This page is intentionally left blank.

Mission Planning for the Mitigation of Hazardous Near Earth Objects

By

Brent William Barbee, B.S.

Thesis

Presented to the Faculty of the Graduate School

of The University of Texas at Austin

in Partial Fulfillment

of the Requirements

for the Degree of

Master of Science in Engineering

The University of Texas at Austin

December 2005

Mission Planning for the Mitigation of Hazardous Near Earth Objects

APPROVED BY

SUPERVISING COMMITTEE:

_____

Wallace T. Fowler

_____

Cesar A. Ocampo

Mission Planning for the Mitigation of Hazardous Near Earth Objects

by

Brent William Barbee, M.S. E.

The University of Texas, 2005

SUPERVISOR: Dr. Wallace Fowler

The problem of mitigating the threat posed by hazardous Near Earth Objects (NEOs) is examined and addressed. The concept of hazardous NEO mitigation is presented, along with background on the NEO population and its characteristics. A set of philosophies and hierarchies of decision-making principles and protocols are devised to aid in the design of spacecraft missions to mitigate threatening NEOs, leading to the construction of a generalized approach to NEO mitigation mission planning. The orbital mechanics involved in rendezvousing with a NEO and performing proximity operations in its vicinity for the purposes of science and deflection system deployment are studied. The need and opportunity to perform rigorous asteroid/comet science in the context of NEO mitigation missions is also discussed. The construction of optimal NEO deflection maneuvers is also examined and the particular case of impulsive deflection maneuvers is given more thorough treatment. NEO deflection systems, both practical and theoretical, are analyzed and discussed. In particular, the standoff nuclear detonation deflection method is examined in detail. A case study is conducted in which a fictitious threatening Near Earth Asteroid (NEA) is mitigated using the techniques developed within.

TABLE OF CONTENTS

LIST OF TABLES

LIST OF FIGURES

NOTATION AND MATHEMATICAL CONVENTIONS

Philosophy

Efficient and accurate communication of technical information is crucial to a healthy, functioning academic community and this author wishes to achieve such communication with this work.

While this author has attempted to use what most technical readers will recognize as some form of standard mathematical notational convention throughout, the definition of standard mathematical notational convention tends to vary within the academic community. Therefore, this brief section has been dedicated to outlining the mathematical notation format presented herein in order to promote clarity and avoid confusion.

In addition to the attempt to adhere to the notational convention presented below throughout, an attempt is also made to fully define each quantity when presented and to present each in a context that makes its nature and meaning clear.

Scalar Quantities

Scalar quantities are those that have only magnitude and no direction. Such quantities presented herein shall include but are not limited to angles, velocity magnitudes, distances, thrust magnitudes, masses, and spatial dimensions. Time is also considered a scalar quantity even though it has an implicit direction since the direction of the flow of time is constant, at least for the physics examined in this work.

Italicized, unbolded characters taken from both the Greek and English alphabets, both lowercase and uppercase, shall be used to represent scalar quantities in this work. Some examples are:

$$\omega, \Omega, \Delta v, R, X, Y, Z, m$$

Vector Quantities

Vector quantities are those that possess both magnitude and direction. Such quantities presented herein shall include but are not limited to position vectors, velocity vectors, thrust vectors, angular momentum vectors, and basis vectors of unit length.

Italicized, unbolded characters taken from both the Greek and English alphabets, both lowercase and uppercase, shall be used to represent vector quantities in this work. These characters shall each be distinguished from scalars by the inclusion of an embellishment denoting their type. For vectors of length other than unity a right arrow above the character shall be used while vectors of unit length shall have a "hat" placed above them. Some examples are:

non-unit vectors: $\vec{r}, \vec{v}, \vec{h}, \vec{T}$

unit vectors: $\hat{i}, \hat{j}, \hat{k}$

Additionally, vectors are defined according to the frame of reference in which they are coordinated. The frame in which a vector is coordinated shall be indicated by a right-side subscript, especially when ambiguity is possible. In cases where ambiguity is not likely, the subscript may be omitted. Some examples are:

$$\vec{r}_{XYZ}, \vec{v}_{RTN}$$

Matrix Quantities

Matrix quantities are those that contain a series of scalar numbers arranged in rows and columns according to the definition of the matrix in terms of linear

algebraic relationships. Such quantities presented herein may include, but are not limited to, rotation or transformation matrices and state transition or propagation matrices.

Italicized and unbolded uppercase characters taken from both the Greek and English alphabets shall be used to represent matrix quantities in this work. Additionally, an underbar will distinguish these quantities. Some examples are:

$$\underline{R}, \underline{T}, \underline{\Phi}$$

In the special case of rotation or transformation matrices, the reference frames between which the matrix transforms shall be indicated by right-side superscripts and subscripts; the superscript shall denote the reference frame from which the matrix transforms while the subscript shall denote the reference frame to which the matrix transforms. Additionally, the angle(s) through which the transformation matrix rotates vectors may also be indicated in parentheses directly to the right of the character denoting the matrix. Some examples are:

$$\underline{R}_B^A(\theta), \underline{T}_C^B(-\alpha)$$

Hence, $\underline{R}_B^A(\theta)$ may be translated as: *the rotation (or transformation) matrix that transforms a vector coordinated in the A reference frame to a vector coordinated in the B reference frame via a positive rotation through angle* θ.

Time Derivatives

Time derivatives are denoted by dots above the variable, which can be a scalar or a vector, for which the derivative is taken. For instance,

$$\frac{d}{dt}(r) = \dot{r}$$
$$\frac{d^2}{dt^2}(\vec{r}) = \ddot{\vec{r}}$$

Note that the first derivative of a quantity with respect to time is denoted by a single dot and the second derivative with respect to time is denoted by a double dot.

Partial Derivatives

Partial derivatives are always written out fully with no shorthand notation. Examples are:

$$\frac{\partial}{\partial v}(E)\ ,\ \frac{\partial}{\partial x \partial y}(\vec{R})\ ,\ \frac{\partial}{\partial t}(r)$$

Note that the partial derivative with respect to time in the above examples is not abbreviated with a dot; partial derivatives with respect to time will not ever be abbreviated.

Other Derivatives

Derivatives with respect to quantities other than time are always written out fully, just as partial derivatives are. Some examples are:

$$\frac{d}{dx}(G)\ ,\ \frac{d}{d\alpha}(\Delta v)$$

1. INTRODUCTION

When I grow weary of it, I have business
Amongst the stars, which these poor creatures deem
Were made for them to look at. 'Twere a jest now
To bring one down among them, and set fire
Unto their ant hill: how the pismires then
Would scamper o'er the scalding soil, and, ceasing
From tearing down each others nests, pipe forth
One universal orison! Ha! Ha!
- Lord Byron (1822)

1.1 Mission Statement

The primary goal of this work is to present a systematic approach to planetary defense against Near Earth Objects (NEOs). NEOs consist of asteroids and comets whose orbits bring them in close proximity to Earth's orbit; some have orbits that cross or intersect Earth's. Potentially hazardous NEOs are those whose Minimum Orbital Intersection Distance (MOID) is very small, meaning that their path through space brings them dangerously close to Earth's path through space. Astronomical observatories all over the world have been concentrating their efforts on discovering NEOs and determining their orbits in order to ensure that none of them will collide with Earth in the foreseeable future. The logical conclusion is that if a NEO were found to be on a collision course with Earth, humanity would act to prevent the collision, thereby averting what could be a civilization-ending cataclysm. The purpose of this study is to analyze the nature of the NEO-Earth collision problem and formulate methods for preventing such a collision.

1.2 Human Opportunity and Responsibility

Human beings have survived and, by some estimations, thrived on our homeworld by learning to adapt to our environment and, in some cases, shield ourselves from aspects of our environment that might harm or kill us. It is generally accepted that humans have a will to live, usually choosing to fight when faced with mortal danger. The impending collision of a NEO with Earth constitutes a mortal

danger of the gravest sort. The collision of a sufficiently massive NEO with Earth would release tremendous amounts of energy, owing to the extreme mass of the NEO and the large magnitude of the relative velocity between the NEO and the Earth at the time of impact. If a massive enough NEO, of mean diameter 1 km or greater, were to strike Earth, the amount of energy released would be unprecedented in known human history, sending enough debris into the atmosphere to block out all sunlight for weeks or months, sending enormous tsunamis to batter coastlines all along whichever ocean is struck if the NEO impacts an ocean, and creating an enormous crater if the NEO impacts land, sending forth a huge shockwave that would wipe out everything in its path for many kilometers from the impact point. The massive shock to our ecology and climate would dramatically shift the weather, creating a long series of devastating storms and perhaps even ushering in a premature ice age. The mechanical shock delivered beneath the Earth's surface could spark a horribly destructive spell of volcanic activity and/or earthquakes. Millions, if not billions of people would be killed and human civilization might not survive in its present form or at all. Even a relatively small NEO could lay waste to an entire metropolis or continental region were it to strike land in a densely populated area.

There is no question that humanity would choose to prevent a NEO collision with overwhelming unanimity. However, given our ability to think rationally and plan ahead, it follows that such an act of self-preservation ought to be a conscious choice resulting from a sense of responsibility rather than a last-minute reaction resulting from fear of annihilation. Moreover, a hasty response to a threat of such magnitude would likely fail. Recently, the Deep Impact spacecraft mission to the comet Tempel 1 only succeeded in delivering an impactor to the comet after years of careful and dedicated mission planning, coupled with the most optimal conditions possible given natural constraints, and constant tending by mission controllers on the ground. Scientists and engineers will not have the luxury of choosing their target when an Earth-impacting NEO is discovered; nature will have chosen the target, and its potentially challenging physical and orbital characteristics, for us. Moreover, the

Tempel 1 impactor was only guided into a head-on impact with the comet; an optimal impulsive NEO deflection strike would have to be oriented in a particular way relative to the NEO's velocity vector, which requires more precise positioning.

Ultimately, humanity has a responsibility to itself, and to the myriad species with whom we share this planet, to execute the best defense possible should an impending NEO collision event be discovered. This is both an honor and an opportunity. Never before, to the best of our historical knowledge, has any species on Earth had the capability to perform NEO mitigation; this capability marks a milestone for our civilization. If we prove that we have the ability to deflect or destroy an incoming NEO, the only forces that could lay us to waste are the Sun going nova, which will not happen for approximately 4.5 billion years, massive geological activity, a massive pandemic, or ourselves. While we could not conceivably prevent the Sun from going nova or stop a worldwide wave of earthquakes and volcanic eruptions, we are working hard to prevent disease and we ostensibly can evolve past the sorts of behaviors that would lead us to destroy ourselves. Thus, the only remaining threat to our survival that is within our power to mitigate but that we have not yet demonstrated the ability to mitigate is NEO collision.

Surely, the act of successful NEO mitigation, or a successful mission demonstrating NEO mitigation technology, will call upon the resources of the entire planet, owing to the extreme complexity of the problem, logistical conundrums, and the sheer energy required. Thus, apart from being a species milestone for its own sake, the act of consciously choosing to develop NEO mitigation systems as a safeguard against future calamity also represents a tremendous opportunity for the human race. Rather than coming together out of fear in the final hour, we can come together now by virtue of an unforced and conscious choice, choosing to unite across national and ethnic boundaries in the development and execution of a spacecraft mission that demonstrates to the entire world that all the sacrifices and turmoil that have led to our current level of technology have not been in vain; while the development of our technology may have dearly cost us socially, culturally, and

ecologically, it has given us the ability to defend ourselves from one of the few remaining cataclysmic threats to our existence, if we choose to employ it in that capacity.

Additionally, the threat of NEO impact is a threat to the entire species, not just one nation or ethnicity. The impact of a massive NEO would instantly affect the entire world, making the mitigation of such a NEO both the responsibility and the birthright of the entire human race. This fact cements the basis for a worldwide effort, both for testing NEO mitigation systems and for executing an actual mitigation mission.

There are some people who do not see the merit of such efforts, claiming that a NEO collision is such a low probability event that it isn't worth expending resources on designing and testing NEO mitigation systems. It would perhaps be more accurate to say that NEO collisions of sufficient magnitude to devastate an entire species are low frequency events, relative to human history. Small extraterrestrial objects collide with our planet quite often, and they mostly go unnoticed until someone discovers the meteor on or beneath the ground. Other "small" impacts, such as the Tunguska (Siberia) event of 1908, which leveled 2000 km^2 of forest, have the potential to devastate a region extending many kilometers from the impact site [1]. Even though the impact site was fortunately remote, people were injured and two were reportedly killed. This sort of impact by even such a small NEO over a densely populated region would be locally catastrophic and absolutely worth preventing. It is estimated that this class of collision occurs about once per century [2]. It is also estimated that the mean diameter of the colliding NEO in the Tunguska event was a mere 60 m [3]. NEOs with mean diameters on the order of 100 m are more plentiful by several orders of magnitude than their civilization-ending counterparts of mean diameter greater than 1 km; they are also far more difficult to detect.

1.3 Current State of NEO Mitigation Readiness

To date, no NEO mitigation system has ever been experimentally tested. While various scientists, theorists, and engineers have hypothesized about NEO mitigation techniques, none have ever been tried. Though some proposed techniques are beyond the capabilities of current and foreseeable technology, others are possible today or in the very near future. Given the great uncertainties involved in such novel applications of technology, a given mitigation system cannot be depended upon until it has been tested and verified in the field, which means carrying out a test mitigation mission on a non-threatening NEO. Proper choice of the target NEO for testing will ensure that there is no possibility of inadvertently placing the NEO onto a collision course with Earth.

However, perhaps the most crucial ingredient in a successful NEO mitigation attempt is advance warning. Even the most capable NEO mitigation system may prove useless without sufficient advance warning of the impending NEO collision with Earth. Towards this end, teams such as LINEAR, Spacewatch, the Catalina Sky Survey, and Spaceguard are constantly searching the skies in an effort to discover as many NEOs as possible and, most importantly, to use the observational data to predict the orbit of the NEO well enough to determine whether there is any chance that the NEO will collide with Earth in the future. The Spaceguard goal of discovering 90% of all Near Earth Asteroids (NEAs) by 2008 was established in May of 1998. At the time of this writing in 2005, Spaceguard has discovered an estimated 73% of all such NEAs, to the best of our knowledge [4].

Another crucial ingredient in a successful NEO mitigation attempt is NEO science. The amount of physical data that can be gathered on NEOs via remote observation on Earth is limited at best. A maximally effective NEO mitigation can only be designed and executed with adequate knowledge of the NEO's physical properties, most especially composition and internal structure. In fact, insufficient knowledge of these quantities could cause a NEO mitigation to fail; deflecting a porous, "rubble-pile" NEO, for example, requires a very different amount of energy

applied in a different way than deflecting a solid, monolithic NEO does. Therefore, sending the wrong mitigation payload due to inadequate scientific knowledge of the NEO could prove utterly catastrophic.

Thus, the ideal NEO mitigation mission always begins with a preliminary science mission to the NEO, providing crucial data that will determine the final design of the actual mitigation mission. However, there are conceivable NEO collision scenarios in which the warning time is very short, on the order of a few years, meaning that there would not be enough time to precede the deflection mission with a science mission.

1.4 Low Frequency, Low Probability, High Impact Events

It is an unfortunate aspect of human nature that most people wait until an accident happens to institute preventative measures against future accidents. In some cases it is because people only feel justified in expending the effort to take such preventative measures once they have felt the pain of a particular accident. In other cases, a politician may personally feel that it is worth spending money and time on a certain preventative measure, but the people whom the politician represents disagree.

Whatever the cause of negligence, there is one common factor. This common factor is the typical human response to low frequency, low probability, high impact events. These are sharply distinguished from low frequency, low probability, low impact events; such events are only worth taking measures against if the energy required to take the measures is extremely small. However, the issue of taking measures against the high impact events is more complex.

Generally, people give little regard to low frequency, low probability events. However, these events occur: people win state lotteries, aircraft crash, cosmic rays strike electronic equipment and cause malfunctions. More seriously, natural disasters are a matter of record. In 2004, a terrible tsunami spawned by an earthquake killed over 118,000 people in Indonesia, Thailand, and India. Within the past few months, as of the time of this writing, a Hurricane named Katrina slammed into New Orleans

and devastated the city, killing approximately a thousand people. For many years, people had been saying that a hurricane striking New Orleans would be a terrible disaster. Yet little action was taken to protect the city, such as constructing better levees and shoring up existing ones. No one was prepared to properly evacuate the city. Rescue response was pitifully slow. People simply were unprepared. They were unprepared because a hurricane making a direct strike on New Orleans was a low frequency, low probability, high impact event. While the consequences were imagined to be grave, the threat was far away and unlikely, making it easy for people to ignore. Now, millions of those people are jobless and homeless.

This is not to suggest that we should live in a perpetual state of fear regarding the next possible disaster or threat to come our way; that would be a needlessly unpleasant way to live. Nor is it to suggest that we as a species have the resources or technology to mitigate every single threat in our environment; in some cases effective damage control and adroit disaster response is the best we can do. Rapid, organized response can dramatically reduce the net impact of a disaster by saving lives and minimizing damage to infrastructure.

What *is* being suggested here is that no potential threat should be ignored. The fact that a particular threat is of the low frequency, low probability category is no excuse to do nothing about it when that same threat is also of the high impact category. It is possible, with some forethought, to institute protective measures efficiently without excessive expenditure of resources. Moreover, even if the potential threat never occurs, the technology and techniques developed to prepare for the mitigation of the threat frequently have other applications and generally advance the level of our science and engineering capabilities.

However, we are currently taking no action to prepare ourselves for mitigating the threat posed by a hazardous NEO, other than searching what sections of the sky we can see from ground-based observatories for incoming NEOs. There are entire orbital regions that NEOs inhabit that we cannot see from ground-based observatories. Yet there are no plans for putting observatories in orbit to address this

deficiency. Most importantly, there have been no tests of possible NEO mitigation systems. It appears that humanity at large is content to operate under the assumption that we will simply fire a few nuclear warheads at the incoming asteroid and that will solve the problem. Unfortunately, the general public does not have the technical background to even begin to grasp the incredible complexity of such an operation. Nor does the general public understand that nuclear devices might not operate as predicted or hoped in the space environment. Such devices might also not deliver energy to a NEO the way we hope they will. There are a host of unanswered questions regarding NEO mitigation in general and these questions cannot be answered with simulation and calculation; direct experimentation in the field is required. Yet we are doing nothing.

If a NEO were discovered tomorrow that was going to impact Earth in several years, even ten years, we would be completely unprepared and whatever our mitigation effort was would be shaky at best. It would be preferable to have a knowledge base built on field tests of mitigation systems and a more expansive catalogue of NEOs and their physical properties. Such a knowledge base can be accumulated only through testing of actual mitigation systems and the study of NEOs in the field.

NEO science missions are becoming more common, fortunately. The Near Earth Asteroid Rendezvous (NEAR) mission, which studied the large asteroid Eros, was a great success. More recently, the Deep Impact mission collided a small impactor with comet Tempel 1 in order to excavate subsurface material and create an ejecta plume to be studied by a nearby monitoring spacecraft. This mission has also been very successful, with interesting results already being garnered from the currently collected data.

NEO science missions such as these must continue. Not only do NEO science missions better prepare us for mitigating the threat posed by a hazardous object, but they also provide unique knowledge regarding the state of matter in the early solar system. Comets and asteroids are like time capsules because the material within them

has been preserved since these objects formed during the earliest days of our solar system. The scientific quest to understand our origin as a species will advance further and further as our spacecraft technology for rendezvousing with and studying asteroids and comets improves and more of these missions are performed.

However, all the sky-searching, NEO cataloguing, and deployments of NEO science missions will amount to nothing unless we also test our proposed NEO mitigation systems in order to identify the ones that are viable and learn how to improve them. The more comfortable and practiced we are with the process, the far less likely it is that our mitigation efforts would fail in a true emergency.

The recommendation of this author is that NEO mitigation system testing should begin immediately. Adequate and proper personnel, resources, and funding should be allocated to NEO mitigation system mission design and testing should begin shortly thereafter. The general public should be educated regarding the complex nature of the NEO mitigation problem so that they can appreciate the successes and failures of the NEO mitigation system design teams. Most importantly, the general public and the scientific community alike need to recognize that the act of demonstrating the ability to mitigate an incoming hazardous NEO represents the first time that we know of where a species on this planet was able to defend itself against one of the few remaining threats to the entire species. Demonstrating that we, as a species, have evolved enough to be capable of saving ourselves from annihilation at the hands of an asteroid or comet is a milestone unlike any other and should serve to remind us of our mortality, our strength, and our inherent connection to each other. Everyday we live as peoples of different and often disagreeing nations. But on the day that we are called upon to defend ourselves from the ultimate threat that poses a danger to all, we will act as one. At least, that is the hope of this author. The greatest hope is that we as a species are motivated to work together now and lay aside our differences by conscious choice now rather by fear in the final hour.

1.5 Scope of This Work

This work will present an overview of the NEO population but will focus more on asteroids than comets. A discussion of some potential NEO mitigation methods will be presented, but the focus will be on the mitigation techniques characterized by impulsive deflection. A variety of NEO mitigation systems will be presented and some will be analyzed, however the primary focus will be on nuclear devices as mitigation systems. This is with the caveat that the operation of nuclear devices in space and the coupling between the output of a nuclear device and a NEO are all highly theoretical and their efficacy remains to be proven.

Additionally, the techniques and capabilities for deflecting solid, monolithic asteroids will be considered while the techniques and capabilities for deflecting strengthless asteroids (rubble piles) will be not be considered in as much detail; their deflection has specific and separate requirements.

A top-level design system for generating NEO mitigation spacecraft missions with a generalized approach will be developed and presented. However, some design details, such as attitude control, communication bandwidth, data handling, etc. are not considered in detail. After being developed and summarized, the generalized NEO mitigation mission design philosophy will be applied to a case study.

A design space search method for determining optimal impulsive NEO deflection parameters is developed that bypasses difficult explicit optimization techniques. Most importantly, the design space search method shows the structure of the entire solution space and provides critical intuition as to the nature of the solutions.

Discussions of the societal and philosophical issues associated with NEO mitigation will be presented where appropriate. These philosophical issues will also play a role in the overall mitigation mission design philosophy.

The details of orbital mechanics and orbital simulation methods will be expounded upon since it is these techniques that lie at the heart of the experimental procedure used to generate most of the results in this work.

2. NEO POPULATION AND TAXONOMY

2.1 Introduction

Near-Earth Objects (NEOs) primarily consist of a family of asteroids, specifically termed Near-Earth Asteroids (NEAs), whose orbits lie close to that of Earth. Thus they are differentiated from the rest of the asteroids in the solar system that have orbits fully outside of Earth's orbit, such as main belt asteroids between Mars and Jupiter. NEOs may also include comets whose orbits bring them in close proximity to Earth, though comets are much less numerous and hence not a major focus of this work.

NEAs are further subdivided according to two criteria: orbital characteristics and composition. The categories of each subdivision are overviewed below.

2.2 NEA Orbit Classifications

Near-Earth Asteroids (NEAs) are placed into one of three main groups according to key features of their orbits. The Apollo asteroids are Earth-crossing asteroids with a semi-major axis greater than 1.0 AU and a perihelion distance less than 1.107 AU. The Aten asteroids are Earth-crossing asteroids with a semi-major axis less than 1.0 AU and a perihelion distance greater than 0.983 AU. The Amor asteroids are Mars-crossing asteroids with a perihelion distance less than 1.3 AU and greater than 1.017 AU [5].

The most dangerous objects inhabit Apollo or Aten orbits. Aten asteroids can be particularly dangerous because the observation of these objects is greatly hindered by their typical position relative to the Earth and the Sun. Thus, warning times for impactors on Aten orbits can potentially be very short.

2.3 NEA Composition Classifications

There are three main composition classifications of NEAs. S-type asteroids, which are silicaceous, account for approximately 17% of known asteroids and

comprise the majority of the inner asteroid belt. They are composed of iron mixed with iron- and magnesium-silicates. M-type asteroids are mostly composed of metallic iron and comprise most of the middle asteroid belt. C-type asteroids, which are carbonaceous, include more than 75% of all known asteroids [6].

2.4 Observed and Predicted NEA Orbital Characteristics

Statistical predictions of the evolution of NEA orbital characteristics based upon solar system dynamics have been made by Bottke, *et. al.*, and the debiased orbital characteristics distributions normalized to 960 NEAs of absolute magnitude less than 18 ($H < 18$) are shown in figure 2.1 below.

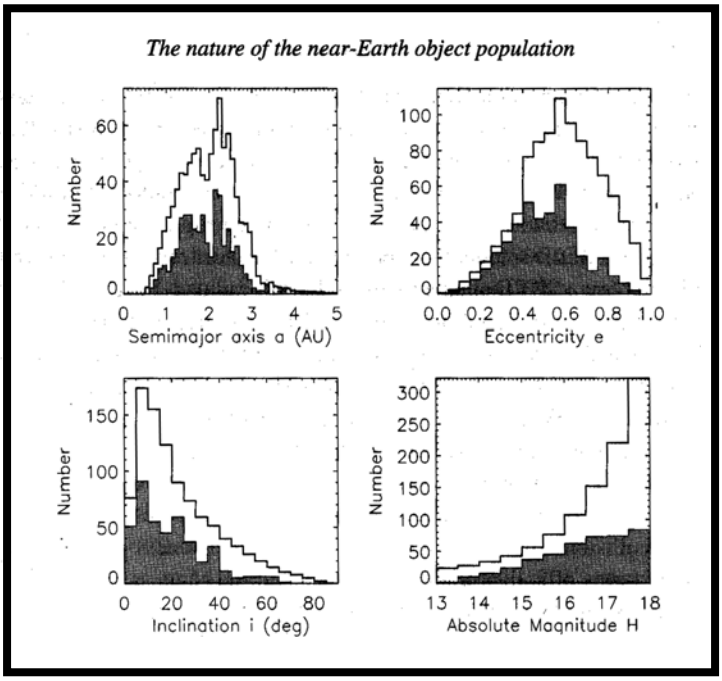

Figure 2.1: Debiased Orbital and Size Distribution of NEAs for $H < 18$ [5]

The absolute magnitude, *H*, is a logarithmic measure of the brightness of an object, in this case a NEA, typically in the V spectral band, corrected to a heliocentric and geocentric distance of 1 AU and a solar phase angle of 0°. Essentially it is a measure

of the physical size of a NEA,with H = 18 corresponding to NEOs of approximately 1 km in mean diameter. The darkened portions of the plots in figure 2.1 represent the actual observed distributions of 426 NEAs based on data current as of the year 2000. This provides some validation of the orbital models used to arrive at the statistical predictions as it can be seen that the observational data is nicely filling in the predicted distributions.

2.5 Orbital Characteristics of Earth-Impacting NEAs

Just as predictions have been made regarding the overall distribution of NEAs based on solar system dynamics, predictions have also been made regarding the orbital characteristics of NEAs on orbits that impact Earth by Chesley, *et al.* and their results are presented in figure 2.2 below.

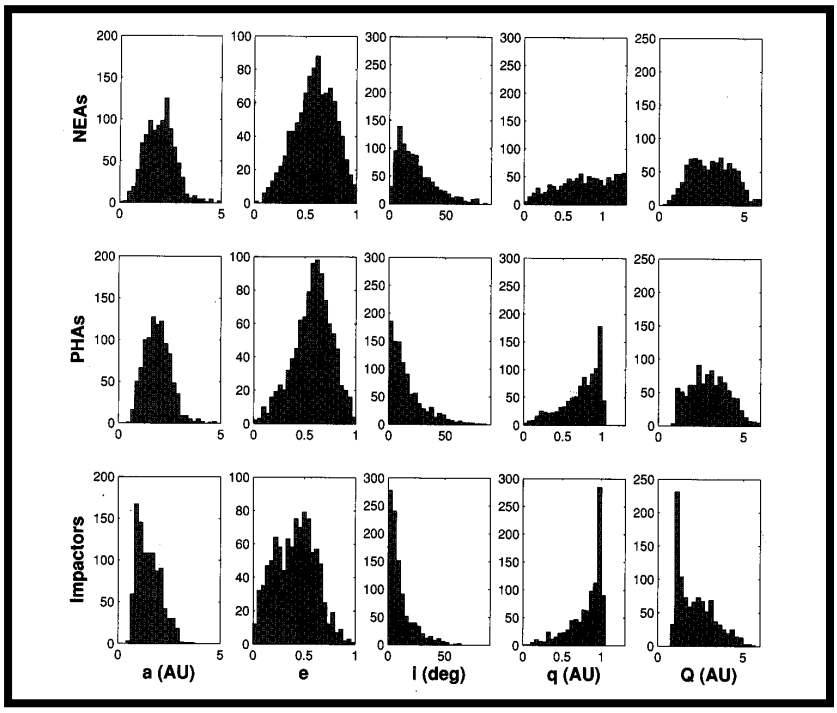

Figure 2.2: Simulated Orbital Elements of NEAs, PHAs, and Impactors [7]

The chief result from *Chesley, et al*, is that many (but not all) simulated impactors *tend* to have low (but not necessarily zero) inclination, low eccentricity, and a semimajor axis near 1 AU. Comparing these trends to the distributions in figure 2.1 above, it is clear that potential impactors are lurking in the NEA population. This evidenced by the many NEAs that have made very close approaches to Earth in the past. There is a definite predominance of low (but not zero) inclination orbits in the observed and predicted distributions though the eccentricities seem to tend more towards moderate values. There are certainly a large number of known NEAs with semi-major axes near 1 AU, though the majority are predicted to have semi-major axes of around 2 AU.

2.6 Structural Classifications of NEOs

In addition to being separated according to orbit and elemental composition, asteroids and comets are also classified according to the characteristics of their physical structure. This classification is predicated on the level of material strength and cohesion present in the NEO, ranging from no strength or cohesion at all, e.g., a "rubble pile," to fully monolithic NEOs that are fully coherent. Ground-based observations can provide some clues as to the physical character of NEOs, but science missions are required to be certain.

2.6.1 Strength, Coherence, and Porosity

A NEO's structural character may be described in terms of strength, coherence, and porosity. Generally speaking, the strength is the usual mechanical material strength, representing the material's resistance to applied forces, including shear forces, which would otherwise deform it. Conversely, it is also a measure of the required energy to disrupt the object.

The coherence of the object is related to its strength. Essentially, the coherence is a measure of to what degree the object is an unfragmented solid. An

object of zero or near-zero coherence is one that is merely a conglomerate of small, disparate chunks of material that are not bound strongly to each other; even miniscule applied forces will move the pieces of material apart, constituting a disruption. Such objects are also said to be strengthless as their ability to resist forces is negligible.

The porosity of an object refers to how porous it is, indicating how much of its internal structure is pockets of empty space. The overall material may still be coherent though. The key effect of porosity is on the transmission of mechanical force through the object. Highly porous objects are able to absorb larger amounts of force since the empty spaces within them cannot transmit the force well and generally simply are crushed, thus absorbing energy. Hence, the force applied to the object is attenuated according to how porous the object is. This is of particular concern to NEO mitigation techniques characterized by impulsive deflection that rely on the NEO material to transmit the applied force effectively, leading to the desired acceleration on the NEO's center of mass.

It is for this reason that rubble pile NEOs pose a unique problem in terms of how they might be mitigated. Impulsive forces from explosive devices would be strongly attenuated by such NEOs and hence have minimal effects on the NEO's orbit, though some analyses have shown they can still be made effective. The anchoring of high or low thrust systems to such NEOs would be infeasible since there would be no cohesive structure to transmit the thrust to the NEO's center of mass. The best solution to mitigate a rubble pile NEO may be to position explosive devices, probably nuclear devices, within the rubble pile and attempt to blast it apart. Depending on the size and composition of the rubble pile, this process might have to be executed several times in series to sufficiently reduce the rubble pile such that it no longer poses a threat.

There is currently a debate in the NEO science community as to whether most large NEOs are of the rubble pile, rather than monolithic, variety. While it is impossible to answer this question decisively from ground-based observations, some inferences may be made. As stated previously, the only way to be certain is to sample

the NEO's impulse response either with seismic sensors planted on the NEO, as is done in the Don Quixote mission currently being designed by ESA, or by observing the results of an energetic collision with the NEO, as has been done with the recent Deep Impact mission to comet Tempel 1. The nature of the crater formed by an energetic impact provides critical information about the NEO's physical structure; there is an observable difference between craters formed in the strength regime and those formed in the gravity regime, and this difference can be ascertained by visual inspection of the shape and extent of a crater resulting from a collision of known energy. The impact crater resulting from the energetic projectile that was smashed into comet Tempel 1 indicates that the comet surface is weak and powdery in nature, held together only by gravity [8]. This does not bode well for an attempt to alter the comet's orbit adequately for mitigation purposes using an impulsive technique or a technique that requires anchoring to the comet's surface. For example, were Tempel 1 on a collision course with Earth and nuclear devices were used on it in an attempted mitigation, the effort would likely have failed. This example demonstrates the need for conducting NEO science in preparation for any mitigation effort.

2.6.2 Ground-Based Observations

While ground-based observations cannot confirm that a given NEO is indeed a rubble pile, these observations can determine that a given NEO is not a rubble pile since the sustained rotation rate of a NEO implies a minimum tensile strength across its equator. The key to this determination lies in the fact that most NEOs are rotating (as well as precessing and nutating, generally) about a spin axis. A consequence of physics is that there is a critical rotational speed past which any strengthless object will fly apart. Hence, any object observed to be rotating faster than this speed cannot be a strengthless rubble pile. Conversely, objects observed to be rotating slower than the critical rate might be rubble piles, but this cannot be confirmed without a mission such as the Deep Impact mission.

The critical rotation speed can be derived as follows. The first assumption is that the object is a sphere rotating at a constant rate. Though most NEOs are irregularly shaped and have nutating and/or precessing spin axes, the deviations are not large and thus the given set of assumptions is acceptable for a cursory analysis. A diagram for the situation is presented in figure 2.3 below.

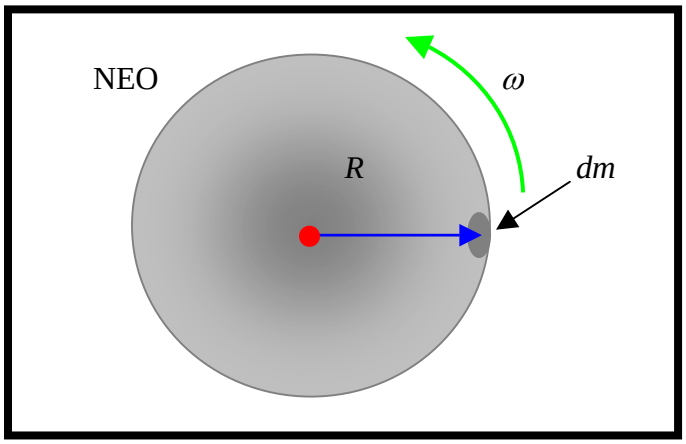

Figure 2.3: Spherical NEO Rotating at a Constant Rate

R is the radius of the object, dm is a differential mass element located right at the surface of the NEO, and ω is the rotation rate of the NEO; the rotation axis as shown is coming directly up and out of the page.

The next step is to draw a Free Body Diagram (FBD) for the differential mass element, shown in figure 2.4 below.

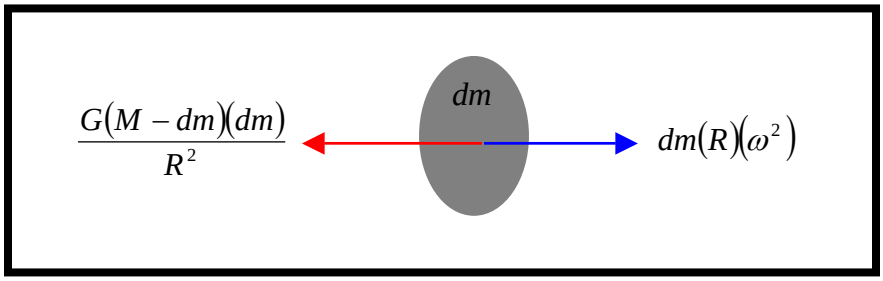

Figure 2.4: Free Body Diagram of Differential Mass Element

As shown in figure 2.4, the only forces acting on the differential mass element are the gravity of the rest of the NEO and the centripetal “force”.

Next, the forces are equated in order to generate an equilibrium condition, resulting in the following equation

$$\frac{G(M-dm)(dm)}{R^2} = dm(R)(\omega^2) \tag{2.1}$$

At this point it is necessary to make the reasonable assumption that the differential mass element is much, much smaller than the total asteroid mass such that

$$M - dm \approx M \tag{2.2}$$

Thus reducing the equilibrium equation to

$$\frac{G(M)(dm)}{R^2} = dm(R)(\omega^2) \tag{2.3}$$

Next, dividing both sides by the differential mass element dm and solving for ω^2 yields

$$\omega^2 = \frac{GM}{R^3} \tag{2.4}$$

Since our asteroid is spherical, we can rewrite the mass in terms of the density and volume as

$$M = \rho V = \rho \frac{4}{3} \pi R^3 \tag{2.5}$$

Substituting equation (2.5) into equation (2.4) gives

$$\omega^2 = \frac{4G\rho\pi R^3}{3R^3} \tag{2.6}$$

Dividing out the R^3 term in equation (2.6) and rearranging gives

$$\omega^2 = \frac{4\pi G\rho}{3} \tag{2.7}$$

Thus, the critical rotation rate for which material on the NEO's surface becomes orbital is

$$\omega = 2\sqrt{\frac{\pi G\rho}{3}} \tag{2.8}$$

Note that this rate is approximate due to the assumptions listed above. However, it provides a working estimate that can be used to assess NEO observations made on the ground.

Current results for ground observations are that none of the approximately 1000 asteroids larger than 150 m in mean diameter with a reliably measured spin rate rotates fast enough to require that the asteroid is coherent [9]. Furthermore, a fast rotator named 1998 KY26 is rotating fast enough to require cohesion, however its minimum required tensile strength according to its spin rate is orders of magnitude less than the tensile strength of snow [9].

The primary result of these analyses is that many NEOs may in fact be rubble piles due to frequent collisions in the past that shattered them. However, there is no basis for a model of this intense collisional history, though many asteroids do bear evidence of substantial cratering. The only way to be certain of a given NEO's structural integrity is to fly a science mission equipped with mechanisms for assessing the NEO's cratering and/or seismic response. Another option is seismic imaging, e.g., using dual-wavelength radar tomography, which has been recently refined for kilometer-scale geologic masses [9]. This sort of remote sensing of a NEO's seismic properties and hence internal structure is preferable, especially for NEOs that possess a loosely-packed regolith that would impede the anchoring of seismic sensors, which require coupling with the NEO body in order to take proper measurements.

3. NEO SCIENCE OPERATIONS

3.1 Introduction

Asteroid and comet science is one of the most valuable means for humanity to study its own origins, as well as the origins of the solar system. Asteroids and comets are comprised of material that is the direct legacy of the earliest days of the solar system's formation, allowing researchers studying that material to peer into the distant past, testing theories as to how the solar system formed and how life on Earth began.

This same science also allows for the characterization of NEOs in the context of hazardous NEO mitigation. The physical properties of a NEO are the primary drivers in the selection of the mitigation system that will be the most effective for that particular NEO; NEO spin rates and surface compositions strongly impact the efficacy of attached thrusters (as well as the ability to attach and optimally point thrusters in the first place) and the NEO's internal composition and structure determine its impulse response. Without the accurate knowledge of a NEO's physical composition and dynamic state that comes from flying a science mission to the NEO, a mitigation mission planner is left with the best guesses provided by ground based observations, which are quite coarse.

Funding and politics currently dominate the deployment of scientific missions to asteroids and comets for purely scientific purposes, though no such restrictions would ostensibly limit science missions to potentially catastrophic NEOs. Instead, the factors that limit science on hazardous NEOs will be purely logistical. Essentially, if there is enough time before Earth impact to deploy a science mission and collect sufficient data before the time window for constructing and launching the mitigation spacecraft arrives, then a science mission will invariably be deployed; in the extreme case where there is not sufficient warning time to conduct a science mission before the mitigation, we will have no choice but to base design decisions on ground observation data and include the largest margins for error possible. A detailed

discussion of the methodology behind deriving physical data for NEOs from ground observations is beyond the scope of this work. Suffice it to say that these methods exist and are regularly employed.

Thus, while it may not always be possible to deploy a NEO science mission prior to mitigation, it is always desirable to do so. Hence, when available, NEO science mission data is a critical component of mitigation planning and this section is devoted to developing the most pertinent NEO science techniques and explaining how the results of such science influence the mitigation mission design process.

3.2 NEO Properties of Interest

The mission objectives for a science mission to a hazardous NEO are largely driven by the specific physical properties of the NEO that must be known for effective mitigation system design and implementation. It is of note that these physical properties are generally the same as those that would be of interest to science survey missions conducted on an asteroid or comet in a purely scientific context. Thus, the data collected is valuable both in the effort to understand NEOs and solar system origins and in the effort to determine the best mitigation technique.

The specific physical properties of interest for NEO science in the context of mitigation planning are listed in table 3.1 below.

Table 3.1: NEO Physical Properties of Interest

Property
Mass and Density
Shape and Volume
Center of Mass Location
Internal Structure and Seismic Properties
Internal Composition
Surface Composition and Properties
Thermal Characteristics
Spin Rate and Spin Axis Orientation

Methods for determining some of the quantities listed in table 3.1, as well as the significance of those quantities in mitigation system design, are discussed below.

3.2.1 Mass

The primary effect of mass is to displace other nearby masses due to mutual gravitational attraction. Therefore, the best way to measure the mass of a NEO is to measure the attraction it exerts on a nearby body at a known distance. This attraction manifests as an acceleration experienced by the nearby body. This methodology was employed by the NEAR spacecraft on the asteroids Mathilde and Eros with favorable results.

The Near Earth Asteroid Rendezvous mission (NEAR), which sent a survey craft to the asteroid Eros, estimated its mass by measuring the perturbation due to Eros' gravitational field on the NEAR spacecraft. Owing to the mission timeline and the sheer size of Eros (33×13×13 km), the spacecraft was able to orbit the asteroid for an extended period, allowing a relatively detailed determination of the asteroid's mass properties and gravitational field [9].

While an exposition of the exact mathematical techniques employed by the NEAR mission are beyond the scope of this work, the capabilities they imply are central to this work. The important point is that measurement equipment precision and associated techniques are sufficiently mature to allow the accurate detection of the gravitational pull of a relatively small solar system body amidst other perturbations of (often) similar magnitude. For instance, spacecraft in interplanetary space are subject to solar radiation pressure, primary attraction by the Sun, N body "perturbations" from the other planets in the Solar System, and other more obscure (and difficult to model) forces, such as the Yarkovsky Effect (uneven thermal reradiation from the NEO), and yet the NEAR spacecraft was still able to sense the specific forces it was experiencing due to Eros' gravity despite being affected by the additional aforementioned forces.

However, not all NEOs are as massive as Eros and none are as massive as the Earth, of course. The Near Earth Asteroid (NEA) population is comprised of thousands of asteroids on the order of several kilometers in mean diameter, and there are many more that are several hundred meters in mean diameter or less [5]. It is not feasible to place spacecraft in captured orbits around these objects due to their low gravity, though it is feasible to construct trajectories around these smaller NEOs using the Clohessy-Wiltshire (CW) equations and an appropriate guidance and control system, as will be demonstrated later. While in proximity to the NEO, sensors will determine the gravitational pull of the NEO and hence its mass. Consider the simple case of a spacecraft traveling behind a NEO along the same heliocentric orbit, as shown in figure 3.1 below.

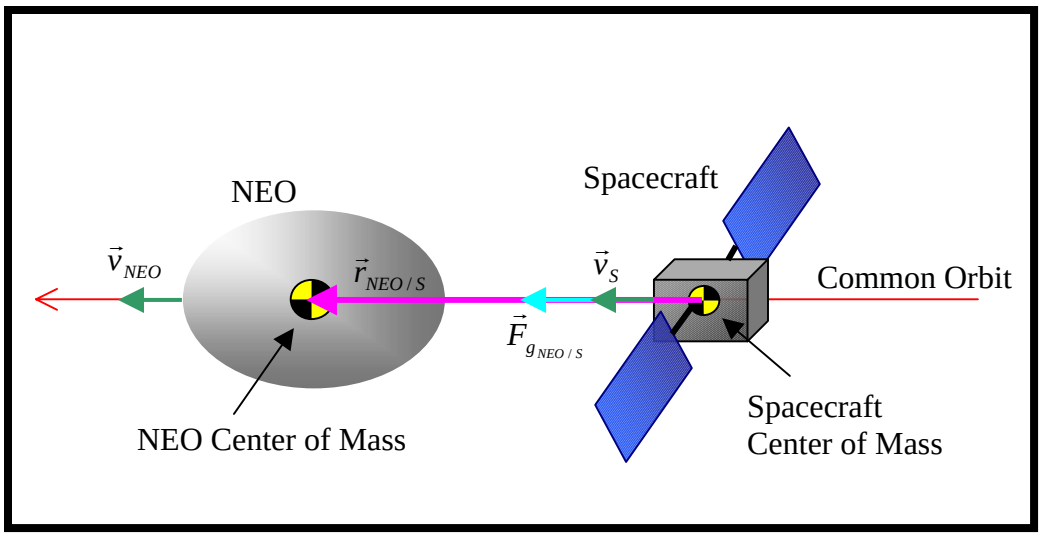

Figure 3.1: Relative Geometry of NEO and Spacecraft On Orbit

The vector quantities depicted in figure 3.1 are defined as follows:

$\vec{v}_S$ = spacecraft velocity vector

$\vec{v}_{NEO}$ = NEO velocity vector

$\vec{r}_{NEO/S}$ = position vector from the spacecraft's center of mass to the NEO's center of mass

$\vec{F}_{g_{NEO/s}}$ = force due to the NEO's gravity acting on the spacecraft

The force acting on the spacecraft due to the NEO's gravity is computed according to Newton's law of gravitation as follows:

$$\vec{F}_{g_{NEO/S}} = \frac{GM_{NEO}M_S}{\left\|\vec{r}_{NEO/S}\right\|^3}\vec{r}_{NEO/S} \qquad (3.1)$$

where

G = universal gravitational constant

M_{NEO} = mass of the NEO

M_S = mass of the spacecraft

The only unknown on the right-hand side of equation (3.1) is the mass of the NEO, which is the quantity of interest. The relative position vector between the NEO and spacecraft centers of mass can be determined with attitude and ranging sensors, perhaps augmented by reflective targets placed on the asteroid's surface. The asteroid's center of mass location can be determined by methods such as those employed by the TALON system, which will be discussed briefly later [10]. The spacecraft's center of mass relative to the mounting point of sensors is known. Finally, the mass of the spacecraft is also known. Therefore, to solve for the NEO's mass, the only remaining task is to measure the left-hand side of equation (3.1), which is the gravitational force experienced by the spacecraft due to the NEO. This force will manifest as an acceleration acting on the spacecraft's center of mass as follows:

$$\vec{a}_{g_{NEO/S}} = \frac{\vec{F}_{g_{NEO/S}}}{M_S} \tag{3.2}$$

where

$\vec{a}_{g_{NEO/S}}$ = acceleration experienced by the spacecraft due to the NEO's gravity

The gravitational force due to the NEO can be directly computed by rewriting equation (3.2) to isolate the force on the left-hand side of the equation. The acceleration indicated by equation (3.2) is the quantity that must be measured precisely, filtering out the accelerations from all other perturbations in the

spacecraft's environment. As discussed above, doing so is within the capability of modern technology and computing.

Finally, once the gravitational force due to the NEO has been measured with sufficient accuracy, an accurate estimate of the NEO's mass may be computed by rewriting equation (3.2) as follows:

$$M_{NEO} = \frac{\left(\left\|\vec{F}_{g_{NEO/S}}\right\|\right)\left(\left\|\vec{r}_{NEO/S}\right\|^2\right)}{GM_S} \tag{3.3}$$

The only errors in the estimate of the NEO's mass provided by equation (3.3) will come from the errors in the measurement of each term on the right-hand side. Thus, minimizing the error in each measurement will lead to a good estimate of the NEO's mass.

To quantify the sorts of accelerations the spacecraft will experience due to the NEO during a characteristic science operation, the acceleration felt by a spacecraft due to a NEO's gravity, as described by equation (3.2) above, was computed for a range of characteristic NEOs at a spacecraft separation distance of 100 m. The radii of the NEOs range from 100 m to 10 km and they are assumed to be spherical with a mean density of 3.0 g/cm^3. The accelerations felt by the spacecraft for each characteristic NEO are plotted versus NEO mass in figure 3.2 below.

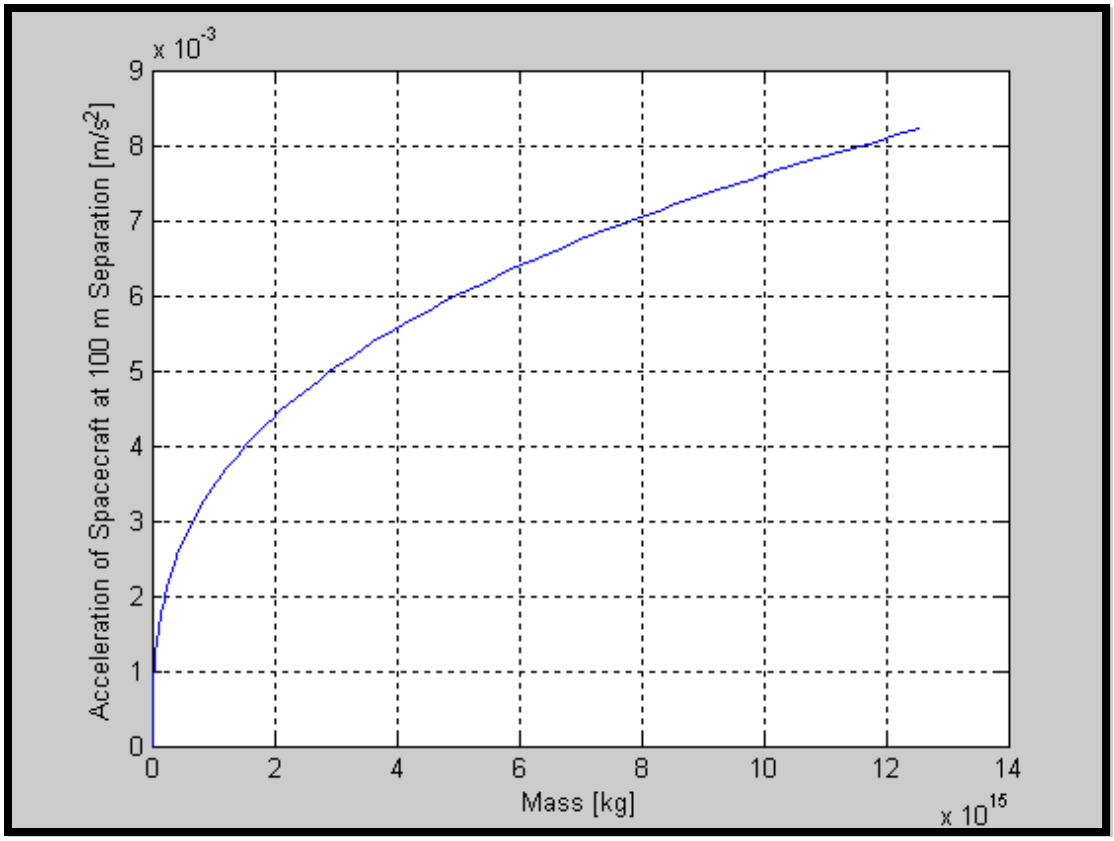

Figure 3.2: Spacecraft Acceleration versus NEO Mass at a Separation Distance of 100 m

The accelerations range from 2.0963×10^{-5} m/s^2 for a 100 m NEO to 8.2198×10^{-3} m/s^2 for a 10 km NEO. Due to the sensitivity of current instrumentation, these accelerations are sufficient to be detected in the presence of the accelerations on the spacecraft due to the planets, the Sun, and environmental forces such as solar radiation pressure.

3.2.2 Importance of Mass Determination

The mass of the NEO is a measure of its inertia, which is indicative of how much it will resist an attempt to impulsively change its velocity. Moreover, if the volume of the NEO is also known, the mean density of the NEO may be determined,

which is an important quantity for computing the required yield of a nuclear device for standoff nuclear detonation deflection. Finally, the mass of the NEO, along with the NEO's velocity relative to Earth at impact, determines the energy released by the NEO should it impact Earth, which quantifies the threat to Earth represented by the NEO.

Additionally, the mean density of a NEO can be compared to its dimensions and composition to indicate what its porosity might be. The porosity of a NEO is a secondary parameter and is related to the NEO's seismic properties. It is indicative of how well the NEO transmits impulsively applied forces internally, which has implications for attempts to deflect the NEO with impulsive forces; poor transmission of force internally throughout the NEO will result in adverse attenuation of the applied impulse, thus reducing the overall efficacy of the deflection attempt.

3.2.3 Volume

The volume of the NEO is simply the space contained within the boundaries of the NEO's surface, as per the usual definition of the volume of an object. Determining the exact volume of a NEO is difficult because most of them are shaped very irregularly. While some are excessively irregular in shape, having lobes or being "bone" shaped, most can be approximated as ellipsoids. If this approach is to be used to approximate the volume of a NEO, the equation for the volume of an ellipsoid is required, given by:

$$V_{ellipsoid} = \left(\frac{4}{3}\right)\pi\left(\frac{l}{2}\right)\left(\frac{w}{2}\right)\left(\frac{h}{2}\right) \tag{3.4}$$

where

$V_{ellipsoid}$ = volume of the ellipsoid

l = length dimension of the ellipsoid

w = width dimension of the ellipsoid

h = height dimension of the ellipsoid

The length, width, and height of the ellipsoid specified above correspond to the three axes of the ellipsoid. Estimates of these dimensions can be obtained from measurements taken by spacecraft sensors.

Another approach to computing the volume of a NEO, particularly a very irregularly shaped one, is to combine measurements of its dimensions with a surface map of the NEO generated by surface scans. With this data the volume may be approximately numerically by applying algorithms to the three-dimensional models generated for the NEO's shape.

3.2.3 Importance of Volume Determination

The primary importance of accurate NEO volume determination is its use in determining the mean density of the NEO for use in computing the required yield of a nuclear device for a given deflection. Additionally, physical measurements of the NEO's size and shape help determine the distance between a given point on its surface and its center of mass, which is an important quantity in the proper positioning of a nuclear device before detonation.

3.2.4 Density

The mean density of the NEO may be determined once the mass and volume are known by simply dividing the mass by the volume, as indicated in the following equation:

$$\rho_{NEO} = \frac{M_{NEO}}{V_{NEO}} \tag{3.5}$$

where

ρ_{NEO} = mean density of the NEO

M_{NEO} = mass of the NEO

V_{NEO} = volume of the NEO

It is important to note that this quantity is an average value for the entire NEO; the mass distribution and composition of the NEO may not be homogenous (in fact, this is quite likely). However, this average quantity is quite useful for mitigation calculations, and this will be detailed in subsequent sections.

3.2.5 Importance of Density Determination

As stated above, the mean density of a NEO is an important quantity in NEO mitigation application calculations. The mean density of the NEO, coupled with knowledge of the NEO's composition, gives a measure of how porous the NEO is and hence how well it will transmit impulsive force through its interior, which determines the efficacy of an applied impulse for the purposes of deflection.

For example, if a given NEO is known to be composed of a certain material and the volume of the NEO is known, then the expected density of the NEO can be computed since the density of the material of which it is composed is known. However, once the mass of the NEO is measured directly, the actual mean density of the NEO may be computed, and it may differ from the expected value considerably. For instance, if the sensed mean density is about half of the expected value, this indicates that, on average, the NEO has a porosity of 50%.

An actual example of this case occurred during the NEAR mission. While traveling to the asteroid Eros, which was the primary target of the mission, the

spacecraft encountered the asteroid Mathilde. Mathilde's mass was determined to be $\sim 1.0 \times 10^{20}$ g from the deflection experienced by the spacecraft, in a fashion similar to that described in section 3.2.1 above, and the best-fit ellipsoid dimensions were determined to be 66×48×46 km. Applying the methods of section 3.2.4 indicated that the measured mean density was about half of the expected value based on the asteroid's composition, indicating an average porosity of approximately 50% [9].

3.2.6 Determining Internal Structure and Composition

While the internal structure and composition of a given NEO are important factors in the selection of an appropriate mitigation system, they are difficult to ascertain. One option is to collide an impactor with the NEO and study the spectra of the ejecta plume, such as was done with the Deep Impact mission to comet Temple 1. Other options are to detonate small explosives either on the NEO's surface or within the NEO, after placing seismic sensors on the surface, in order to ascertain the internal structure from the NEO's response to shocks. However, the logistics of such science operations are complex. Another option that may be useful is dual-wavelength radar tomography, which has recently been refined for kilometer scale geologic masses. However, the mass of such equipment and its power requirements would have to be assessed prior to consideration for a spacecraft mission to a NEO.

There are also indirect methods for assessing a NEO's internal properties. For instance, the surface composition and mineralogy of the NEO can be determined from sensor scans of the surface, as was done during the NEAR mission to Eros. Assuming the composition does not change radically throughout its interior, this knowledge leads to an expected value for the NEO's density. The NEO's mean density may also be computed based on sensed mass and measured volume estimates. If this mean density is reasonably close to the density expected based on scans of the NEO's surface composition, then it is reasonable to assume that the NEO is solid and of mostly homogenous internal composition and structure. If the density values

differ, inferences may be made regarding the NEO's internal structure. For instance, if the mean density computed from the estimated mass and volume is lower than the density as determined from surface composition scans, the NEO may have a porous interior, as previously discussed.

3.2.7 Scientific Determination of Other Quantities

To determine other physical, elemental, and electromagnetic properties of a NEO, including elemental composition, mineral composition, magnetic field strength, and spin dynamics, other sensors and methods apart from those described above are required. Table 3.2 below lists some of the sensors used on the NEAR spacecraft to characterize the asteroid Eros, and these sensors are good choices for general NEO science missions.

Table 3.2: NEO Sensors and Their Characteristics

Sensor	Measurements	Range	Resolution	Power Usage	Mass
Multi-Spectral Imager (MSI)	Rotation rates, size, surface composition	35 km	3-5 m	6.92 W	7.7 kg
Near-Infrared Spectrograph (NIS)	Mineral composition	35 km	300 m	15.1 W	15.15 kg
X-Ray Gamma-Ray Spectrometer (XGRS)	Composition analysis (Mg, Al, Si, Ca, Ti, O, Fe, H, Radioactive elements)	35 km	5 m	24 W	26.9 kg
Magnetometer	Magnetic field strength	35 km	10 nT	1.5 W	1.5 kg
Laser Rangefinder	Range, surface maps	50 km MAX	Variable	16.5 – 20.7 W	5 kg

For a more thorough description of these devices and their capabilities, refer to appendix C.

3.3 NEO Proximity Operations

The environment in the immediate vicinity of a NEO presents some unique challenges to spacecraft operating in its proximity. Large NEOs, which have substantial gravity, will have a very irregular gravitational field, requiring a spacecraft operating in proximity to the NEO to be able to counteract the prominent non-spherical gravitational effects using a control system and sensors as it moves around the NEO. Very small NEOs will have extremely weak gravity, meaning that in order to execute maneuvers around the NEO in a timely fashion, or at all, a spacecraft will have to navigate around the NEO without relying on the NEO's gravity for a NEO-centered orbit of some kind. However, even a small NEO causes a substantial gravitational perturbation on a spacecraft at close range over time.
As previously mentioned, it is possible to enter captured orbits about very large NEOs, as was done in the NEAR mission to Eros. However, these large NEOs are quite few in number compared to the thousands of kilometer size and the millions of hundred-meter size NEAs. These smaller objects, which are quite capable of devastating Earth, are perhaps even more important to study because they are so numerous and hence the probability of an impact by one of them is higher than for a much larger NEA. Since their gravity is so low, entering captured orbits around them is not practical and other methods are therefore required.

While some researchers have developed models for the gravitational fields of elongated or otherwise non-spherical bodies, sometimes including the effects of non-uniform density, these models will not presented here. Special attention will be given to the case where the NEO's gravity is not relied upon for proximity operations maneuvers and is instead treated as a perturbation that the spacecraft's guidance, navigation, and control (GNC) system will have to sense and reject.

An excellent approach to proximity operations with respect to bodies of low gravity is to employ the linearized Clohessy-Wiltshire (CW) equations of relative motion[1]. These equations allow precise navigation relative to a target object, and the position and velocity vectors are conveniently coordinated in the Radial-Transverse-Normal (RTN) frame, whose origin is at the center of mass of the target. See appendix A for a complete treatment of the RTN frame. One drawback to using these equations is that they are linearizations and hence are not perfectly accurate. They are also derived for a target body that is in a circular orbit about the primary attractor. However, the linearization only deviates significantly from the true trajectory far away from the target, and most proximity operations will be taking place near the NEO, within the linear range. Additionally, the linearization breaks down over long time intervals. However, most NEO orbits are elliptical, and this will have to be accounted for.

The CW equations of relative motion are written with x, y, and z corresponding to the radial, transverse, and normal axes, respectively. They are given by [11]

$$\begin{aligned} \ddot{x} - 2n\dot{y} - 3n^2 x &= 0 \\ \ddot{y} + 2n\dot{x} &= 0 \\ \ddot{z} + n^2 z &= 0 \end{aligned} \tag{3.6}$$

where

$$n = \sqrt{\frac{\mu}{\|\vec{r}\|^3}}$$

[1] The CW equations are also referred to as Hill's equations in some texts. Hill developed these equations in 1878 and then Clohessy and Wiltshire rediscovered them independently in 1960.

with μ equal to the gravitational parameter of the primary attractor and $\vec{r}$ equal to the position vector of the target body in a circular orbit about the primary attractor. Thus n is simply the mean motion found in two-body orbital mechanics.

All maneuvers are assumed to be impulsive and hence thrust is not included. Making some approximations leads to the linearized equations of motion, given in the form of a partitioned state transition matrix as [11]

$$\begin{aligned}\vec{r}(t) &= \Phi_{rr}\vec{r}_0 + \Phi_{rv}\vec{v}_0 \\ \vec{v}(t) &= \Phi_{vr}\vec{r}_0 + \Phi_{vv}\vec{v}_0\end{aligned} \tag{3.7}$$

where

$$\begin{aligned}\Phi_{rr} &= \begin{bmatrix} 4-3\cos\omega & 0 & 0 \\ 6(\sin\omega-\omega) & 1 & 0 \\ 0 & 0 & \cos\omega \end{bmatrix} \\ \Phi_{rv} &= \begin{bmatrix} \frac{1}{n}\sin\omega & \frac{2}{n}(1-\cos\omega) & 0 \\ \frac{2}{n}(\cos\omega-1) & \frac{4}{n}\sin\omega-\frac{3}{n}\omega & 0 \\ 0 & 0 & \frac{1}{n}\sin\omega \end{bmatrix} \\ \Phi_{vr} &= \begin{bmatrix} 3n\sin\omega & 0 & 0 \\ 6n(\cos\omega-1) & 0 & 0 \\ 0 & 0 & -n\sin\omega \end{bmatrix} \\ \Phi_{vv} &= \begin{bmatrix} \cos\omega & 2\sin\omega & 0 \\ -2\sin\omega & -3+4\cos\omega & 0 \\ 0 & 0 & \cos\omega \end{bmatrix}\end{aligned} \tag{3.8}$$

$$\omega = nt \tag{3.9}$$

and

$$\vec{r}(t)=\begin{bmatrix} x(t) \\ y(t) \\ z(t) \end{bmatrix}, \vec{r}_0 = \begin{bmatrix} x_0 \\ y_0 \\ z_0 \end{bmatrix}$$
$$\vec{v}(t)=\begin{bmatrix} \dot{x}(t) \\ \dot{y}(t) \\ \dot{z}(t) \end{bmatrix}, \vec{v}_0 = \begin{bmatrix} \dot{x}_0 \\ \dot{y}_0 \\ \dot{z}_0 \end{bmatrix} \tag{3.10}$$

These equations provide the position and velocity of an impulsively maneuvering body relative to the target at any time. Equations (3.7) can also be solved using matrix inversion methods to compute the necessary impulsive velocity changes to send the maneuvering body to any desired position relative to the center of mass of the target body. In this fashion, relative navigation can be performed accurately.

The CW equations are derived assuming that the target object is in a circular orbit, meaning that the angular rate of the target object is constant along its orbit. However, this is not true for elliptical orbits, and asteroid orbits are elliptical rather than circular, which poses a problem. One solution is to make the assumption that the orbit rate is constant over short time intervals even though in truth it is changing slightly. This will naturally introduce some error, but it will be very small. The maneuvering spacecraft will already be fighting against a host of perturbations and will require a robust Guidance, Navigation, and Control (GNC) system in any case. Therefore the GNC system will be relied upon to correct for the slight errors that result from assuming the orbit rate is constant over short intervals. A “short” interval might be on the order of ten or several tens of days, which is a small fraction of the period of the average NEO orbit; the period typically ranges from slightly less than a year to two years. Thus, the estimate of the orbit rate can be periodically updated in the flight software to minimize the impact of the simplifying assumption of constant orbit rate.

These methods are extremely useful for performing controlled science maneuvers in the proximity of a NEO, as well as for positioning mitigation systems prior to activation, which will be discussed later. A sample NEO fly-around case has been constructed to demonstrate the nature of these methods. The sample trajectory involves a 500 kg spacecraft attempting to navigate around an ellipsoidal NEO with dimensions 110×120×130 m and mean density of 4.0 g/cm^3, yielding a mass for this NEO of approximately 3.594×10^9 kg. The NEO is assumed to be solid and homogeneous. The eccentricity of its heliocentric orbit is approximately 0.28. While the physical model for the NEO is ellipsoidal, a spherical gravity field is assumed.

The fly-around trajectory for this sample case is an octahedron with 4 vertices in the radial-transverse plane and 4 in the radial-normal plane. The spacecraft begins directly behind the NEO (relative to the general direction of orbital motion) at a center of mass to center of mass distance of 160 m, providing a nominal distance to the NEO's surface of 100 m. Thus the initial coordinates in the RTN frame are (0, -160, 0) m. The CW equations presented above have been incorporated into a targeting code that allows point-to-point navigation to be performed, computing the proper velocity vector at each vertex of the octahedron to take the spacecraft from vertex to vertex in sequence. The initial vertex is at the coordinates specified above and the next is at (160, 0, 0) m, placing the spacecraft on the radial axis. From there the spacecraft travels around the NEO in the radial-transverse plane and ends up where it started. From there it then travels around the NEO in the transverse-normal plane, with the next target vertex at (0, 0, 160) m. The NEO ends up back at the initial coordinates once more, completing the octahedral trajectory. The total time of flight for the trajectory was chosen to be 16 days and required a modest total Δv of 0.01494 m/s. A plot of this trajectory is shown in figure 3.3 below.

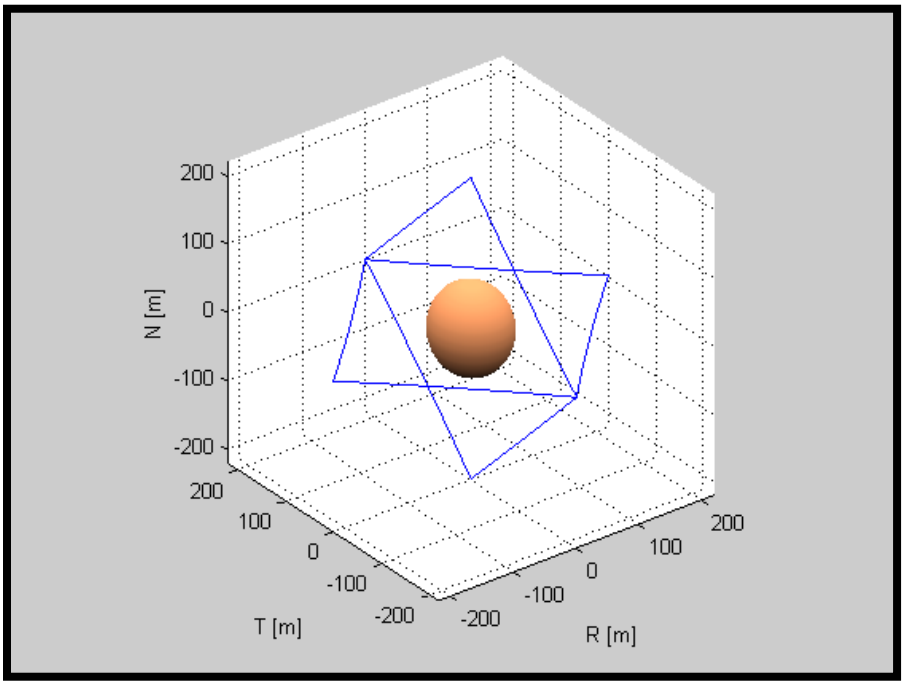

Figure 3.3: Octahedral Fly-Around of NEO with CW Targeting

The octahedron is used as a prototype trajectory because it is simple to construct, illustrative of the process, and provides the spacecraft with a view of the entire NEO surface. The choice of a nominal surface distance of 100 m was arbitrary; in practice there is a preferred nominal surface distance based on the size of the NEO and the resolution of the spacecraft's sensors. A set of trajectories that better approximate circular orbits around the NEO may be constructed by adding more and more vertices, until the fly-around trajectories are rounded as desired.

However, realizing these trajectories in practice requires active spacecraft control. Firstly, the CW equations of motion are only linearizations, and secondly, the mass of the NEO is a strong perturbation on the spacecraft's motion at such close ranges. Moreover, there is the issue of the CW equations being further skewed when the NEO's orbit is non-circular and the mean motion is hence not constant, requiring periodic updates to the flight software. On top of all that, there are other perturbations, such as N-body "perturbations" from the planets and solar radiation

pressure, acting on the spacecraft. The sum of these disturbances is capable of causing severe deviations in the spacecraft's trajectory that require some degree of active control and guidance to adequately overcome. This was investigated by transforming the velocity change vector for each maneuver, $\Delta\vec{v}$, into the Heliocentric Inertial (HCI) frame and applying them to the spacecraft in an N body simulator. The bodies included were the Sun, Earth, NEO, and spacecraft. The spacecraft was started on the same orbit as the NEO by matching the HCI position and velocity of the spacecraft to the NEO. Then an offset was added to the spacecraft's position vector to position it at the initial RTN coordinates specified above. The $\Delta\vec{v}$ for each maneuver was rotated from the RTN frame to the HCI frame according to the procedures in appendix A. Then each segment of the octahedral trajectory was simulated by applying each $\Delta\vec{v}$ at the prescribed time. After simulation the spacecraft trajectories were rotated back into the RTN frame so they could be plotted with the CW trajectories for comparison. The initial results showed that the numerically integrated trajectory was heavily skewed in chaotic ways from the desired trajectory at the given initial separation distance. In fact, the spacecraft passes through the NEO surface (collision physics are not modeled) and is then ejected from the region of space near the NEO. A plot of the trajectories is shown in figure 3.4 below.

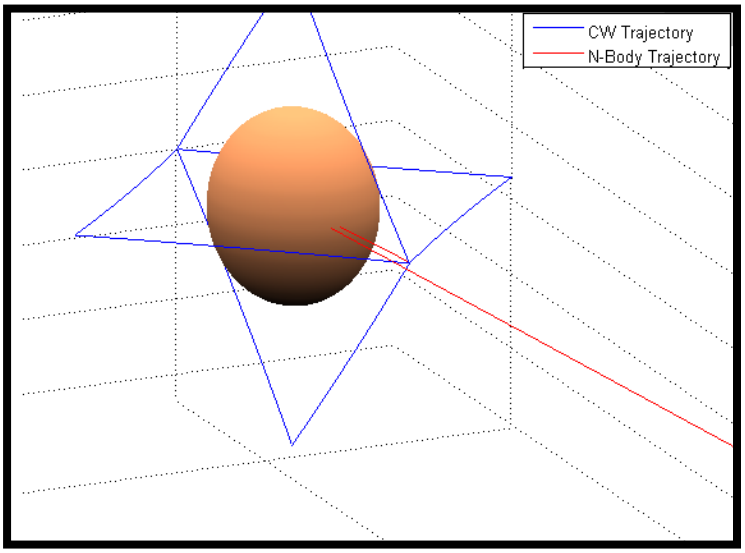

Figure 3.4: Spacecraft Ejected from NEO Proximity at Initial Range of 160 m

The initial idea was that the perturbation from the NEO's gravity was too strong at such a close range. Indeed, it was discovered that the numerically integrated trajectory began to more closely approximate the CW trajectory as the separation distance was increased. The distance was increased until the parity between the trajectories ceased to noticeably improve. A plot of the resulting trajectories, at an initial distance from the NEO of 5.5 km, is shown in figure 3.5 below.

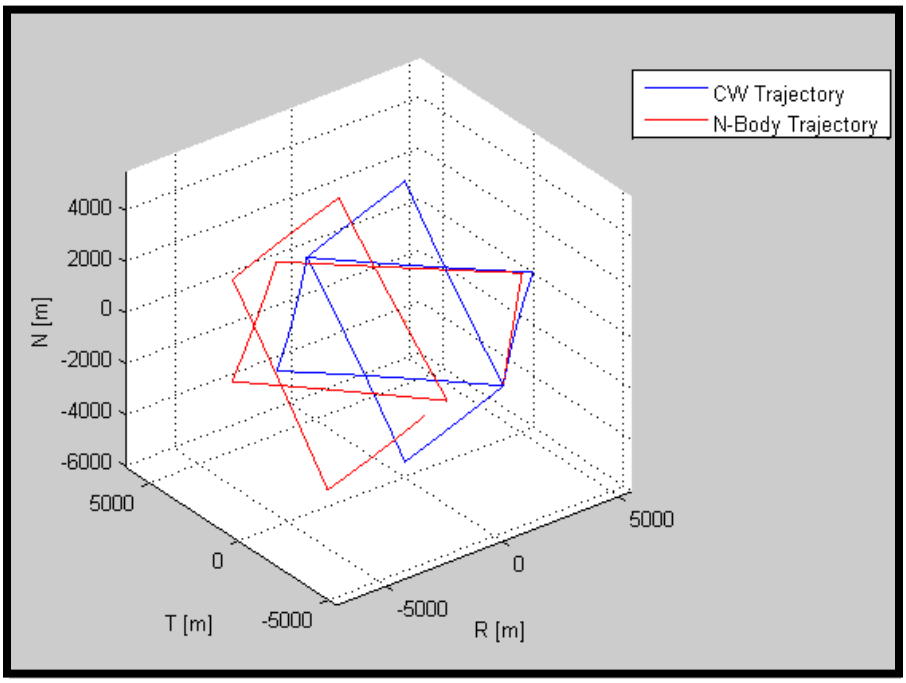

Figure 3.5: Spacecraft Trajectories at Initial Range of 5.5 km

The total flight time was kept at 16 days and the new total Δv increased by an order of magnitude, yielding a value of 0.5137 m/s. Next, it was considered that the flight time might also play a role in the deviation of the numerically integrated trajectory since the gravitational perturbations from the NEO are cumulative over time. Thus, it was reasoned that if the flight time was dramatically decreased, the trajectories should then match up reasonably well even at close range. This turned out to indeed be the case. Figure 3.6 below shows the trajectories for a total flight time of 2.22 hours at the initial separation distance of 160 m.

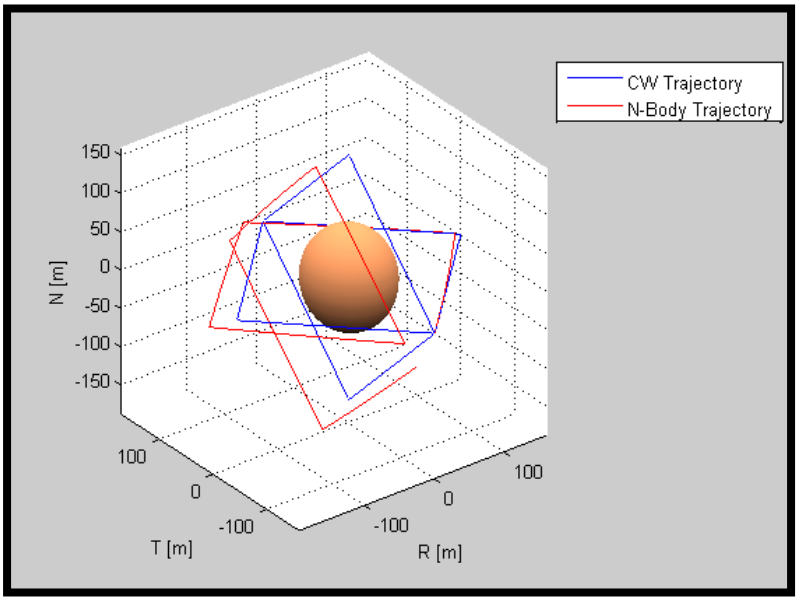

Figure 3.6: Spacecraft Trajectories at Initial Range of 160 m with 2.22 hour Flight Time

As expected, the total Δv increased by two orders of magnitude with respect to the original 160 m, 16 day case, yielding a value of 2.5384 m/s.

There are obviously trade-offs to be made in terms of flight time and nominal range from the NEO. For close range and short flight times the required Δv is relatively high and the required GNC input is reduced somewhat. Conversely, for close range and long flight times, the total Δv prescribed by the CW equations is greatly reduced but much more GNC input is obviously required. The investigation of these considerations and the design of GNC systems to accomplish given fly-around trajectories in proximity to NEOs for the purposes of science missions is an excellent avenue for further research.

3.3.1 Constraints and Requirements

Finally, a general description of the constraints and requirements for a spacecraft conducting proximity operations around a NEO is outlined below. A

spacecraft operating in the vicinity of NEO must be able to accurately navigate relative to the NEO in the presence of the following perturbations and error sources:

- General on-orbit perturbations such as solar radiation pressure, the Yarkovsky effect (uneven thermal reradiation), N body perturbations from planets, and, occasionally, collisions with small pieces of debris;
- Gravitational perturbation by the NEO itself;
- Accuracy limits of sensors;
- Measurement noise;
- Net uncertainties in position and velocity relative to the NEO.

The following are the general requirements that apply to spacecraft performing science and/or mitigation operations around a NEO:

- The spacecraft must not collide with the NEO except in the special cases where this is desired and planned accordingly[1];
- The spacecraft must not lose control and fly away from the NEO in an unplanned, uncontrolled fashion;
- The spacecraft must be able to maintain its position, velocity, and trajectory relative to the NEO within the tolerances required for scientific data collection and/or mitigation system positioning.

These generalized constraints and requirements will be quantified depending on the specific physical parameters involved in a given NEO mission.

[1] This has actually happened. The NEAR spacecraft mission culminated with a soft crash landing of the spacecraft on the surface of the asteroid Eros. Furthermore, some schemes to collect samples of NEO material require the spacecraft to make a series of controlled minor collisions with the NEO.

4. NEO IMPACT HAZARDS AND COLLISION MECHANICS

4.1 Introduction

The previous chapters have provided background on the characteristics of NEOs, the characteristics of the general NEO population, and how NEOs are studied scientifically. The next step is to quantify the threat a given NEO may pose if it impacts Earth. Some of the broader effects were discussed in the introduction to this work, such as tsunamis, earthquakes, massive shockwaves and craters, induced volcanic activity, contamination of the atmosphere, and blockage of sunlight for an extended period of time. The severity and duration of the effects ranges from localized damage to global catastrophe and is a function of the energy delivered by the NEO due to its mass and impact velocity.

This section will survey the way that the threat posed by a given NEO is quantified and expressed, as well as the evidence in the geological record for past impacts and their consequences. The fact that impacts are known to have occurred in the past means they will occur in the future; the NEO population still exists and is ever-evolving. In point of fact, meteor impacts are continuously reported up to the present day. Such small objects are only capable of killing a single person or destroying a car or the roof of a house. Their larger counterparts are far less gentle, as previously discussed.

4.2 The Torino Scale and Palermo Technical Scale

Scales for rating the level of threat posed by a given asteroid or comet exist for the purposes of communicating the impact hazard level to the general public as well as to other members of the scientific and engineering community. By design, the scale best used for communicating with the general public is the Torino Scale, and the best scale for technical communication is called the Palermo Technical Scale. The goal of both scales is to cross-reference the two primary quantities that determine the level of threat posed by a given NEO: probability of Earth impact and energy released

upon impact should it occur. A diagram of the Torino Scale is shown in figure 4.1 below [2].

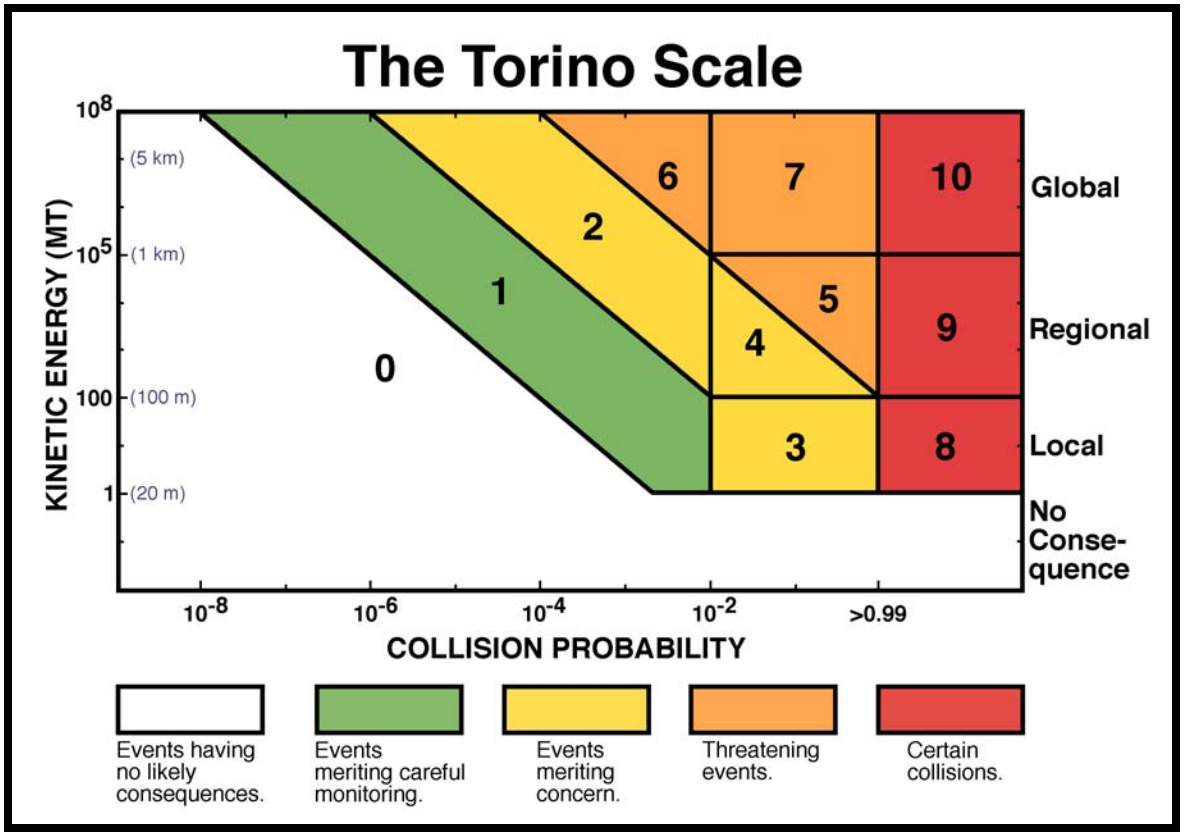

Figure 4.1: The Torino NEO Hazard Threat Index Scale

Probability values are indicated according to the general convention for probabilities, which is that events with zero probability of occurring are assigned the value 0 and events that are certain to occur are assigned the value 1.

Impact energy is generally expressed in megatons (Mt) and is equal to the kinetic energy of the asteroid at the time of Earth impact, given by:

$$E_{IMPACT} = \frac{1}{2} M_{NEO} \left\| \vec{v}_{IMPACT} \right\|^2 \tag{4.1}$$

where

E_{IMPACT} = impact energy

M_{NEO} = mass of the NEO

$\vec{v}_{IMPACT}$ = velocity vector of the NEO with respect to the Earth at impact

If the mass of the NEO is measured in units of kg and the velocity is measured in units of m/s, then the units for the impact energy are Joules (J). To convert J to Mt, it is necessary to divide by the conversion factor of 4.2×10^{15} J/Mt.

This scale is easier for the general public to understand as it uses simple integer values ranging from 0 to 10. However, the collapsing of multiple dimensions into a single parameter causes an inevitable loss of technical information, making this scale less useful for the professional NEO community. It is for this reason that the Palermo Technical Scale was developed.

The development of the Palermo Scale began with the definition of a normalized probability parameter developed by Binzel, expressed as [2]

$$M = \frac{P_i}{P_B \Delta T} \tag{4.2}$$

where

P_i = probability of impact

P_B = annual background probability for an object of the same kinetic energy

ΔT = time in years before impact

The Palermo Scale was later defined by Chesley, *et al.* in the year 2002 after extensive consideration. The final definition is given by

$$P = \log_{10}(M) \tag{4.3}$$

The Palermo Technical Scale is the primary communication tool within the professional NEO community [2].

As mentioned previously, the destructive force of a NEO impact is measured by its kinetic energy at the time of Earth impact, given above by equation (4.1). For reference, typical impact velocities for asteroids range from 10 – 20 km/s while impact velocities for comets may reach 40 km/s [12]. Assuming a spherical shape and a mean density of 2.65 g/cm^3 for the NEO material (conservative approximations), the impact energies for a range of NEOs has been computed to give an idea of their destructive potential. Figure 4.2 below shows the impact energy surface for a spectrum of NEOs ranging from 60m to 6 km in mean diameter and ranging from 10 to 40 km/s in impact velocity.

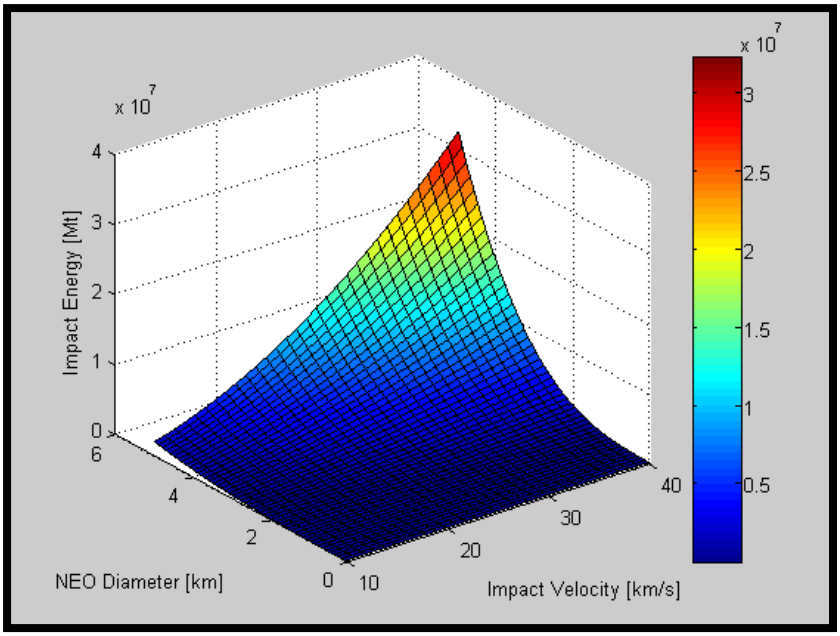

Figure 4.2: NEO Impact Energy as a Function of Mean Diameter and Impact Velocity Ranging from 60 m to 6 km and 10 to 40 km/s, Respectively

The comets deliver the highest impact energies in the spectrum of figure 4.2, approaching $3-4\times10^{7}$ Mt. These are globally devastating values. Figure 4.3 below restricts the spectrum to the most typical asteroid impact velocities, ranging from 10 to 15 km/s.

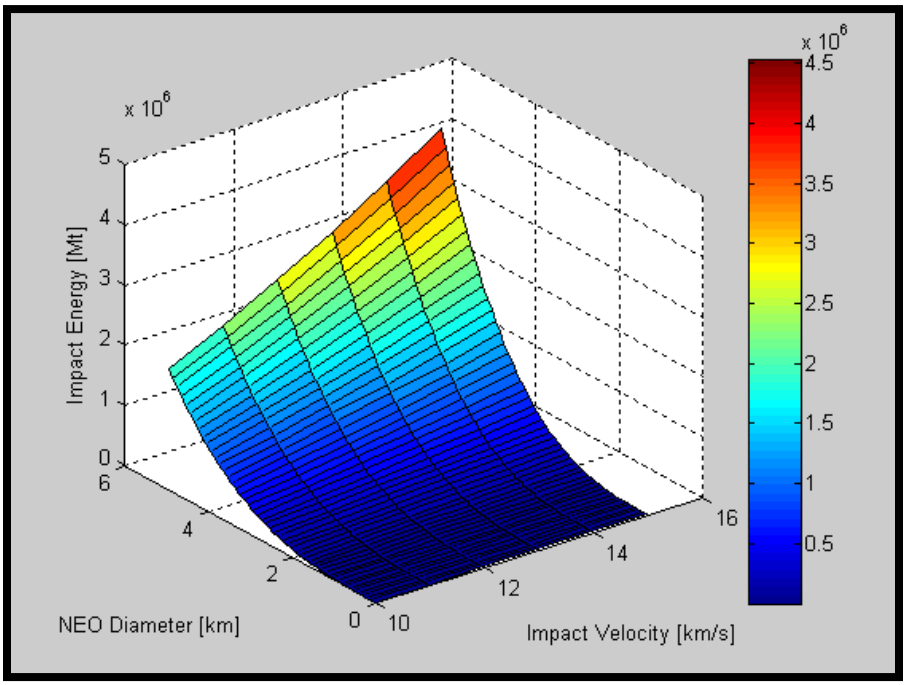

Figure 4.3: NEO Impact Energy as a Function of Mean Diameter and Impact Velocity Ranging from 60 m to 6 km and 10 to 15 km/s, Respectively

In figure 4.3, the maximum impact energy is $3-4\times10^{6}$ Mt, though most impact energies are in the $0.5-1\times10^{6}$ Mt range, which is at the estimated threshold for global catastrophe. For reference, the smallest NEO of 60 m mean diameter still tends to deliver ~100 Mt upon impact, which is almost twice as large as the largest nuclear device ever tested by humanity. Such an impact in an ocean near a coast would cause destructive tsunamis and an impact on land in a populated area would yield horrific casualties; the Tunguska impact of 1908 is though to have involved a 60 m asteroid and 2000 km^2 were devastated, fortunately in an unpopulated region.

Finally, to focus in on the impact energy spectrum for the most common classes of NEOs, figure 4.4 is presented below.

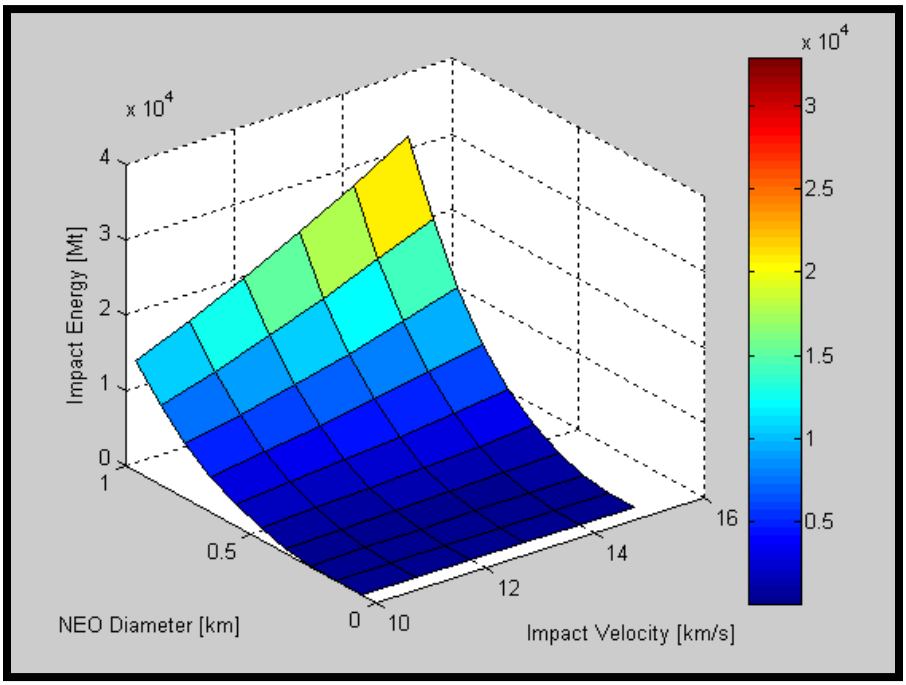

Figure 4.4: NEO Impact Energy as a Function of Mean Diameter and Impact Velocity Ranging from 60 m to 1 km and 10 to 15 km/s, Respectively

In figure 4.4, the impact energy spectrum is constrained to asteroids ranging from 60 m to 1 km. The upper impact energy is approximately 2×10^4 Mt, placing the 1 km class of impactor at the cusp for global devastation. These impact energy results are all biased downwards slightly from the representative values in the Torino Scale, likely because of the conservative mean density estimate used in the calculations herein.

4.3 Earth's Collision History

It is a somewhat little known fact that the Earth has a rather rich NEO collision history. People today regularly see "shooting stars" when looking at the night sky and even the occasional fireball, which is a particularly bright meteor. It is

important to understand the nomenclature here: objects outside of Earth's atmosphere are dubbed asteroids or comets as appropriate, objects that enter Earth's atmosphere are called meteors, and a meteor that survives atmospheric passage and impacts the surface is typically called a meteorite. In addition to spurious meteors and the occasionally fireball, there are of course the annual meteor showers, such as the Leonids or Perseids, which are the result of Earth's passage through debris left behind in comet tails.

The modern day experience with NEOs for the average person does not extend beyond these very tiny objects, which dissipate all their energy when they ablate into oblivion as they speed through the atmosphere due to the intense pressure that heats them during the fastest portion of the their atmospheric entry. A common misconception is that meteors burn up due to atmospheric friction. The results of the impacts of such small meteors, most of which are only a few kilograms after impact, are generally anticlimactic; they may create a small crater if they hit land and are generally readily found sometime later by an enterprising individual sporting a metal detector. This author knows of one man who makes his living hunting for meteorites and selling them; meteorite material is rather valuable, both to scientists and museums and to private collectors and jewelry makers.

Perhaps the most infamous and certainly the most catastrophic known impact event was that which caused the Cretaceous/Tertiary (K/T) boundary extinction approximately 65 million years ago. The crater left behind from the impact is near the Yucatan peninsula and is estimated to be 180 km in diameter. It is the legacy of a massive NEO that struck there approximately 65 million years ago, devastating the biosphere. It is estimated that sunlight was blocked out for months or years and the tremendous energy released is sure to have caused dramatic shockwaves and earthquakes. Evidence has also been discovered recently indicating massive lava flows over the surfaces of landmasses during extinction periods, raising the possibility that NEO impacts led to increased volcanic activity and allowed lava to

reach the surface in copious quantities. Relatively few species survived; the dinosaurs were made completely extinct.

The fact that it was a NEO impact that caused the K/T boundary extinction was debated heatedly until the early 1980s when the crater was found. Even then skeptics were unconvinced, until the strata in the geological record for the K/T boundary extinction era was dug up and examined. It was found that this strata contained high amounts of iridium, which is not found in any sort of abundance on Earth, though it is common in NEOs. Furthermore, this iridium signature was present in the strata all over the world, consistent with a massive collision event that spread debris all throughout the atmosphere.

More recent research into the periodicity of mass extinctions as indicated by evidence in the fossil record shows a strong periodicity of about 62 ± 3 million years [13], leading to the chilling conclusion that the next mass extinction may occur soon since the previous one happened about 65 million years ago. If massive NEOs are indeed striking Earth at such regular intervals, it begs the question of why and how. Specifically, the origin of these massive NEOs needs to be understood. One theory examined was that the Sun has a dark companion star that is in 65 million year orbit and that whenever this "Nemesis" star passes near the solar system, it dislodges objects from the Oort cloud and sends them raining into the inner solar system where one or more have a good chance of striking Earth. However, studies have shown that orbits for this "Nemesis" star are not stable in the presence of perturbations by other passing stars. Furthermore, the Nemesis star has never been found and no direct evidence for it exists [13]. However, new things are being discovered all the time; as of the time of this writing, Pluto was discovered to have two more moons than previously thought, for a total of three. The dynamical origins of these moons are currently baffling researchers.

There are a variety of small NEO impacts recorded over the past several thousand years of human history, dating from 1420 BCE up to the present day. In

1998 a meteorite struck the ground 1 meter away from a man playing golf [1]. More serious recorded impacts have resulted in death when the meteor struck a human, or destruction when the meteor struck a building or a vehicle [1]. Appendix D contains an extensive table that details these numerous recorded events, clearly illustrating that NEO collision is not some remote possibility that isn't worth paying serious attention to. Rather, it is yet another part of life on Earth.

4.4 NEO-Earth Collision Mechanics

The strict definition of a collision is the attempt of any portion of two bodies composed of matter to occupy the same spatial coordinates at the same time coordinates, all in the same space-time reference frame. If the spatial coordinates of any given points on the two bodies, designated body 1 and body 2, are given by *x, y,* and *z* and the time coordinates are given by *t* then the mathematical condition that a collision attempts to satisfy is:

$$\begin{bmatrix} x \\ y \\ z \\ t \end{bmatrix}_1 = \begin{bmatrix} x \\ y \\ z \\ t \end{bmatrix}_2 \tag{4.4}$$

Because these bodies have mass, a collision event will release energy, equal to the kinetic energy at the time of impact, and will result in the change of the momenta of the objects. In the case where one object is of significantly greater mass than the other, i.e., $m_1 << m_2$, the less massive object will generally be either utterly destroyed or will accrete with the larger mass. Note that plastic, rather than elastic, collisions are assumed due to the high energies and the planetary materials involved.

Additionally, if the magnitude of the relative velocity at the moment of impact is exceedingly high, the larger body will likely exhibit a crater at the site of impact and considerable ejecta will be dispersed. If the larger body is not exceedingly larger

than the smaller body, then the larger body may fracture internally or spall off fragments that are a significant portion of its size prior to impact. The former case is relevant to a NEO-Earth collision while the latter is pertinent to the case of NEO mitigation methods that attempt to deflect the NEO by colliding a high-velocity kinetic impactor with it.

In fact, the recent spacecraft mission to comet Tempel 1 delivered just such a kinetic impactor to the comet. In this case, the collision was more akin to a NEO colliding with Earth in that the impactor was not large enough to fracture or fragment the comet and instead formed a modest impact crater on the comet's surface.

4.4.1 Collision Geometry

The relative geometry between the NEO and the Earth in the Heliocentric Inertial (HCI) reference frame is shown in figure 4.5 below.

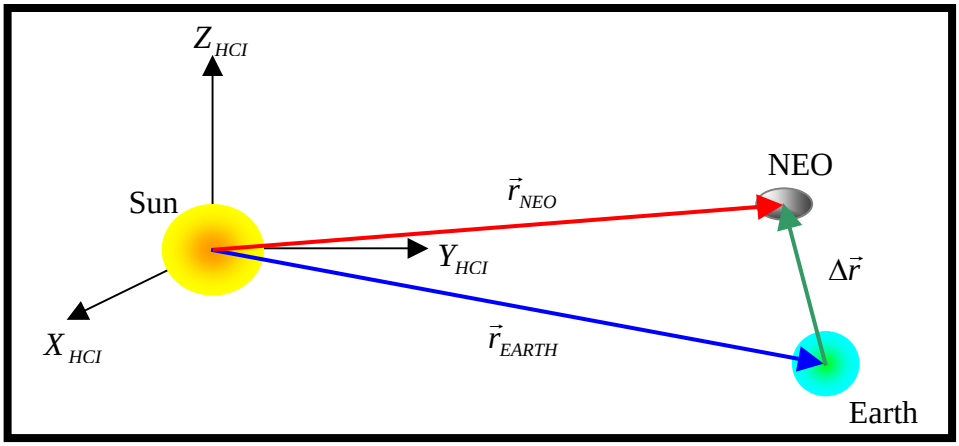

Figure 4.5: NEO-Earth Relative Geometry

where

$\vec{r}_{NEO}$ = HCI position vector of the NEO

$\vec{r}_{EARTH}$ = HCI position vector of the Earth

$\Delta\vec{r}$ = HCI position vector of the NEO relative to the Earth

The relative position vector between the NEO and the Earth at any time is given by equation (4.5) below.

$$\Delta\vec{r} = \vec{r}_{NEO} - \vec{r}_{EARTH} \tag{4.5}$$

Thus, the distance between the NEO and the Earth, as a function of time is

$$\Delta r(t) = \left\|\Delta\vec{r}(t)\right\| \tag{4.6}$$

Each of the vector quantities defined above is a function of time, and all vectors are computed for the same time indices by definition and are thus implicitly time-synchronous. Therefore, the mathematical condition for a NEO-Earth collision is given by

$$\Delta r(t_{coll}) \leq R_{EARTH} \tag{4.7}$$

where

t_{coll} = the time of collision.

R_{EARTH} = the equatorial radius of the Earth[1]

4.4.2 Minimum Orbital Intersection Distance (MOID)

Both the NEO and Earth travel on elliptical orbits about the Sun, though the Earth's orbit is nearly circular. Since the paths of both bodies are relatively fixed in

[1] Since the Earth is actually an oblate spheroid, rather than a perfect sphere, it has polar and equatorial radii, which are approximately 6356.7 km and 6378.1 km, respectively. For the purposes of defining a collision envelope around the Earth, the larger of the radii, this being the equatorial radius, is used to define a spherical collision envelope around the Earth that contains the entire oblate Earth.

space, neglecting the minor orbital perturbations they experience due to the space environment and gravitational attraction from other solar system bodies, which are very small, there are specific conditions which a NEO's orbit must satisfy if it is to be a candidate for collision with Earth at some point in time. These conditions lead to the definition of the Minimum Orbital Intersection Distance (MOID).

4.4.3 MOID Geometry and Definition

The majority of NEO orbits are inclined with respect to the XY plane of the Heliocentric Inertial frame, while Earth's orbit is virtually contained in this plane[2]. Since we have established that to collide two bodies must attempt to inhabit the same point in space at the same time, a NEO with non-zero orbital inclination must intersect the ecliptic plane when the Earth is at that exact point of intersection in order to collide with Earth. The distance of this point from the Sun must be at almost precisely the distance of Earth from the Sun at that point along the Earth's orbit. The fact that satisfying these conditions is exceedingly difficult comes as no surprise when considering the massive volume of interplanetary space and the relatively tiny size of NEOs and planets. Thus it is also no surprise that impacts by massive NEOs are quite infrequent. For the case of a NEO with a zero inclination orbit, its orbital trajectory would have to intersect the Earth's orbital trajectory and the NEO would have to arrive at an intersection point at the exact same time as the Earth in order for a collision to occur. However, the majority of asteroid orbits have non-zero inclination and therefore the geometry of an inclined NEO orbit will be considered in more detail.

Considering an inclined NEO orbit, the MOID is defined as the distance between the point where the NEO intersects the ecliptic plane and the nearest point on the Earth's orbit. This quantity is illustrated in figure 4.6 below.

[2] The plane of the ecliptic, which is the XY plane of the heliocentric inertial (HCI) frame, contains the *mean* orbit of the Earth by definition.

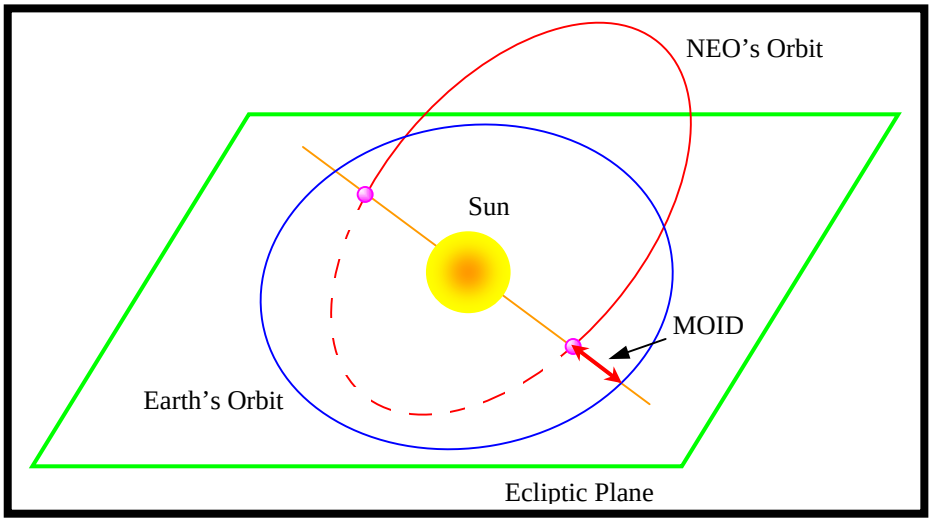

Figure 4.6: Minimum Orbital Intersection Distance

The MOID is used to divide the NEO population into those objects that are potentially hazardous objects (PHOs) and those that are not. In the case of NEAs, these are termed PHAs. PHAs are NEAs greater than 150 m in mean diameter with a MOID $\leq$ 0.05 AU. Currently, 586 such objects are known [14].

Thus it is clear that the potential for given a NEO to collide with Earth depends heavily on the shape of the NEO's orbit. It follows then that impacting NEOs will tend to have ranges of values for their orbital elements, and this was found to be true in the study by Chesley, *et al*, the results from which were presented previously in section 2.5. A complete explanation of Keplerian orbital elements is presented in appendix A.

The above results and geometrical considerations define the nature of NEO-Earth impact geometry and serve as a basis for evaluating the potential threat posed by a given NEO. However, the determining factor is simulation of the NEO's orbit with increasing accuracy, until the error associated with the propagation is sufficiently reduced such that the uncertainty regarding whether an impact with Earth

will occur is eliminated. While most NEOs can be determined to not be threats based on ground observations, some NEOs pass so close to Earth that eliminating them as threats can only be accomplished with more accurate knowledge of their orbit. Such accurate orbit determination is achieved by placing a radio transponder beacon on the NEO, followed by rigorous computer simulation of the telemetry. However, the identification of a threatening NEO and the determination that its potential threat level warrants the placement of such a beacon in the first place is predicated on the type of analysis discussed above. Note that radio transponder beacons can provide position accuracies on the order of ~100 m and velocity accuracies on the order of ~1 mm/s, leading to precise orbit determination [15].

Now that the geometry and definitions that describe a NEO-Earth collision have been established, the discussion will be completed with an examination of the contributions from orbital dynamics.

4.4.4 Orbital Dynamics Considerations

When considering how low the MOID must be for the probability of a collision to be high, it is necessary to consider the Earth's capture cross-section, which is given by [7]

$$C_C = \frac{R_{EARTH} v_{IMPACT}}{v_\infty} \tag{4.8}$$

where

C_C = capture cross-section

v_{IMPACT} = NEO impact velocity at Earth's surface

v_∞ = hyperbolic excess velocity

The capture cross-section forms a toroid around the Earth's orbit, and a potentially hazardous NEO will have an MOID that lies within this toroid. However, to truly be

a danger, the NEO must also enter this toroid at such a time that the Earth is in the same vicinity, i.e., the distance between the Earth and the NEO is less than or equal to the Earth's capture cross-section.

Mathematically speaking, the impact velocity is given by the magnitude of the difference between the NEO's and Earth's heliocentric velocity vectors at the time of collision, t_{coll}, which can be derived by taking the first derivative with respect to time of equation (4.6) above.

$$v_{IMPACT} = \left\| \Delta \dot{\vec{r}}(t_{coll}) = \dot{\vec{r}}_{NEO}(t_{coll}) - \dot{\vec{r}}_{EARTH}(t_{coll}) \right\| = \left\| \vec{v}_{EARTH}(t_{coll}) - \vec{v}_{NEO}(t_{coll}) \right\| \qquad (4.9)$$

where

$\vec{v}_{EARTH}(t_{coll})$ = The Earth's heliocentric velocity vector at the time of impact

$\vec{v}_{NEO}(t_{coll})$ = The NEO's heliocentric velocity vector at the time of impact

Note that this is also the basis for computing the kinetic energy released in a NEO-Earth collision as specified in equation (4.1) above. It is also nearly equal to the hyperbolic excess velocity, V_{∞}, since the asteroid has a much weaker gravitational field than that of the Earth.

4.4.5 Keyholes and Resonant Returns

Considering the application of orbital dynamics to the collision conditions as described above led to the development of the concept of Minimum Orbital Intersection Distance (MOID) and the Earth's capture cross-section. This further leads to the concepts of keyholes and resonant returns.

A keyhole is a region in three-dimensional space near the Earth defined such that if a NEO were to pass through this volume of space, it would return to collide with Earth some time in the future due to the system dynamics. The return of the

NEO to collide with Earth at a later time is termed a resonant return. It is therefore undesirable for a NEO to pass through a keyhole and be placed upon a resonant return trajectory. Thus, any attempt to deflect a NEO should be constructed such that the NEO is not inadvertently directed through a keyhole if possible. Additionally, if it is determined that an incoming NEO will miss Earth by a narrow margin, it should also be determined that the NEO will not pass through a keyhole; if it is determined that a NEO will pass through or near a keyhole, the NEO should be deflected such that it misses not only Earth, but also the keyhole by a safe margin.

5. THREATENING NEO MITIGATION METHODS

Who knows whether, when a comet shall approach this globe to destroy it, as it often has been and will be destroyed, men will tear rocks from their foundations by means of steam, and hurl mountains, as the giants are said to have done, against the flaming mass? – and then we shall have traditions of Titans again, and of wars with Heaven.
(Medwin's Conversations of Lord Byron, 1824)

5.1 Introduction

As previously discussed, Near Earth Objects (NEOs) have devastated Earth in the past and will strike Earth again in the future, at any time. It follows that humanity would choose to mitigate the threat posed by an incoming NEO should one be discovered. This involves sending a spacecraft to the threatening NEO with the means to take action that will avert the impending collision of the NEO with Earth.

Accomplishing the mitigation, either through deflection or destruction of the NEO, requires a mitigation method and corresponding system for effecting the mitigation. In fact, the design of both the mitigation spacecraft and the corresponding spacecraft mission are directly driven by the choice of mitigation system.

The scientific and engineering communities have proposed a variety of possible NEO mitigation methodologies and effectors, ranging from those that are possible with current technology to those that will never be practical, absent unforeseen leaps in humanity's knowledge of physics. Selected mitigation systems are described and assessed in the following section, with a special focus on standoff nuclear detonation techniques for NEO deflection.

5.2 Mitigation Modes

There are three possible mitigation modes: annihilation, fragmentation, and deflection. These modes are explained and discussed below.

5.2.1 Annihilation

The annihilation of an entire NEO refers to its reduction to a gas or fine-grain dust cloud via energetic vaporization or pulverization, respectively. This method of NEO mitigation would deliver the highest degree of certainty that the danger of catastrophic impact had indeed been averted. However, the energy requirements are prohibitive given current and near-future technologies. Tentative figures for the energy required to vaporize 40m mean diameter NEOs is approximately 1500 TJ [16], which would require a 3.6 Mt nuclear device with 10% neutron energy yield. This energy requirement increases exponentially with NEO size, so vaporizing NEOs several hundred meters or several kilometers in size is out of the question. Pulverizing a NEO requires one or more high kinetic energy impacts, i.e., by massive spacecraft traveling at ultra-high velocities. Other techniques for utterly destroying a threat NEO include some technologies that may be feasible only in the distant future, including antimatter devices to literally annihilate the NEO matter or mechanical, biological, or chemical "eaters" that could consume the threat NEO until only gas or dust particles remained. These techniques are far beyond the reach of current and foreseeable technology and are hence eliminated from consideration.

5.2.2 Fragmentation

While it is clear that total annihilation of the threat NEO is not feasible now or in the near future, fragmentation of a threat NEO may be more tractable. Fragmentation refers to the sudden or gradual reduction of a NEO body into a collection of smaller chunks. In order for these chunks to all burn up in Earth's atmosphere, if the bulk of them were to remain on a collision course subsequent to the mitigation, each must be 30 – 50 m in mean diameter or less [17].

Fragmentation, like annihilation, generally requires the sudden delivery of a certain amount of energy to NEO. The result is that the NEO is shattered, reducing it to a strengthless body that may then be dispersed. It is also possible to supply enough

energy all at once to both disrupt the NEO and disperse it, sending the fragments out in different directions. As stated, these fragments must all be less than ~ 40 m in mean diameter or must all be perturbed off of an Earth-impacting trajectory. It is not possible to achieve these outcomes in controlled manner, making deliberate fragmentation of a threatening NEO a risky proposition.

The estimated energy required to shatter a NEO is only 100 J/kg of NEO material [12], and most nuclear bursts near a NEO will impart at least that much energy during even a deflection attempt, meaning that shattering a NEO when attempting to deflect it with a nuclear burst is usually unavoidable anyway. The threshold for dispersion of the NEO fragments is estimated to be 1000 J/kg or more [12], and this is still within the range of nuclear device capabilities. However, as previously stated, the outcome of dispersion is uncontrollable and therefore this mode of mitigation is not advisable unless multiple nuclear devices are used in a tested configuration that provides high assurance that all fragments are less than ~ 40 m in size or that all the fragments will miss Earth.

Aside from nuclear device detonations, other more exotic methods of fragmentation have been proposed, such as positioning a spacecraft near the NEO that then fires several salvos of tungsten bullets connected by wires in a grid configuration to literally cut the NEO into pieces. These methods are beyond the reach of current technology.

Finally, the dispersion of a shattered NEO is further complicated in the case of large NEOs because self-gravity tends to retard the dispersion, which can be advantageous depending on the mission goals.

5.2.3 Deflection

The deflection of a threatening NEO amounts to perturbing its orbit through an applied force and is the most controllable mitigation mode, thus providing the most reliable outcomes. Additionally, due to their more tractable energy

requirements, most deflection techniques are within range of current and near-term technology. However, some of them require logistics that are too complex to be considered in missions where failure is truly not an option.

5.3 Types of Deflection Techniques

NEO deflection techniques fall into two main categories, these being impulsive and gradual. Each type of technique has specific applications. The governing philosophy is that gradual techniques are preferred when all of the following conditions are met:

- Adequate warning time, generally on the order of a decade or more;
- Technical and technological feasibility;
- The target NEO is not structurally coherent enough to efficiently transfer the force of an impulsive deflection maneuver but can be accelerated effectively by low thrust;
- Reasonable assurance of efficacy, as indicated by design, simulation, and, hopefully, experimentation;
- The NEO is structurally coherent enough to accommodate the mounting of thrusters.

Applying a gradual deflection technique to a given NEO is generally complicated by the following factors:

- The NEO's spin state;
- Autonomous anchoring of the required equipment to the NEO's surface;
- Controllability.

The science of NEO deflection poses a problem in which the target of interest, this being the threatening NEO, possesses tremendous translational and rotational inertia. This makes it exceedingly difficult to de-spin an NEO or even reorient its spin axis. Furthermore, the task of applying a translational deflection to the NEO's motion involves a very tiny margin for error; great amounts of energy and/or time must be expended simply to achieve tiny changes in the NEO's velocity vector. This creates a situation where the optimal deflection maneuver may be the only effective deflection maneuver given constraints on time, technology, and energy-generation resources.

Thus, both the issues of controllability of the gradual deflection maneuver and the issue of the NEO's spin state are crucial. There is, in general, an optimal direction along which the thrust vector of the gradual deflection being applied to the NEO must point and this direction will likely be time-varying. Therefore, unless the NEO's spin axis remains aligned with this optimal thrusting direction (extraordinarily unlikely) or the NEO can be de-spun, which is nearly impossible given a NEO's high mass and hence tremendous rotational inertia, the amount of time required to achieve the necessary direction may be magnified so much as to negate the efficacy of the gradual deflection maneuver. This is because the thruster may only be activated during time intervals when the NEO's spin brings the thrust vector of the mounted low-thrust device near enough to the optimal direction. Even if the issues relating to NEO spin are somehow surmounted, the question of whether the gradual thrust maneuver can be controlled precisely enough to achieve the necessary optimal direction remains to be answered and the answer will depend on the specific dynamics and equipment involved in a given NEO deflection scenario. The inevitable conclusion is that gradual techniques are problematic in a variety of ways, making their use in a critical NEO mitigation mission questionable.

Returning to the philosophy behind the application of gradual or impulsive NEO deflection techniques, impulsive techniques are preferred when:

- Warning time is short, on the order of a decade or a few years;
- The NEO is so large that it would resist gradual techniques enough to render them infeasible over the available timespan;
- The NEO is highly structurally sound, allowing the force of an impulsive deflection maneuver to propagate through it efficiently;
- Gradual techniques are otherwise deemed infeasible due to the specific dynamics and characteristics of the particular NEO deflection scenario at hand.

There is certainly a bias towards gradual techniques in general because they are often more energetically efficient and more elegant in application, whereas impulsive techniques generally rely on brute force coupled with precise calculations and timing.

However, there are situations for which impulsive deflection maneuvers are not only appropriate but also required, such as cases where an impending NEO collision is discovered with very little advance warning. Situations in which there is very little advance warning are quite plausible. While most of the NEOs which are roughly 1 km in mean diameter or larger have been discovered, there are still many waiting to be found. NEOs may also inhabit orbits mostly within Earth's orbit, causing them to be silhouetted by the Sun during much of the period during which they are observable from Earth. Such NEOs are nearly impossible to detect from ground observatories and one that is on a collision course with Earth might only be found a few years before the collision event. This is an excellent reason to field space-based NEO observatories. Furthermore, there are a great many smaller NEOs that have not yet been discovered, possibly on the order of millions. These smaller NEOs range in size from tens of meters to hundreds of meters. While NEOs ~ 40 m or less in mean diameter will generally burn up upon entering the atmosphere and hence pose no threat, there are many NEOs between 100 and 300 m in mean diameter which pass very closely to the Earth and are often not discovered until after they have

passed their point of closest approach with Earth. These NEOs are certainly not the civilization killers that their 1 km and greater counterparts are, but they are still capable of laying large regions to waste wherever they hit Earth's surface.

Impulsive techniques are generally characterized by the following attributes or features:

- Explosions of either conventional or nuclear devices;
- Firing of chemical thrusters or rocket engines attached to the NEO;
- Collisions that transfer high amounts of kinetic energy.

Both impulsive and gradual NEO deflection techniques require optimal application in order to be effective because the applied velocity change magnitude is so small compared to the NEO's massive momentum due to the limits of current and foreseeable technology. Generally speaking, the direction of the applied force is the primary quantity to be optimized such that the following deflection conditions are satisfied, in this order of priority:

- The target NEO that would have collided with Earth must miss Earth by some predetermined margin;
- The target NEO should not return to the vicinity of Earth in the future in a specific manner that leads to a subsequent impending collision. Note that there are a variety of NEOs, large and small, that have made close approaches to Earth at one point or another but are not ever going to be on a collision course with Earth in the future. Additionally, one might indeed expect a freshly deflected NEO that was only deflected by a small margin to return to the vicinity of Earth at some point in the future, depending on the ratio of the NEO's and Earth's orbital periods. So it is not that we wish to avoid any future proximity of the NEO to Earth, it is only that we wish to avoid a

specific configuration that would lead to a second collision threat in the future.

The first condition is obviously the most important one because even if it is discovered that the NEO is going to come back to collide with Earth in the future, at least the first collision has been averted and there is time to plan the second deflection mission. Moreover, the very fact that the first collision could be averted means that, precluding catastrophic mission failure, the second impending collision can be averted in the same manner. That being said, if it is possible to deflect a threatening NEO, either with impulsive or gradual techniques, such that any future collisions of that NEO with Earth are ruled out, then the deflection maneuver that achieves that condition is certainly the maneuver of choice. The following sections detail selected NEO deflection systems and discuss their requirements, advantages, disadvantages, and feasibility.

5.3.1 Non-Impulsive Methods

Non-impulsive threatening NEO mitigation techniques generally fall into the deflection, rather than disruption or annihilation, regime, due to their gradual natural. By definition these techniques require years, usually several decades, to impart enough momentum to the NEO to accomplish deflection, depending on the type and magnitude of the method and the characteristics of the target NEO. For this reason, non-impulsive NEO mitigation methods are only feasible when the threatening NEO is discovered long in advance of its future collision with Earth, on the order of decades. Several proposed techniques for gradual NEO deflection are discussed in turn below.

5.3.2 Low-Thrust Attached Thrusters

For the purposes of this discussion, low-thrust devices may either be ion engines or mass drivers. Ion engines accelerate charged particles with magnetic

fields to generate thrust, and these devices have been successfully tested on spacecraft. However, their current thrust levels are only in the micro-newton range, meaning that, to be effective against NEOs, extremely large-scale low-thrust engines would have to be developed that could operate continuously for decades. Such devices are far beyond the reach of current technology.

Mass drivers use electromagnetic fields to accelerate metallic "buckets" of NEO material away at high velocity, thereby imparting thrust through momentum exchange. These devices have yet to be reliably tested and the power requirements for a mass driver operating at a level sufficient for NEO mitigation would likely be extremely high.

Both of these methods of low-thrust deflection also suffer from being directed non-optimally by the NEO's natural spin state. Additionally, both require robust anchoring to the NEO's surface, which can be problematic and would certainly have to be tested prior to using such methods in an actual threat mitigation situation.

5.3.3 Utilization of the Yarkovsky Effect

The Yarkovsky effect is the acceleration experienced by NEOs due to the reradiation of thermal energy absorbed from the Sun as the NEO surface rotates into and out of direct sunlight. This small force is extremely difficult to model, making its net effect on a given NEO difficult to estimate. However, this force occurs naturally and has a strong effect on a NEO's orbit over time. If the NEO's natural motion, which includes the contributions from this force, is leading it to a collision with Earth, then even a small change in the Yarkovsky effect force it experiences could deflect it from Earth impact if the change was initiated with enough lead time.

Methods for changing the acceleration due to the Yarkovsky effect are aimed at changing the NEO's solar flux absorbance. This can be accomplished by changing the thermal properties of the NEO's surface, possibly through the application of some pigmented material. Thus, the NEO's surface could be "painted" by dusting it with

something of a certain color. If the NEO is dark in color, it could be painted white; if light in color, it could be painted black. This change in surface color would dramatically alter the Yarkovsky effect.

One drawback to this method, aside from the fact that is has never been tested, is that the payload of pigment could be prohibitively large due to the massive surface area of most NEOS. Another drawback is that the Yarkovsky effect is exceedingly difficult to model, as mentioned above, making the outcome of this deflection method unpredictable.

5.3.4 Solar Concentrators

A solar concentrator is essentially a large parabolic mirror that focuses sunlight into an intense beam that heats a spot on the surface of the NEO, causing either vaporization of the surface material or sufficient heating to release any volatiles that may be present naturally in the NEO. The result in either case is a small gas jet streaming away from the NEO, imparting a small force that gradually deflects the NEO over time. The difficulties in applying this technique are attaining accurate pointing for extended periods and constructing a very large mirror that can withstand the rigors of the space environment. This technique requires a lead time on the order of decades, and it can be very effective over such time periods. A conceptual design of a solar concentrator is shown in figure 5.1 below.

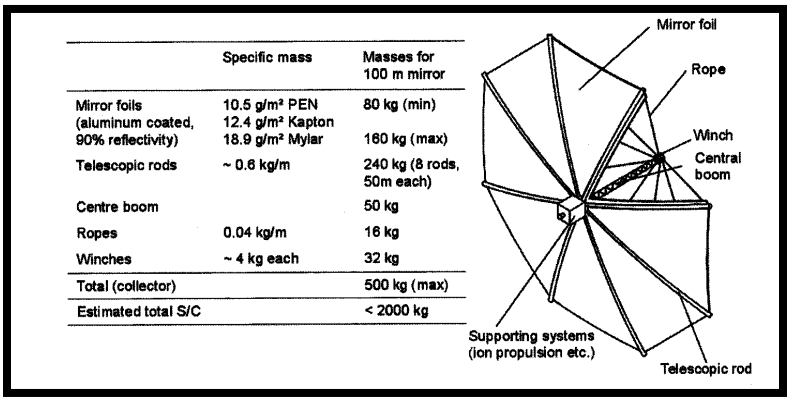

Figure 5.1: Conceptual Design of a Solar Concentrator [17]

Plots showing the simulated effectiveness of a solar concentrator in the deflection of a NEO are presented in figure 5.2 below.

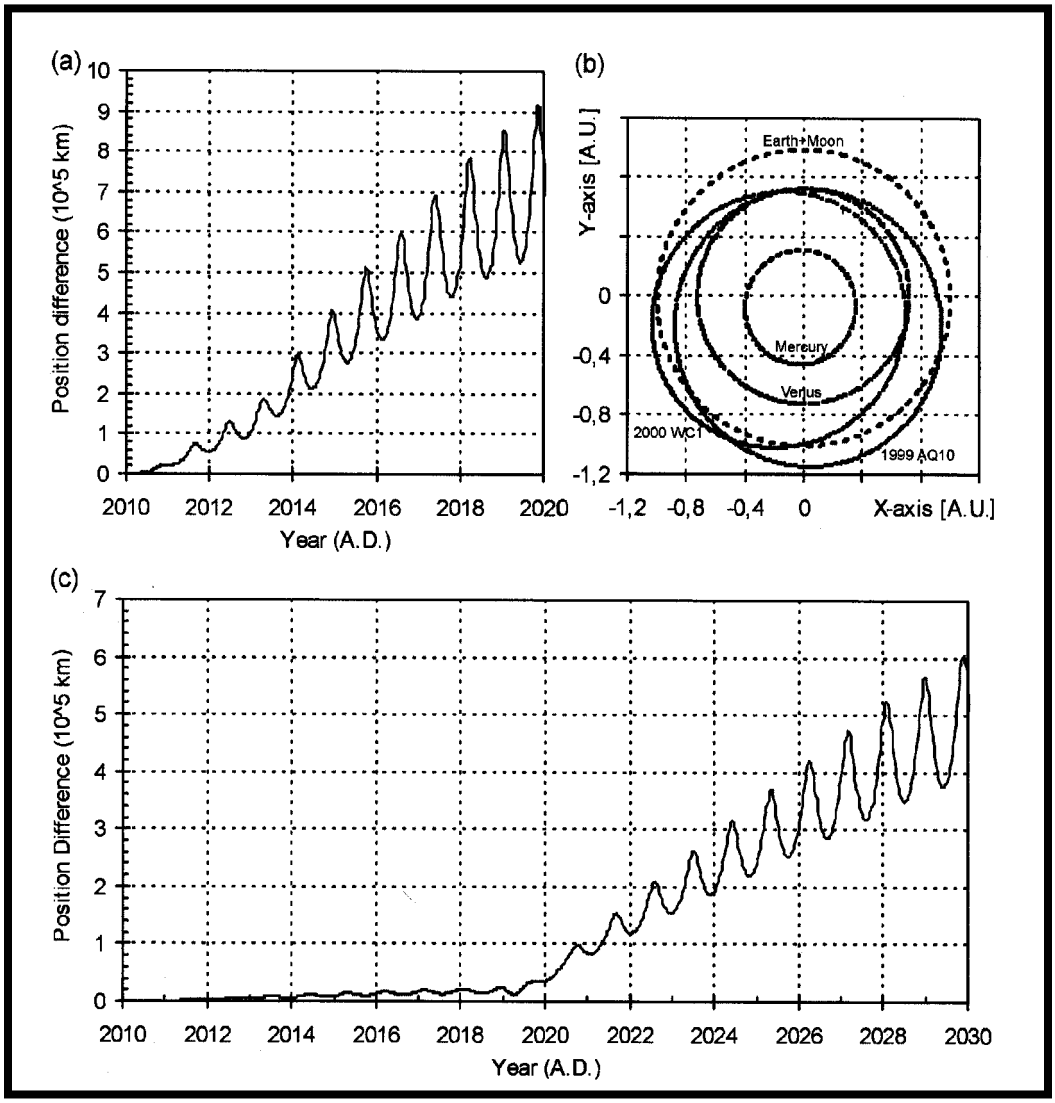

Figure 5.2: Efficacies of Solar Concentrator Applications Over Time [17]

The data in figure 5.2 was generated by simulating the computed applied force of a solar concentrator over time for two cases. Actual NEOs were used in the simulations and the force was applied parallel to each NEO's velocity vector, which

is not necessarily the optimal direction, as will be shown later, but is often close. The forces were applied for a period of 400 days and the subsequent deviations in the NEO's position, measured as the time-varying distance between the NEO on the perturbed and unperturbed trajectories, is shown. It is clear that this technique has the potential to be quite effective, but it takes at least a decade for the deflection to become substantial. Drawbacks to this technique include the fact that the concentrator mirror is likely to be degraded over time by the jet of vaporized NEO material streaming off of the surface [17].

5.3.5 Attached Solar Sails

Solar sails are large pieces of reflective material that are pushed by the photons from the sun that strike the sail's surface, much in the same fashion that terrestrial wind pushes on cloth sails and propels maritime vessels. These devices have been proposed for providing propulsion to spacecraft and it has thus been postulated that such a device could be attached to a threatening NEO for the purposes of deflection. It is likely that the required size for such a solar sail would be quite large, and it requires anchoring to the NEO's surface, which is always problematic. The NEO's natural spin state also complicates achieving proper sail orientation.

5.3.6 Impulsive Methods

Impulsive threatening NEO mitigation techniques may fall into any of the deflection, disruption, or annihilation regimes, depending on the magnitude and type of impulsive method and the characteristics of the target NEO. These techniques take effect nearly instantaneously, acting on timescales ranging from fractions of a second for detonations to several minutes for high-thrust thruster operations. While such techniques are of course just as feasible as non-impulsive techniques for long-term deflection missions, impulsive techniques are the only option when lead-time is short, i.e., the threatening NEO is discovered only a few years before its impending

collision with Earth. Some currently postulated impulsive techniques are each discussed below.

5.3.7 High-Thrust Attached Thrusters

High-thrust attached thrusters may be solid rockets or liquid rockets using conventional liquid oxygen and liquid hydrogen. They may also be more exotic high-performance nuclear rockets, which have yet to be tested. The obvious problem with using these systems is the sheer mass of fuel required and the complexities of anchoring such massive equipment reliably to a NEO's surface. Note that the anchoring mechanism has to be robust enough to withstand up to several minutes of extremely high stress while the thrusters are operating. The NEO's spin state does not complicate the application of these systems much because the thruster burn times are generally on the order of several minutes at most, which is only a small fraction of the rotation period of most NEOs.

Given the fact that the solar concentrator in the above example had a total mass of 2000 kg [17] and the mass of high-thrust thruster and fuel systems could be several orders of magnitude above this, high-thrust systems are clearly not attractive for their energy per unit mass performance. The use of attached high-thrust systems has to be carefully considered for a given NEO scenario, but it will always most likely be out-performed by other systems. The exception to this is when lead time is short. However, the thrust requirements in such a scenario may necessitate a combined thruster and fuel mass be delivered to the NEO that is beyond current launch system capabilities, effectively rendering the technique useless. These systems are discussed for completeness but are not recommended for use in NEO deflection, generally speaking.

5.3.8 Nuclear Fission/Fusion Devices

Nuclear weapons, in the form of both fission and fusion devices, have been under development since World War II. It was a 20 kiloton (Kt) yield nuclear fission bomb that devastated the Japanese city of Hiroshima on August 6, 1945, heralding the end of the second World War. Since that time, nuclear device technology has progressed considerably, largely due to the Cold War between the United States and Russia, which only ended within the past two decades. There are currently multiple nations with the capability to produce nuclear weaponry, and the energetic yields of these devices are now on the order of megatons (Mt), rather than Kt. Aside from being used to create ultra-destructive weaponry, the nuclear fission process has also been used as a power source for military, civilian, and space applications; fusion reactors are still under development and impractical at the time of this writing.

Much of the energy released during a nuclear detonation is in the form of X-rays and neutron radiation, making nuclear devices attractive for threatening NEO mitigation; the neutron radiation from a nuclear device detonated near the surface of a NEO should penetrate its outer surface beneath the blast point, instantaneously vaporizing a layer of the surface material and causing it to blow off to zero pressure, thereby imparting momentum to the NEO [12]. However, the standoff detonation distance must be computed correctly for these effects to be realized. This process will be discussed in much greater detail presently.

Most preliminary calculations by various researchers have indicated that nuclear device yields on the order of 1 Mt are required for imparting velocity changes on the order of ~ 1cm/s to kilometer-scale NEOs, and this velocity change value is sufficient to deflect a NEO given adequate lead time, even only a few years. Nuclear devices of this yield are certainly available today, and thermonuclear (fusion) devices can achieve yields of several MT, even up to 50 MT, with current technology. Thus, a nuclear device is currently a viable threatening NEO mitigation effector in terms of production, containment, and deployment capabilities. Moreover, nuclear devices

offer the highest energy density, making them attractive from the point of view of minimizing the payload mass for the spacecraft that delivers the deflection system, thereby allowing for more powerful spacecraft maneuvers and overall shorter flight times, which helps to maximize the overall effectiveness of the deflection.

5.4 Nuclear Device Application Methods

Nuclear detonations can be applied in several different modes. The first mode is the standoff detonation mode, which was described above. The second mode is a surface explosion, and the third mode is a penetration explosion in which the nuclear device is buried to some depth within the NEO and then detonated. The surface and penetration modes are not going to be considered in detail because they necessitate more complex mission logistics without offering significant gains in terms of effectiveness. In fact, the required mass for the penetration device combined with the nuclear device leads to a reduced overall energy per unit mass for the deflection method [12].

5.4.1 Standoff Nuclear Detonation Theory

A variety of theories have been researched regarding the outcome of applying impulsive forces to solid and porous bodies that are thought to resemble NEOs in structure and composition. Experimental data for the energy thresholds for disrupting and dispersing such objects are numerous and varied though reasonable estimates may still be made. Additionally, theoretical research into the results of a standoff nuclear detonation has been performed in the form of analytical treatments and computer simulation. Several key studies were performed by Ahrens and Harris in the early and mid 1990s and, more recently, by Holsapple. Holsapple's results are based upon the most detailed models, incorporating one dimensional wave physics calculations [12]. He has shown his data to be a significant improvement over

previous work in the field, and thus his models will be used as the basis for nuclear device yield requirements calculations in this work.

5.4.2 Standoff Nuclear Device Mechanics

As stated previously, the energy generated by the nuclear detonation takes the form of X-rays and neutrons. However, it is expected that the neutrons are more effective than the X-rays and therefore the focus is on the neutron energy. The basic assumption for most nuclear devices is that the neutron energy produced is 10% of the total device yield [12].

The neutrons generated by the detonation are assumed to penetrate some depth into the NEO surface, and the generally accepted value for penetration depth is 20 cm. This, in combination with a given NEO's physical properties, leads to a specific energy (energy per unit mass) deposited into the surface layer, which then determines the momentum imparted to the NEO per unit area. Multiplying this value by the affected surface area on the NEO, which is computed through spherical geometry, assuming a spherical body, and then dividing by the NEO mass yields the total impulsive velocity change imparted to the NEO [12]. An artist's conception of a standoff nuclear detonation applied to a NEO is shown in figure 5.3 below.

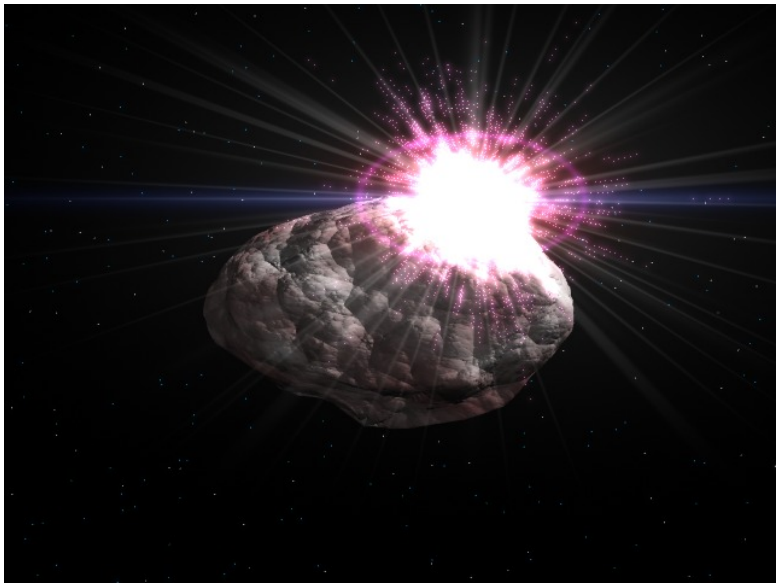

Figure 5.3: Artist's Conception of a Standoff Nuclear Detonation Applied to a NEO [18]

There are, however, a variety of assumptions one can make which lead to disparate results for the above calculations. Some researchers assume that the energized surface layer vaporizes while others assume that it blows-off in the form of fragments. Holsapple's approach is to use a three-phase equation of state for an approximate NEO material (alpha-quartz, SiO2) and simulate the application of the energy to determine the results, including a one-dimensional modeling of the resulting wave propagation through the material as it loads and unloads due to the intense stresses [12]. Holsapple's data and results for a specific case study he performed will be scaled in order to apply them to a case study presented later in this work. The details of the scaling calculations are presented below.

5.4.3 Standoff Nuclear Detonation Results Scaling

The equation for computing the total velocity change imparted to a NEO for a given standoff nuclear detonation is presented below.

$$\Delta v = \frac{p_A A_e}{M} \tag{5.1}$$

where

Δv = the impulsive velocity change to the NEO's velocity

p_A = the specific momentum (momentum per unit area) imparted to the NEO

A_e = the surface area on the NEO affected by the nuclear detonation

M = the total mass of the NEO

The affected area on the NEO is a function of the standoff detonation distance and the application of spherical geometry to the NEO body. The specific momentum imparted to the NEO is a function of the specific energy in the layer of energized surface material, given by [12]

$$Q = \frac{y}{4\pi d_s^2 \rho l} \tag{5.2}$$

where

y = nuclear device yield

l = neutron penetration depth

d_s = standoff detonation distance

ρ = mean density of NEO

However, Equation (5.2) seems to only be an approximation because Holsapple's results from numerically integrating the deposition of a differential amount of energy over a set of "rings" of surface area yields a different value than what equation (5.2) provides for his scenario parameters. This will be apparent in the subsequent presentation of numerical results. A plot showing how Holsapple determines the

optimal standoff detonation distance is presented in figure 5.4 below and the parameters for his test case are presented in table 5.1 below.

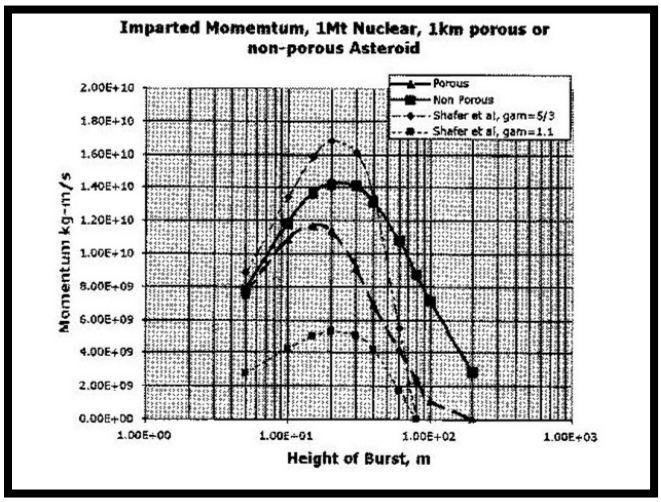

Figure 5.4: Imparted Momentum to 1 km NEO Test Cases [12]

Table 5.1: Holsapple's Standoff Nuclear Detonation Simulation Parameters and Results [12]

Quantity	Value
Neutron penetration depth, l	20 cm
Mean NEO density, ρ	2.65 g/cm^3
NEO diameter (spherical NEO), D	1000.0 m
Nuclear device yield, y	1 Mt
Optimal standoff detonation distance, d_s	23 m
Momentum imparted to NEO, P	1.4×10^{10} kg-m/s
Percent of NEO surface area affected, A_e	2.2%
Percent of total neutron energy absorbed	35%
Specific energy below detonation point, Q	1200.0 MJ/kg
Energy per unit mass of NEO material, E_{sp}	100 J/kg
Imparted velocity change, Δv	1 cm/s

While these results are of course applicable to any NEO that very closely resembles the one modeled by Holsapple, it is desirable to scale these results for optimal NEO standoff detonation distance and imparted Δv for a different NEO for deflection simulation purposes and first-order deflection mission sizing, which is performed in a subsequent case study within this work. This is the motivation for determining the required scaling relationships.

Holsapple provides a plot of specific momentum as a function of the specific energy below the detonation point, and this is shown in figure 5.5 below. However, the specific energy found by Holsapple, 1200 MJ/kg, is beyond the range of this plot.

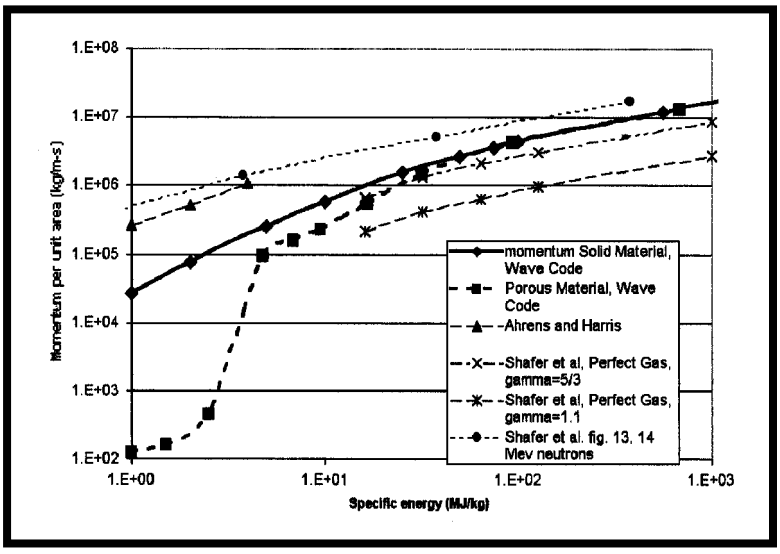

Figure 5.5: Specific Momentum as a Function of Specific Energy Below Detonation Point [12]

Note that at the final value for specific energy in figure 5.5 (~ 1000 MJ/kg), the imparted momentum is slightly more than 1×10^{7} kg/m-s. Computing the affected area on Holsapple's NEO using the spherical model and the quoted value of 2.2% for the affected surface and then dividing the total imparted momentum by this number yields a specific momentum of 2.026×10^{5} kg/m-s, which corresponds to between 1 and 10 MJ/kg in figure 5.5, much different than the stated value of 1200 MJ/kg.

Therefore, the data from figure 5.5 will not be used in subsequent calculations since a functional relationship that matches Holsapple's results cannot be established.

Instead, the specific momentum for another NEO will be scaled according to Holsapple's specific momentum and specific energy as follows.

$$p_A = \frac{Q}{1200} \times 2.026 \times 10^5 \tag{5.3}$$

Additionally, equation (5.2) above for the specific energy below the detonation point yields a value of 733.6 MJ/kg for Holsapple's parameters, instead of the expected value of 1200 MJ/kg. Therefore, equation (5.2) will be scaled by the ratio of Holsapple's numerically integrated value to the analytical value, which is 1.636, as follows

$$Q_{actual} = Q \times 1.636 \tag{5.4}$$

The standoff distance will be scaled according to the ratio of the other NEO's radius to Holsapple's. The percentages of 2.2% for the affected surface area and 35% for the amount of absorbed neutron energy are both geometric results and will be assumed to be the same for any spherical NEO if the standoff distance is scaled proportionally as described above.

Finally, Holsapple notes that the computed value of 100 J/kg for the energy per unit mass of NEO material is about the threshold value for shattering the object but is a "factor of 10 or more below that required to also disperse it." This consideration will be used to determine the maximum nuclear device yield for a given NEO that will shatter but not disperse it. This is important because, as previously discussed, it is often desired that the object not be dispersed; if any of the dispersed fragments proceed to collide with Earth later and any are large enough to survive

atmospheric entry, one or more of them could still cause considerable damage over localized regions.

5.5 Antimatter Devices

Antimatter has fueled the imaginations of engineers and engineering enthusiasts for nearly 100 years. Indeed, matter/antimatter reactors power the warp drives of Federation starships in the Star Trek universe, conceived by Gene Roddenberry in the 1960s. However, while antimatter is certainly fantastic, it is not fictitious. The existence of antimatter was predicted by Dirac's theory of quantum mechanics in 1928 and confirmed by Carl Anderson soon after that [19]. Antimatter is currently created and studied at particle physics research facilities throughout the world to glean insights into the fundamental nature of physics and the universe, yielding precious clues to both humanity's origins and future.

The nature of antimatter is such that when it is combined with normal matter, both quantities of material completely annihilate, creating a burst of pure energy. This energy production is governed by Einstein's famous equation for the *rest energy* of matter, given as [20]

$$E = mc^2 \tag{5.5}$$

where E (sometimes written as E_0) is termed the *rest energy*, m is the mass of the matter, and c is the speed of light. Equation (5.5) has two important implications; first, that matter has energy, even when its kinetic energy is zero, due to the fact that it has mass, and secondly that mass and energy are therefore equivalent. It has been experimentally verified at particle physics laboratories such as CERN that equation (5.5) holds true; when equal quantities of matter and antimatter are combined, the burst of energy generated during the subsequent annihilation is indeed of the amount

predicted by equation (5.5). Note that in the case of a matter-antimatter reaction, the energy produced is calculated as follows:

$$E_{produced} = \left(m_{antimatter} + m_{matter}\right)c^2 \tag{5.6}$$

The energy burst produced by such a reaction could theoretically be used to divert or destroy an incoming NEO in a similar fashion to a nuclear detonation, thereby accomplishing the NEO mitigation mission objective. An example of computing the required mass of antimatter for a NEO mitigation mission is given below.

First, the energy density of the antimatter/reaction can be computed as follows:

$$\rho_{\varepsilon} = c^2\left[\frac{J}{kg}\right] \times \frac{1[MJ]}{1\times 10^6[J]} = 8.98740441\times 10^{10}\left[\frac{MJ}{kg}\right] \tag{5.7}$$

where

c = speed of light in a vacuum = 2.9979×10^8 m/s [20]

Assume that the required detonation energy is 1 MT (4.2×10^9 MJ). With the required energy, E_{req}, and the energy density both known, the required mass of matter for the reaction can be computed as follows.

$$m_{req} = \frac{E_{req}}{\rho_{\varepsilon}} = \frac{4.2\times 10^9[MJ]}{8.98740441\times 10^{10}\left[\frac{MJ}{kg}\right]} = 4.6732\times 10^{-8}[kg] = 4.6732\times 10^{-5}[g] \tag{5.8}$$

Since equal portions of matter and antimatter are combined in a matter/antimatter reaction, only half of the mass resulting from equation (5.8) is antimatter, yielding a final value for the required mass of antimatter of 2.3366×10^{-5} g.

While the above calculations show that a matter/antimatter reaction device is quite attractive in terms of extremely low payload mass, there are difficulties in handling and producing antimatter that will preclude its use in such a capacity for the foreseeable future. These limitations manifest in terms of both storage and production capabilities.

Antimatter must be stored such that it never is in contact with particles of normal matter, else it will instantly annihilate and be lost. Since antiparticles have an electric charge just as normal particles do, an electromagnetic "bottle" serves the purpose of suspending a quantity of antimatter away from the material walls of the containment device. Furthermore, a vacuum must exist within the bottle.
The problem lies in the fact that only antiparticles of the same charge may be stored together. In the case of antiprotons, for example, if both positive and negative particles are brought together, they attract and form anti-hydrogen atoms, which are electrically neutral and thus are no longer affected by the magnetic field; such neutral particles would soon annihilate with the material walls of the containment system. However, if too many particles of the same charge are stored together, the repulsive forces between them eventually overcome the magnetic field. Thus, only small amounts of antimatter consisting of particles with like charges may be stored in a given containment device. These containment devices are also bulky and require power to operate because they are electromagnetic. Essentially, not enough antimatter can be accumulated at a high enough density 19].

Currently, antimatter is produced at high-energy particle physics laboratories such as CERN. The production process involves colliding high-speed protons into tungsten blocks, creating a hail of particles, including antiprotons, which are then collected, albeit with great difficulty and losses. CERN quotes a production rate of

about 10^7 antiprotons per second, which means that to amass one gram of anti-hydrogen (6×10^{23} antiprotons) would take approximately 2 billion years. Thus it is obvious that creating the required 23.366 grams of antimatter in the example above is, for all intents and purposes, impossible. Even if such quantities of antimatter could be produced in a timely fashion, containment would not be feasible 19].

For the reasons explained above, this author does not foresee antimatter becoming a viable effector for threatening NEO mitigation. However, as the calculations of equation (5.8) show, it would be a highly efficient and effective mitigation effector if the fundamental problems of production and storage were solvable.

In recent times the scientific and engineering communities have expressed aversion to employing nuclear devices in NEO mitigation. It appears that this is largely for moral reasons; many scientists and engineers seem to feel that nuclear devices are "tainted" because they are intended for use as weapons of mass destruction against other human beings. While this author certainly does not agree with the usage of nuclear devices for that purpose, this author does not have any moral issue with employing nuclear devices against NEOs in the defense of humanity. In fact, it seems most fitting that humanity's weapons of mass destruction should be transformed into humanity's instruments of planetary defense for all humankind. It would be the penultimate instance of swords turning into plowshares.

Thus, it is curious that some scientists and engineers even cite antimatter devices as attractive NEO mitigation systems. Were antimatter devices to be produced on a large enough scale to be viable NEO mitigation effectors, such devices would also be far more powerful weapons than current nuclear devices. Therefore, it would seem that the same scientists and engineers who loathe nuclear devices and refuse to acknowledge their extreme merit as NEO mitigation effector candidates would loathe antimatter devices even more and speak out against antimatter research. Yet this author has heard no such rhetoric.

It is clear that some scientists and engineers have simply adopted a stance against the use of nuclear systems for any purpose merely because of the social stigma associated with nuclear devices. The origin of this stigma is understandable, given that humanity lived in fear of nuclear annihilation throughout the latter half of the twentieth century and still has to acknowledge the existence of this threat today. However, technology cannot ever be disinvented; the best thing that can happen is for society to mature and for highly energetic devices to be used for purposes that benefit all humankind. To propose that nuclear devices be discarded, prohibited, or forgotten is impractical, naïve, and inappropriate as it would remove a valuable tool from our resource pool and set the stage for malicious persons to rediscover and re-implement that technology in the future when it is least expected. Human beings will kill each other regardless of the available technology until humanity as a whole evolves past the desire to commit such acts. Therein lies the true problem; it is not the technology, it is how humans choose to employ it. The scientists and engineers who decry the use of nuclear devices for any purpose would do well to understand that concept. Moreover, if those scientists and engineers are truly passionate about ending the threat of humans destroying each other on massive scales, they should devote energy to solving the true problems of unwarranted human aggression and greed rather than impeding the efforts of other scientists and engineers, such as this author, to find safe, beneficial uses for otherwise destructive technology.

5.6 Conclusions

Standoff nuclear device detonations offer the best NEO deflection performance in terms of mission simplicity, imparted momentum to the NEO, and payload mass. These devices are readily available with current technology but must be tested in order to confirm their theoretical effectiveness against a NEO. NEO deflection using these devices will be the focus during the remainder of this work.

The above information has detailed the magnitude of the Δv that standoff nuclear detonations are capable of delivering to a target NEO but say nothing about

the optimal direction in which to orient the resulting $\Delta\vec{v}$ vector that is applied to the NEO's center of mass. The next part of this work will present a new method for determining this optimal $\Delta\vec{v}$ orientation and then employ this technique in a NEO mitigation case study.

6. NEO DEFLECTION MECHANICS

6.1 Introduction

As previously discussed, deflection, rather than fragmentation or annihilation, is the NEO mitigation mode that will be the focus of this work. This section details the mechanics of impulsively deflecting NEOs.

6.2 Deflection Principles

To deflect a body traveling through space is to alter its trajectory such that it does not arrive at the same sets of space-time coordinates that it would have arrived at absent interference. In truth, the trajectories of all objects traveling through the solar system are constantly being deflected from simple, identically repetitive orbital motion. The space environment provides forces that act on orbiting bodies, including solar radiation pressure, magnetic fields, the Yarkovsky effect, atmospheric drag when within a planet's exosphere, and collision with debris. Additionally, the effects of relativity, though minute, are still present. Finally, the gravitational forces due to all other bodies in the solar system also act to cause a given body's orbital motion to deviate from the pure Keplerian model.

However, for the purposes of NEO deflection, the undeflected motion of the NEO is defined to be its motion under the influence of all natural forces, including, but not limited to, the various forces and effects described above. For it is this motion, which is the product of all such effects, that leads to the threatening NEO's collision with Earth, the condition that NEO deflection has the goal of preventing.

Thus, to deflect a NEO is to alter its natural path through space by means of some sort of energetic intervention, which, since impulsive rather than gradual techniques are being considered, will take the form of some impulsive force being applied to the NEO at some time. Whatever the mechanism involved or the method of delivery, an impulse applied to a NEO will result in some net, effectively

instantaneous, change in the NEO's orbital velocity vector, hereafter referred to as the "delta-v," denoted symbolically by $\Delta\vec{v}$.

The mathematical definition of a deflection is given by the converse of equation (4.7) above for collision, which is

$$\Delta r\left(t \in \left\{t_{coll-} < t < t_{coll+}\right\}\right) > R_{EARTH} \tag{6.1}$$

where

t_{coll-} = time shortly before the original time of collision on the original orbit

t_{coll+} = time shortly after the original time of collision on the original orbit

The meaning of "shortly" in the above definitions is somewhat ambiguous and will be refined in subsequent sections. Suffice it to say that the deflected NEO will still closely approach at a slightly different time than the original epoch of impact though it won't collide, and the goal of the deflection is to ensure that the condition of non-collision holds over the interval of time surrounding the original time of collision. The goal of making the non-collision condition hold for the rest of time is more difficult and subtle, as discussed in the previous section on orbital keyholes and resonant returns. Generally, maximizing the distance between the NEO and Earth is the best way to avoid a resonant return.

6.3 Deflection Results

A deflection may be interpreted as the forced transition of a NEO-Earth collision event to a NEO-Earth close approach event. The application of a $\Delta\vec{v}$ to the NEO will change its trajectory from the point in time of application forward. Thus, if the $\Delta\vec{v}$ is applied correctly and applied at a sufficient time prior to when impact would have occurred absent intervention, the NEO will fly past Earth rather than collide with Earth. This event is defined as a close approach.

Therefore, the goal of a deflection is to *maximize the minimum close approach distance*. Note that the close approach resulting from deflection will in general not occur at the same exact time as the time when the unmitigated collision would have occurred. Thus, deflection analyses must account for this by analyzing a time interval that extends slightly beyond the time at which impact would have occurred. The amount of time to consider past the original time of collision is generally subjective, but a few days is generally sufficient; the $\Delta\vec{v}$ magnitudes being considered are only tiny perturbations in comparison to the NEO's orbital velocity and hence the difference between the perturbed and unperturbed trajectories will be correspondingly small. The exception to this is when the deflection is applied many years before the predicted impact date. In these cases it may be necessary to analyze a time interval that extends weeks past the original, unmitigated impact date.

More formally, the analysis must encompass a time interval up until the point at which close approach has passed. Mathematically, this will occur when the first time derivative of the distance between the NEO and the Earth changes sign from negative (approaching) to positive (receding). The time of closest approach is the time for which the derivative is zero. These mathematical relationships are formally defined in the equations below.

The condition on the NEO-Earth distance rate immediately prior to the time of closest approach is given by

$$\Delta\dot{r}(t) < 0 \tag{6.2}$$

where

$t \in \{t_{CA-} < t < t_{CA}\}$

t_{CA} = time of closest approach

t_{CA-} = times immediately prior to closest approach time

and the condition on the distance rate at the time of closest approach is thus

$$\Delta\dot{r}\left(t_{CA}\right) \equiv 0 \tag{6.3}$$

which leads to the condition on the distance rate for the times immediately following the time of closest approach, given by

$$\Delta\dot{r}\left(t\right) > 0 \tag{6.4}$$

where

$t \in \left\{t_{CA} < t < t_{CA+}\right\}$

t_{CA+} = times immediately after the time of closest approach

It is important to note that the above conditions are guaranteed to apply only in the temporal region surrounding the time of original collision. If the deflection is (preferentially) applied several or more orbits prior to the original time of collision, the sign of the time derivative of the distance between the NEO and the Earth will change several times before the time intervals listed above are reached.

While the value of t_{CA} cannot be computed analytically, it can be ascertained by numerically computing the first derivative of the NEO-Earth distance and finding the time at which that derivative is zero. It can also be estimated by visually examining a plot of the distance over time for a given deflection case.

6.4 Deflection Application

The $\Delta\vec{v}$ applied to deflect the NEO has two aspects, as all vectors do, which affect the efficacy of the deflection attempt: magnitude and direction. The maximum available velocity change magnitude, denoted by $\Delta v \equiv \left\|\Delta\vec{v}\right\|$, is generally fixed by the

energy of the deflection mechanism, the physical and structural properties of the NEO, and the coupling efficiency between the deflection device and the NEO. Maximizing Δv amounts to choosing the best available deflection device for the given NEO from among those available with the technology of the time.

However, the applied $\Delta\vec{v}$ may generally be oriented as desired in three-dimensional space, except in cases where physical limits exist, such as the available angles of incidence for kinetic impactors on intercept orbits. In the case where thrusters are mounted on the NEO or a standoff nuclear detonation is executed, the choice of orientation for the resulting $\Delta\vec{v}$ is generally open. The geometry associated with an impulsive deflection is shown in figure 6.1 below.

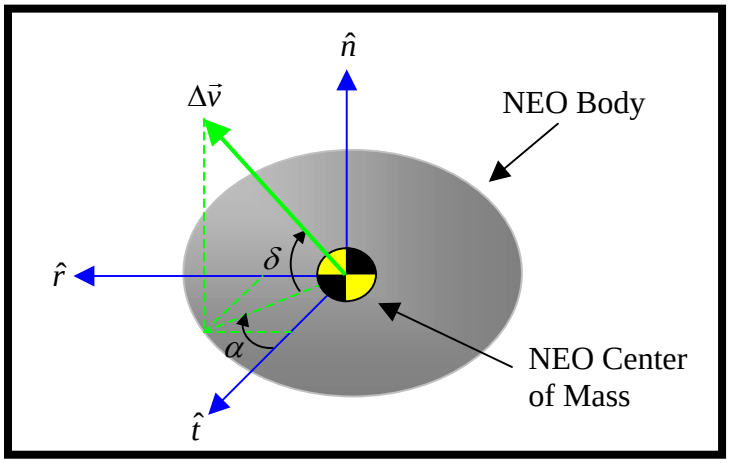

Figure 6.1: Deflection Impulse Orientation Geometry

The spherical coordinate angles, α (azimuth) and δ (elevation) shown in figure 6.1 define the orientation of the $\Delta\vec{v}$ vector in the RTN (Radial-Transverse-Normal) frame, whose origin is at the NEO's center of mass and whose basis vectors are $\hat{r}$, $\hat{t}$, and $\hat{n}$. This frame does not rotate with the NEO body and is also not fixed with respect to inertial space. A complete derivation of the RTN frame and the transformation matrix between it and the inertial frame can be found in appendix A.

The $\Delta\vec{v}$ vector is written in terms of its magnitude and spherical coordinate angles as:

$$\left[\Delta\vec{v}\right]_{RTN} = \begin{bmatrix} \left\|\Delta\vec{v}\right\|\cos(\delta)\sin(\alpha) \\ \left\|\Delta\vec{v}\right\|\cos(\delta)\cos(\alpha) \\ \left\|\Delta\vec{v}\right\|\sin(\delta) \end{bmatrix} \tag{6.5}$$

The full set of deflection $\Delta\vec{v}$ vectors is obtained by allowing α to vary from 0 to 360° (0 to 2π radians) and δ to vary from –90° to 90° ($-\pi/2$ to $\pi/2$ radians), at a given discretization. This discretization will play a prominent role in optimizing a given NEO deflection, and this will be detailed in subsequent sections on that particular topic.

The vector relationships described above are depicted in figure 6.2 below.

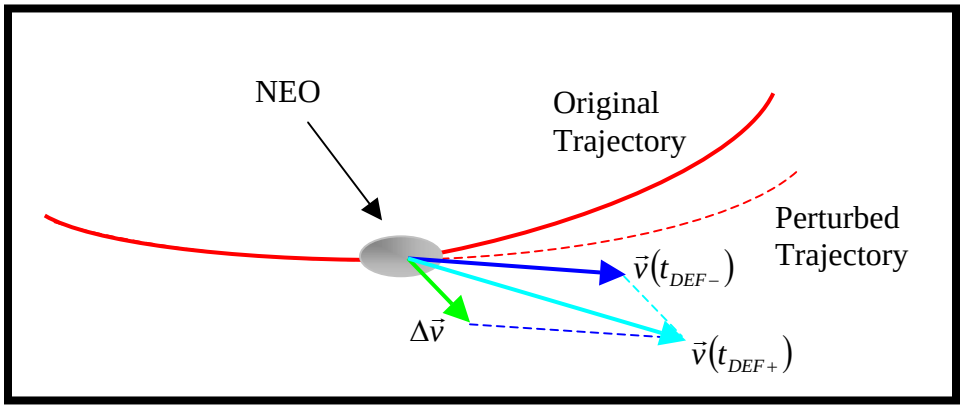

Figure 6.2: Velocity Perturbation Applied to a NEO

Figure 6.2 shows a velocity perturbation being applied to a NEO at some point along its orbit, where t_{DEF-} is the time immediately prior to the deflection and t_{DEF+} is the time immediately after the deflection.

6.4.1 Point of Deflection Application Along NEO Orbit

This raises the question of where along the NEO's orbit to apply the deflection. Two factors are considered here, the first being the effect of lead time and the second being the orbital energy of the NEO. Lead time refers to the amount of time between the time of deflection and the original time of impact. In general, maximizing this amount of time will lead to a maximization of the resulting closest approach distance, which is the desired outcome. However, the earliest time at which a deflection may be applied given logistical constraints may not be the optimal time, owing to the NEO's orbital energy.

Consider the energy of an object in orbit, given by equation (6.6) below.

$$\varepsilon = \frac{v^2}{2} - \frac{\mu}{r} \tag{6.6}$$

where

v = magnitude of the object's orbital velocity

r = distance of the object from the central attractor

μ = gravitational parameter of the central attractor

Taking the partial derivative of equation (6.6) with respect to velocity magnitude leads to

$$\frac{\partial}{\partial v}(\varepsilon) = \frac{\partial}{\partial v}\left(\frac{v^2}{2}\right) - \frac{\partial}{\partial v}\left(\frac{\mu}{r}\right) \tag{6.7}$$

which becomes

$$\frac{\partial}{\partial v}(\varepsilon) = v \tag{6.8}$$

Allowing the partial derivative operator to become a discretized increment, i.e., a Δ, and rearranging yields

$$\Delta\varepsilon = v(\Delta v) \tag{6.9}$$

In equation (6.9) the aforementioned magnitude of the deflection velocity vector, Δv, appears, along with the magnitude of the NEO's orbital velocity at the time of deflection, v. Equation (6.9) therefore says that the greatest change in the NEO's orbital energy may be obtained by applying a velocity increment when the orbital velocity is largest, which is at the orbit's periapsis.

Proceeding with the assumption that the greatest deflection will result from the deflection maneuver that most greatly changes the NEO's orbital energy (and hence orbital shape, particularly the semimajor axis), equation (6.9) is interpreted to mean that the optimal point of application along the NEO's orbit is at perihelion. This implies that if the earliest available time for applying the deflection does not correspond to one of the NEO's perihelion passages, then the deflection should be held until the NEO's first available perihelion passage.

This result has been shown to be true in cases examined by other researchers and will be examined in subsequent sections of this work. Generally speaking, the case study presented in a subsequent section will compare the efficacy of waiting until the first available perihelion passage of the NEO to the efficacy of simply deflecting the NEO as soon as logistically possible, irrespective of the NEO's proximity to perihelion. Simulation data for this case study will shed light on the generality of the result implied by equation (6.9) and how strongly it affects the outcome of a deflection scenario in comparison to the contributions from the non-linearity of the system.

6.4.2 Conditions on Deflection Orientation

Conditions on the orientation of the deflection vector, $\Delta\vec{v}$, may also be speculated upon prior to performing optimization. An extension of the preceding analysis, which indicates that the best place along the NEO's orbit to apply the deflection is at perihelion, is that the best direction in which to apply that deflection is such that the $\Delta\vec{v}$ vector is aligned with the NEO's velocity vector (with or against it) at the time of deflection. However, the current research shows that this is not always the case, owing to the non-linear dynamics of the system.

Furthermore, an intuitive conclusion is that the $\Delta\vec{v}$ vector should lie in the NEO's orbit plane, i.e., the out-of-plane or normal components of the $\Delta\vec{v}$ vector in the RTN frame should be zero. This result stems from the fact that out-of-plane maneuvers are attempting to torque the NEO's orbit, which is resisted by the angular momentum of the NEO's orbit, the magnitude of which is much, much larger than the magnitude of the $\Delta\vec{v}$ vector. It follows then that orienting a $\Delta\vec{v}$ vector such that it has an out-of-plane component will always serve to diminish the efficacy of the deflection attempt. This conclusion will be shown to be true in simulation; thus only in-plane $\Delta\vec{v}$ vectors will be considered in optimization analyses, always setting the elevation angle, δ, equal to zero.

6.4.3 Deflection Optimization

It is desired to determine the set of parameters for deflection that yields the optimal, or most effective, deflection of a NEO. This requires the definition of what precisely is meant by "deflection" because this will be the figure of merit with respect to which the optimization will be performed. Conceptually, this performance index is stated as *the difference of the minimum distance between Earth and the NEO on the deflected trajectory and the minimum distance between Earth and the NEO on the*

undeflected trajectory over a time span that includes the time of closest approach on the deflected trajectory. The equation for this performance index is given by

$$P = \left[\min\left(\Delta r(t)\right)\right]_{DEFLECTED} - \left[\min\left(\Delta r(t)\right)\right]_{UNDEFLECTED} \tag{6.10}$$

where

$$t \in \left\{t_{CA-} < t < t_{CA+}\right\}$$

With the magnitude of the deflection, Δv, fixed *a priori* by the choice of deflection mechanism, the parameters to be varied in the search for an optimal deflection are α, δ, and t_{DEF}. The optimization condition is that P, defined in equation (6.10) above, is maximized. Note that each deflection time, t_{DEF}, also corresponds to a true anomaly value, ν_{DEF}. Thus, specifying a time of deflection also specifies a true anomaly of deflection, and vice versa, since the true anomaly is a function of time.

Additionally, the performance index defined above will indicate when an attempted deflection solution is actually counterproductive because P will be negative for deflection solutions that actually bring the NEO and the Earth closer together in their subsequent motion, which is the antithesis of the desired outcome. This is only a consideration when the event being modified is a close approach rather than an impact; some attempts to increase separation during a close approach will actually push the NEO closer to Earth at close approach rather than further away. This is demonstrated in a subsequent case study.

To summarize, the mathematical expression of the optimal solution for a NEO deflection is

$$\left(\alpha, \delta, t_{DEF}\right) \ni P = \max\left(P\right) \tag{6.11}$$

Thus the design space is three-dimensional and the outcome maps to a one-dimensional deflection solution space. However, since non-zero elevation angles are generally not considered, the dimension of the design space is reduced to two.

6.4.4 Deflection Optimization Techniques

The optimization problem posed in equation (6.11) above is difficult to solve, especially with classical optimal control theory methods. The governing state equations that lead to the computation of P consist of the N body equations of orbital motion for the NEO and for Earth, since the positions of both objects over time are elements of the performance index definition. These state equations are highly non-linear second order differential equations, the analytical solution of which has stubbornly eluded researchers for hundreds of years. This makes the application of analytical optimization techniques impractical and means that other measures must be taken.

The previous work done on this problem has focused on the application of optimization theory to simplified orbital dynamics of the NEO-Earth collision model. Examples include the work done by Park and Ross (1999) [21] and Conway [3], in which optimal or near optimal NEO deflection maneuvers were computed. However, these approaches have their limitations. Park and Ross employ explicit optimization, allowing for arbitrary time until impact, but they assume Keplerian motion and make the assumption that the NEO's orbit lies entirely in the ecliptic plane, i.e., the solution is two-dimensional. In the case of Conway, it is assumed that the impact event will occur before the NEO completes one orbital period (an imminent collision) and thus the time of deflection is not arbitrary. Furthermore, Conway does not employ explicit optimization, but rather examines the linearized dynamics by utilizing the state transition matrix of the two-body NEO orbital dynamics and its eigenspace. This is why the time of deflection is not arbitrary. Furthermore, Conway uses a measure of

"deflection" that turns out to be problematic, which will be discussed in subsequent sections.

The goal in this work is to develop methods for identifying optimal NEO deflection $\Delta\vec{v}$ orientations for general three-dimensional cases with no restrictions on the time at which the deflection is applied, other than the unavoidable real-life constraint that the deflection must occur after the discovery of the threatening NEO but before the Earth-NEO collision event. Therefore, design space search methods were developed that avoid explicit optimization. These methods may also be augmented to make them adaptive if warranted and may lend themselves to modern numerical optimization techniques such as simulated annealing or taboo search.

6.4.5 Current Optimization Approach

Based on the formulation of the problem given above and the parameterization of the design space and deflection solution space, the optimization method is to exhaustively sample all combinations of design space parameters and apply each combination to the non-linear system. The results are propagated and the performance index is computed for each perturbed NEO trajectory. This leads to a large family of perturbed NEO orbits and corresponding performance index values. The performance index values are sorted to find the maximum and the entire deflection solution space is shown in plots as a function of the design space parameters to illustrate the functional relationships. In this fashion intuition may be developed regarding the dynamical response of the system to perturbations applied to the NEO's orbit.

Therefore, the azimuth angles and times of deflection are defined according to a set resolution for both quantities. The resolution, or discretization level, is a subtle issue because resolutions that are too coarse may cause optimal solutions to be missed. Generally speaking, a resolution of one or several degrees for the azimuth is sufficient for initial runs of the search codes and several days to several months is

sufficient resolution for the range of deflection times considered. Regions of the design space surrounding favorable combinations of design parameters may of course be re-scanned at finer resolutions.

As mentioned previously, the family of deflected NEO trajectories that results from an application of all combinations of parameters in the design space is formed by processing each combination of deflection parameters in an N body orbital motion simulation. This simulation system will be briefly introduced in a subsequent section and detailed treatments of the underlying mathematics, physics, and state representations can be found in appendix B.

6.4.6 Design Space Search Methods

For a given deflection $\Delta\vec{v}$ vector magnitude, the number of algorithm iterations is equal to the number of deflection parameter combinations generated to form the search space. For all three parameters (the time from detection at which the deflection is applied and the two angles specifying the $\Delta\vec{v}$ orientation), initial and final values must be selected, along with the aforementioned scan resolutions for each quantity. This information is used to build a scan vector for each quantity as follows.

$$\begin{aligned} t_{scan} &= \left\lfloor t_{init} : t_{res} : t_{final} \right\rfloor \\ \alpha_{scan} &= \left[\alpha_{init} : \alpha_{res} : \alpha_{final} \right] \\ \delta_{scan} &= \left[\delta_{init} : \delta_{res} : \delta_{final} \right] \end{aligned} \tag{6.12}$$

The *init* subscripts indicate the initial values selected, the *final* subscripts indicate the final values selected, and the *res* subscripts indicate the scan resolutions. The quantity *t* represents the time after simulation start at which the deflection maneuver is performed, and the quantities α and δ are the aforementioned spherical coordinate angles which define the orientation of the possible deflection vectors, depicted in figure 6.1 above.

The number of combinations of sampled deflection design parameters may be computed by calculating the number of elements in each scan vector and taking the product as shown in equations (6.13) below.

$$
\begin{aligned}
N_t &= ceil\left(\frac{t_{final} - t_{init}}{t_{res}}\right) \\
N_\alpha &= ceil\left(\frac{\alpha_{final} - \alpha_{init}}{\alpha_{res}}\right) \\
N_\delta &= ceil\left(\frac{\delta_{final} - \delta_{init}}{\delta_{res}}\right) \\
N_{combinations} &= N_t \times N_\alpha \times N_\delta
\end{aligned}
\tag{6.13}
$$

Note that the *ceil* operator refers to a rounding of any decimal value towards positive infinity. The total number of combinations to be sampled, $N_{combinations}$, determines both the processing time and data storage capacity required to perform the analysis. There is a certain amount of data that is stored for each sampled deflection maneuver, and the amount of data storage required per combination can thus be computed analytically. The amount of numerical data stored during each iteration for post-processing and analysis may also be minimized. However, the required processing time may only be estimated since it depends on the performance and varying load state of the processor. The time per combination is also not constant, since as the time from simulation start to deflection, given by t_{scan} in equations (6.12) above, increases with each iteration, the amount of time over which the deflected NEO orbit is simulated decreases.

Finally, the computed performance index for each deflected trajectory is sorted to identify the maximum. Plots showing the multi-dimensional space containing deflection as a function of design space parameters are also generated in order to understand the solution space.

7. STANDOFF NUCLEAR DEVICE POSITIONING

7.1 Introduction

For the case of standoff nuclear detonation, the impulsive force is delivered to the NEO by means of a radiation burst that propagates in a spherical fashion from the nuclear detonation center. While the magnitude of the impulsive force imparted to the NEO is determined by the energy of the nuclear device, the properties and structure of the target NEO, and the standoff detonation distance, the direction of the resultant velocity change vector for the NEO is determined by the location of the detonation center in space relative to the NEO's center of mass. The associated geometry is shown in figure 7.1 below.

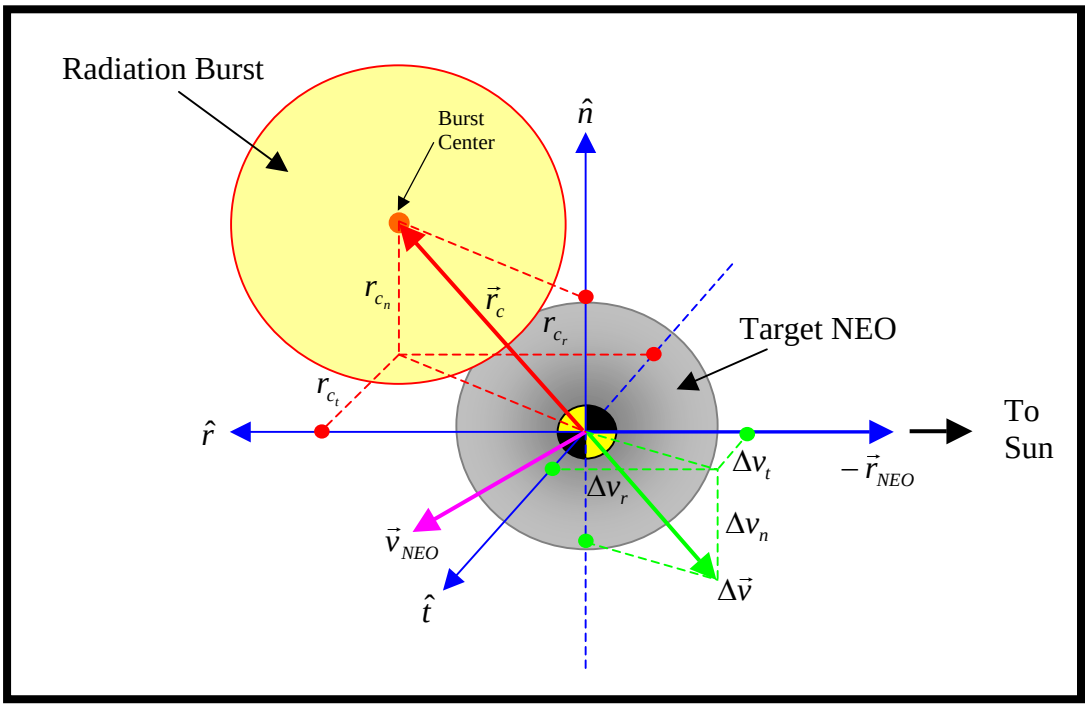

Figure 7.1: Irradiative Burst Targeting Geometry (not to scale)

7.2 Targeting Geometry

It is convenient to coordinate the detonation center location vector and the velocity-change vector in the Radial-Transverse-Normal (RTN) reference frame, centered at the target NEO's center of mass. A full description and derivation of this reference frame is included in appendix A.

Note in figure 7.1 that the target NEO's velocity vector is, in general, not aligned with the transverse direction, owing to the fact that the vast majority of NEO orbits (and the orbits of celestial bodies in general) are non-circular; in fact, most are significantly eccentric. However, the target NEO's velocity vector will always lie in the RT (radial-transverse) plane, by definition.

Following the geometry presented in figure 7.1 it can be seen that the position of the irradiative burst center is given by the following vector in the RTN frame:

$$\vec{r}_c = r_{c_r}\hat{r} + r_{c_t}\hat{t} + r_{c_n}\hat{n} \tag{7.1}$$

The resulting velocity change vector is given by

$$\Delta\vec{v} = \Delta v_r\hat{r} + \Delta v_t\hat{t} + \Delta v_n\hat{n} \tag{7.2}$$

Note that, since the velocity change vector results from the recoil of the target NEO in repsonse to the impulse delivered through its center of mass, the direction of the velocity change vector is exactly opposite the direction of the irradiative burst center position vector in in the RTN frame. If the magnitude of the of velocity change is expressed as $\Delta v = \|\Delta\vec{v}\|$, then the velocity change vector can be expressed as

$$\Delta\vec{v} = \Delta v(\hat{u}_{\Delta v}) \tag{7.3}$$

where $\hat{u}_{\Delta v}$ is the unit vector in the direction of the velocity change vector, given by

$$\hat{u}_{\Delta v} = \frac{\Delta \vec{v}}{\Delta v} \tag{7.4}$$

Thus, if the target NEO's radius, at the point on its surface which is pierced by the negative of the velocity change vector, is given by R_P and the prescribed standoff distance for the irradiative burst is given by d_s, then the position vector of the center of the irradiative burst in the RTN frame may be expressed as

$$\vec{r}_c = -(R_P + d_s)\hat{u}_{\Delta v} \tag{7.5}$$

The expression of equation (7.5) is convenient because the direction of the desired velocity change vector will be computed *a priori* according to an optimization scheme and it will then be the job of the guidance, navigation, and control (GNC) software/hardware onboard the nuclear device delivery craft to position the nuclear device such that the center of the burst will be as near to the coordinates given by equation (7.5) as possible. The set of maneuvers to achieve a given positioning may be computed with linearized dynamics such as the Clohessy-Wiltshire (CW) equations.

7.3 NEO Shape Considerations

Furthermore, the standoff distance for the burst, d_s, is computed in advance and is a function of the nuclear device capabilities and the properties of the target NEO. The target NEO's radius at the point on its surface that is pierced by the negative of the velocity change vector, R_P, will be determined from the results of the science operations as accurately as possible prior to the positioning of the nuclear device. This quantity is diagramed for clarity in figure 7.2 below.

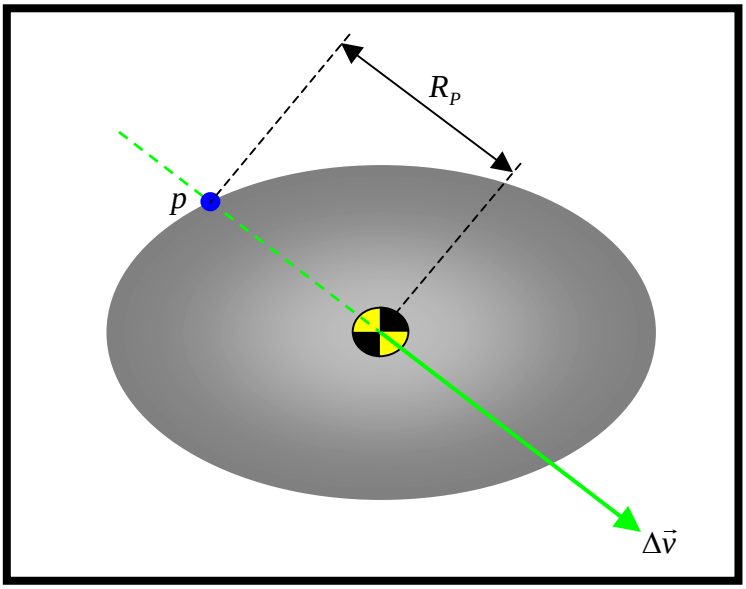

Figure 7.2: Diagram Indicating Target NEO Radius at the Surface Point Directly Below Irradiative Burst Center

Note that the target NEO is sketched as an ellipsoid in figure 7.2 while a spheroidal shape is used in figure 7.1. This is because the vast majority of NEOs are more elliptical than spherical, and are generally irregularly shaped. Therefore the determination of the target NEO's radius at the point of irradiative burst application is nontrivial and will be dependent on accurately determining the target NEO's center of mass and mapping its surface.

7.4 Reference Frame Considerations

It is most convenient to perform calculations for optimal velocity change vectors in the Heliocentric Inertial (HCI) frame, however the flight software that will govern the maneuvering of the nuclear device delivery craft will be operating in the RTN frame, which means that an appropriate transformation between the HCI and the RTN frame is required. The transformation matrix which transforms vectors from the HCI frame to the RTN frame is given by

$$\underline{R}_{RTN}^{HCI} = \begin{bmatrix} \cos(\omega+\nu)\cos(\Omega) - \cos(i)\sin(\Omega)\sin(\omega+\nu) & \cos(\omega+\nu)\sin(\Omega) + \cos(i)\cos(\Omega)\sin(\omega+\nu) & \sin(i)\sin(\omega+\nu) \\ -\sin(\omega+\nu)\cos\Omega - \cos(i)\sin(\Omega)\cos(\omega+\nu) & -\sin(\omega+\nu)\sin\Omega + \cos(i)\cos(\Omega)\cos(\omega+\nu) & \sin(i)\cos(\omega+\nu) \\ \sin(i)\sin(\Omega) & -\sin(i)\cos(\Omega) & \cos(i) \end{bmatrix} \quad (7.6)$$

The transpose of the transformation matrix in equation (7.6) will transform vectors from the RTN frame to the HCI frame. The angles in this rotation matrix are some of the heliocentric Keplerian orbital elements of the NEO. To see the derivation of the matrix in (7.6), refer to appendix A.

Placing the nuclear device delivery craft at the proper location in space relative to the target NEO's center of mass depends on a variety of factors, including how well the target NEO's center of mass location is known. Determining the center of mass of a given NEO is problematic owing to the irregularities found in most NEO's shape and mass distribution.

However, methods do exist for locating the target NEO's center of mass using markers placed on its surface in combination with sensors on the monitoring spacecraft. Development of these methods is beyond the scope of this work and the reader is referred to a dissertation on this very topic entitled "Talon and Cradle – Systems For The Rescue of Tumbling Spacecraft and Astronaunts – A Preliminary Design" by Dunning Idle V [10]. Among many other things, Idle presents a methodology for accurately estimating the center of mass location for a general tumbling body through remote observation. This is precisely the technique required here.

7.5 Conclusions

The impulsive $\Delta\vec{v}$ imparted to a target NEO will be determined prior to a deflection mission such that it is oriented optimally and will thus have maximum effect. The $\Delta\vec{v}$ is caused by the recoil of the NEO in the direction identically opposite the location of the irradiative burst from a standoff nuclear detonation. Therefore, the center of this burst must be located along a vector identically opposite

$\Delta\vec{v}$. Thus, once $\Delta\vec{v}$ is known, the proper coordinates for the nuclear device can be computed, taking into consideration the optimal standoff detonation distance and the radius of the NEO immediately below the detonation center. These coordinates are computed in the RTN frame, relative to the NEO's center of mass, and hence the center of mass location must be determined. Previous research into the dynamics of stabilizing general tumbling bodies in space provides descriptions of techniques for determining an object's center of mass location via remote observation, and such techniques will be applied on-orbit during a NEO deflection mission to facilitate the proper positioning of the nuclear device prior to detonation such that the desired optimal $\Delta\vec{v}$ orientation is achieved and the deflection is maximized.

8. ORBITAL SIMULATION METHODS

8.1 Introduction

The majority of the analysis presented herein is based upon simulating orbital motion and analyzing the results. Thus, the primary software tool utilized is a custom N-body propagator engine that simulates the orbital motion of interest. A complete treatment of the simulation procedures and gravitational physics is presented in appendix B.

8.2 Orbital Mechanics

Orbital mechanics is primarily concerned with the evolution of a system governed by mutual gravitation, though in truth it includes all the factors that contribute to the space environment, including gravitation. While gravitation is the foremost contributor to the evolution of orbits in the solar system, there are other factors which cannot be ignored for ultra-precise simulation, including solar radiation pressure, uneven thermal energy absorption and radiation (Yarkovsky Effect), weak atmospheric drag (when in the region of a planet's exosphere), magnetic forces (when in the region of a planet's magnetic field), the effects of a non-uniform gravitational field (when in the vicinity of a planet), collisions (ranging from tiny impingements by micrometeoroids to crushing collisions between behemoth asteroids), and outgassing (particularly on comets in the form of jets which are most active during the portion of the orbit arc that is close enough to the Sun to sufficiently heat the volatiles). While inclusion of these factors does provide the most complete model of motion for objects in the Solar System, it should be noted that these non-gravitational forces are generally exceedingly small in magnitude and are also very difficult to model accurately.

Hence, a balance must be struck in any analysis by considering how much accuracy will truly be gained over the time interval of simulation and how much more computationally intensive and difficult the simulation becomes with the inclusion of

more and more non-gravitational forces. Generally, when simulations are being run over time intervals more than several years in length, it is necessary to include as many of these natural non-gravitational forces as possible because their effects are cumulative over time. It is even possible to harness this property of the system for NEO deflection in some cases, provided there is on the order of decade's worth of warning time. For instance, dusting an NEO's surface with a certain pigment should change its solar flux absorbance thus changing the impact upon it from the Yarkovsky effect, which changes its position relative to Earth over a long period of time. This could, in theory, avert a NEO-Earth collision under the right conditions, albeit in an uncontrolled and hence unpredictable fashion.

For the purposes of analyzing impulsive NEO deflection, the orbital simulations herein will be restricted to only simulating gravitational forces because processing time is at a premium. Running optimal deflection searches that also compute the effects of natural non-gravitational forces along with the N body equations would take much longer. Most importantly, the level of precision gained is primarily useful for long-term, ultra-precise prediction of planetary or spacecraft positions and this is not a requirement here. What is required is that the simulation be *dynamically* accurate, meaning that it faithfully represents the dynamics of the system and hence gives a good characterization of the evolution of a NEO's orbit subsequent to an applied deflection.

9. MODEL AND METHODOLOGY VALIDATION

9.1 Introduction

This section will demonstrate the validity of the solar system simulation model described in section 8, as well as validate and explore the optimal deflection determination system developed in section 6. The NEO used for benchmark data is the asteroid designated 1991 RB, which has made several close approaches to Earth in the past though there is no danger of it ever colliding with our planet. This is the same asteroid used in a test case for an optimal NEO deflection system developed by another researcher, which will be discussed herein.

The validity of the solar system model will be demonstrated first, and the validity of the optimal deflection determination system will be demonstrated second. Pertinent background information on the scenarios examined will also be provided.

9.2 Asteroid 1991 RB

While the orbit of 1991 RB is fairly well understood, little is known about the asteroid's physical properties. This asteroid was discovered on September 4th, 1991 by R.H. McNaught at the Siding Spring Observatory [22], located in the Warrumbungle Mountains in the central west region of New South Wales in Australia [23]. Its apparent magnitude is 19.00 and its mean diameter is estimated to be 0.5 – 1.1 km [22].

9.2.1 Asteroid 1991 RB Orbital Properties

Asteroid 1991 RB is classified as an Apollo asteroid and follows a fairly eccentric and inclined orbit about the Sun, with an eccentricity and nominal inclination of approximately 0.48 and 19.6°, respectively. The complete orbital elements for 1991RB are given in table 9.1 below.

Table 9.1: Orbital Elements for Asteroid 1991 RB on August 18th, 2005, 00:00:00 UT [24]

a	1.45438360980929 AU
e	0.485604672558029
i	19.5928647606947°
Ω	359.482372416714°
ω	68.7619235043386°
M	306.726124765938°

As mentioned previously, this asteroid has made several close approaches to Earth, and some of these are tabulated in table 9.2 below.

Table 9.2: Selected Close Approaches to Earth of Asteroid 1991 RB [25]

Date/Time	Nominal Distance from Earth [AU]
1984/09/18.71940	0.0442681
1991/09/24.96647	0.0970033
1998/10/03.36949	0.175507
2041/02/21.98607	0.194285

9.2.2 Asteroid 1991 RB Physical Properties

As previously stated, little is known about asteroid 1991 RB's physical properties. However, an estimate of the asteroid's mass is required in order to include it in the solar system simulation model. Therefore, reasonable assumptions about some of its physical properties are made to facilitate subsequent simulations.

Since no shape data is available, this asteroid will be modeled as a sphere with a radius of 0.4 km, determined by averaging the upper and lower bounds for the mean

diameter of 1.1 and 0.5 km, respectively. These estimates are used to compute the volume of the asteroid according to the equation for spherical volume, given by

$$V_{SPHERE} = \frac{4}{3}\pi R^3 \tag{9.1}$$

where

R = radius of sphere

The next assumption is that the asteroid has a mean density[1] of 2.7 g/cm^3. This allows the estimated mass of the asteroid to be computed as follows

$$M_{ASTEROID} = V_{SPHERE} \times \rho_{ASTEROID} \tag{9.2}$$

where

$\rho_{ASTEROID}$ = mean asteroid density

Using the data presented above in conjunction with equations (9.1) and (9.2), the computed value for 1991 RB's mass is approximately 7.2382×10^{11} kg.

9.3 Simulation Results

The validation of the solar system simulation was conducted by performing a series of simulations of asteroid 1991 RB's motion and then comparing the results to known sources. Specifically, the asteroid's orbit was simulated, along with that of

[1] This mean density value is one that is commonly accepted for many NEAs. However, were some compositional taxonomic information available for 1991 RB, a better estimate of the mean density would be possible. Note also that the *mean density* accounts for whatever structural or compositional irregularities the asteroid may actually manifest. Alternatively, this may be interpreted as assuming the asteroid to be identically homogenous structurally and compositionally, and thus the assumed density is simply the constant actual density. However, in that case the density value would still also be the mean density.

Earth, and the distance between the asteroid and the Earth was computed at a selected epoch. This distance was then compared to that given by known, reliable sources, in this case the Near Earth Objects – Dynamics Site (NEODyS), maintained by the University of Pisa in Italy, and the Jet Propulsion Laboratories (JPL) in California, USA. A reasonable agreement between the Earth-Asteroid distance figures given by the current simulation and the two sources given above is taken to be a validation of the fact that the solar system simulation model is working to within required accuracy.

Owing to the many perturbations in the interplanetary space environment, including multi-body gravitational forces, solar radiation pressure, and the Yarkovsky Effect, to name but a few, it is very difficult to model the orbits of solar system objects with extremely high accuracy, especially using custom simulation code on a personal workstation computer. However, the purpose of the current research is to analyze the dynamics of NEO orbits and applied deflections, which only requires that the model be consistent and dynamically accurate, capturing the *character* of the NEO orbit and its response to applied perturbations for the purposes of mitigation efficacy assessment.

9.3.1 Basic Simulation

The selected day and time for analysis is 1998/10/03.36949, and the corresponding distance between 1991 RB and Earth is given as 0.175507 AU in table 9.2 above, which was taken from NEODyS data. In the basic simulation, the only objects included aside from Sun are 1991 RB and Earth. The orbital elements for 1991 RB given in table 9.1 above were used to generate the asteroid's initial state vector according to the methods presented in appendix A. The orbital elements for Earth were obtained at the same epoch from *The Astronomical Almananc For The Year 2005* [26] and will not be presented explicitly herein. A three-dimensional perspective plot of the simulation results is presented in figure 9.1 below.

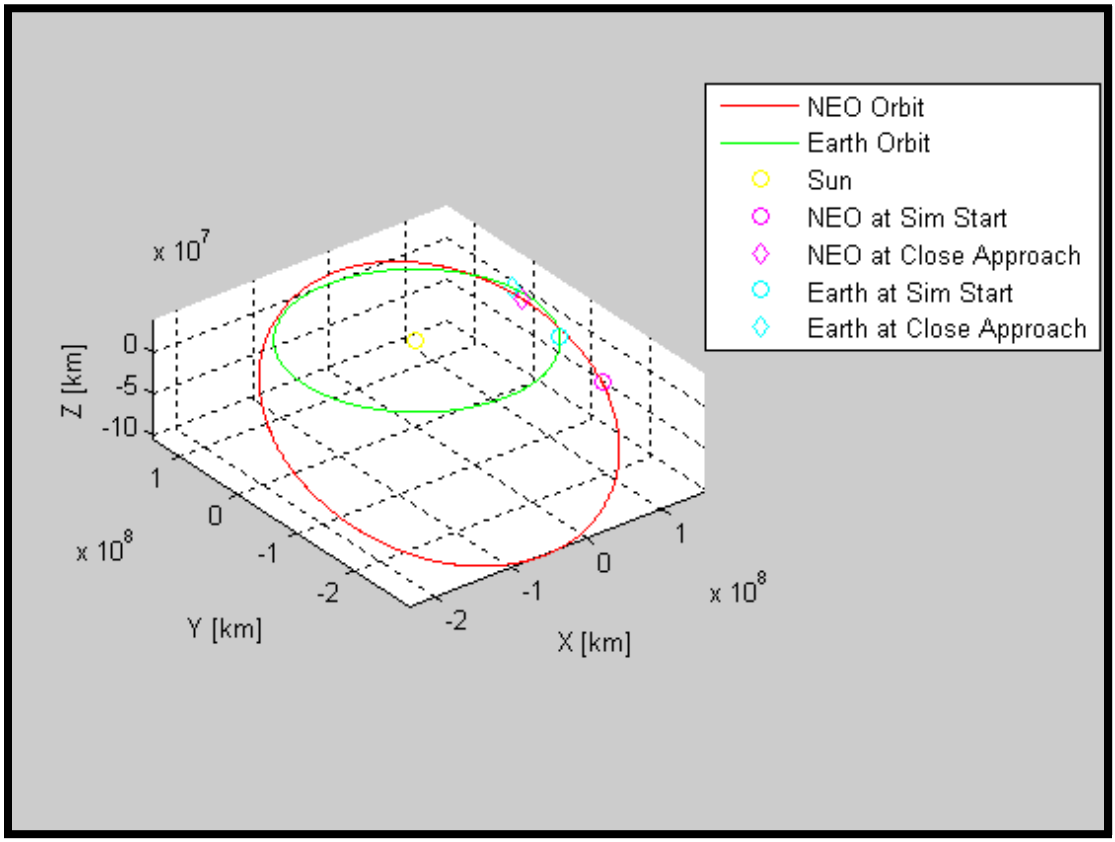

Figure 9.1: Simulated Orbits of Asteroid 1991 RB and Earth with the Final Positions on 1998/10/03.36949 Marked

A plot showing the orbits of 1991 RB and Earth in the ecliptic plane is given in figure 9.2 below, and a corresponding plot from a JPL two-body simulation is shown in figure 9.3 for comparison. Note that the positions shown in those plots agree nicely. Note also the computed distance between the Earth and 1991 RB of 0.172 AU shown on the JPL plot. This value is only approximate of course, owing to the two-body dynamics employed in the JPL simulation, and, given its approximate nature, it is in good agreement with the NEODyS value of 0.175507 AU.

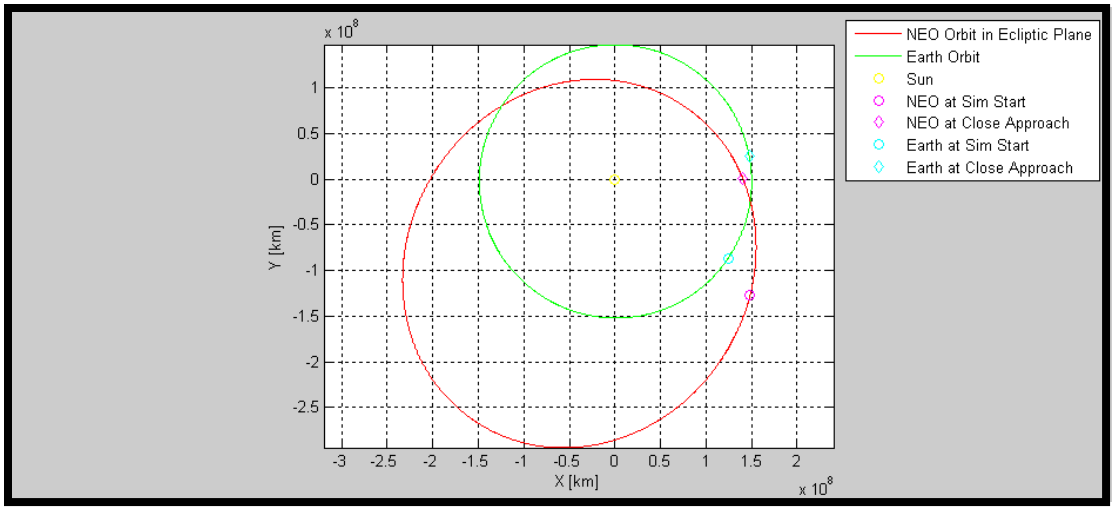

Figure 9.2: Ecliptic Plane View of Earth and Asteroid 1991 RB Orbits with Final Positions on 1998/10/03.36949 Marked

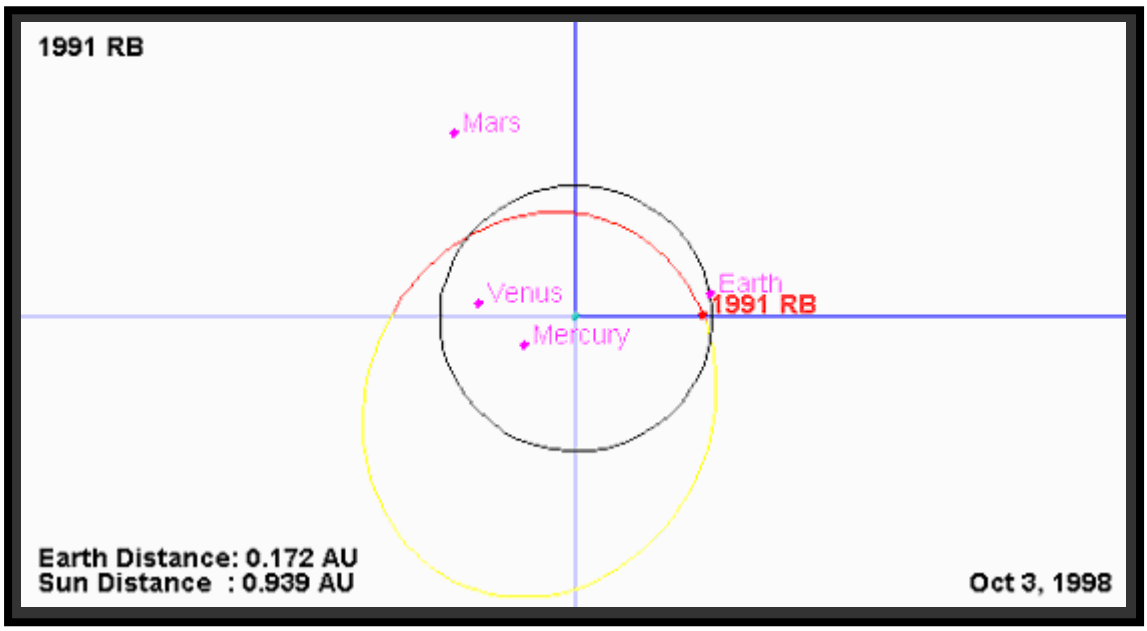

Figure 9.3: JPL Orbit Diagram of Earth and Asteroid 1991 RB on 1998/10/03.36949 using Two-body Dynamics

The computed distance between Earth and 1991 RB for the current simulation on the day and time in question is 0.174794 AU, which agrees well with the actual distance

provided by NEODyS of 0.175507 AU given that only 3 body dynamics are employed whereas the NEODyS data is based on observation and statistical orbit determination techniques.

9.3.2 Extended Simulation

While the accuracy demonstrated by the results of the basic simulation above is quite sufficient for this work, an extended simulation was performed in an attempt to refine the results further. For the extended simulation, all the planets in the solar system, including Earth, of course, are included, along with the asteroid. The ephemeris data for the planets were obtained from *The Astronomical Almananc For The Year 2005* [26] and will not be presented explicitly herein. Such an extensive N body propagation, with a total of 10 bodies orbiting the Sun, is much more computationally intensive than the basic simulation with 3 bodies (Earth and Asteroid orbiting the Sun), and thus this extended simulation will not normally be performed for optimal deflection orientation searches for the sake of expediency. As will be shown later, the difference in accuracy is not sufficient to significantly alter the optimal deflection orientation results, especially when only short time intervals, on the order of several years or less, are considered. The orbital plots resulting from the extended simulation are not presented because they are not visibly different from those presented in the figures above for the basic simulation. The computed distance between Earth and 1991 RB for the extended simulation is 0.175630 AU, an even better agreement with the NEODyS value of 0.175507 AU.

9.3.3 Orbital Model Validation Conclusions

Based on the comparison of current simulation results with the NEODyS database and the JPL two-body propagation, the current simulator is found to be valid within expected, acceptable limits. All results are tabulated in table 9.3 below.

Table 9.3: Comparison of Simulation Results and Other Data Sources

Source	Distance Between Earth and 1991 RB
NeoDys Database	0.175507 [AU]
JPL Two-Body Propagation	0.172 [AU]
Current Basic Simulation	0.174794 [AU]
Current Extended Simulation	0.175630 [AU]

9.4 Optimal Deflection Orientation Determination Validation

The optimal deflection orientation determination method developed previously in section 6 will be validated against the method developed by Conway in his work titled "Optimal interception and deflection of Earth-approaching asteroids using low-thrust electric propulsion" [3]. The first part of Conway's work deals with optimizing the low-thrust trajectory to intercept the asteroid, which is not a major focus of this work. However, the second part deals with maximizing the deflection of the asteroid by optimizing the orientation of the impulse applied to the asteroid at the time of interception, which is at the heart of the current work.

Conway uses asteroid 1991 RB as a test case for the demonstration of his methods, and this is why it was convenient to use 1991 RB in the orbit model validation presented in the previous section.

The relevant portion of Conway's work presents an optimal deflection orientation determination method that utilizes a linearized model (state transition matrix) for the asteroid, allowing the application of velocity perturbations in arbitrary orientations in three dimensions. However, his approach is limited in the sense that it requires that the deflecting impulse be applied at a time such that the asteroid does not make a full revolution around the Sun before collision with Earth, or in the case of 1991 RB, closest approach to Earth; this restriction is a result of the linearization. Conway's approach was motivated in part by the restrictions of previous work in the field of optimal asteroid deflection; for example, Park and Ross explicitly optimize the deflection of asteroids in their work entitled "Two-Body Optimization for Deflecting Earth-Crossing Asteroids" [21], but the derivation assumes that the

asteroid's orbit lies entirely in the same plane as Earth's even though many asteroids have orbits with significant inclinations, as exemplified by 1991 RB with inclination ~ 19°. In a similar fashion, the limitations of Conway's result, that being that the time at which the optimal deflection is applied cannot be arbitrary, motivated the current work, which presents a method for finding optimal deflection solutions for arbitrary NEO orbits and arbitrary deflection times. Conway linearizes because the three-dimensional problem resists explicit optimization and it is also for this reason that design space search methods, rather than attempts at explicit optimization, are employed here.

An intuitive result obtained by Conway, Park and Ross, and the current research is that the efficacy of the deflection increases in an essentially linear fashion with lead time, which is the amount of time between when the deflection is applied and when the collision (or closest approach) would have occurred absent mitigation. This makes clear the importance of determining optimal deflection orientations for arbitrary application times; in a true threat situation, the deflection should be applied at the earliest time possible, hopefully well in advance of the NEO's final solar orbit before collision.

In the sections that follow, the scenario for 1991 RB examined by Conway will be analyzed with the current optimal deflection orientation determination methods and the results will be compared to validate the current method and further explore the finer structures of the deflection solution space.

9.4.1 Close Approach Scenario

As stated, 1991 RB only makes a close approach to Earth and does not collide. Thus, the goal of the optimization of the deflection is not to cause the asteroid to miss Earth (it already misses Earth), but rather to maximize the distance between Earth and the asteroid at the time of closest approach (t_{CA}). Conway provides orbital elements

for asteroid 1991 RB on September 15th, 1991, and these are tabulated in table 9.4 below.

Table 9.4: Asteroid 1991 RB Orbital Elements, 1991/9/15, 00:00:00 UT[1] [3]

a	1.4524 [AU]
e	0.4846
i	19.580°
Ω	359.599°
ω	68.708°
M	328.08°

Conway also states that 1991 RB makes a close approach to Earth on September 19th, 1998[2], coming to within 0.04 AU of our planet. However, an examination of the NEODyS database shows no close approach event on that date. In fact, the close approach on October 3rd, 1998 that was previously referenced in the orbital model validation section is the only close approach to Earth by 1991 RB for the year 1998.

However, table 9.2 above does show a close approach to Earth by 1991 RB of 0.0442681 AU on September 18th, 1984. This author believes it is possible that this close approach is the one that Conway meant to refer to.

In any case, the date that will be used for the subsequent "close approach" scenario is the same date used by Conway: September 19th, 1998, 00:00:00 UT. Simulation results show that the distance between 1991 RB and Earth at this epoch is 0.203242 AU, and the JPL two-body orbit propagator indicates a distance of 0.199 AU, a good agreement considering the disparity between the simulation methods. A plot of the current simulation results is shown, along with a plot from the JPL propagator, in figures 9.4 and 9.5 below.

[1] Conway does not explicitly state that the epoch for the orbital elements is at precisely 00:00:00 UT on the date given, but this author is assuming that is the case.
[2] No time of day is provided to accompany this date. Again, the author is assuming a time of 00:00:00 UT.

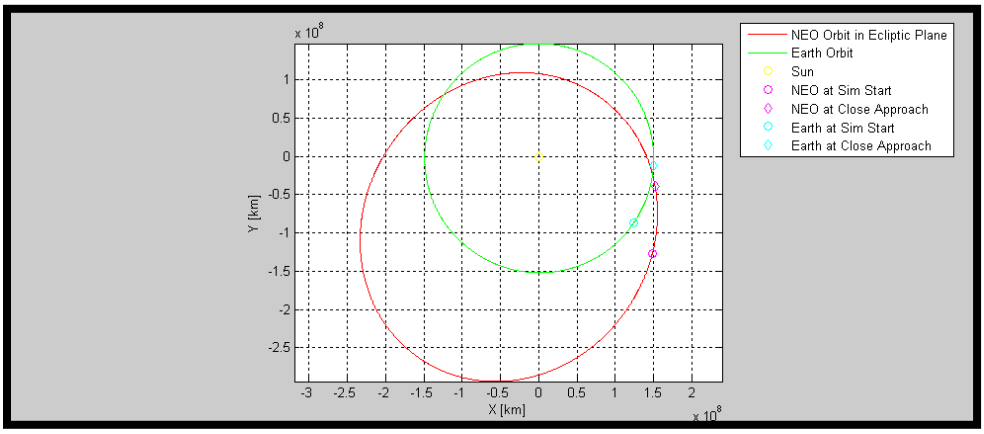

Figure 9.4: Earth and Asteroid 1991 RB on 1998/9/19.00 using the Current Basic Simulation (3-body Dynamics)

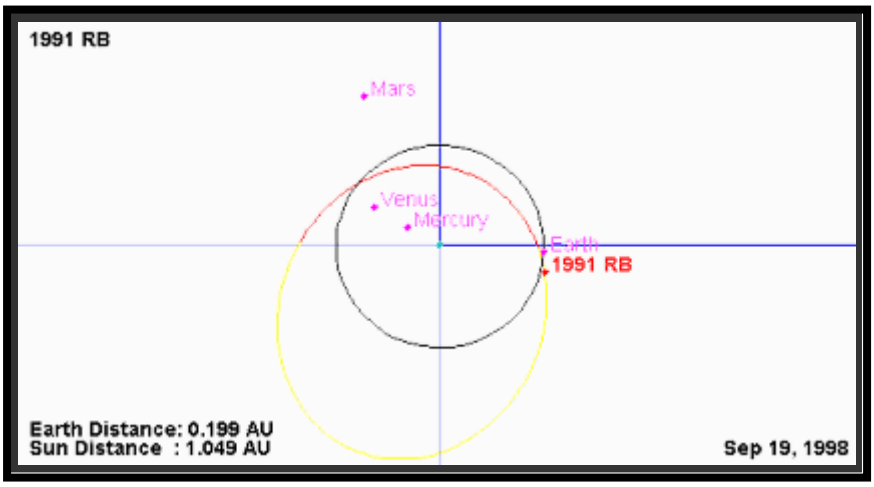

Figure 9.5: JPL Orbit Diagram of Earth and Asteroid 1991 RB on 1998/9/19.00 using Two-body Dynamics

While Conway provides orbital elements for 1991 RB, given in table 9.4 above, the orbital elements from JPL, given in table 9.1, are provided with greater decimal accuracy and thus will be the elements used to generate 1991 RB's initial state, which will then be integrated through time as needed.

9.4.2 Optimal Deflection Study

In this study we will be considering the same deflection times for which Conway provides optimal deflection results, shown in figure 9.6 below.

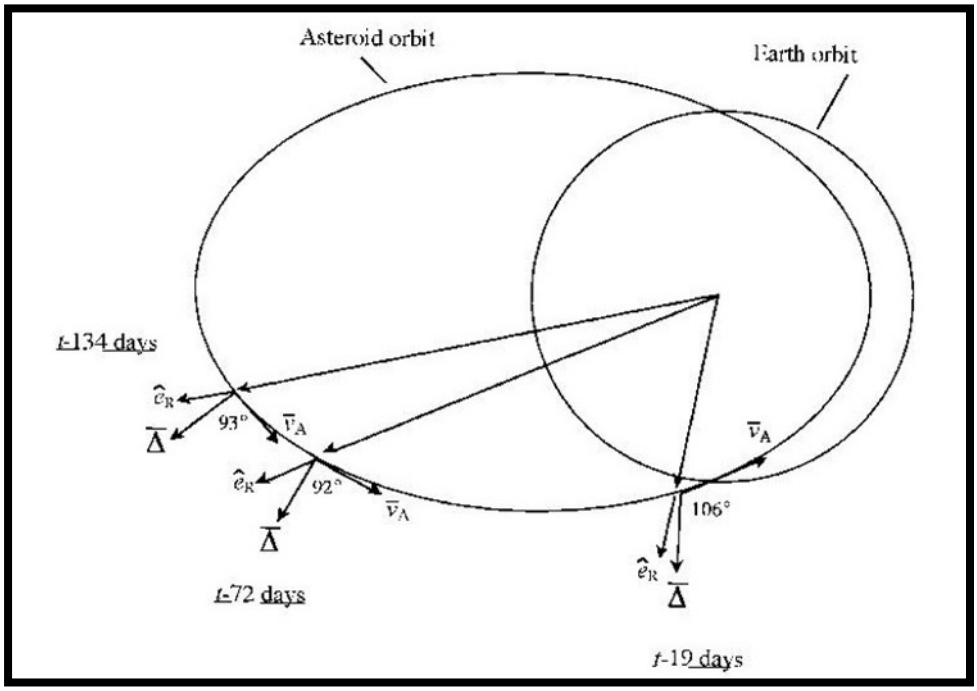

Figure 9.6: Conway's Optimal Directions for Application of Deflection Impulses at Selected Points Along the Asteroid Orbit [3]

Figure 9.6 indicates the orientation of the optimal deflection impulse vectors but not the resulting magnitude of deflection. Conway provides this information in the form of a graph, shown in figure 9.7 below. The magnitude of the perturbing velocity vector, $\Delta\vec{v}$, applied to the asteroid is given by Conway as 1 m/s. He states that this is an unrealistic value, unreachable especially for large asteroids greater than several hundred meters in mean diameter. Thus, this velocity perturbation magnitude is an unrealistic value for 1991 RB, whose mean diameter is somewhere between 500 and 1100 m. However, a smaller velocity perturbation magnitude would not have yielded useful (i.e., on the order of one Earth radii or larger) asteroid deflection results for the short time intervals examined by Conway (a couple of hundred days or less).

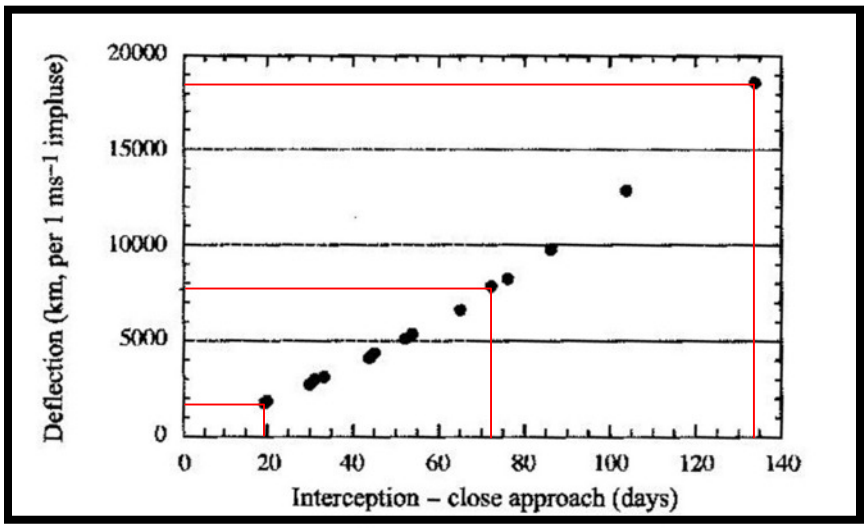

Figure 9.7: Conway's Resulting Optimal Deflection Magnitudes [3]

The red colored lines drawn on figure 9.7 above were placed there by the author to make the data for the three deflection points shown in figure 9.6 easier to read. These values were read from figure 9.7 and are tabulated in table 9.5 below.

Table 9.5: Estimated Values for Conway's Optimal Deflections in Figure 9.7

Time Before Close Approach of Asteroid to Earth [days]	Estimated Deflection from Conway's Graph [km]
19	1700
72	7700
134	18400

9.4.3 Conway's Performance Index

Since Conway's model uses linearized two-body dynamics, his performance index is restricted to be the distance between the asteroid on the perturbed orbit and the asteroid on the unperturbed orbit. The linearized dynamics model takes the form a state transition matrix that provides the perturbation of the asteroid's motion relative to the nominal unperturbed trajectory. These equations are of the form

$$\begin{bmatrix} \delta\vec{r} \\ \delta\vec{v} \end{bmatrix} = \underline{\Phi}(t, t_0) \begin{bmatrix} \delta\vec{r}_0 \\ \delta\vec{v}_0 \end{bmatrix} = \begin{bmatrix} \underline{\tilde{R}} & \underline{R} \\ \underline{\tilde{V}} & \underline{V} \end{bmatrix} \begin{bmatrix} \delta\vec{r}_0 \\ \delta\vec{v}_0 \end{bmatrix} \tag{9.3}$$

Thus the position pertubation is computed by

$$\delta\vec{r}(t) = [R]\delta\vec{v}_0(t_0) \tag{9.4}$$

which leads to the required form of the performance index,

$$P_{CONWAY} = \left\| \delta\vec{r}(t_{CA}) \right\| \tag{9.5}$$

Conway writes a quadratic form for equation (9.4) and uses the eigenspace to find the optimal perturbing velocity vector, $\delta\vec{v}_{OPT}(t_0)$, according to the performance index in equation (9.5).

This performance index measures by how much the asteroid's perturbed position in space changes with respect to its unperturbed position *at what would otherwise have been the exact time of closest approach*. The explicit form of this performance index is given as

$$P_{CONWAY} = \left\| (\vec{r}_{NEO}(t_{CA}))_{DEFLECTED} - (\vec{r}_{NEO}(t_{CA}))_{UNDEFLECTED} \right\| \tag{9.6}$$

The drawback to this performance index is that the distance between the Earth and the asteroid is not considered at all, and this is the crucial quantity of interest in the field of NEO mitigation.

Using this performance index in the current optimal deflection determination system yielded results that closely match those of Conway.

9.5 Optimal Deflection Determination Results

The current optimal deflection determination algorithm was run using Conway's performance index in equation (9.6) for the three cases given in table 9.5 above in an attempt to reproduce Conway's results and thereby provide a measure of validation for the current methods. The results for each case are presented below.

9.5.1 Case 1: 134 Days Before September 19th, 1998

The optimal deflection vector orientation was computed using the current methods and the results are tabulated in table 9.6 below.

Table 9.6: Optimal Deflection Results 134 Days Before Close Approach Date

	Deflection [km]	Angle from Asteroid Velocity Vector	Azimuth Angle in RTN Frame
Current	18182	96.77°	240°
Conway	18400	93°	-

A plot of the relevant vectors is shown in figure 9.8 below, not to scale.

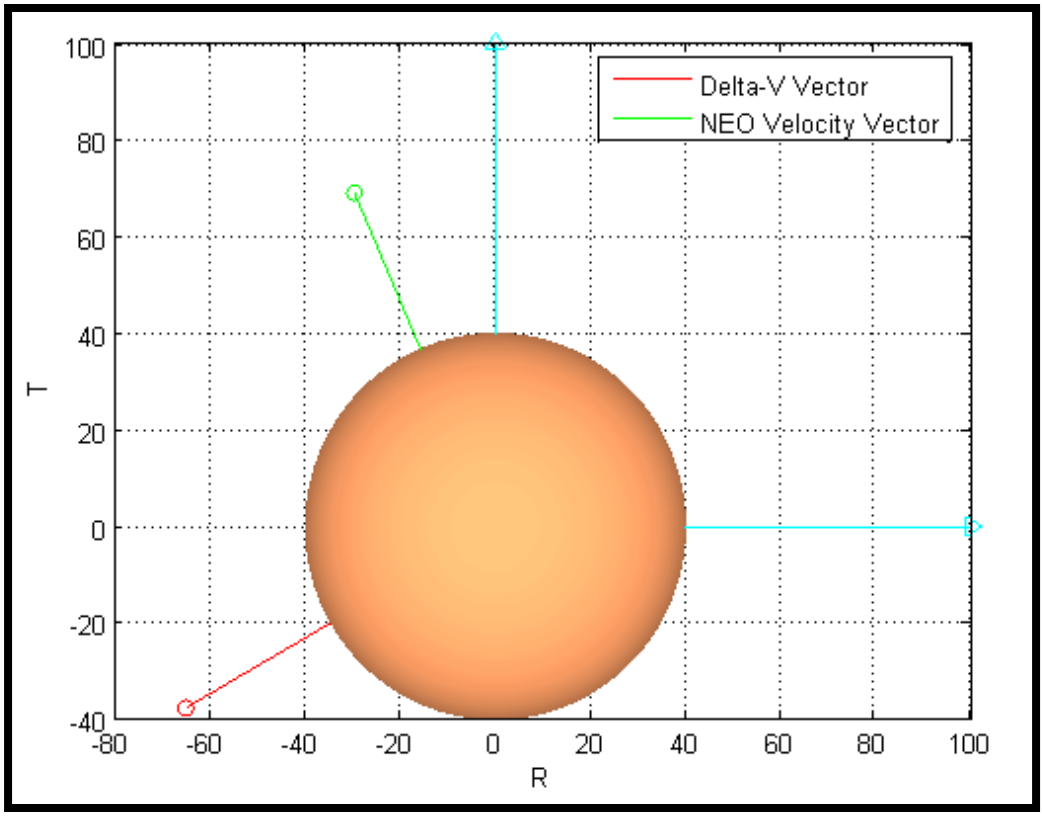

Figure 9.8: Optimal Deflection Vector at 134 Days Before Close Approach Date

Note that this result is actually quite different from that found by Conway. While the values of the angle between the asteroid's velocity vector and the perturbing velocity vector are very close (93° and ~96°), the direction of the optimal perturbing velocity vector found by the current method is nearly ~180° away from the direction of the optimal perturbing velocity vector found by Conway's linearized model. This can be seen by comparing figures 9.6 and 9.8 above. The apparent mystery is solved by examining a plot of the deflection as a function of the azimuth angle, given in figure 9.9 below.

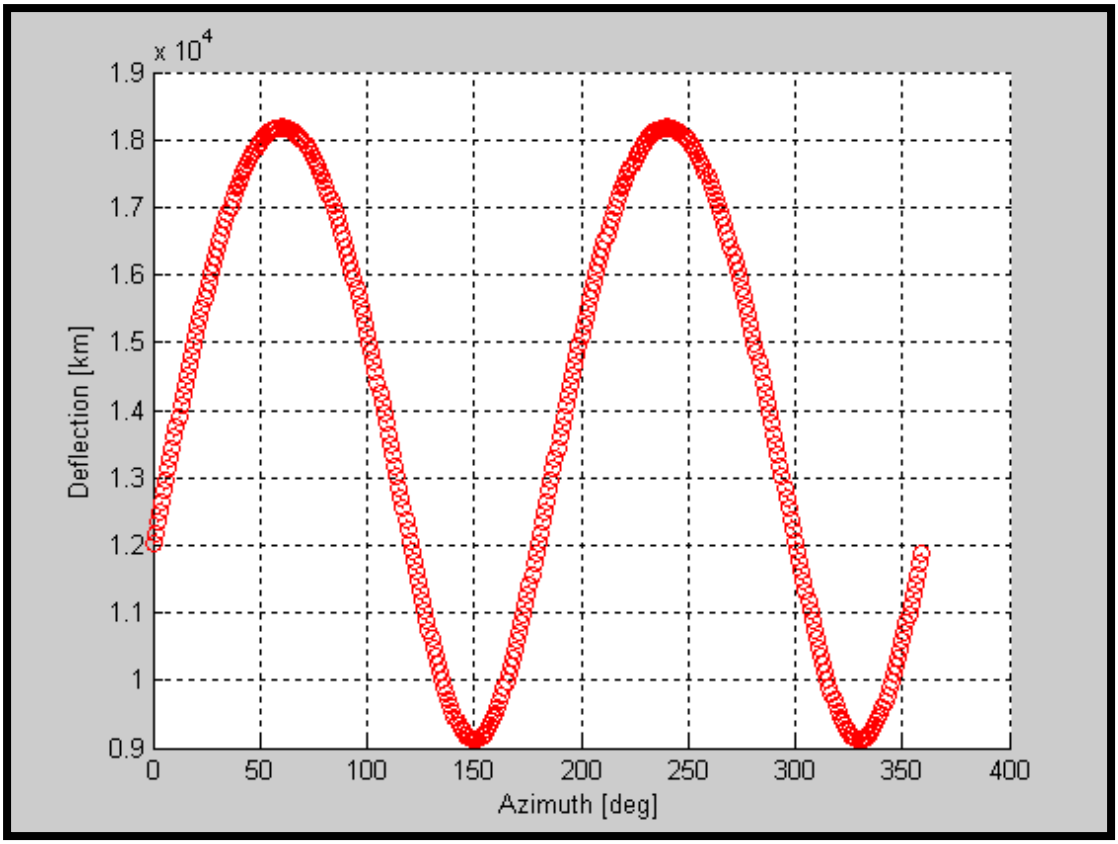

Figure 9.9: Deflection versus Azimuth at 134 Days Before Close Approach Date

The interesting result of the optimization is that there are in fact two excellent deflection solutions rather than just one. This is a result of the performance index Conway employs. The two solutions are very close in magnitude, that is, both solutions provide nearly the same amount of deflection. The data for the near optimal solution is provided in table 9.7 below.

Table 9.7: Near Optimal Deflection Results 134 Days Before Close Approach Date

	Deflection [km]	**Angle from Asteroid Velocity Vector**	**Azimuth Angle in RTN Frame**
Current	18181	83.22°	60°
Conway	18400	93°	-

Note that the near optimal solution, separated from the optimal solution by exactly 180° in azimuth, is only less than the optimal by 0.804711 km, or 0.004%, which is negligible. Note also that this near optimal solution is actually most likely the non-linear version of the linearized solution found by Conway. While the difference in the angles between the asteroid velocity vector and the perturbing velocity is approximately 10° (~83° vs. 93°), the *character* of the solutions is the same, and this can be seen by comparing figure 9.10 below to figure 9.6 above.

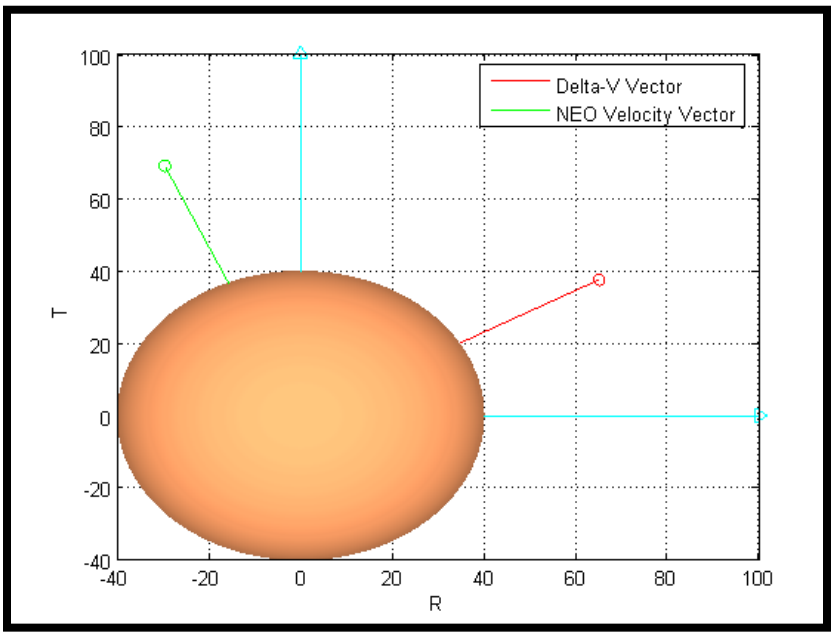

Figure 9.10: Near Optimal Deflection Vector at 134 Days Before Close Approach Date

Another interesting result is that there are also two worst solutions, as shown by figure 9.9 above. Even more interesting is that these worst solutions are actually only approximately 50% less effective than the best solutions, as shown in figure 9.11 below, which shows the deflection, normalized such that the optimal deflection value is 1, versus azimuth angle.

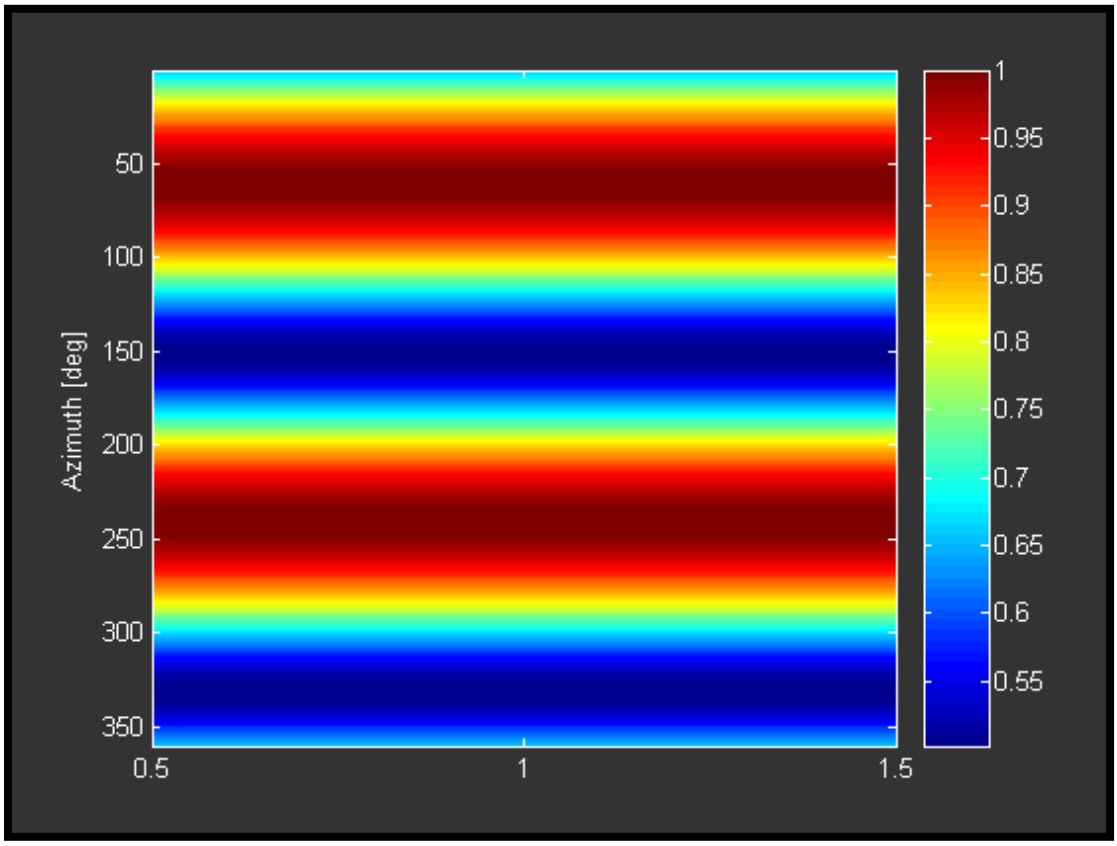

Figure 9.11: Colormap of Normalized Deflection versus Azimuth at 134 Days Before Close Approach Date

Thus even the worst solutions in this case appears to still deflect the asteroid by approximately 9000 km, more than one Earth equatorial radius.

9.5.2 Case 2: 72 Days Before September 19th, 1998

The character of the solutions found for this case is the same as that of the solutions discussed in the previous case. The relevant data are tabulated in tables 9.8 and 9.9 below, and the relevant figures follow.

Table 9.8: Optimal Deflection Results 72 Days Before Close Approach Date

	Deflection [km]	Angle from Asteroid Velocity Vector	Azimuth Angle in RTN Frame
Current	7682.7	82.35°	249°
Conway	7700	92°	-

Table 9.9: Near Optimal Deflection Results 72 Days Before Close Approach Date

	Deflection [km]	Angle from Asteroid Velocity Vector	Azimuth Angle in RTN Frame
Current	7682.6	97.64°	69°
Conway	7700	92°	-

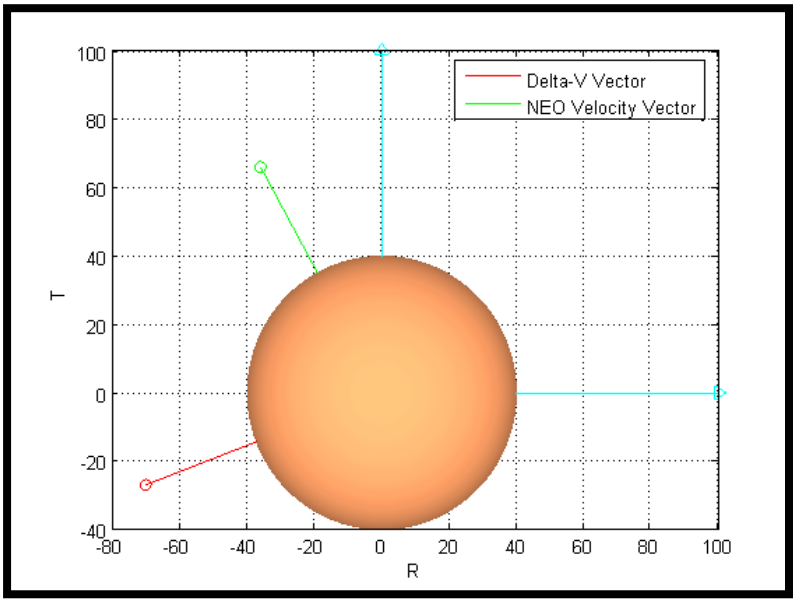

Figure 9.12: Optimal Deflection Vector at 72 Days Before Close Approach Date

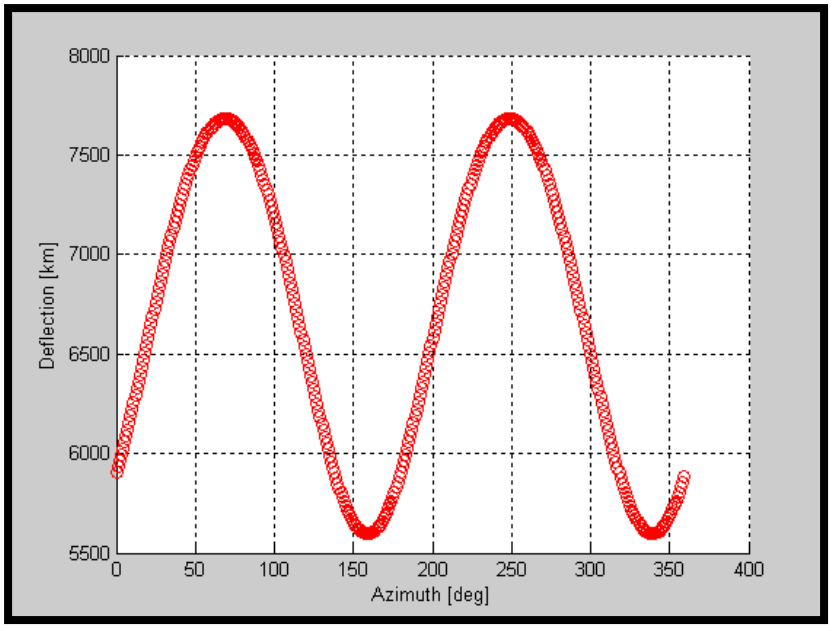

Figure 9.13: Deflection versus Azimuth at 72 Days Before Close Approach Date

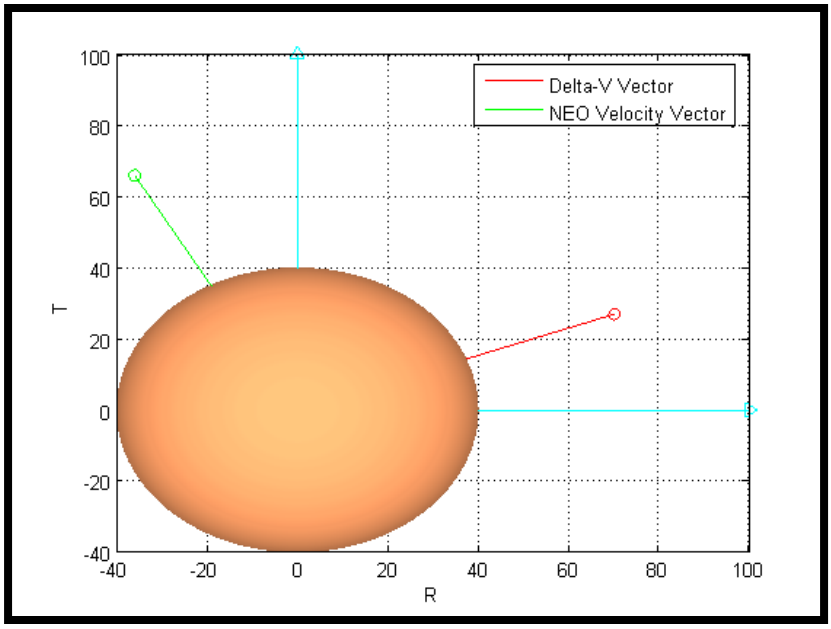

Figure 9.14: Near Optimal Deflection Vector at 72 Days Before Close Approach Date

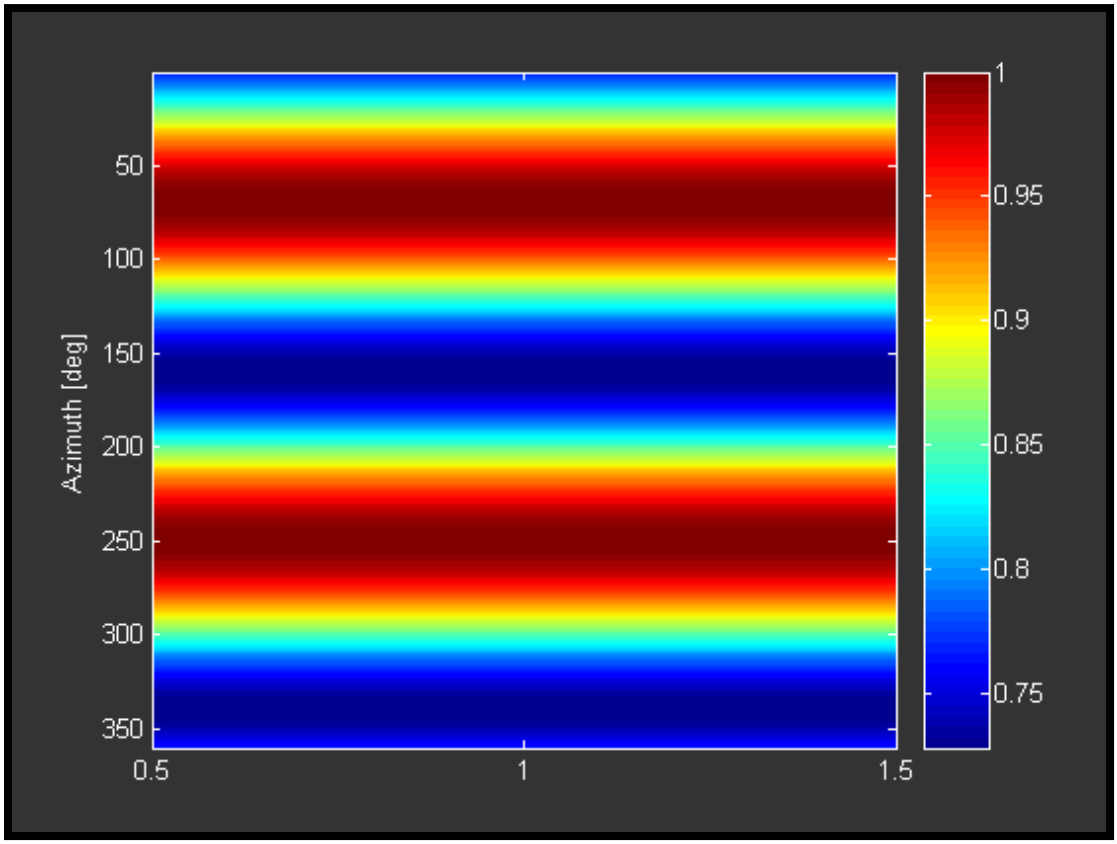

Figure 9.15: Colormap of Normalized Deflection versus Azimuth at 72 Days Before Close Approach Date

Figure 9.15 above illustrates the only difference between this case and the previous case, this being that the worst solutions are only approximately 27% less effective than the optimal and near-optimal solutions, whereas in the first case the worst solutions were 50% less effective than the optimal and near-optimal.

9.5.3 Case 3: 19 Days Before September 19th, 1998

The character of the solutions found for this case is the same as that of the solutions discussed in the previous two cases. The relevant data are tabulated in tables 9.10 and 9.11 below, and the relevant figures follow.

Table 9.10: Optimal Deflection Results 19 Days Before Close Approach Date

	Deflection [km]	Angle from Asteroid Velocity Vector	Azimuth Angle in RTN Frame
Current	1691.807	70.55°	262°
Conway	1700	106°	-

Table 9.11: Near Optimal Deflection Results 19 Days Before Close Approach Date

	Deflection [km]	Angle from Asteroid Velocity Vector	Azimuth Angle in RTN Frame
Current	1691.806	109.45°	82°
Conway	1700	106°	-

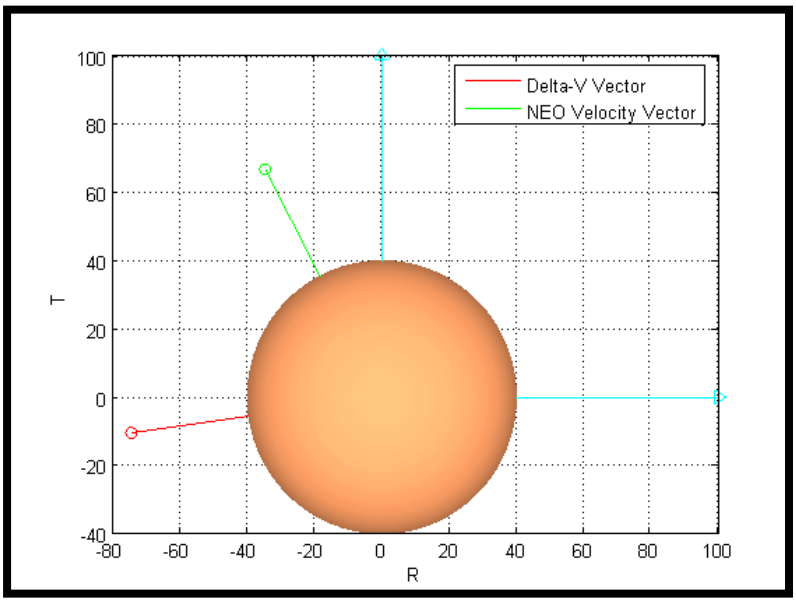

Figure 9.16: Optimal Deflection Vector at 19 Days Before Close Approach Date

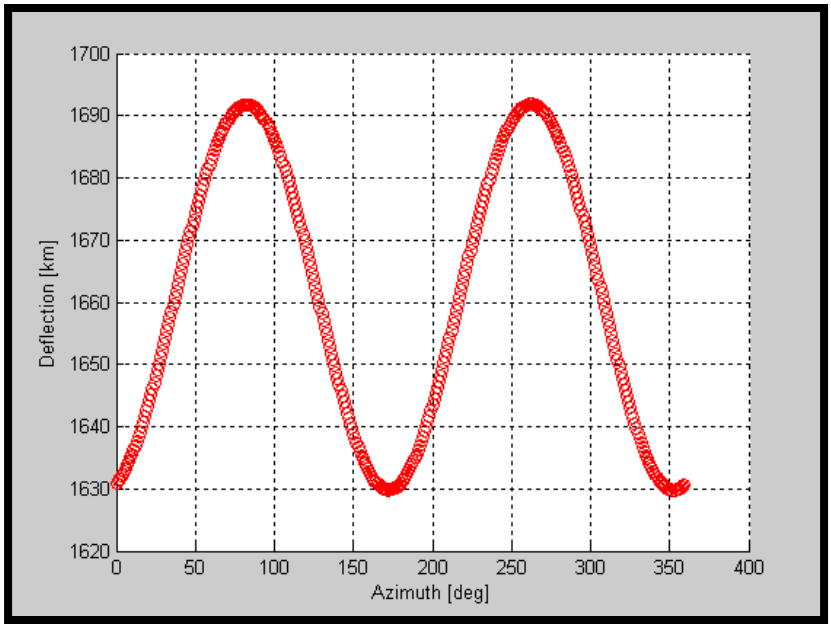

Figure 9.17: Deflection versus Azimuth at 19 Days Before Close Approach Date

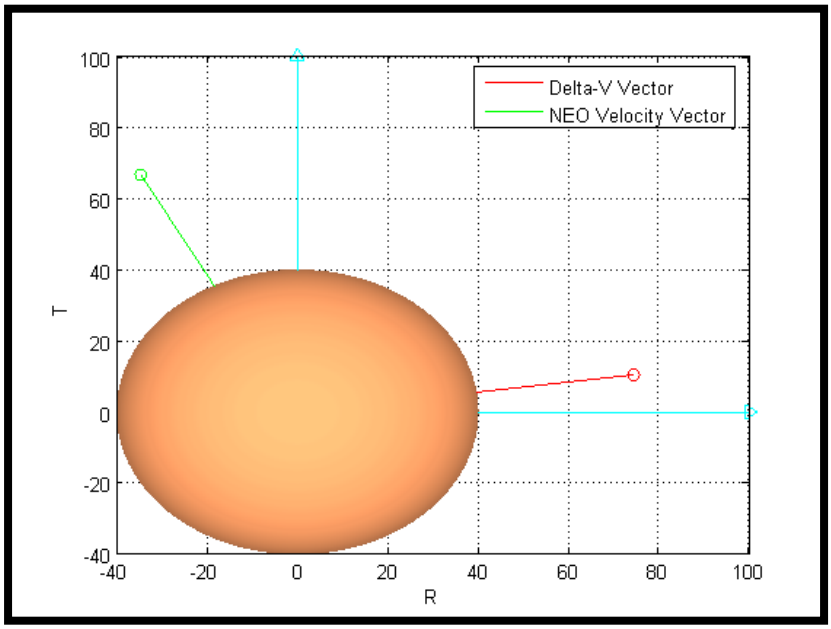

Figure 9.18: Near Optimal Deflection Vector at 19 Days Before Close Approach Date

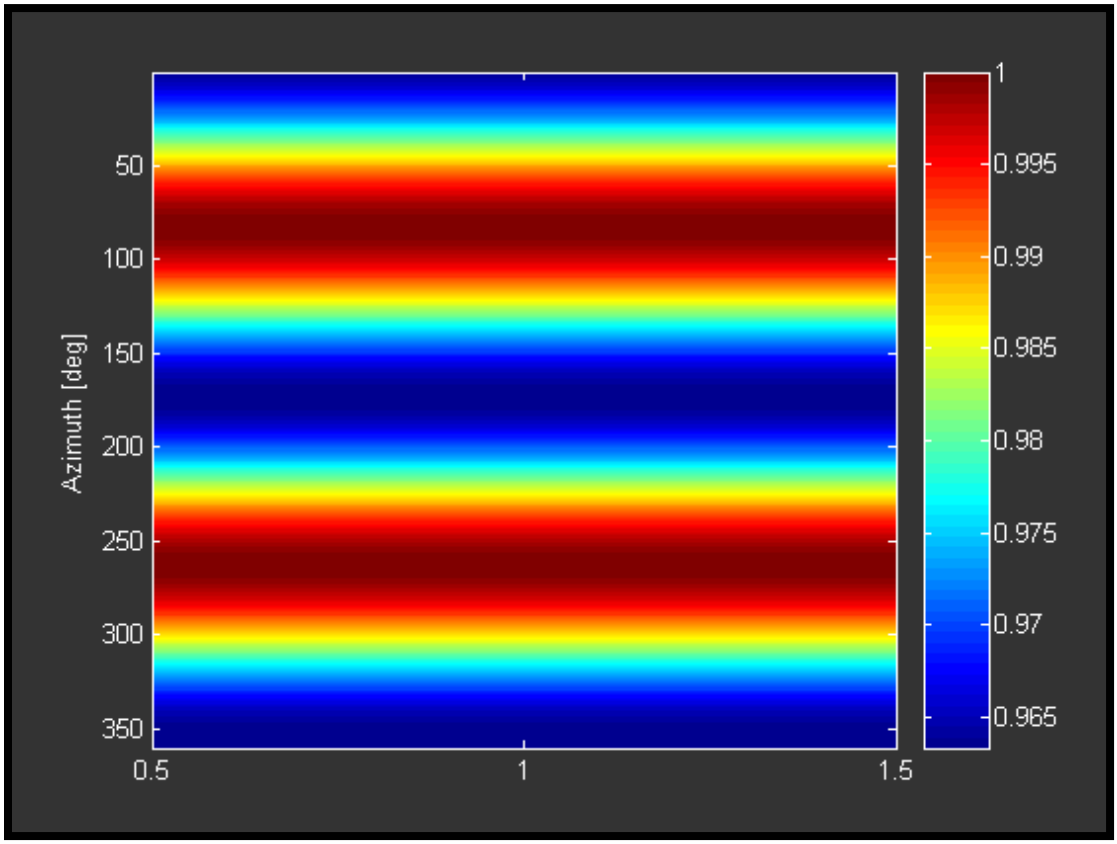

Figure 9.19: Colormap of Normalized Deflection versus Azimuth at 19 Days Before Close Approach Date

Figure 9.19 above illustrates the only difference between this case and the previous two cases, this being that the worst solutions are only approximately 3.5% less effective than the optimal and near-optimal solutions, whereas in the first case the worst solutions were 50% less effective than the optimal and near-optimal and in the second case the worst solutions were approximately 27% less effective.

9.5.4 Case 4: 134 Days Before September 19th, 1998 Revised

A final test case was examined in which the author's preferred performance is used instead of the performance index used by Conway. This preferred performance index is given in equation (6.10) and restated below for clarity.

$$P = \left[\min\left(\Delta r(t)\right)\right]_{DEFLECTED} - \left[\min\left(\Delta r(t)\right)\right]_{UNDEFLECTED}$$

This performance index is the best measure of by how much the asteroid is moved away from Earth in the absolute sense because it causes the optimization search to identify solutions that increase the distance between the Earth and the asteroid during the *post-deflection closest approach*, which generally occurs at a different time than the original close approach or collision event, inherently accounting for the following factors:

- The relative dynamics between the Earth and the asteroid;
- The gravitational influence of the Earth on the asteroid;
- The fact that the exact time of closest approach may shift from the original time of close approach for the unperturbed asteroid trajectory.

However, in this case the asteroid is continually moving closer to Earth until the actual date of close approach, which is 10/3/1998. Therefore, the time t at which the performance index is evaluated is constrained to be 9/19/1998 in order to be able to make comparisons with Conway's methods. The results for this case are tabulated in table 9.12 below.

Table 9.12: Optimal Deflection Results 134 Days Before Close Approach Date with Preferred Performance Index

	Deflection [km]	Angle from Asteroid Velocity Vector	Azimuth Angle in RTN Frame
Current	15464.59	104.22°	81°
Conway	18400	93°	-

Note that the "deflection" achieved by the current methods in this case cannot be directly compared to the "deflection" found by Conway because the current method is now employing a different performance index, and hence a different method of computing "deflection," than that used by Conway. That being said, the optimal deflection achieved in this case by the current methods is approximately 3000 km less than that found by Conway, illustrating that using a less meaningful performance index can give a false sense of the efficacy of a given deflection maneuver. Moreover, if Conway's computed optimal direction were used, the achieved deflection would be reduced a bit more. That being said, the direction of the optimal deflection impulse vector for this case is still in the neighborhood of the direction found by Conway (~11° difference), and this can be seen by comparing figure 9.20 below to figure 9.6 above.

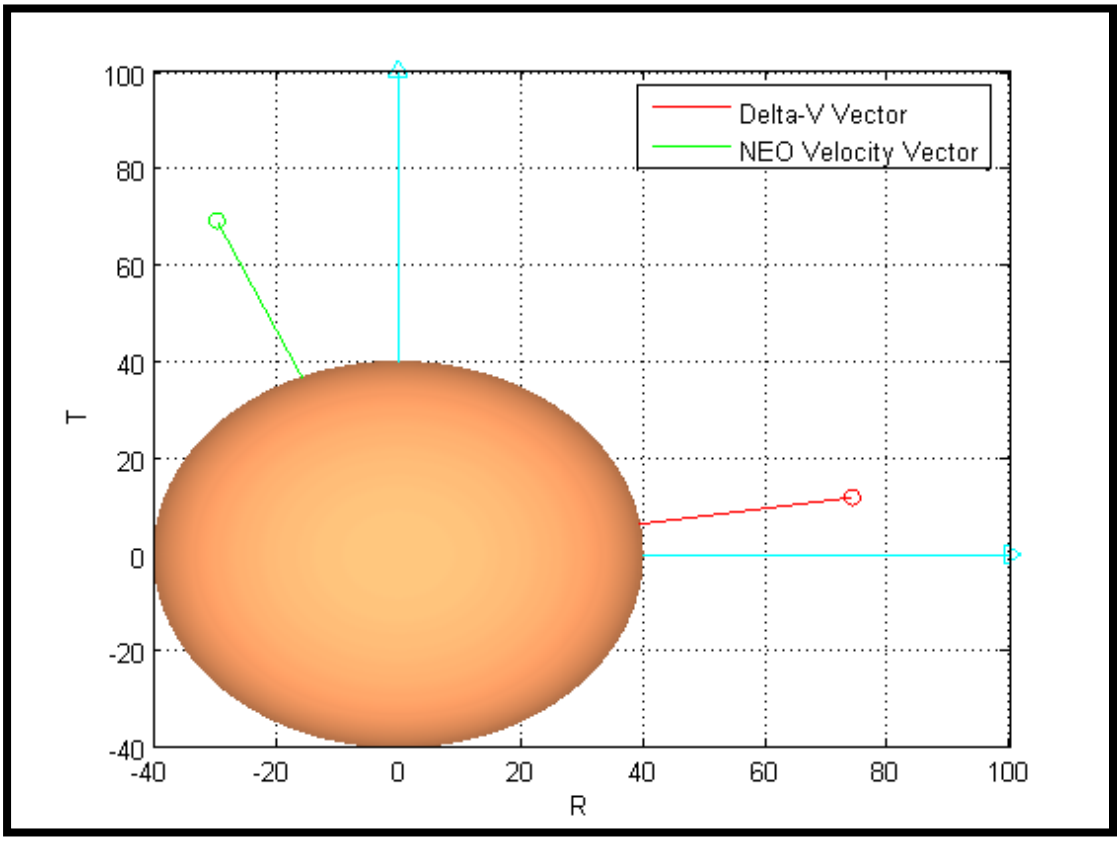

Figure 9.20: Optimal Deflection Vector at 134 Days Before Close Approach Date with Preferred Performance Index

The most dramatic difference between this case and the previous cases is the fact that there is only *one unique optimal solution* rather than the two found in the previous cases. Moreover, the worst solution actually brings the asteroid *closer* to Earth, and this can be seen in figure 9.21 below.

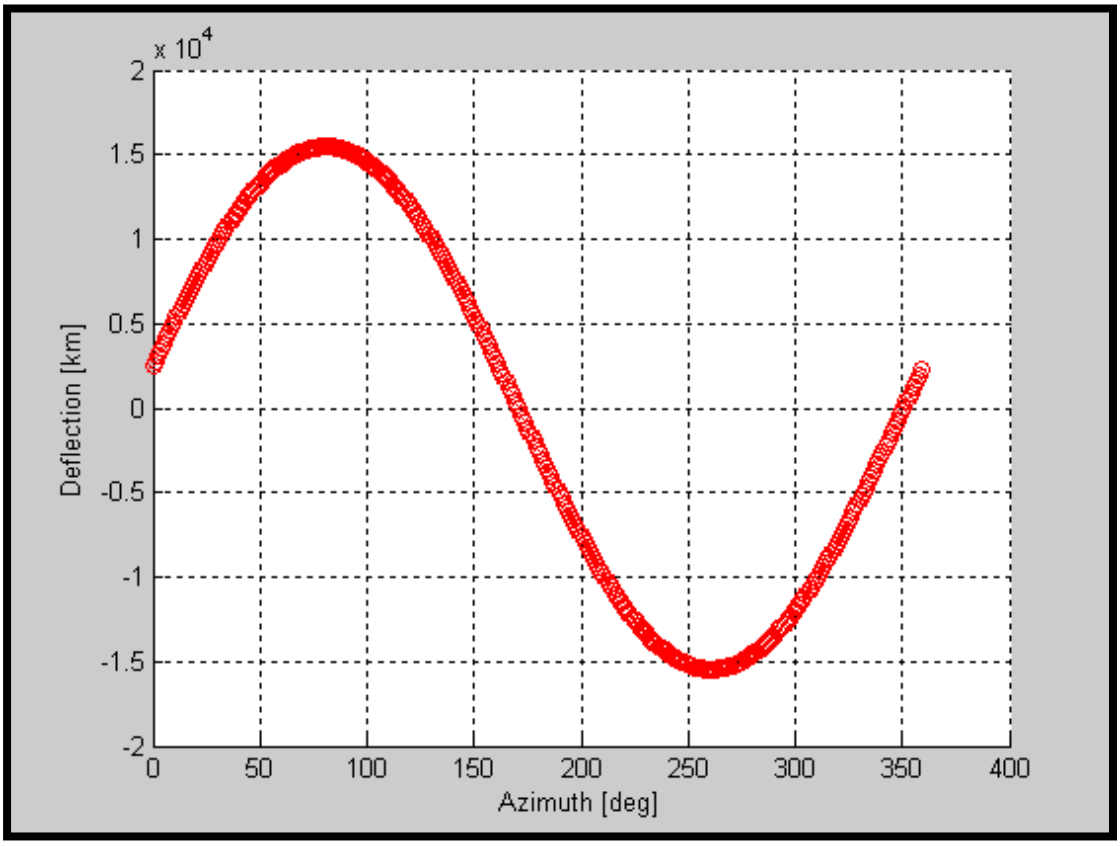

Figure 9.21: Deflection versus Azimuth at 134 Days Before Close Approach Date with Preferred Performance Index

The negative values of the curve shown in figure 9.21 show deflection vector orientations that actually cause the asteroid to come closer to Earth than it would have on the unperturbed trajectory, a very undesirable outcome. There are also deflections that effectively produce no change in the asteroid's distance to Earth as shown by the values for the performance index that are zero and near zero. Note that the absolute optimal deflection vector found in the first case had an azimuth angle of 240°, which actually causes the asteroid to end up approximately 15000 km *closer* to Earth than it would have otherwise, according to figure 9.21 above. Thus in each of the cases above that use Conway's performance index, one of the two apparent optimal solutions was actually an anti-optimal solution that made the situation worse. This

clearly illustrates the superiority of the preferred performance index and highlights the dangers of using other performance indices.

Finally, it is of note that the worst solution in this case moves the asteroid closer to Earth by approximately the same amount that the optimal solution moves the asteroid away, again making clear the importance of identifying the absolute optimal solution. This is shown in figure 9.22 below.

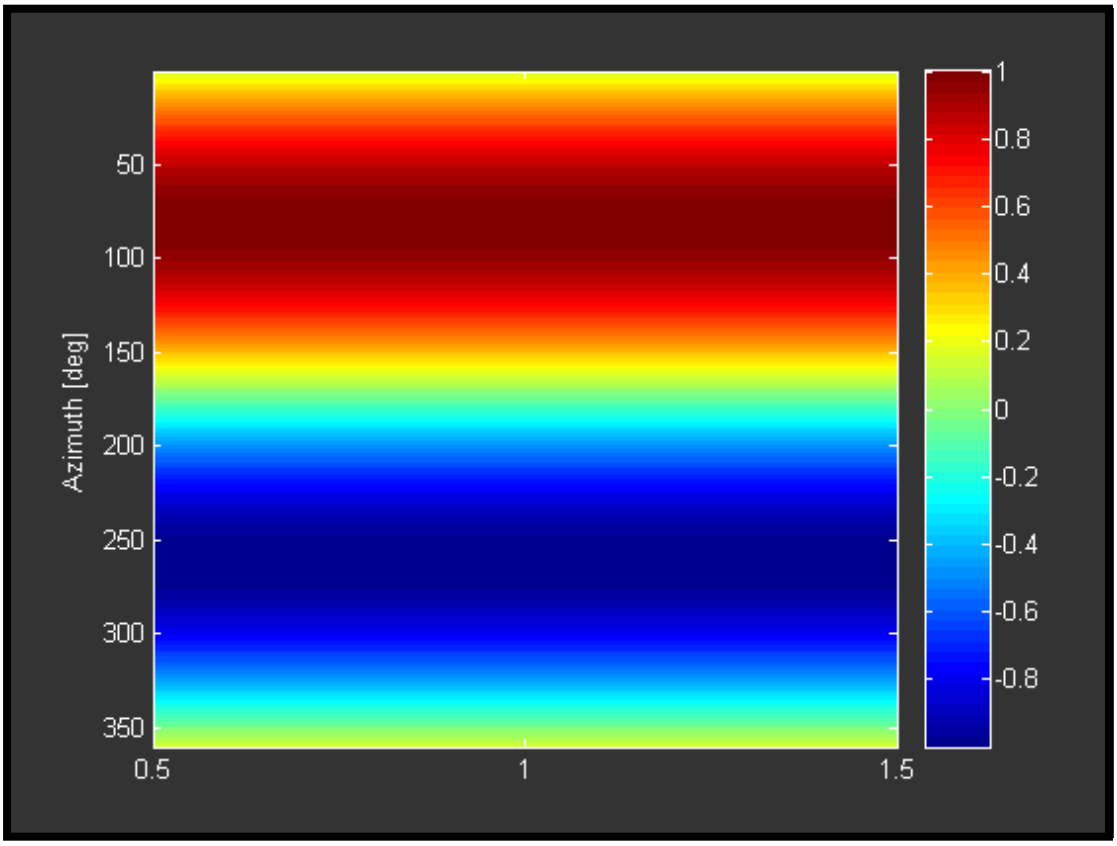

Figure 9.22: Colormap of Normalized Deflection versus Azimuth at 134 Days Before Close Approach Date with Preferred Performance Index

9.5.5 Elevation Angle Effects

In section 6.4.2 it was reasoned that non-zero elevation angles, i.e., $\Delta\vec{v}$ vectors with non-zero normal components, would only serve to reduce the efficacy of

the deflection. The basis for this reasoning is that the massive orbital angular momentum of the NEO's orbit would resist out of plane perturbations too strongly for them to be optimally effective. This result manifests in spacecraft navigation; maneuvers that change the inclination of an orbit always require more Δv than in-plane maneuvers.

This postulation was explored by allowing the elevation angle, δ, to vary from -90° to 90° at a discretization of 10°. The resulting three dimensional deflection solution space is shown in figure 9.23 below.

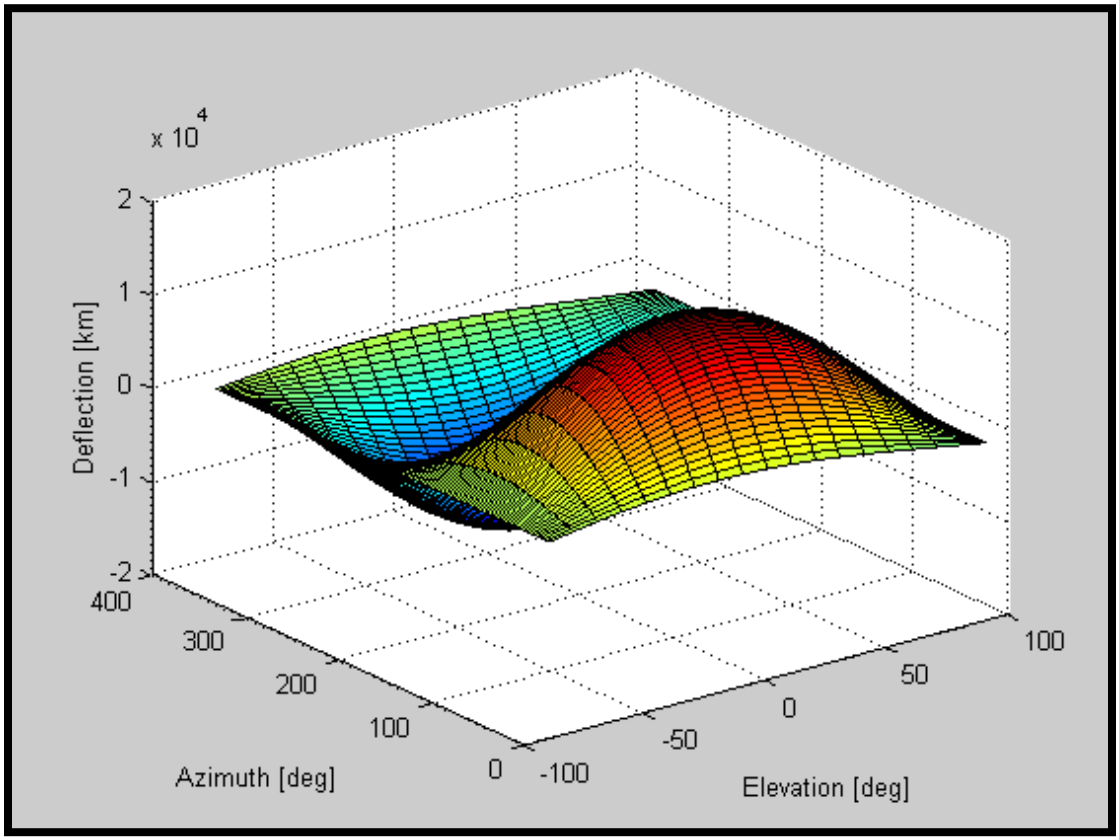

Figure 9.23: Three-Dimensional Deflection Solution Space Including Elevation

It is clear that the global maximum for the deflection still occurs at an elevation angle of zero degrees and that moving the elevation away from zero degrees never has a

positive effect on the deflection. The plot in figure 9.24 below, which contains multiple deflection curves varying in azimuth, further illustrates this fact. Each curve is for a different elevation angle. The curve for which the maximum deflection occurs corresponds to an elevation angle of zero.

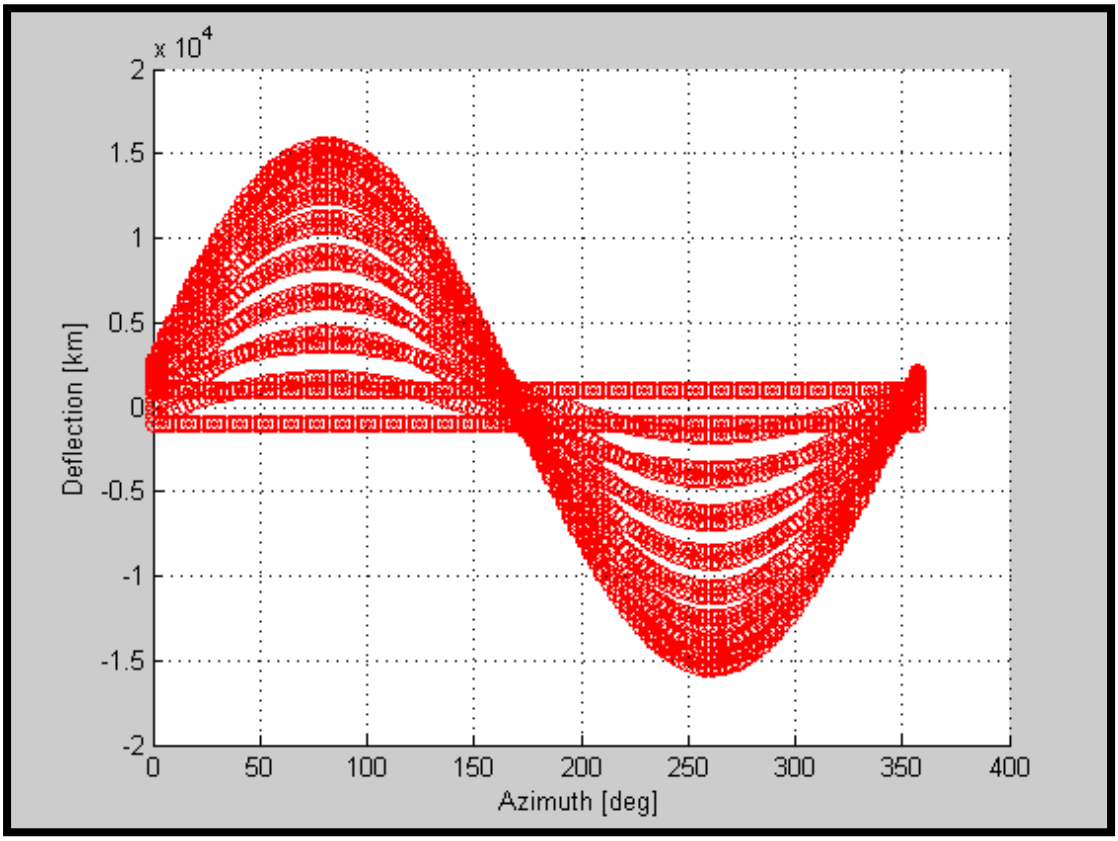

Figure 9.24: Deflection Curves at Different Elevations

Finally, plotting the deflection values with respect to elevation directly clearly demonstrates that peak deflection occurs at zero elevation. This is shown in figure 9.25 below. The encouraging aspect of the results is that the achieved deflection does not fall off sharply until approximately ±30° from 0°, meaning that slight out-of-plane components will not severely impact a deflection action, relaxing the required orientation accuracy a bit.

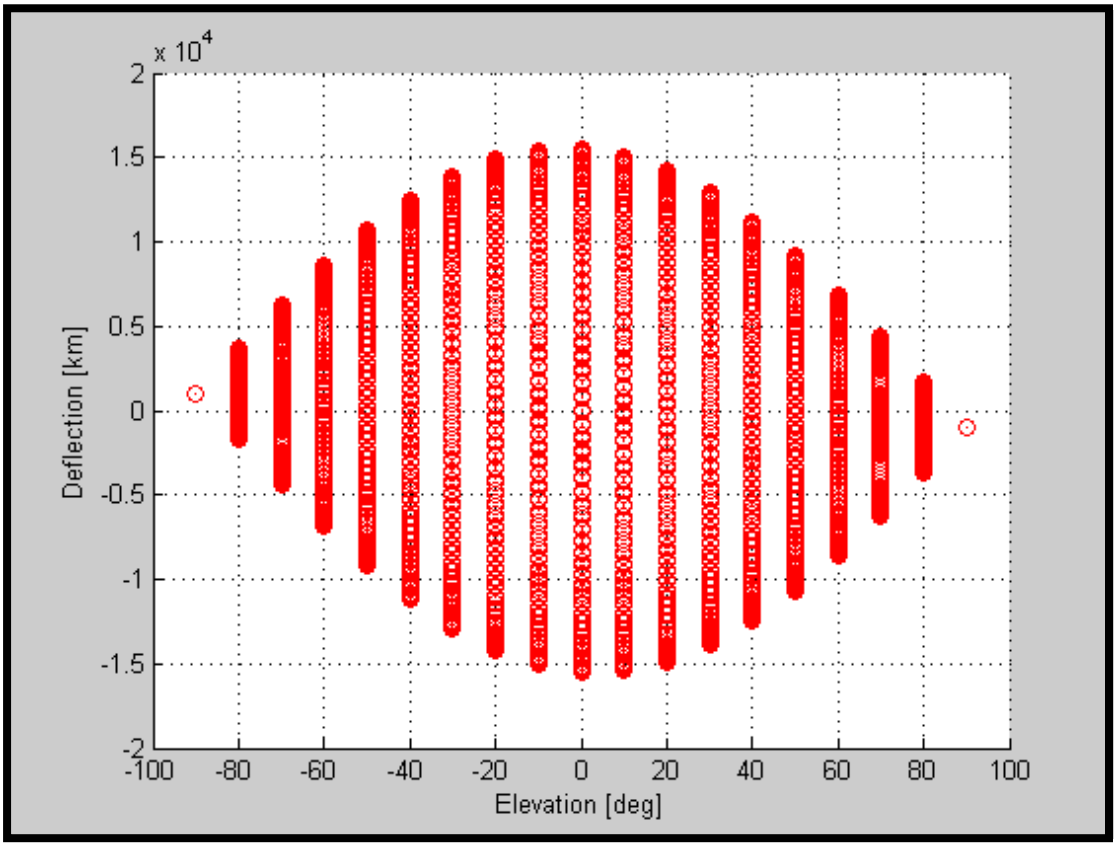

Figure 9.25: Ranges of Deflection Values at Specific Elevations

9.6 Conclusions

The results found by Conway are reproduced fairly accurately by the current methods, considering the fact that Conway uses linearized two-body orbital dynamics whereas the current methods utilize non-linear three-body methods. Moreover, the current methods refine these results and deliver an optimal deflection solution that is 15-20% more accurate in terms of actual deflection achieved and the corresponding optimal orientation of the applied $\Delta\vec{v}$. Additionally, the appropriate choice of performance index eliminates the ambiguity in the structure of the deflection solution space that manifests when Conway's performance index is used. Thus, the current

optimal deflection determination methods are not only validated, but have also been shown to improve upon the quality achieved by previous work in the field. This case was also run with the entire solar system but the solution only changed by 0.08%, likely due to the relatively short run time. Including the entire solar system also increased the time it took for the algorithm to finish by a factor of 4.4.

Note the colormap in figure 9.22 above shows that deflections applied within approximately ±10° of the optimal azimuth angle are at least 95% as effective, meaning that there is a comfortable margin of acceptable error in the realization of the optimal azimuth angle for a given deflection action, increasing the chances of success. Non-zero elevation angles are also conclusively shown to negatively impact the deflection solution space, as was predicted in previous sections.

Finally, the design spaces and deflection solution spaces did not include the dimension of deflection time and corresponding true anomaly at deflection discussed in previous sections on deflection optimization techniques since Conway only considers individual specific times of deflection rather than a continuum. It is almost certain that considering such a continuum would simply have shown that the achieved deflection increased nearly linearly as the time before "close approach" increased since the asteroid did not pass perihelion during the portion of its orbit arc that was examined. Therefore the assertion that perihelion passage is an advantageous time for applying a deflection could not be tested experimentally. This issue will be treated in a subsequent section that does consider a range of deflection times for a fictitious NEO that does make several perihelion passages over the range of times considered.

Paths for future research include the application of numerical optimization techniques, such as simulated annealing or taboo searches, to the computer model presented herein. It would be advantageous to incorporate these techniques if they can converge on optimal solutions with reduced algorithm run times, data accumulations, and processor loads.

10. HAZARDOUS NEO MITIGATION MISSION PLANNING

10.1 Introduction

As previously discussed, vigorous NEO search programs and robust NEO science are two primary ingredients for successful hazardous NEO mitigation. The third crucial ingredient is NEO mitigation mission planning. Achieving the goal of attaining scientific knowledge regarding NEOs requires the planning and execution of investigative missions to expand the body of scientific knowledge concerning NEOs and test proposed mitigation systems, which will provide the baseline for any actual mitigation missions that become necessary in the future.

This section will outline the NEO mitigation mission planning process, culminating in the presentation of a generalized design flow that applies to a wide range of hazardous NEO scenarios. This design flow takes the form of a hierarchy of decision-making principles for an iterative design process. This process will converge on an optimal mitigation plan for a given NEO, which amounts to the best combination of optimal mitigation system selection, optimal mitigation system delivery to the hazardous NEO, and optimal mitigation system application to the hazardous NEO.

10.2 The Holistic NEO Mitigation Optimization Problem

The overall NEO mitigation problem is an optimization problem with a rich character. Specifically, it is a multi-dimensional, multi-segment optimization problem for which each segment of the problem is optimized as part of a whole. Moreover, it is a problem for which the quality of a mitigation effort is not solely measured in a relative sense according to appropriate performance indices; in the final analysis, either the NEO strikes Earth or it doesn't. The only middle ground occurs when a mitigation effort places the NEO onto a resonant return trajectory, meaning that the NEO will collide with Earth in the future, at a later time than the original collision date. A mitigation that places the NEO onto a resonant return trajectory

does still achieve the goal of preventing the first imminent collision, though additional future mitigations will be required. This sort of mitigation does not perform as well as a different mitigation that does not lead to a resonant return. However, the fact that humanity would still be alive and capable of performing future mitigations is still a resounding success, even if a resonant return will occur in the future and require another mitigation.

That being said, it is still possible to design mitigations such that resonant return conditions are avoided by maximizing the physical distance between the Earth and the NEO at what would have been the time of collision, which is desirable anyhow. Thus, while the first layer of the mitigation design is to simply achieve the condition that the NEO misses Earth, in many cases it is possible to optimize the mitigation such that the NEO misses Earth by the widest possible margin given the constraints of the particular scenario.

Another segment to be optimized is the trajectory taken by the mitigation spacecraft to intercept or rendezvous with the NEO. For an actual emergency, it is only necessary to optimize this trajectory such that the flight time is minimized within the constraints of technology; fuel and power are concerns only if they are in danger of being exhausted prior to the completion of the mission, but there is no need to conserve fuel or power otherwise during an actual NEO emergency. Thus, all trajectories in a NEO mitigation mission are first optimized with respect to time rather than fuel/power efficiency and then are optimized for fuel/power efficiency only if necessary, with the constraint that the mission still meets the minimum timeline requirements such that the mitigation effort has sufficient time to indeed cause the threatening NEO to miss Earth.

10.3 Response Time

While the quality and thoroughness of NEO discovery and tracking programs dictates the available warning time for mitigating a NEO, the quality and thoroughness of the design and testing of NEO mitigation systems dictates the

minimum response time. Typically, it takes years for a spacecraft to be designed, tested to the extent possible on Earth, constructed, and launched into space. Our space programs will not have the luxury of these years to plan, design, and build if a NEO is found that will collide in only a matter of years. Therefore, it would be wise for the space programs of the world to collaborate on NEO mitigation systems now, designing modular spacecraft that can be assembled and prepared for launch rapidly. As previously discussed, the effectiveness of a mitigation attempt is directly proportional to the length of the time interval between the time of mitigation system application and what would have been the time of impact.

10.4 Threat Determination

Given the limitations imposed by observing NEOs solely from tracking stations on Earth, there is a time interval between the time at which a threatening NEO is first observed and classified as a potential threat and the time at which the fact that a non-zero probability exists that the NEO will collide with Earth on a future date, absent mitigation, is confirmed. Several days or weeks of gathering observations of the NEO are required to refine its orbit after its initial discovery, and it is during this interval that all apparently threatening NEOs as of the time of this writing have been found to in fact be harmless. However, in the event that the NEO still appears to have a non-zero probability of colliding with Earth after this initial orbit refinement period, the next step is to apply yet more rigorous orbit propagation techniques to the observed NEO orbit. These calculations and predictions are peer reviewed by the NEO science community to rule out erroneous results, and if the NEO still has a probability of Earth collision that cannot be ruled out, the time to take action has arrived. This process can take months or even a year with current capabilities. If the NEO is unobservable for some time interval after initial discovery, this can make the process take even longer.

Some discussion of what the probability of Earth collision means is warranted here, though a detailed presentation of the mathematics and methods of statistical

orbital mechanics is beyond the scope of this work. Essentially, there are a collection of error sources that cause some maximum accumulated error in the predictions of the NEO orbit, and the result is that rather than a precise track though space, the computations produce a sort of tube with an elliptical cross section that represent all the possible NEO trajectories given the known accumulated errors in the orbit propagation. There is a non-zero probability that the NEO will end up at any point in this collection of possible locations in space-time, and if the Earth's location coincides with any of these points, a possibility of Earth collision exists that cannot be ignored.

The accumulated error is the result of uncertainties in the observations of the NEO's orbit due to the limitations of ground based tracking station equipment as well as the error that accumulates during numerical integration of the NEO's orbit on a computer. These error sources can only be minimized, not eliminated, given current science and technology, and so the field of statistical orbital mechanics has arisen to provide the best methods possible to minimize the overall error in the calculations and quantify the probabilities of a given trajectory being correct.

That being said, the error ellipses associated with NEO trajectory propagations are the best information we have to work with and so they must form the baseline for our mitigation planning and response protocols. Even if the collision of the NEO with Earth is not completely certain, we are compelled to take action if the chance of a collision cannot be ruled out. It is at this point in time, when the refinements of the NEO's trajectory are complete and a non-zero probability of Earth collision remains, that the NEO mitigation mission planning process begins.

The subsequent actions to be taken are entirely dependent on the time available. The first step is to catalog everything that is currently known about the NEO, including its likely size and composition. The next step is to evaluate how much time is available to take action, which will drive almost every subsequent decision in the mitigation planning process. It is mostly likely, given current and foreseeable technology, that deflection will be the chosen mode of mitigation.

Preliminary analyses can be performed on a computer model of the Earth-NEO collision scenario, using optimal deflection determination techniques that were developed in previous sections of this work to evaluate by how much the NEO can be optimally deflected as a function of how long we wait to apply the deflection. This gives us a measure of what our final time window to mitigate the NEO is, and this dictates how much time we have to prepare and take preliminary action. However, the mitigation system must first be delivered to the NEO in order to take effect, so the time required to travel to the NEO must also be taken into account. This travel time should also be minimized using trajectory optimization techniques.

These preliminary calculations provide a time window for conducting operations in support of the mitigation. If the time window is too small to permit such operations, then the only thing to be done is to design and construct the mitigation and delivery spacecraft with the information currently available and design with the largest margins for error possible. However, if time permits, there are other actions that must be taken.

The first thing to be done, time permitting, is to send a spacecraft to deliver a transponder beacon to the NEO. This spacecraft may be very small and fast, using high thrust and low payload mass to minimize the flight time to the NEO. All that is required of the spacecraft is to deliver a beacon/power source package to be planted on the NEO, probably by colliding with the NEO in a controlled manner and lodging the beaconing mechanism in the NEO surface using a penetrator system. The design and operation of a mostly autonomous targeting system to guide the penetrator to the target NEO is quite feasible, as demonstrated by the recent Deep Impact mission to comet Tempel 1, which guided an impactor to collide with the comet. Planting a beacon will allow extremely precise determination of the NEO's orbit, which will aid subsequent mitigation calculations. The expected accuracies for a characteristic beacon system with 5 watts of radio frequency power and a low-gain antenna on the beacon system coupled with a 35 m receiving dish on Earth are on the order of 0.1 mm/s in velocity and 100 m in position within a geocentric range of 2 AU [15]. It is

entirely possible that the refinement of our knowledge of the NEO's orbit will show that a collision will not in fact occur and at this point mitigation efforts are no longer an issue.

If possible, a science spacecraft should also be sent with the beacon delivery system in order to gather accurate physical data on the NEO, as discussed previously in the section on NEO science. This data will be invaluable in designing a mitigation system specifically tailored to the actual NEO, which will greatly enhance the effectiveness of the mitigation. The time to perform science operations on orbit, receive the data, and process the results must also be taken into account. All of that could take many months, and if that time is not available, then the design and construction of the mitigation system and delivery spacecraft must proceed based on estimates of the physical data for the NEO that can be inferred from processing ground based observations, which are generally coarse in comparison to on-orbit sensor data.

At this point, there are three possibilities: no beacon or science missions have been sent and only ground observation data is available, only a beacon mission has been sent, or a beacon and science combination mission has been sent. In any case, whatever data is available on the NEO will be processed to determine the NEO's orbit and physical properties as accurately as possible. The next step is to select a mitigation system that will maximize the magnitude of the deflection imparted to the NEO, given the technology available at the time. This selection of the most effective NEO mitigation system will fix the value of the maximum available $\Delta\vec{v}$ magnitude that can be applied to the given NEO, which is a function of the NEO's physical properties, and it only remains to determine the optimal time, which also corresponds to a point along the NEO's orbit, to apply the deflection maneuver, as well as the optimal orientation for the resulting $\Delta\vec{v}$.

The methods for determining optimal NEO deflection maneuvers described in previous sections will now be applied, as well as rigorous trajectory optimization of

the rendezvous or interception trajectory to be used to deliver the mitigation package to the NEO. These calculations will yield the required maneuvers for the mitigation spacecraft, allowing the spacecraft systems to be designed and the thrusters and fuel systems to be selected. If the overall spacecraft mass to be launched into orbit is too large for current launch systems to handle, the spacecraft may be launched in pieces and assembled on orbit, and a mission will have to be planned to achieve that. Conversely, if there is additional launch payload mass available, it is desirable to include a science craft in the design to monitor the mitigation event from a distance. The data collected would be inherently scientifically valuable and would also provide information for planning future mitigation missions should they be required. This will lead to an overall design of the NEO spacecraft, including the mitigation system payload and possible science payload, and selection of the best launch vehicle will follow. These design choices, coupled with the mission phases dictated by the trajectory maneuvers, form the overall spacecraft mission plan for the mitigation. At this point the initial design cycle is complete and must be evaluated for effectiveness and feasibility. If necessary, the design cycle can be repeated until a design and mission that are both feasible and effective are converged upon. The next and final step is to execute the mission.

The generalized hierarchy of decision-making principles and mitigation mission design methods discussed above have been used to construct a comprehensive mitigation planning flowchart that illustrates the sequence of events during the handling of a NEO mitigation scenario and the interdependencies between critical phases of the planning process. This flowchart is presented in figure 10.1 below.

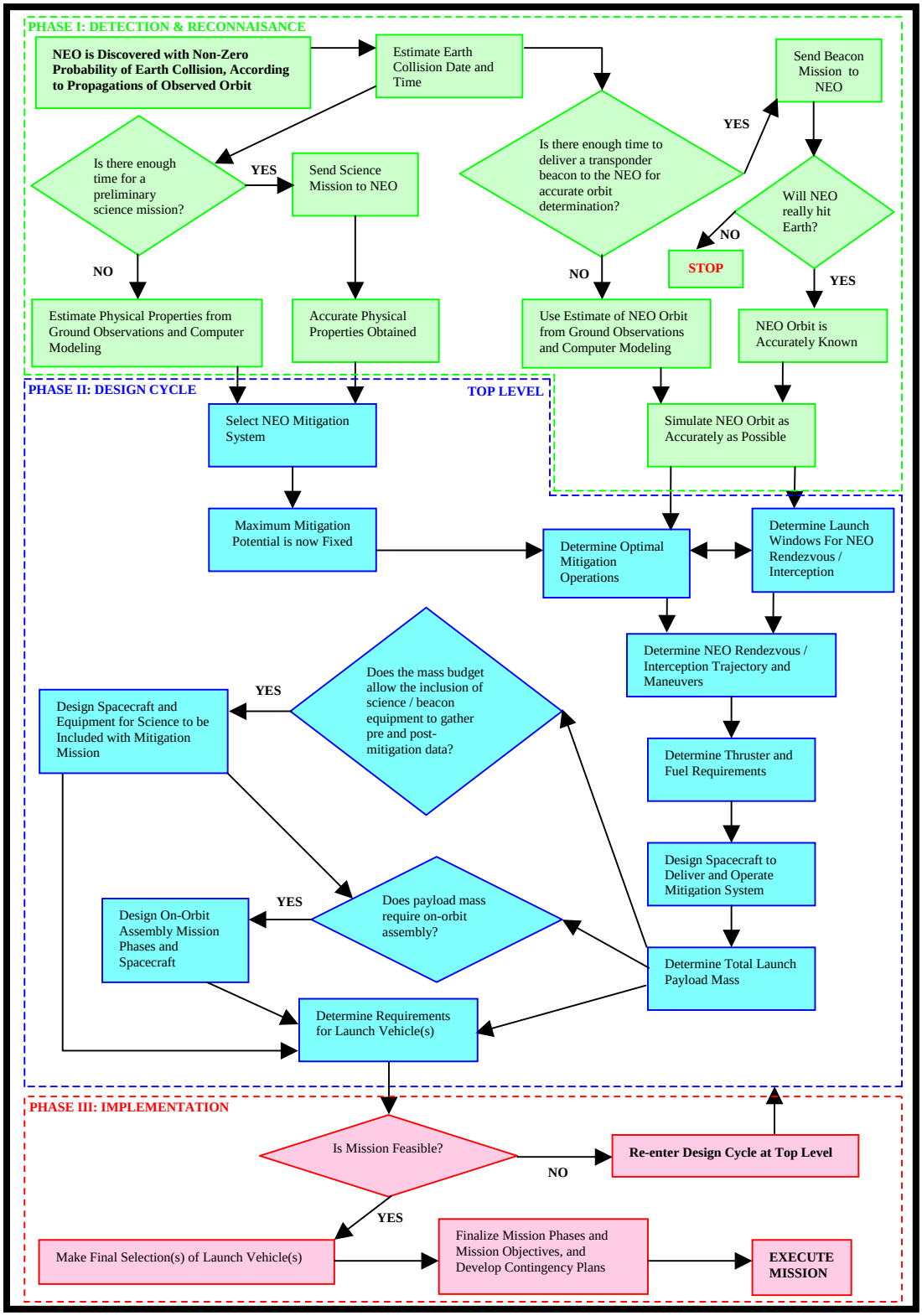

Figure 10.1: NEO Mitigation Mission Planning Flowchart

11. NEO MITIGATION CASE STUDY

11.1 Introduction

In this section a case study will be presented in which the theories and principles of NEO mitigation mission planning developed heretofore will be applied. The parameters for the sample NEO selected for this case study were obtained from *Athos, Porthos, Aramis & D'Artagnan: Four Planning Scenarios for Planetary Protection* by David K. Lynch, Ph.D. and Glenn E. Peterson, Ph.D. of The Aerospace Corporation, a document which contains four fictitious Defined Threat (DEFT) scenarios [27]. Each scenario is a set of parameters for an impacting NEO and the intention of the document is to pose these scenarios as challenges for NEO mitigation mission planners with the goal of raising awareness of the NEO mitigation problem and inviting solutions from the academic community. The physical and orbital characteristics of each sample NEO are presented in detail, forming unique scenarios that the authors believe are representative of part of the spectrum of NEO mitigation situations that might actually be encountered.

This author chose to examine D'Artagnan because the associated scenario is well suited to the focus in this work on rapid response NEO mitigation with impulsive deflection maneuvers.

11.2 Sample NEO Physical Characteristics

The synthetic impactors in the DEFT scenarios are given names that were not currently assigned to existing NEOs as of the time of the writing of the document (2004). The name of the impactor chosen for this case study is D'Artagnan. D'Artagnan is a monolithic, S-type (silicaceous), ellipsoidal, Aten asteroid, detected on February 22, 2004, 00:00:00 UT. The date of Earth impact is September 14, 2009. Its orbit is slightly inclined with respect to the ecliptic plane, its orbital period is a little less than a year, and its mass is approximately 3.594×10^9 kg. This mass value is computed from the asteroid's given dimensions and average density, which are

$(130 \times 120 \times 110)$ m and 4.0 g/cm^3, respectively. An idealized structural diagram of the asteroid is given in figure 11.1 below.

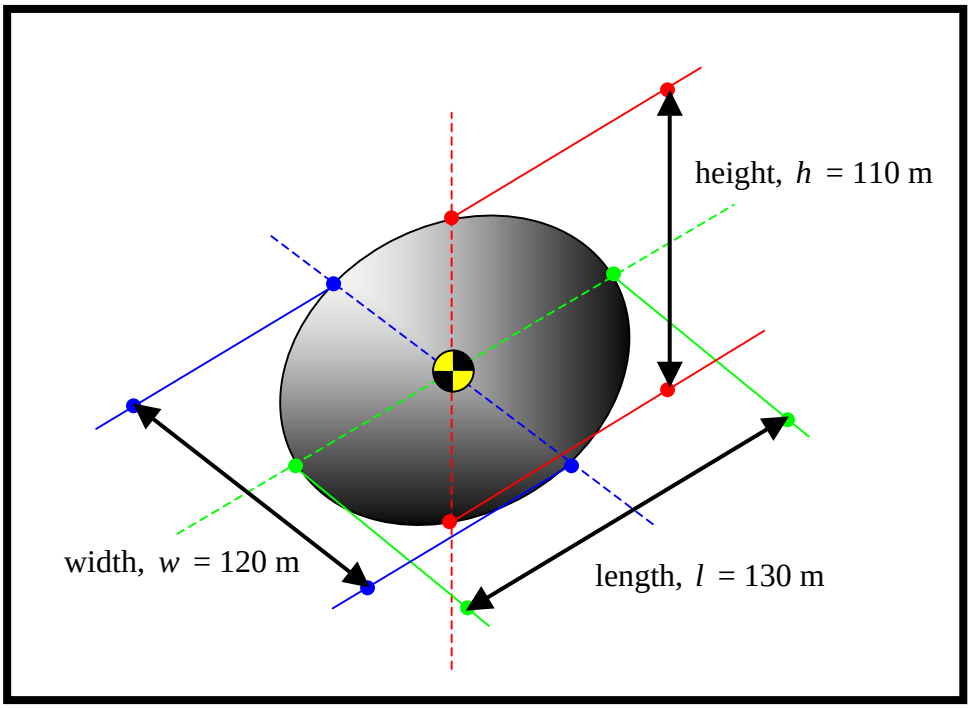

Figure 11.1: Idealized Structural Diagram of Asteroid D'Artagnan

To determine the value for D'Artagnan's mass that will be used in subsequent simulation and analysis, the volume was first computed using the given dimensions, shown in figure 11.1 above, and the formula for ellipsoidal volume given by:

$$V_{ellipsoid} = \left(\frac{4}{3}\right)\pi\left(\frac{l}{2}\right)\left(\frac{w}{2}\right)\left(\frac{h}{2}\right) \tag{11.2}$$

Next, the mass of the asteroid was calculated by multiplying the volume by the given density as follows:

$$M_{asteroid} = V_{ellipsoid} \times \rho_{asteroid} \tag{11.3}$$

It is assumed that the density given for the asteroid is the mean density and that the asteroid is an approximately homogenous solid monolith of silicaceous (type S) composition.

The given and computed values for the asteroid's physical properties are presented in table 11.1 below:

Table 11.1: Given and Computed Physical Properties for Asteroid D'Artagnan

Property	Symbol	Value
Length $[cm]$	l	13,000.0
Width $[cm]$	w	12,000.0
Height $[cm]$	h	11,000.0
Density $[g/cm^3]$	$\rho_{asteroid}$	4.0
Volume $[cm^3]$	$V_{ellipsoid}$	898,495,498,926.7
Mass $[kg]$	$M_{asteroid}$	3,593,981,995.7
Structure	--	Solid, Monolithic
Taxonomic Type	S	S – silicaceous

A computer-generated model of what D'Artagnan might look like is shown in figure 11.2 below.

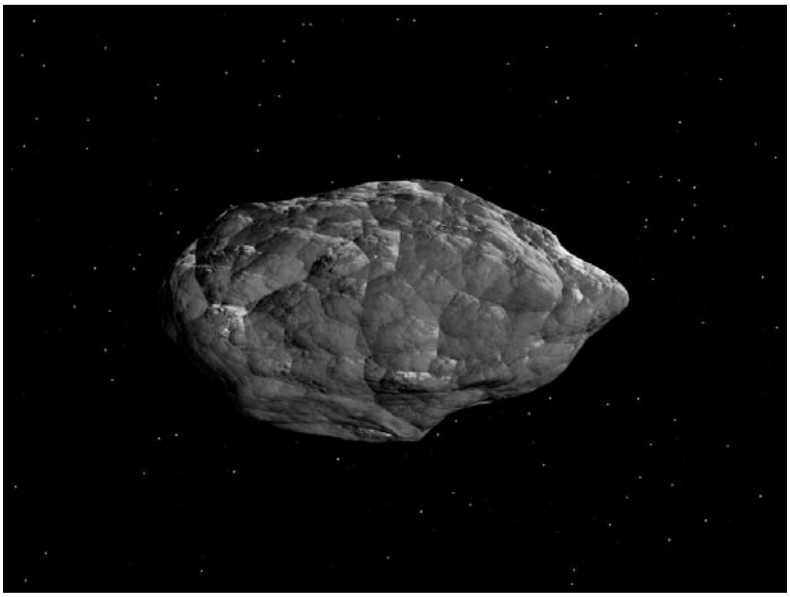

Figure 11.2: Computer-generated Model of Asteroid D'Artagnan [18]

11.3 Sample NEO Orbital Characteristics

The taxonomic type of D'Artagnan's orbit is Aten, meaning that the asteroid spends most of its time closer to the Sun than the Earth, making it difficult to observe. As discussed in previous sections, the definition of an Aten orbit is that the semi-major axis is less than 1.0 AU and the aphelion distance is greater than 0.9833 AU.

The document from which all the parameters for this fictitious asteroid were obtained includes an explicit set of approximate orbital elements for the asteroid at the time of detection and an exact state vector (position, velocity) for the asteroid in the ECEF frame at the time of collision. The authors explicitly state that the given orbital elements at the time of detection are only approximate and that mission analysts should integrate the asteroid's ECEF state vector at the time of collision backwards in time to provide a robust set of initial conditions to be used for further simulation and analysis of the collision event and its mitigation. This is the method used by this author and the construction of the colliding orbit for the asteroid is described below.

11.4 Construction of Impact Trajectory

In order to simulate the collision of D'Artagnan with Earth, initial conditions for both celestial objects are required. The reference frame for the simulation is the Heliocentric Inertial (HCI) frame, and Earth's heliocentric orbital elements were obtained from the *Astronomical Almanac* [26]. These orbital elements were converted into a heliocentric position and velocity state vector and then propagated to the epoch time of D'Artagnan's collision, September 14, 2009, 11:04:26.117 UT. This provided the state vector of the Earth in the heliocentric frame at the time of impact by D'Artagnan.

Next, D'Artagnan's state at the time of impact was converted from the Earth-Centered, Earth-Fixed (ECEF) reference frame to the HCI frame according to the procedures detailed in appendix A and then summed with Earth's HCI state at the time of impact to yield the HCI state vector for D'Artagnan at the time of impact. Now, with the HCI state vectors of both the Earth and D'Artagnan known at the time of impact, these states were propagated backwards through time to the time of detection to provide the initial conditions for the collision scenario.

The orbits were simulated using a three-body orbital dynamics model including the Sun, Earth, and D'Artagnan. The details of the gravitational physics and simulation methods are presented in appendix B. The resulting initial orbital elements for D'Artagnan are presented in table 11.2 below.

Table 11.2: Approximate and Computed Values For D'Artagan's Orbital Elements for the Epoch 2/22/204, 00:00:00 UT

	Approximate Value [27]	Computed Value
a	0.8976 AU	0.89949569016432 AU
e	0.288063	0.282208717191371
i	4.788754°	4.52052114106094°
Ω	350.540144°	351.896987833313°
ω	230.740220°	231.0711730104°
M	254.275083°	271.974701522753°

It is clear from table 11.2 that the computed values are nearly identical to the approximate values given in the reference document. The differences are mostly likely due to disparate simulation models and methods, though the disparity is obviously small. The simulated orbits for both the Earth and D'Artagnan are presented in three dimensions and in the plane of the ecliptic in figures 11.3 and 11.4 below, respectively.

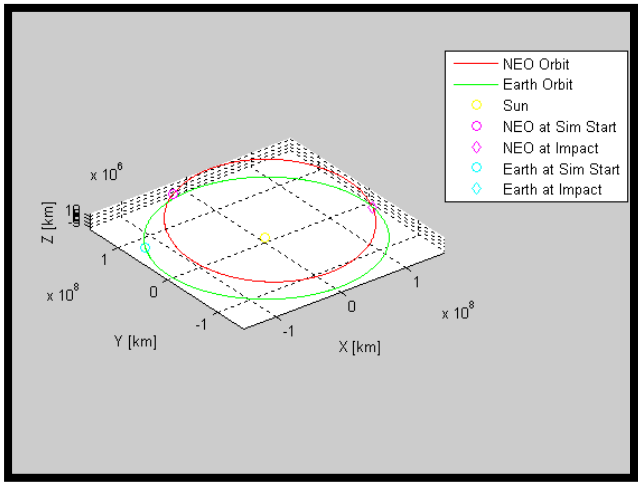

Figure 11.3: Earth and D'Artagnan Orbits in Three Dimensions

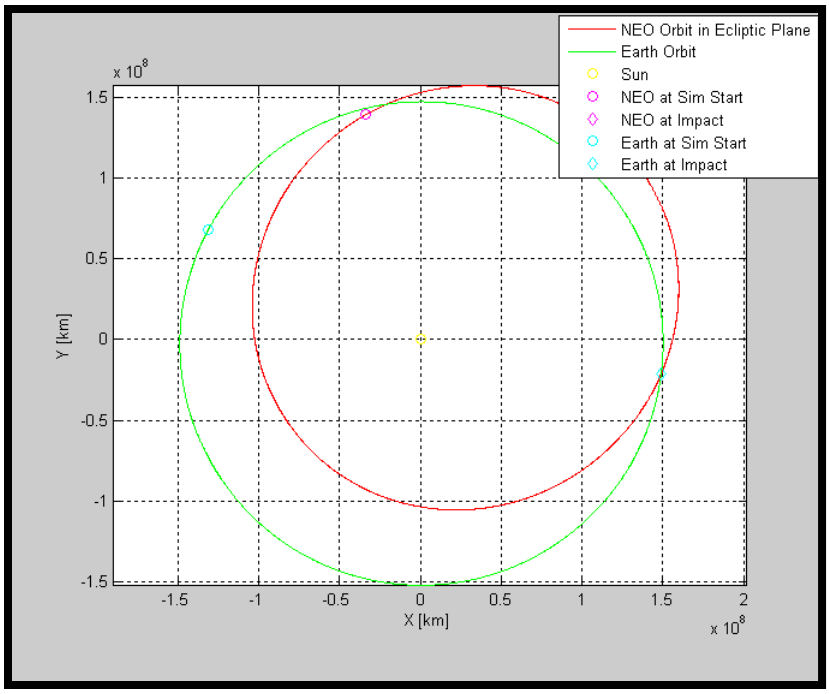

Figure 11.4: Earth and D'Artagnan Orbits in the Ecliptic Plane

The distance between Earth and D'Artagnan was also calculated for the duration of the simulation and is plotted in figure 11.5 below. The times at which D'Artagnan was at perihelion were also determined and are indicated in this plot. The corresponding times of perihelion passage are going to be included in the time vector of the design space for the optimal deflection velocity change vector determination since perihelion passages are theorized to be advantageous for deflection maneuvers, as described in previous sections. Note that D'Artagnan makes two close approaches to Earth within the first year after initial detection. It is unfortunate that NEO mitigation systems were not at the ready prior to the time of detection, because these close approach events, particularly the close approach of approximately 0.124 AU 0.855 years after detection, provide excellent opportunities for both the rendezvous of the deflection spacecraft with D'Artagnan and the application of the deflection itself. As verification that the collision event occurs in

simulation, the final distance between the asteroid's center of mass and that of Earth is 6368.315779 km, 10 km less than the Earth's equatorial radius.

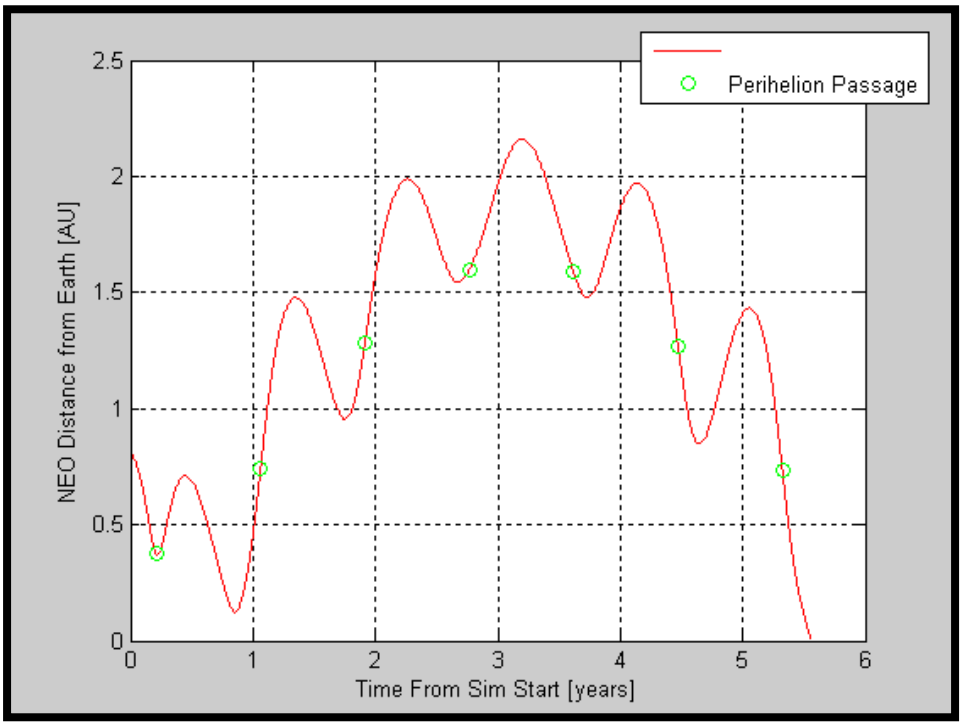

Figure 11.5: Distance between Earth and D'Artagnan over the Time between Initial Detection and Impact 5.5617 years Later

11.5 Collision Effects

As stated previously, D'Artagnan is initially detected on February 22nd, 2004 and collides with Earth on September 14th, 2009, 11:04:26.117 UT. The location of the impact on the Earth's surface is Lyon, France. The impact velocity quoted in the reference document is 14 km/s and the value computed here is 13.999237 km/s, an excellent agreement. Thus, the kinetic energy of the impact was computed to be 83.85 Mt according to equation (4.1). This energetic yield is nearly twice as large as the largest nuclear device ever tested by humanity. Lyon is France's third-largest city and second-largest urban area, with populations of 415,000 and 1.26 million, respectively [28]. Were D'Artagnan not mitigated, the death toll would be unquestionably catastrophic.

11.6 Mitigation of Asteroid D'Artagnan

The previous sections have completely defined the collision scenario for asteroid D'Artagnan and made clear the devastating consequences of failure. At this point the modeling of the mitigation will begin, according to the NEO mitigation mission planning flowchart presented previously in figure 10.1. At each step appropriate assumptions will be made to facilitate the analysis because it is not possible to simulate every single aspect of the scenario precisely. The culmination of this design process is a complete mission plan for successfully mitigating the threat posed by D'Artagnan.

11.6.1 Phase I: Detection and Reconnaissance

As previously stated, D'Artagnan is first detected on February 22nd, 2004, 00:00:00 UT. At this time as many observations as possible are made of it in an attempt to determine its orbit accurately enough to assess whether or not a future impact with Earth is possible. Fortunately, the Sentry system at Jet Propulsion Laboratory and the NEODyS system at the University of Pisa in Italy are continuously scanning the orbital data for NEOs in order to identify threatening objects as soon as possible. Thus, it is assumed that the calculation of Earth collision probabilities begins right away once D'Artagnan is discovered. The question is how much time passes before it is determined that D'Artagnan is indeed a threat worth mitigating, i.e., it has an unusually high probability of Earth impact. There are currently no established threshold values for collision probability past which a mitigation mission is deemed to be necessary, so a simulation of NEO detection and threat assessment will be referenced here to provide reasonable estimates.

The simulated threat assessment referenced is that created by Chesley, *et al.*, in which the observations of a newly discovered NEO are simulated, with modeled uncertainties, and the evolution of the probability of Earth impact is determined as a function of the length of the data arc, that is, the length of time over which the NEO is

observed. It is of note that due to orbital geometry there are periods where observation of a given NEO are not possible, meaning that the object is lost for some period of time. Generally, it is reacquired at the next viewing opportunity. The case presented by Chesley, *et al.*, is for a NEA that is discovered in 1983 and will impact in 2000, 17 years later. Thus time from discovery til impact is approximately 3 times longer than for D'Artagnan. Since the errors in the propagation of the orbit are smaller for a shorter propagation time, it will be assumed that perceived probability of D'Artagnan impact will grow more rapidly than for the Chesley *et al.* impactor.

A plot of the perceived probability of impact and corresponding threat index ratings is presented in figure 11.6 below.

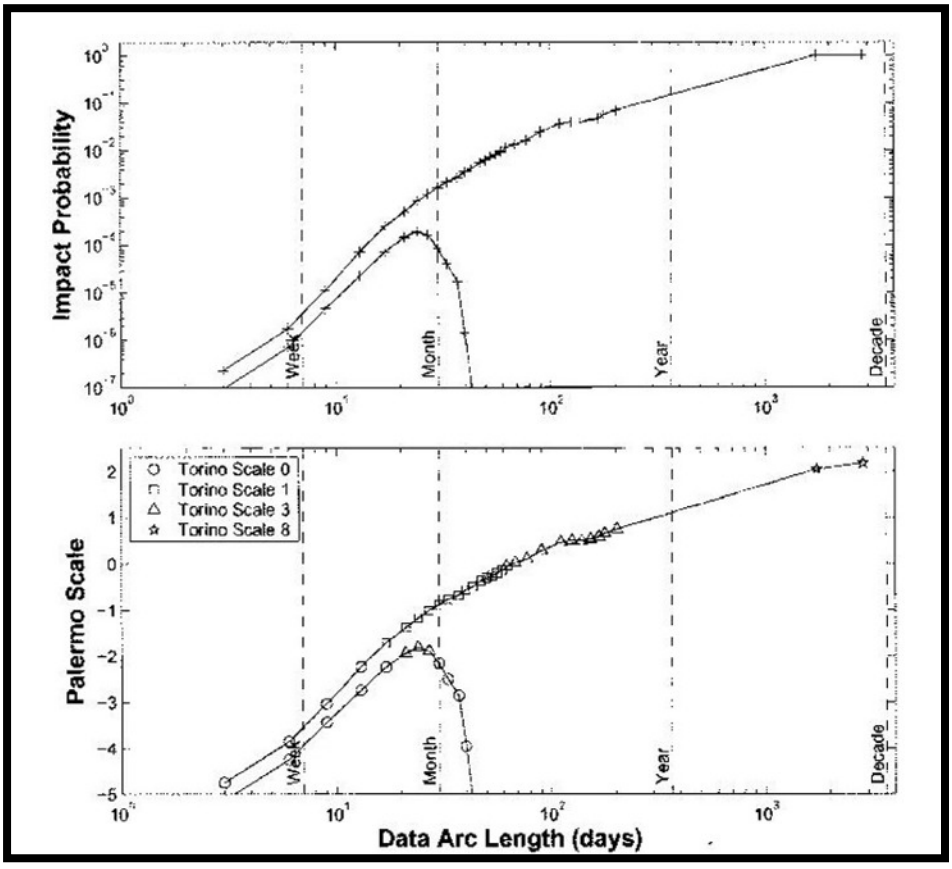

Figure 11.6: Perceived Impact Probability and Corresponding Threat Rating as a Function of Observed Data Arc [7]

For simplicity it will be assumed that D'Artagnan can be continuously observed subsequent to discovery. In figure 11.6 the target NEO was observed for more than 6 months and then lost for 4 years. The likelihood of impact at the time the NEO was lost was 7% and it quickly grew to more than 50% after being reacquired. Thus it is assumed that for an uninterrupted observation arc, the probability of impact would have grown to an alarming value, say > 50%, with approximately a year of observational data and orbit propagation.

As a first order approximation, it will be assumed that D'Artagnan is found to have an alarming likelihood of impact after 6 months of continuous observation. This marks the actual entry into the first block in the NEO mitigation mission planning flowchart on page 151. At this point it is known that the collision of Earth impact is too high to ignore and the approximate date of collision is known.

At this point approximately 5 years remain until impact. The energy of the impact has been estimated fairly accurately and the impact site is approximately known. It would be wise at this point to begin planning the evacuation of the potentially affected areas, though this is a very daunting task. Nevertheless, whatever can be done on the ground to help control the damage in the event that mitigation is unsuccessful is helpful.

With only 5 years remaining until impact, it is not feasible to send a preliminary beacon or science mission to the NEO, unfortunately. The NEAR mission to Eros took about 3 years to design, build, and launch, and the Deep Impact mission took about 6 years. Thus, the design and construction of the mitigation spacecraft and mission have to begin right away, forgoing further reconnaissance. This means that deflection optimization and rendezvous trajectory design will have to be performed with the best available estimates, and ground-based observation data will have to be relied upon for estimates of the NEO's physical parameters. A summary of the assumed estimates for these physical parameters is outlined below.

11.6.2 Assumptions Regarding Estimated Scenario Parameters

As stated previously, neither a beacon nor a science mission to D'Artagnan is possible given the time constraints. Therefore it will be assumed that the physical parameters of the NEO are not known precisely and these slightly incorrect values will be used to plan the mission; the actual parameters will be used in simulation to illustrate the effect of the inaccurate parameters on the results. However, for the sake of simplicity, the actual simulated orbit of the NEO will used for deflection optimization and trajectory planning rather than a skewed one. The assumptions regarding D'Artagnan's physical parameters are tabulated in table 11.3 below.

Table 11.3: Estimated and Actual Physical Parameters for D'Artagnan

Quantity	Estimated Value	Actual Value	Error
Shape	Spherical	Ellipsoidal	-
Size	120 m diameter	110×120×130 m	-
Density	3.0 g/cm^3	4.0 g/cm^3	25%
Mass	2.7143×10^9 kg	3.5940×10^9 kg	24.476%

It will be assumed that spectral data gathered on the ground is not terribly erroneous and thus D'Artagnan is thought by observers to probably be an S-type asteroid. The DEFT scenario specifies that the asteroid has a rotation period of 19 to 24 minutes, meaning that its slowest rotation rate is $2\pi/(24\times60) = 0.0043633$ rad/s. For a density of 3.0 g/cm^3, the critical rotation rate computed according to equation (2.8) is 0.0009156978, meaning that D'Artagnan is rotating faster than its critical rate by a factor of approximately 4.77. However, this alone is not indicative of a sold, monolithic structure (assuming that the ground observations can even provide a good estimate of the spin rate). For example, the small, fast rotator 1998 KY26 (~30 m diameter, ~11 minute spin period, ~1.3 g/cm^3 density) is rotating approximately 15.8 times faster than its critical rate and yet even a cohesive body rotating at this rate only

requires a tensile strength orders of magnitude weaker than that of snow [9]. However, mission planners will draw the conclusion that D'Artagnan is a probably a solid monolith based on the estimates of the mean diameter and density relative to the estimated compositional type.

This marks the end of Phase I: Detection & Reconnaissance. The NEO has been determined to have a high enough chance of collision to warrant mitigation after 6 months of observation. The time until impact is too small to allow a beacon and/or science mission, so estimates of the NEO's physical and orbital parameters will be relied upon for mitigation mission planning. At this point, the design cycle phase for the mitigation mission begins.

11.6.3 Phase II: Design Cycle

The design cycle begins with the best available estimates for the NEO's physical and orbital parameters. The first task is to determine the best mitigation system given the overall scenario constraints. It will be taken as a given that deflection will be mitigation mode of choice. Annihilation is beyond the means of current technology, and fragmentations and dispersals are too unpredictable, as previously discussed. Next, the deflection solution space will be examined by applying the optimal deflection design methods presented previously to map-out the available maximum deflections over a range of times until impact, which also correspond to orbital locations for the NEO; the times for which the NEO is at perihelion are specifically included in the set of time values considered as previously discussed. Trajectories that will bring the mitigation spacecraft to a rendezvous with the NEO are also examined, with the goal of rendezvousing as early as possible since the achieved deflection tends to linearly increase with the time between deflection application and the original time of impact. These design branches will be considered separately and together, as appropriate.

It is also necessary to model the time required for the mission and spacecraft design as well as the construction and preparation of the spacecraft and launch vehicle. This will fix the earliest possible time of launch, which fixes the earliest possible time of deflection application. At this point 6 months have already elapsed, and the next phase to model is the mission and spacecraft design and planning phase. It will be assumed that some of the construction of the hardware can proceed concurrently with the design phase, once a critical mass of design work has been completed.

The following factors are considered. First, the NEAR mission went from conception to launch in 3 years. This mission bears a great deal of similarity to a mitigation mission and is thus a good baseline to examine. However, there is no set organization or group of organizations to respond to a NEO impact hazard, meaning that there is likely to be some initial confusion and inefficiency in the design and planning phase. Overall it will be assumed that the mission planning will take 6 months to reach the critical mass that allows construction and preparation of the spacecraft and launch vehicle to begin.

Finally, it will be assumed that, once the process picks up momentum, the construction and preparation of the spacecraft, including the mitigation system, will be able to be completed in 1 to1.5 years. This is one-third to one-half the time required by NEAR, and the reasons for this assumption are that everyone involved will most likely be highly motivated and cost should not be an issue. For a civilization-threatening NEO, it can be easily assumed that cost will not be a limiting factor in the process, though this unfortunately comes into question for a smaller NEO such as D'Artagnan, which only affects a given country or group of countries. It is assumed that cost is not an issue internally for the affected country or countries in terms of what they are willing to expend, but the question of how much the rest of the world is willing to spend to help them is open. This author would like to assume that all capable nations would contribute to the mitigation effort without hesitation, but this cannot be guaranteed. This issue is mentioned for completeness, but its thorough

analysis requires a rigorous treatment of the geopolitics and global economics involved, which are beyond the scope of this work. Thus it will be assumed that there is full global cooperation in the mitigation effort for the purposes of this case study. It is likely than any delays in cooperation in a real low warning time scenario would severely cripple or even nullify the mitigation attempt because the time scale is so short and imminent action is required for success.

11.6.4 NEO Mitigation System Selection

It will be assumed that a standoff nuclear detonation will be selected as the deflection system for D'Artagnan for the following reasons. One, a standoff detonation is one of the simplest deflection methods. It does not require a spacecraft to be guided into a high-speed impact, it does not require any equipment to be anchored to the NEO's surface, and it provides the highest energy density of any system. In short, the mission logistics are not complex, meaning that there is less to go wrong with the mission, and the nuclear device delivers a great deal of deflection power for the payload mass it requires.

11.6.5 Maximum NEO Velocity Change Magnitude

At this point the NEO mitigation system has been selected and the timeline for the design cycle has been specified. The next step is to determine the maximum deflection magnitude possible with the selected mitigation system. In this case, the standoff nuclear detonation is being considered, using the scaling methods described for Holsapple's models in section 5.4.3 and the estimated NEO parameters presented above in table 11.3.

The first step in sizing the nuclear device yield is the choice of outcome. As previously stated, it is desired that the NEO not be dispersed as there is no guarantee that some or all of the fragments will not proceed to collide with Earth. Furthermore, there is no guarantee that these fragments will be small enough to burn up in the

atmosphere if they do indeed collide. Therefore the most powerful nuclear device that does not disperse the NEO will be selected. It is of note that shattering or fracturing of the NEO is permissible. In fact, given the tremendous stress waves that are induced through the NEO material, shattering and fracture are unavoidable. However, as long as the shattered NEO is deflected as desired and does not disperse, the desired conditions are met. It is of note that this is challenging for a small asteroid such as D'Artagnan because self-gravity cannot be relied upon to help prevent dispersion. For larger asteroids, self-gravity is predicted to play a larger role.

Thus the first step is to compute the maximum nuclear device yield for a given disruption threshold. The disruption threshold is generally expressed as a specific energy for the entire NEO mass. This is determined by computed the total neutron energy delivered to the entire NEO mass in terms of the nuclear device yield and solving for the device yield as follows

$$Y_{MAX} = \frac{D \times M_{NEO}}{0.35 \times 0.1} \tag{11.4}$$

where

Y_{MAX} = maximum nuclear device yield [J]

D = disruption threshold (energy per unit mass) [J/kg]

M_{NEO} = total mass of the NEO [kg]

The factor of 0.1 in equation (11.4) is due to the assumption that only 10% of the device energy is neutron energy, and the factor of 0.35 accounts for the fact that it is assumed that only 35% of the neutron energy is absorbed by the NEO. Section 5.4.3 details the basis for these assumptions.

Next, the specific energy directly below the nuclear device detonation point is computed according to equations (11.4) and (11.5), given as

$$Q = \frac{Y_{MAX} \times 0.1}{4\pi\left(d_s^2\right)\rho l} \times 1.636 \tag{11.5}$$

where

l = neutron penetration depth [cm]

d_s = standoff detonation distance [m]

ρ = mean density of NEO [g/cm^3]

All appropriate units conversions are made. The factor of 1.636 is required to match the results to those given by Holsapple, as explained in section 5.4.3. Again, the factor of 0.1 accounts for a 10% production of neutron energy. The neutron penetration depth is assumed to be 20 cm as described in section 5.4.3. The standoff detonation distance is scaled according to Holsapple's optimal value by the ratio of the radius of D'Artagnan to the radius of Holsapple's asteroid. His asteroid has a 500 m radius and D'Artagnan's estimated radius is 60 m, yielding a ratio of 0.12. Holsapple's optimal detonation distance is 23 m, which thus scales to 2.76 m for D'Artagnan.

With the specific energy known, the imparted momentum per unit area can be computed according to the relationship established based on Holsapple's optimal detonation parameters as previously discussed. The scaling equation is reprinted here for continuity

$$p_A = \frac{Q}{1200} \times 2.026 \times 10^5$$

where

p_A = imparted momentum per unit area

The value of 1200 is the specific energy for Holsapple's optimal detonation in units of MJ/kg and the value of 2.026×10^5 is Holsapple's corresponding imparted momentum per unit area in units of kg/m-s. This proportional scaling relationship is almost certainly not the exact behavior but it serves for a first-order approximation for lack of a computer model such as Holsapple's.

Next, the total momentum imparted to the NEO is calculated by multiplying the imparted momentum per unit area by the affected area on the NEO's surface, which is purely a function of geometry and hence scales directly. As previously stated, Holsapple reports that 2.2% of the NEO surface receives energy deposition at the optimal detonation distance and the same value will be used here. Thus, the total momentum imparted to the NEO is given as

$$P_{TOTAL} = p_A \times 4\pi R_{NEO}^2 \times 0.022 \tag{11.6}$$

where

P_{TOTAL} = total momentum imparted to the NEO [kg-m/s]

R_{NEO} = NEO radius

Finally, the total velocity change imparted to the NEO is computed by dividing the total imparted momentum by the total NEO mass as follows

$$\Delta v = \frac{P_{TOTAL}}{M_{NEO}} \tag{11.7}$$

All assumed values for D'Artagnan pertaining to this set of calculations are tabulated in table 11.4 below.

Table 11.4: Standoff Nuclear Detonation Parameters for D'Artagnan

Quantity	Value
Neutron penetration depth, l	20 cm
Mean NEO density, ρ	3.0 g/cm^3
NEO diameter (spherical NEO), D	120.0 m
Optimal standoff detonation distance, d_s	2.76 m
Percent of NEO surface area affected, A_e	2.2%
Percent of total neutron energy absorbed	35%

Equations (11.4) thru (11.7) above were placed into a computer model to study the available nuclear device yields and Δv values for a range of dispersion thresholds. It was mentioned in section 5.4.3 that Holsapple talks about 100 J/kg being an approximate threshold for shattering and that the threshold for dispersion is a factor of 10 (or more) higher than this. This indicates that 1000 J/kg might be a nominal threshold value for dispersion, but it could be larger than this. The computer model results are presented in figures 11.7 and 11.8 below.

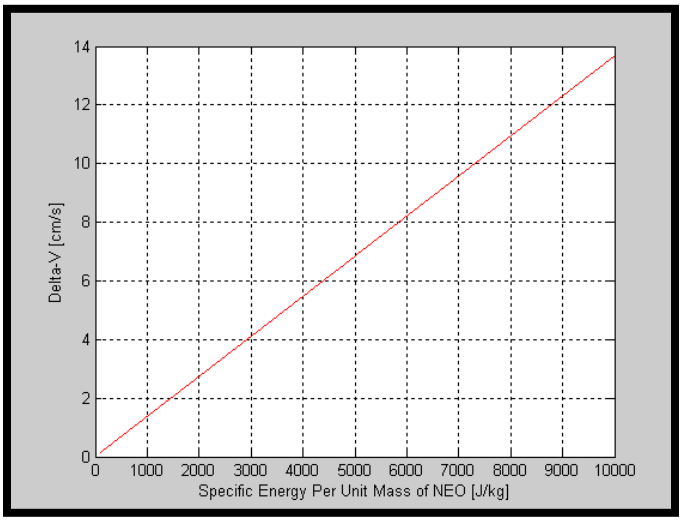

Figure 11.7: Imparted Velocity Change as a Function of Specific Energy

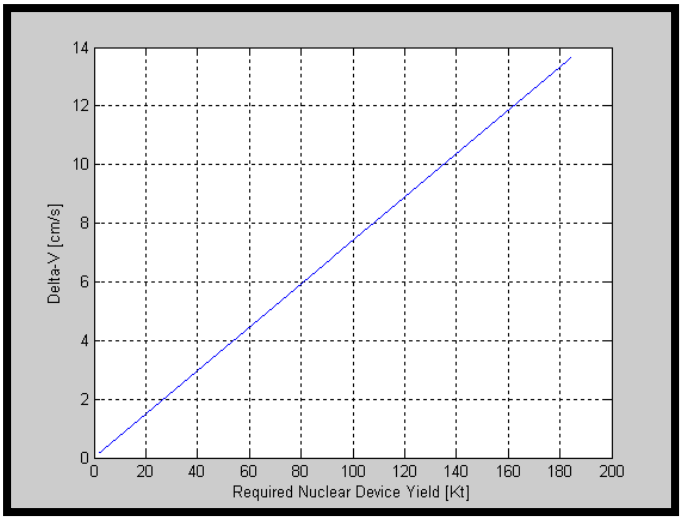

Figure 11.8: Imparted Velocity Change as a Function of Nuclear Device Yield

It is of course desired to maximize Δv with the constraint that the NEO is not dispersed. Assuming a dispersion threshold of 1000 J/kg, it can be seen from figure 11.7 that the maximum Δv is then 1.3672 cm/s and figure 11.8 thus indicates a nuclear device yield of 18.465 Kt. The question is how large a dispersion threshold can be assumed. Table 11.5 below tabulates a small range of values for the problem.

Table 11.5: Standoff Nuclear Detonation Values

Specific Energy	Δv	**Nuclear Device Yield**
732 J/kg	1.0000 cm/s	13.52 Kt
1000 J/kg	1.3672 cm/s	18.465 Kt
1463 J/kg	2.0000 cm/s	27.01 Kt
3657 J/kg	5.0000 cm/s	67.53 Kt

Mission planners are faced with a difficult choice at this point. A small Δv of only 1-2 cm/s is not likely to deflect the asteroid very much over the short time scales involved, meaning that the 1.3672 cm/s Δv at 1000 J/kg, which is 10 times the 100 J/kg shatter threshold and hence is the lower bound for the dispersion threshold range,

is not likely to provide much deflection. The 5 cm/s Δv at 3657 J/kg looks much more attractive, but the high specific energy, ~37 times the shatter threshold rather than 10, causes concern because it places the asteroid in danger of being dispersed in an uncontrolled manner, which is undesirable. However, because the true dispersion threshold is so uncertain and the smaller Δv values are unlikely to be effective, mission planners decide to risk dispersion and plan for a Δv of 5.0 cm/s and thus select a yield of ~ 68 Kt for the nuclear device.

Of course, this expected Δv will differ from that which is actually achieved since the mission planners are using erroneous values for D'Artagnan's physical parameters. This result of this discrepancy will be examined later.

Preliminary research into nuclear weapons parameters has shown that a nuclear device with a 68 Kt yield will have a mass of approximately 350 kg. This is based on the W-85 U.S. nuclear warhead, which has a nominal mass of 400 kg and a variable yield ranging from 5 to 80 Kt [29].

11.6.6 Trajectory and Spacecraft Design

At this point the mass of the nuclear device is known and it only remains to determine the mass of the delivery spacecraft, not including fuel. The amount of fuel required by rendezvous is a function of the trajectory, which has not yet been designed. The goal is to determine the combination of launch date, arrival date, and corresponding trajectory parameters that yields a feasible mission. In this case feasibility means that a launch vehicle and rendezvous thruster exist that are physically capable of carrying out the mission given the constraints of spacecraft mass and fuel mass.

A variety of trajectory optimization schemes are possible here, and the method chosen for this study was to create a lambert targeting algorithm and scan a range of departure dates and flight times. The required rendezvous fuel mass and launch energy were computed for each pair of departure and arrival dates and compared to

the capabilities of current launch systems to evaluate the viability of the design. The launch vehicle selected was the Boeing Delta-IV Heavy (4050H-19) and the rendezvous thruster selected was the Pratt & Whitney RL 10. The RL 10 has a dry mass of 167 kg and a specific impulse, I_{SP}, of 451 seconds [30]. It was decided to make a high-energy launch from Earth directly to rendezvous with D'Artagnan, so the high-energy launch performance of the Delta IV Heavy was considered. Its launch capabilities are shown in figure 11.9 below.

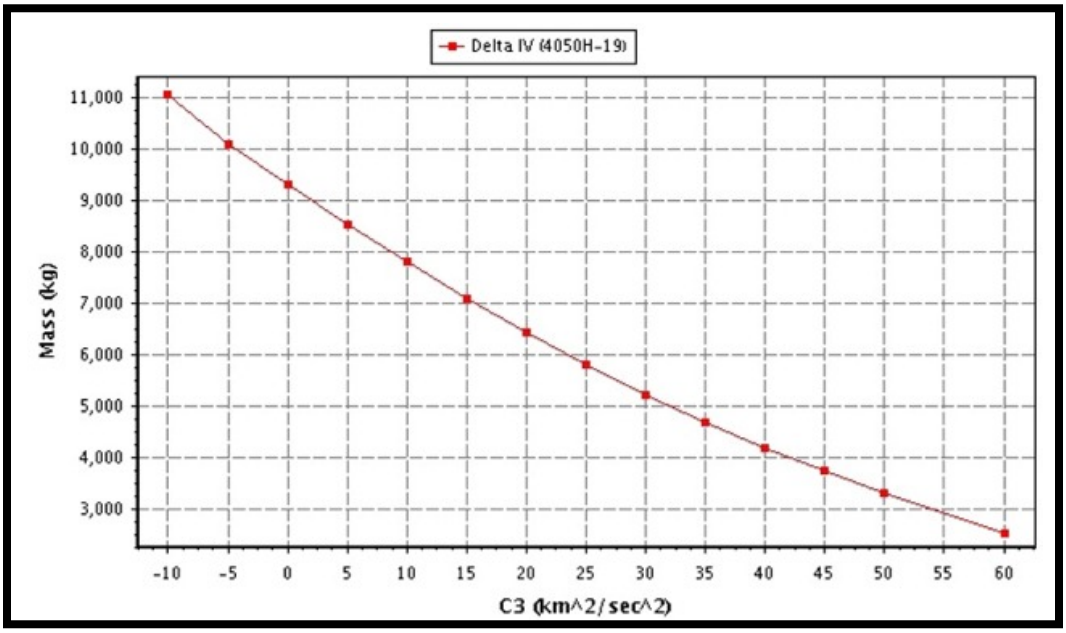

Figure 11.9: High-Energy Launch Performance for the Delta-IV Heavy [31]

The fuel-mass equations used to determine the amount of fuel required by the RL 10 thruster to perform the rendezvous maneuver as well as the resulting total mass to be launched by the Delta IV Heavy are

$$m_{fuel} = m_{dry}\left(e^{\frac{\Delta v}{gI_{SP}}} - 1\right) \qquad (11.8)$$
$$m_{total} = m_{fuel} + m_{dry}$$

where

m_{fuel} = required mass of fuel for rendezvous maneuver

m_{dry} = mass of mitigation spacecraft without rendezvous fuel

Δv = magnitude of the rendezvous maneuver

g = acceleration of gravity on Earth's surface (9.8 m/s^2

I_{SP} = specific impulse of rendezvous thruster

The dry mass of the mitigation spacecraft includes the mass of the rendezvous thruster, the mass of the nuclear device, and the mass of the supporting spacecraft structure and equipment. At this point an estimate of the spacecraft structure and equipment mass is required. The NEAR spacecraft, which had a dry mass of 487 kg was examined as a baseline [32]. The mitigation craft in this scenario will not require the extensive science equipment carried by NEAR, though it will require similar equipment for guidance, navigation, control, and communication. Such equipment includes communications antennae, onboard computer, star tracker, laser rangefinder, inertial measurement unit, and small maneuvering thrusters with fuel. This is because the spacecraft only has to travel D'Artagnan, match its orbit at some initial distance, maneuver in close to the asteroid until it arrives at the optimal detonation point at the optimal time, and then detonate the nuclear device. Therefore, given that the mass of the NEAR spacecraft was 487 kg and the current mitigation spacecraft will not require all of the NEAR equipment, the working estimate of the spacecraft mass in this case was chosen to be 300 kg.

This brings the total dry mass of the spacecraft, including the RL 10 thruster and minimized W-85 nuclear device, to 817 kg. Lambert trajectories were examined for a range of departure and arrival date pairs, with the earliest departure date considered being 1 year after initial threat determination (1.5 years after initial detection). After iterating and evaluating the viability of each trajectory, it was determined that the best rendezvous trajectory left Earth at 1.5 years after initial

detection of D'Artagnan and arrived at a rendezvous point 10 km ahead of the asteroid after an approximately 13.7 month cruise. The resulting trajectory is shown in the plane of the ecliptic in figure 11.10 below.

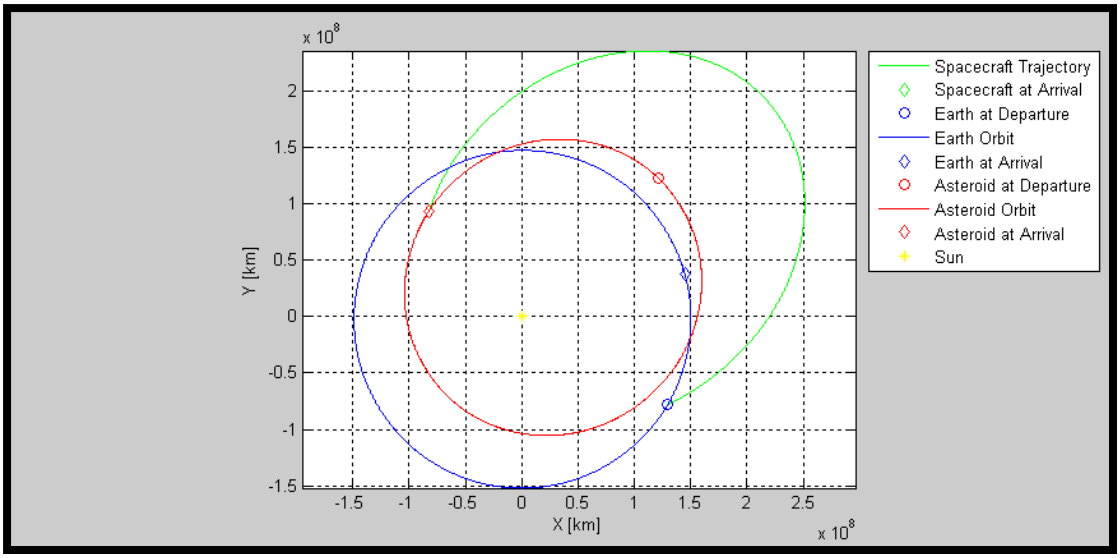

Figure 11.10: Trajectory for Rendezvous with D'Artagnan

The date of departure is 8/25/2005, 00:00:00 UT, and the date of arrival 10 km ahead of D'Artagnan along its orbit is 10/8/2006, 00:00:00 UT. The time of flight is 13.733 months, the C3 value for the launch is 8.019 km^2/s^2, the hyperbolic departure angle is 95.6°, the rendezvous Δv is 10.05 km/s, and the total spacecraft mass, including rendezvous fuel, is 7930.7 kg. Comparing the C3 value and spacecraft mass to launch performance of the Delta IV Heavy in figure 11.9 above shows that the launch vehicle is able to achieve the required performance.

At this point the mitigation system has been selected, along with the best available spacecraft and launch systems. The departure date has been set at 1 year after initial threat determination, which means that the design and construction teams must work quickly in order to be ready to launch on time. Additionally, the arrival date is known, which fixes the first available time for applying the deflection to

D'Artagnan at 2.644 years after initial detection. This now limits the range of times that can be scanned in the search for the optimal deflection orientation, which is the next step in the design process.

11.6.7 Optimal Deflection Design

The next step is to construct a map of the available deflection solution space according to the methods developed previously in section 9. D'Artagnan's actual orbital parameters will be used, along with the aforementioned $\Delta\vec{v}$ magnitude of 5.0 cm/s. The arrival date is fixed to be 2.644 years after initial detection of D'Artagnan, so the range of times to be scanned was set to begin at 2.5 years after detection and end 3 months before the projected date of impact in order to get a good look at the deflection solution space. The times for the four perihelion passages D'Artagnan makes over this interval were also included in the scan times. Time was initially scanned at a resolution of 5 months and azimuth was allowed to vary from 0° to 359° at a 1° resolution. The maximum deflections obtained for each deflection time are shown in figure 11.11 below.

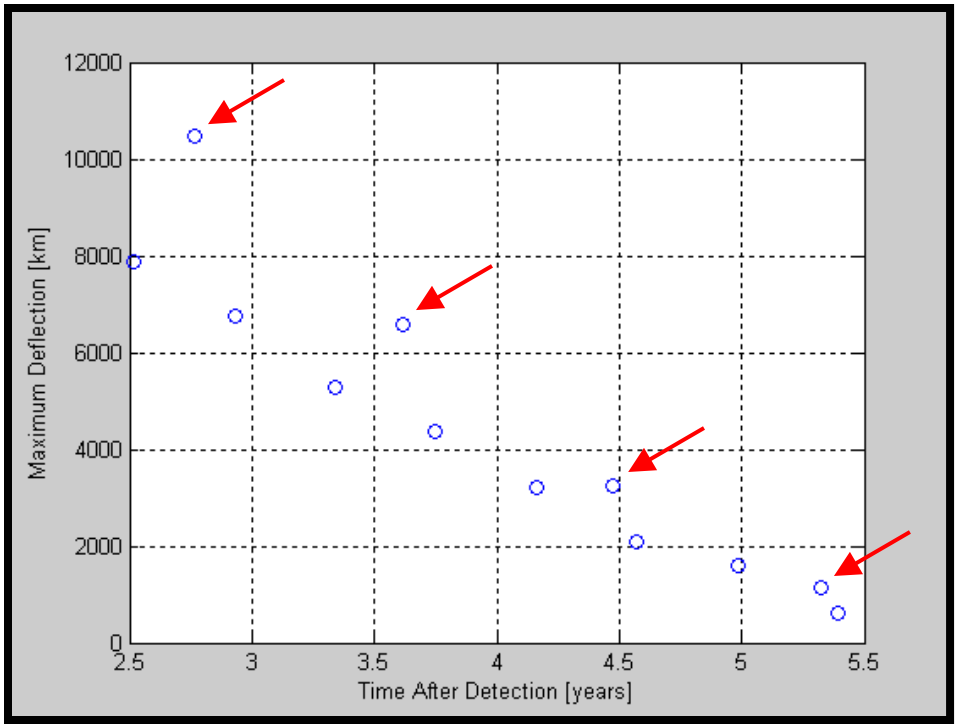

Figure 11.11: Maximum Deflection at Each Deflection Time

At this point the issue of how advantageous perihelion deflections are is revisited. The deflection times that correspond to the asteroid's perihelion passage are marked in figure 11.11 with red arrows. It is clear that the deflections applied at perihelion are substantially more effective than those that are applied several months previous. For example, the perihelion deflection at approximately 3.6 years after detection is almost exactly as effective as a deflection applied at approximately 2.9 years after detection. Additionally, the deflection time of 2.5 years is outperformed by the later perihelion passage time of 2.75 years by over 2000 km. Thus it is found to be true that the earliest available deflection time does not always perform better than a subsequent time that corresponds to a perihelion passage.

The best deflection in the range of times considered is clearly obtained at the perihelion passage that occurs at approximately 2.75 years after detection. This fits with the prescribed mission trajectory, which brings the spacecraft to a rendezvous

with D'Artagnan at 2.644 years after detection. The predicted deflection magnitude is approximately 10487 km, or about 1.644 Earth radii. This is certainly a tremendously close approach, but the goal of preventing a collision with Earth is achieved. Passing by Earth at such a low altitude raises the possibility of the asteroid colliding with Earth-orbiting satellites and spacecraft or perturbing their orbits; proper measures should be taken regarding potentially affected satellites and any humans on orbit should return to Earth immediately.

The deflections shown in figure 11.11 are each for the optimal deflection orientation at that point. The precise chosen time of deflection is 2.767 years and the corresponding optimal deflection orientation is an azimuth of 182°, which is 178.06° apart from the asteroid's instantaneous velocity vector at the time of deflection. For reference, the deflection solution space curves for azimuth are shown in figure 11.12 below. Each curve corresponds to a different time of deflection. The curve with the largest magnitude corresponds to the selected deflection at 2.767 years after detection. The exact optimal deflection date selected is 11/28/2006, 14:24:00 UT.

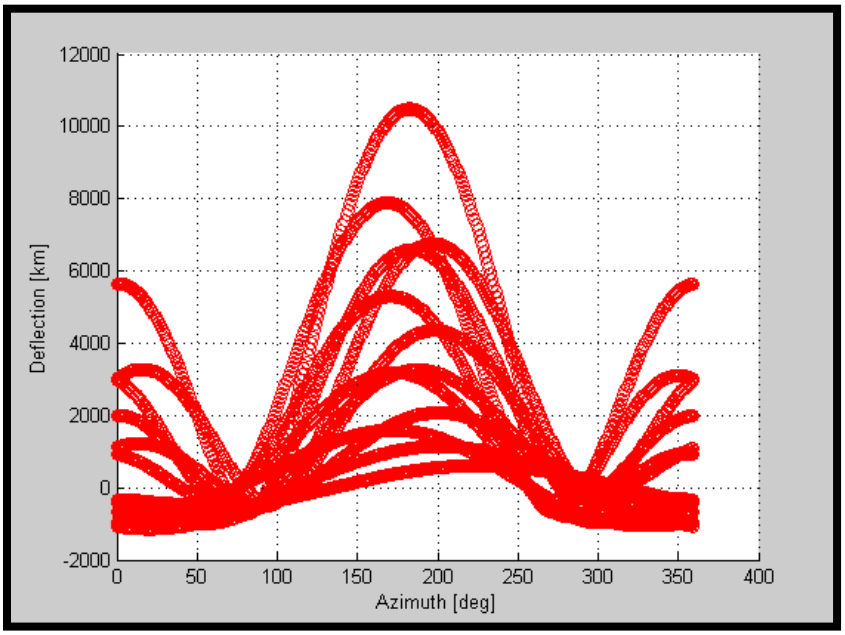

Figure 11.12: Deflection Solution Space

For reference, the optimally oriented deflection at 2.767 years for a Δv of 1.0 cm/s was computed to be only 1315 km, a value that is certainly too close for comfort. This validates the decision by mission planners to select the Δv of 5.0 cm/s even if it means a risk of undesirable dispersion of the asteroid.

11.6.8 Proximity Operations For Mitigation Operations

The only remaining design task is to plan the proximity operations that will position the nuclear device at the proper location relative to the asteroid at the proper time to achieve the optimal deflection orientation computed previously. The optimal azimuth angle, α, is 182°, and the optimal elevation angle, δ, is 0°, which allows the unit vector in the direction of the optimal $\Delta\vec{v}$ to be computed according to equation (6.5) as

$$\hat{u}_{\Delta v} = \begin{bmatrix} \cos(\delta)\sin(\alpha) \\ \cos(\delta)\cos(\alpha) \\ \sin(\delta) \end{bmatrix} = \begin{bmatrix} -0.0349 \\ -0.9994 \\ 0 \end{bmatrix}$$

Recalling that the optimal standoff detonation distance was previously computed to be 2.76 m and the radius of the asteroid beneath the detonation point is 60 m, the corresponding optimal coordinates for the nuclear device in the RTN frame can be calculated according to equation (7.5) as

$$\vec{r}_c = -(R_P + d_s)\hat{u}_{\Delta v} = (62.76)\begin{bmatrix} 0.0349 \\ 0.9994 \\ 0 \end{bmatrix} = \begin{bmatrix} 2.190 \\ 62.722 \\ 0 \end{bmatrix}[m]$$

Thus it is the task of the GNC system to maneuver the spacecraft to the above RTN coordinates from a starting position 10 km ahead of the asteroid, given by the

coordinates [0, 10000, 0] m in the RTN frame. The CW navigation methods discussed in section 3.3 are used to determine the magntiude and direction of the maneuver that will place the spacecraft on a nominal trajectory towards the desired coordinates, as well as the terminal manuever to bring the spacecraft to rest at those coordinates immediately prior to detonation. As discussed in section 3.3, the spacecraft will be fighting an array of perturbations during the proximity operations, including the gravity of the asteroid, and thus a robust controller will be required, the design and implementation of which is quite feasible. The date and time of the initial spacecraft rendezvous is 10/8/2006, 00:00:00 UT and the optimal date for the deflection is 11/28/2006, 14:24:00 UT, giving the spacecraft 51.6 days to position itself.

For simplicity it will be assumed that the spacecraft places itself onto a trajectory towards the optimal detonation coordinates shortly after arriving 10 km ahead of D'Artagnan and stabilizing itself. Thus the CW trajectory takes 51.6 days and the computed Δv required to initiate the maneuver is 0.24 cm/s. The Δv required to bring the spacecraft to rest at the optimal detonation coordinates is also 0.24 cm/s, requiring a total Δv of 0.48 cm/s. Adding a set of 6 DASA CHT monopropellant thrusters, each with a dry mass of 0.36 kg and a specific impulse of 235 seconds to carry out the required maneuvers yields a tiny required mass of maneuvering fuel. Even multiplying the fuel mass by a factor of 10 to account for correction maneuvers and adding that into the original trajectory calculations only raises the total spacecraft mass from 7930.7 kg to 7959.8 kg, still within the performance capabilities of the Delta IV Heavy. The nuclear device positioning maneuver is shown in the Transverse-Radial frame in figure 11.13 below, and a close-in view of the final spacecraft position at the optimal detonation coordinates is shown in figure 11.14.

This completes Phase II: Design Cycle. At this point the mission plan is complete and it only remains to fill in the details of guidance, control,

communication, etc. It is assumed that these details are dealt with in sufficient time and that the spacecraft and launch vehicle are prepared for launch on the specified launch date.

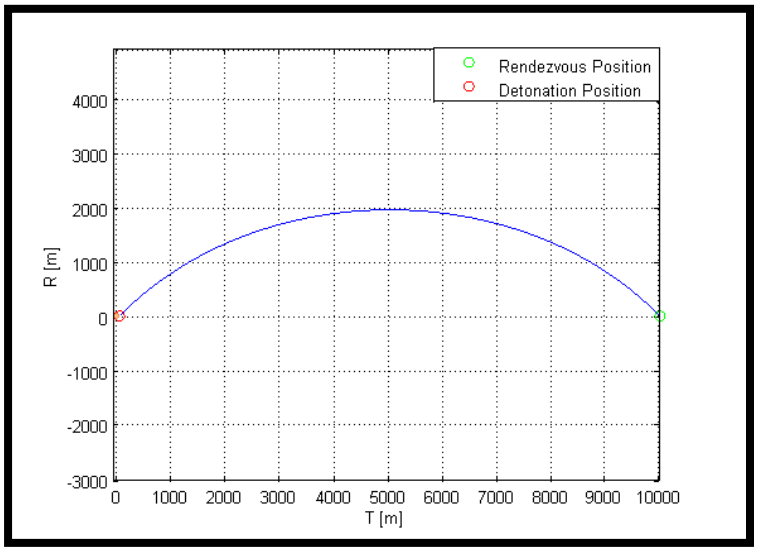

Figure 11.13: Spacecraft Trajectory to Optimal Detonation Coordinates

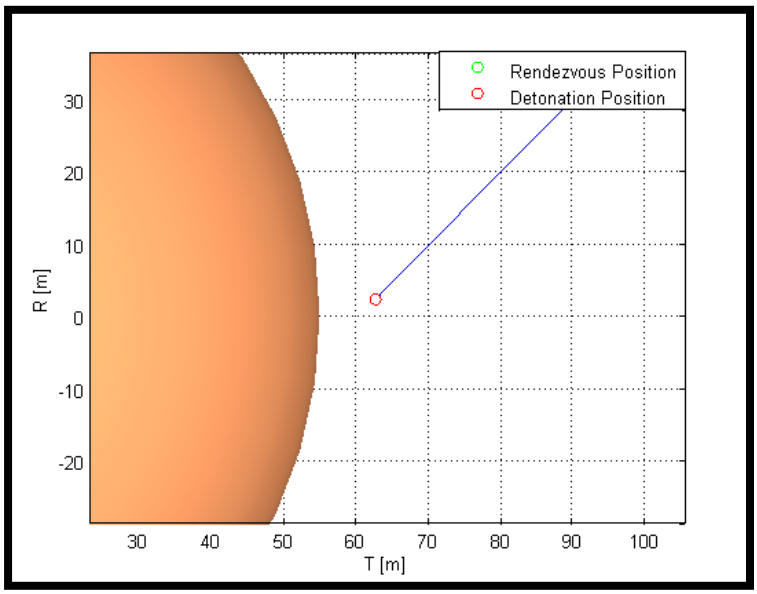

Figure 11.14: Close-In View of Spacecraft at Optimal Detonation Coordinates

11.6.9 Phase III: Implementation

At this point the final phase of the mitigation mission planning flowchart in figure 10.1 has been reached. The designs are complete and the construction of the spacecraft and launch vehicle complete in time to launch on the specified date of 8/22/2005. It is assumed that the mission goes as planned and that the spacecraft performs the rendezvous and proximity operations with only minimal difficulties, culminating in the detonation of the 68 Kt nuclear device on 11/28/2006, 14:24:00 UT as planned. The expected velocity change imparted to the asteroid is 5.0 cm/s, and computed resultant deflection is 10487 km. However, as mentioned previously, mission planners were forced to use flawed estimates of D'Artagnan's physical parameters because there was not enough time to deploy a science mission to the asteroid. The effect of using the incorrect physical parameters is explained below.

The mission planners were using the estimated values in table 11.3 above, essentially assuming that D'Artagnan is spherical with a 60 m radius, rather than ellipsoidal, and, most importantly, assuming that its density is 3.0 g/cm^3, rather than the actual value of 4.0 g/cm^3. Using the actual values and the chosen nuclear device yield of 68 Kt to compute the actual Δv imparted to D'Artagnan yields a value of 2.85 cm/s rather than the expected 5.0 cm/s. The resulting deflection for D'Artagnan, using the computed optimal azimuth angle of 182°, is approximately 5110 km, which is less than the expected value of 10487 km by 5377 km or 51.273%.

The outcome of the mitigation mission is that D'Artagnan is indeed deflected, albeit by a much smaller amount than anticipated due to inaccurate knowledge of its physical parameters.

It is of note that no provisions were made to ensure that D'Artagnan was not deflected through a keyhole location, making it possible that the asteroid will return to collide with Earth sometime in the future. To check this, D'Artagnan's deflected orbit was propagated for 10 years after the deflection in order to ascertain whether a

resonant return is indeed a danger. The resulting simulated distance between the asteroid and Earth over time is shown in figure 11.15 below.

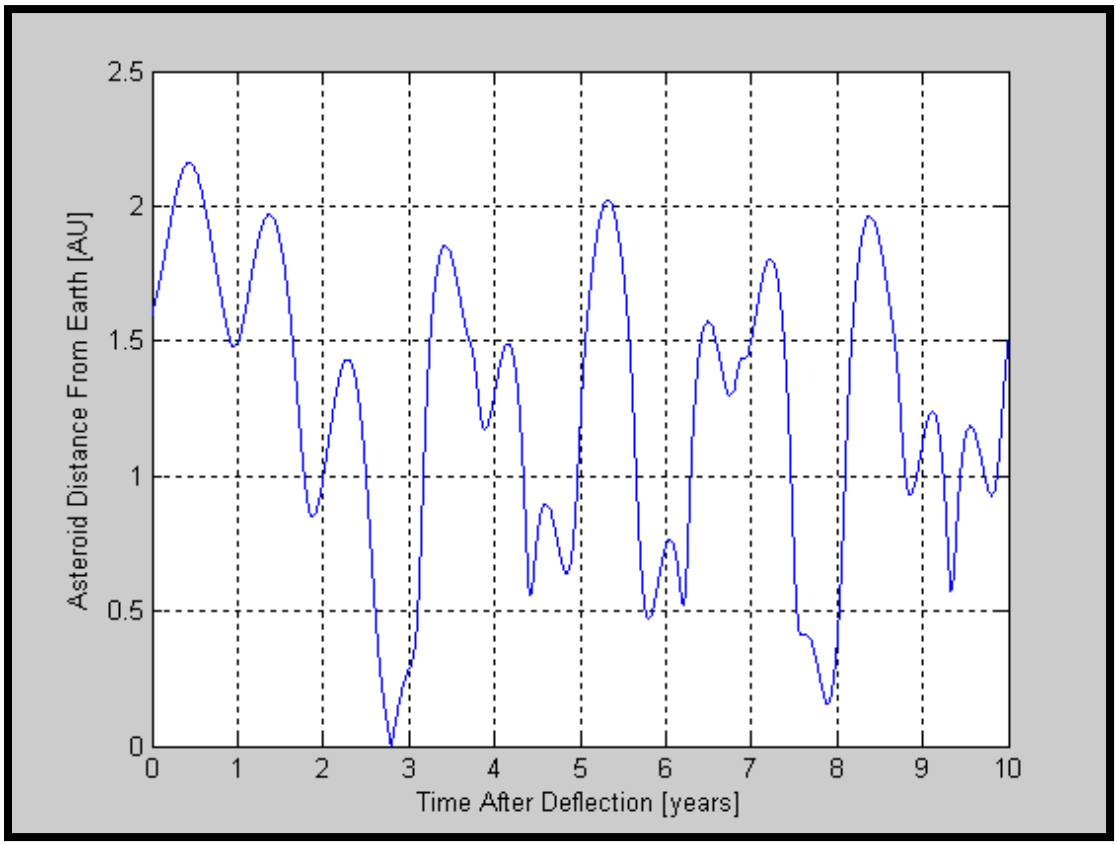

Figure 11.15: Distance Between D'Artagnan and Earth For 10 Years After Deflection

Figure 11.15 shows that D'Artagnan does not make any dangerous close approaches to Earth after the deflection, except of course for the close approach of 5110 km at about what would have been the time of collision absent mitigation.

11.7 Conclusions

Asteroid D'Artagnan was successfully mitigated with a mission generated by using the NEO mitigation mission planning procedures presented in section 10 in conjunction with the optimal deflection determination methods presented in sections

6 and 9. While this illustrates the effectiveness of these procedures and methods, the ultimate outcome of the mitigation serves to underscore deficiencies in the current state of NEO mitigation preparedness.

Firstly, an orbital observatory would mostly likely have discovered D'Artagnan earlier than ~5.5 years prior to impact, as was the case in this scenario, which would have allowed for a much more effective deflection because the asteroid could have been struck earlier. Therefore the first recommendation is that an orbital observatory be put in place to extend our capabilities for inner solar system astronomy and NEO discovery.

Secondly, increased warning time would probably have meant that a preliminary science mission could have been sent to D'Artagnan to accurately ascertain its physical properties. The use of estimated physical properties in the mitigation mission planning process severely reduced the efficacy of the deflection, and it could have been worse.

Thirdly, advancement in NEO search and automatic threat warning systems must continue. The ability to accurately predict a NEO's orbit based on observation data leads to an earlier determination that a newly discovered NEO is actually a hazard requiring mitigation. Earlier warning allows mitigation spacecraft to be deployed more quickly and have better opportunities to strike threatening NEOs at the most advantageous times.

Finally, it would be prudent to start organizing and planning for NEO mitigation missions now, establishing protocols for cooperation between nations capable of spaceflight. This will increase efficiency in the event of an actual emergency and allow for more rapid launches of NEO mitigation missions when required. Additionally, developing modular NEO mitigation spacecraft and systems that can be prepared to launch a general mitigation system quickly in the event of an emergency would further increase response time. The sooner a mitigation spacecraft can launch once a threat is identified, the better the chances of being able to strike the NEO at the earliest advantageous time.

12. CONCLUSIONS

12.1 General Summary

The goals of this work were to conduct in-depth research into the overall hazardous NEO deflection problem, develop new insights into optimal impulsive deflection solutions, design mission planning protocols for addressing hazardous NEO mitigation scenarios, and demonstrate the efficacy of all developed techniques through the use of simulation. At this point these goals have all been achieved.

The NEO mitigation problem is a very challenging one with a rich dynamic character that was not truly explored until recently. In past years this problem was thought to be outlandish rather than a true threat. However, as NEO search programs have continued to advance, they are painting a clearer picture of the space environment near Earth, a picture that shows our planet hurtling around the Sun in a veritable shooting gallery. The evidence for past NEO impacts on Earth is now undeniable, leading the question of when, not if, it will happen again.

12.2 Future Goals

Thus, the penultimate goal of this work is to start laying the foundation for planetary defense against NEOs now, while there is time to explore the problem and conduct experiments. This author and other researchers have been and will continue pursuing better and better solutions to the NEO mitigation problem. JPL's Sentry program and the NEODyS system at the University of Pisa will continue striving to identify threatening NEOs as soon as possible. However, there are key ingredients still missing from a robust planetary defense.

The first missing ingredient is experimentation. Despite all the effort that has gone into theorizing about NEO mitigation strategies, there have been no field tests or serious efforts made to create rapid response spacecraft. Thus it is imperative that NEO mitigation system testing begin immediately. In the process of creating these systems and learning to apply them adroitly to NEOs in challenging ways, we will

only serve to increase our scientific and technological knowledge, whether our mitigation systems are ever needed or not.

The second missing ingredient is cooperation. There is currently no research center, design team, or launch vehicle provider designated as being responsible for planetary defense. Were a threatening NEO discovered tomorrow, the mad dash to act would be chaotic and initially counterproductive. NEO impacts are a global problem and therefore they need to be addressed globally, hopefully through the establishment of international organizations to oversee the creation and advancement of field-tested NEO mitigation technology, as well as its emergency preparedness.

12.3 Future Work

The research begun in this work has a long way to go. Applications of classical optimal control theory, as well as applications of numerical optimization methods, may be well-suited to the deflection orientation optimization problem formulated herein and solved through simulating N body systems. Additionally, the refinement and extension of the generalized NEO mitigation mission planning flowchart could lead to a robust software tool that provides a mission planner with a virtual NEO collision mitigation mission design space in which the effects of altering individual design parameters for the overall deflection, not just the orientation of the deflection vector, can be examined in the context of the overall problem. The difficulties inherent to mitigating the collision of threatening “rubble-pile” NEOs must still be addressed.

12.4 Important Results

One important result from this work is the demonstration that three-body and above methods yield the best results when attempting to ascertain the true deflection achieved by a given solution. This is in contrast to methods used by other researchers that employ two-body dynamics or linearizations thereof. Even more importantly, the choice of performance index is absolutely crucial. It became clear than an

inappropriate performance index gave results that were dangerously misleading and incorrect. Therefore this author strongly recommends the use of non-linear simulation methods coupled with the preferred performance index defined within this work for the purpose of optimal impulsive NEO deflection determination.

12.5 Final Remarks: Asteroid Apophis

In closing I will refer to the current case of asteroid Apophis. Apophis is the Greek name for the ancient Egyptian god of death and destruction, which is rather ominous, to be sure. This asteroid is going to make a historic close approach to Earth on April 13th, 2029, passing within ~ 30,000 km of our planet [33].

Apophis is estimated to have a mass of 4.6×10^{10} kg and a mean diameter of 320 m [33]. For reference, its mass is approximately equivalent to the mass of 130,000 fully loaded 747 airliners. Additionally, its impact velocity, if it indeed hits Earth, is estimated at 12.59 km/s (~ 28,000 mph), placing its energy yield at ~ 870 Mt. This is a huge amount of destructive energy considering that the largest nuclear weapon ever tested on Earth had a yield of 50 Mt. For reference, 870 Mt is equal to 43,5000 Hiroshima bombs. Thus Apophis has the potential to cause extensive regional devastation, depending on where it hits Earth's surface. Preliminary models have shown that Apophis is likely to strike somewhere in the Pacific Ocean if it does impact Earth, which would lead to large tsunamis on the adjacent coastlines and possibly large earthquakes. A collision of Apophis with Earth is clearly worth preventing.

There is a possibility during the 2029 close approach that Apophis will pass through one of the aforementioned "keyhole" locations in space near Earth. If that happens, it is almost certain that the asteroid will return to collide with Earth in the year 2036. This is only the most likely outcome; depending on which keyhole Apophis were to pass through, the actual resonant return could occur on 2034, 2035, 2036, or 2037 [33].

Currently, the estimated probability of an impact occurring is about 1/5560, which is twice the probability of any given person having an automobile accident on a given day [33]. This perceived collision probability will either increase or decrease as more observational data becomes available. The asteroid will come close to Earth on 2014, leading to the possibility that we might be able to either send a mission to study it, deflect it, or both. The most important thing is to place a beacon on the asteroid before doing anything else. The beacon will show the true asteroid orbit, removing a great deal of error and allowing for accurate orbit predictions. This sort of accurate knowledge is required to intelligently design optimal deflection maneuvers. Moreover, if it is found that the asteroid's natural motion takes it clear of the dangerous zone, then there is no need to take further action beyond observing and learning what we can from the asteroid.

Discovering Apophis so early before the upcoming close approach and potential collision is a golden opportunity. Never before has science been performed on a smaller asteroids such as Apophis, and there are many unanswered questions about the large population of small NEOs that such science would address. Therefore, this author recommends that NASA prepare and launch a discovery-class mission to Apophis as soon as possible. The sooner we know what we are dealing with the sooner we can act intelligently. Catching the asteroid so far before potential impact means that even a small deflection now can have a profound cumulative effect much later on the asteroid's subsequent motion. If we wait until the last minute to attempt to deflect it, will take dramatically more energy to safely deflect Apophis. If the case study presented in this work has shown anything, it is that deflection operations that take place only several years before the original impact date suffer from severely reduced performance. With this result known there is no reason to put ourselves in that situation by waiting to act until Apophis passes through a keyhole and we suddenly have a nearly guaranteed impact.

As a final closing remark, I hope that the field of NEO mitigation study continues to grow and that I can continue to be a positive force within it. There is a

vast array of NEOs out there for us to interact with, learn from, and defend ourselves against. They are beautiful, mysterious, and terrifying all at once, like so many things in nature. But on the day when the human race successfully changes the orbit of a NEO, we will not have to fear them any longer.

APPENDIX A: REFERENCE FRAMES AND TRANSFORMATIONS

This appendix contains a specification for each reference frame used in this work. Reference frames are formed by a set of orthogonal basis vectors that allow for vector quantities to be described consistently. In this case, the reference frames are all three-dimensional and are chiefly used for defining vectors for position, velocity, and acceleration as applied to orbital motion. The reference frames presented are the Heliocentric Inertial (HCI) frame, the Radial-Transverse-Normal (RTN) frame, the Earth-Centered Inertial (ECI) frame, and the Earth-Centered, Earth-Fixed (ECEF) frame. Linear transformations to convert vectors coordinated in one frame to vectors coordinated in another frame are presented where appropriate.

A.1 Heliocentric Inertial Reference Frame

The Heliocentric Inertial (HCI) reference frame is centered at the center of mass of the Sun, nominally, and the X-axis of this reference frame is directed at the first point in Aries. The *XY* plane, also called the ecliptic plane, contains the orbit of the Earth by definition. This is generally the reference frame of choice for describing planetary motion, NEO motion, and interplanetary spacecraft trajectories. A diagram of the HCI frame is given in figure A.1 below.

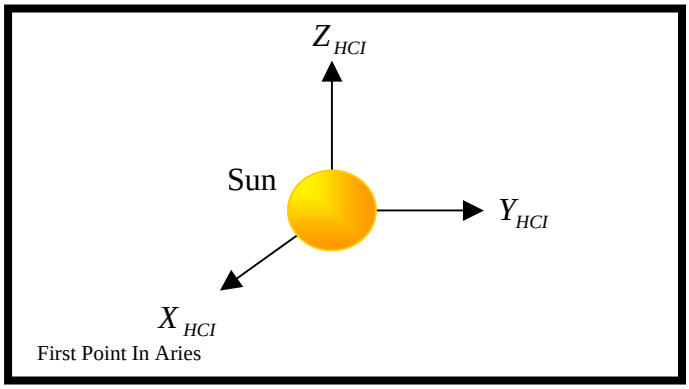

Figure A.1: Heliocentric Inertial (HCI) Reference Frame (J2000)

A.2 State Representations

It is necessary to be able to fully define the dynamic state of an object at any time in a given reference frame, and there are two primary state representations that are used in this work. The first is a pair of position and velocity vectors for an object at a specified time. In astrodynamics parlance, this time is called the epoch. Position and velocity vectors are both three-dimensional and hence each has three components, meaning that six dynamical values plus an epoch are required to completely describe the instantaneous dynamic state of an object. Alternatively, the state may be described by six parameters that describe both the shape of an orbit and the object's location along the orbit at a given epoch. These orbital parameters are typically referred to as orbital elements, and there are a variety of systems for defining them. The orbital element definitions used in this work are those for the classical Keplerian elements.

A.2.1 Position and Velocity Vectors at an Epoch

The position and velocity vectors for an object relative to the HCI frame are shown in figure A.2 below.

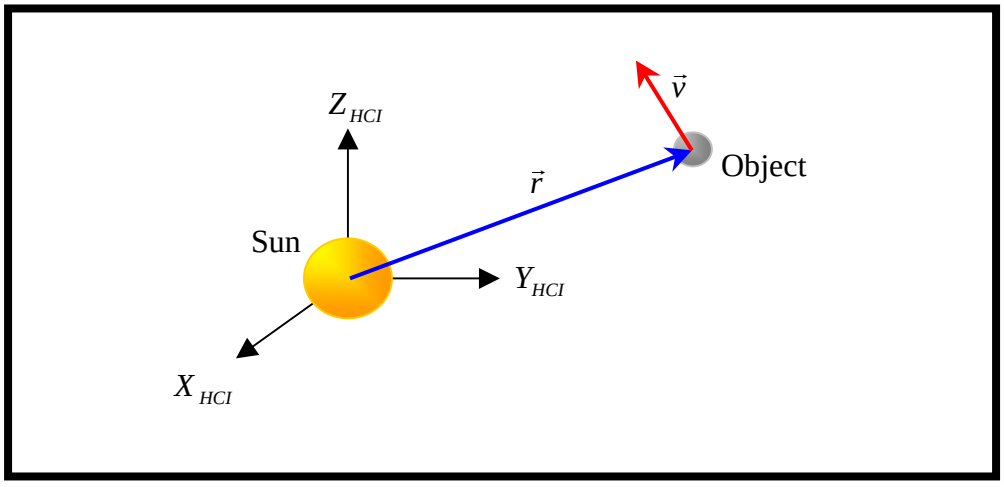

Figure A.2: HCI Position and Velocity Vectors

Unless specifically stated otherwise, all positions and velocities are for the center of mass of an object. As indicated previously, all position and velocity vectors are three-dimensional and are of the form given by

$$\begin{aligned} \vec{r} &= r_X \hat{i} + r_Y \hat{j} + r_z \hat{k} \\ \vec{v} &= v_X \hat{i} + v_Y \hat{j} + v_z \hat{k} \end{aligned} \tag{A.1}$$

where r_X, r_Y, and r_Z are the components of the position vector and v_X, v_Y, and v_Z are the components of the velocity vector. The basis vectors are expressed as $\hat{i}$, $\hat{j}$, and $\hat{k}$, and these correspond to the X, Y, and Z axes, respectively. This correspondence is a general convention and it may be assumed throughout this work unless specifically stated otherwise.

The position and velocity vectors are both functions of time, $\vec{r}(t)$ and $\vec{v}(t)$, and a particular time value is called an epoch, as previously stated. The epoch consists of both a date and a time of day, and there are a variety of systems available for expressing this information. Typically, the epochs given in this work are in terms of a day, month, and year, combined with a time of day expressed as a decimal fraction of one solar day, which is 86400.0 seconds long. Other time expressions may be used, such as the Julian Date (JD) or the Modified Julian Date (MJD), and their mathematical descriptions will not be detailed here. For more information, please consult any astrodynamics text. Time values, like vectors, are expressed with respect to a temporal reference point and conversions are thus required to equate times expressed in different reference systems. Time values in this work will be stated in Universal Time, UT, unless otherwise noted. Please consult any astrodynamics text for a complete description of UT.

A.2.2 Orbital Elements at an Epoch

Aside from position and velocity vectors, classical Keplerian orbital elements will also be used in this work to describe the dynamic state of an orbiting object at a particular epoch. A diagram of the classical Keplerian orbital elements is presented in figure A.3 below.

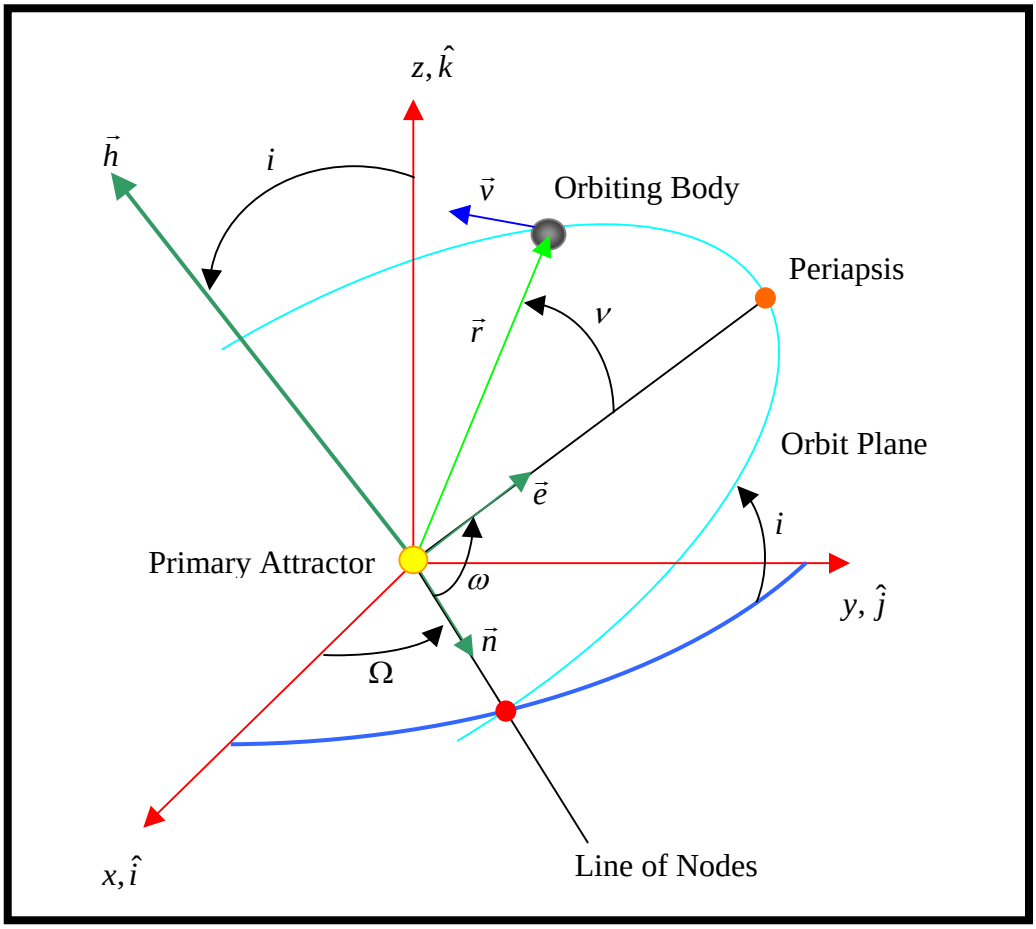

Figure A.3: Diagram of Classical Keplerian Orbital Elements

The definition of the orbital elements are with respect to the inertial frame centered at the center of mass of the primary attractor, which is the Sun for the case of the HCI

frame. These orbital element definitions also apply in the case of an inertial reference frame centered at the center of mass of planet, such as in the case of the Earth-Centered Inertial (ECI) frame that will be discussed in a subsequent section. The individual orbital elements are defined in table A.1 below.

Table A.1: Classical Keplerian Orbital Elements

Symbol	Meaning
a	Semi-major axis
e	Orbital Eccentricity
i	Orbital Inclination
Ω	Right Ascension of the Ascending Node
ω	Argument of Periapsis
ν	True Anomaly at Epoch

In order to convert the state represented by a set of orbital elements to a position and velocity vector coordinated in the inertial frame, it is required to first write the position and velocity vectors expressed in the perifocal (PQW) frame, which is centered at the primary attractor's center of mass and for which the P axis points to the object's periapsis, W is normal to the orbit plane, and Q completes the right-handed set. A diagram of the perifocal frame is presented in figure A.4 below.

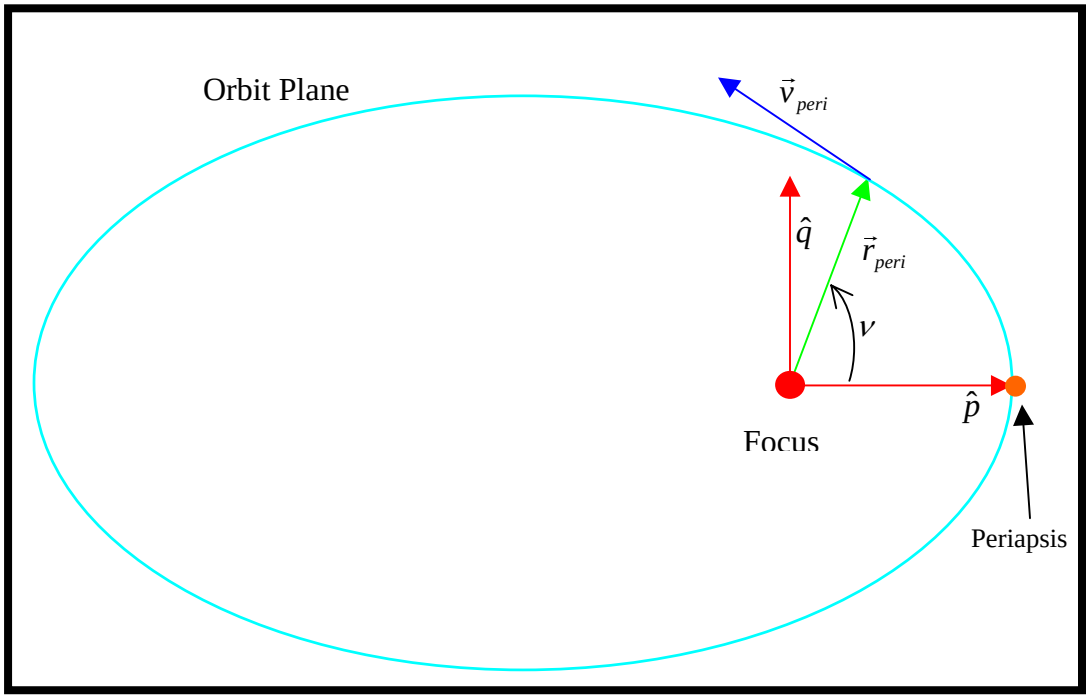

Figure A.4: Diagram of Perifocal Reference Frame in the Orbit Plane

The position and velocity in the PQW frame are expressed as follows.

$$\vec{r}_{peri} = \begin{bmatrix} \frac{a\left(1-e^2\right)\cos(\nu)}{1+e\cos(\nu)} \\ \frac{a\left(1-e^2\right)\sin(\nu)}{1+e\cos(\nu)} \\ 0 \end{bmatrix} \tag{A.2}$$

$$\vec{v}_{peri} = \begin{bmatrix} -\sqrt{\frac{\mu}{a(1-e^2)}}\sin(\nu) \\ \sqrt{\frac{\mu}{a(1-e^2)}}(e+\cos(\nu)) \\ 0 \end{bmatrix} \tag{A.3}$$

where

μ = gravitational parameter of the primary attractor, GM

G = universal gravitational constant

M = mass of the primary attractor

The elliptical geometry used to arrive at the expressions in equations (A.3) and (A.4) above is presented in figure A.5 below.

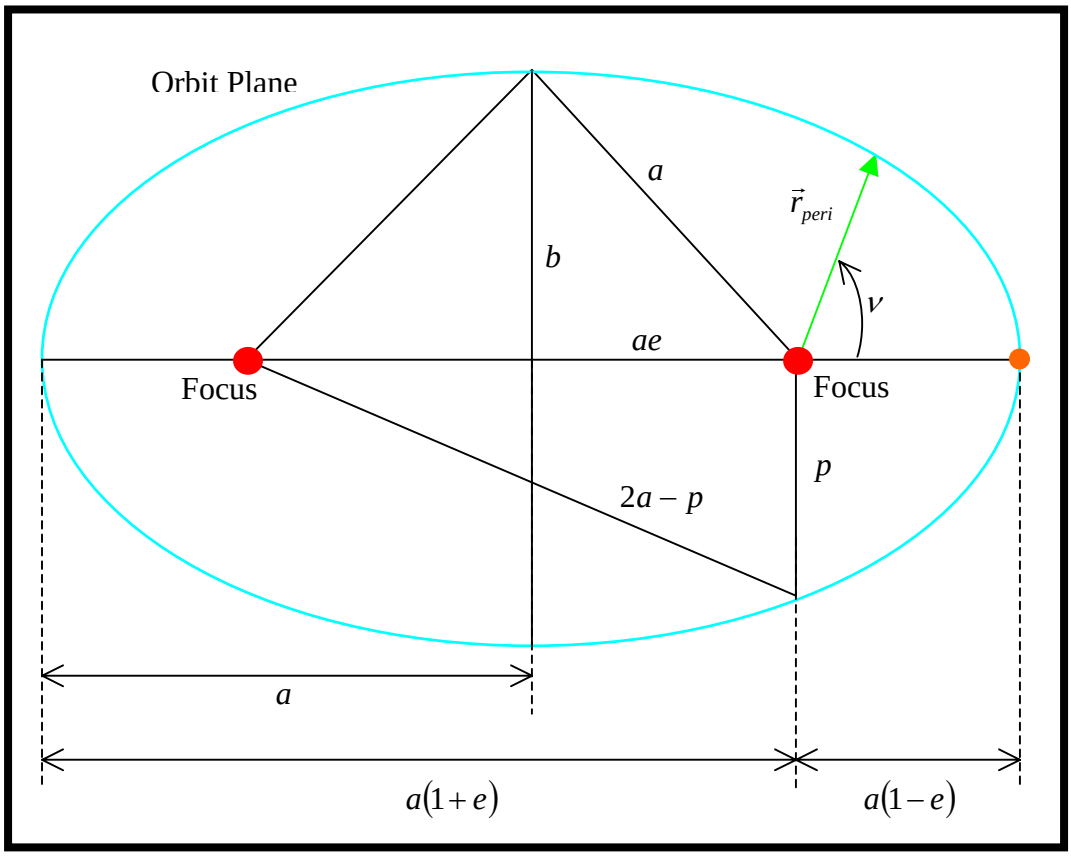

Figure A.5: Diagram of Ellipse Geometry with Orbital Element Quantities

After expressing the position and velocity in the PQW frame, it only remains to transform the PQW position and velocity vectors from the PQW frame to the inertial frame. This requires one linear transformation that is composed of a series of rotations about each coordinate axis.

The first rotation is about the Z-axis by the negative of the argument of perigee. This brings the eccentricity vector down into the equator plane, coincident with the line of nodes. The matrix for this rotation is given as

$$\underline{R}(-\omega) = \begin{bmatrix} \cos(-\omega) & \sin(-\omega) & 0 \\ -\sin(-\omega) & \cos(-\omega) & 0 \\ 0 & 0 & 1 \end{bmatrix} \tag{A.5}$$

The second rotation is about the X-axis by the negative of the inclination. This brings the Z-axis of the PQW frame into alignment with the Z-axis of the inertial frame and makes the XY planes of both frames coincident. The matrix for this rotation is

$$\underline{R}(-i) = \begin{bmatrix} 1 & 0 & 0 \\ 0 & \cos(-i) & \sin(-i) \\ 0 & -\sin(-i) & \cos(-i) \end{bmatrix} \tag{A.6}$$

The third rotation is about the Z-axis by the negative of the right ascension of the ascending node. This brings the X-axes of both frames into alignment, completing the rotation sequence. The matrix for this rotation is

$$\underline{R}(-\Omega) = \begin{bmatrix} \cos(-\Omega) & \sin(-\Omega) & 0 \\ -\sin(-\Omega) & \cos(-\Omega) & 0 \\ 0 & 0 & 1 \end{bmatrix} \tag{A.7}$$

The compound rotation matrix that transforms PQW vectors to inertial vectors is the product of equations (A.5) thru (A.7) and is given by

$$\underline{R}_{INRTL}^{PQW} = \underline{R}(-\Omega)\underline{R}(-i)\underline{R}(-\omega) \tag{A.8}$$

Multiplying a PQW vector by the rotation matrix of equation (A.8) will yield the corresponding vector in the inertial frame.

A set of inertial position and velocity vectors may also be converted to classical Keplerian orbital elements as follows. First, the orbital angular momentum of the object is given by

$$\vec{h} = \vec{r} \times \vec{v} \tag{A.9}$$

This leads to the following computation of the inclination i of the orbit

$$i = \arccos\left(\frac{h_{\hat{k}}}{\|\vec{h}\|}\right) \tag{A.10}$$

The eccentricity vector of the orbit is computed by the following equation

$$\vec{e} = \frac{\vec{v} \times \vec{h}}{\mu} - \frac{\vec{r}}{\|\vec{r}\|} \tag{A.11}$$

and the value of the eccentricity is then simply the magnitude of the eccentricity vector, given by

$$e = \|\vec{e}\| \tag{A.12}$$

The line of nodes is the line defined by the intersection of the orbit plane with the equator plane, as shown in figure A.3 above. A unit vector called the node vector can be defined along this line, and since it is perpendicular to both the Z axis of the inertial frame and the angular momentum vector, this vector is computed as follows

$$\vec{n} = \hat{k} \times \vec{h} \tag{A.13}$$

Note that for an orbit where the orbit plane coincides with the XY plane, the line of nodes and any parameters referenced to it are undefined. In this case, other orbital element systems are available for use but are not discussed here.

Next, the right ascension of the ascending node is computed as the angle between the X axis of the inertial frame and the line of nodes, given by

$$\Omega = \arccos\left(\frac{n_{\hat{i}}}{\|\vec{n}\|}\right) \tag{A.14}$$

The length of the semi-major axis of the orbit can be computed from previously defined quantities as follows

$$a = \frac{\|\vec{h}\|^2}{\mu\left(1-e^2\right)} \tag{A.15}$$

The argument of perigee is the angle in the orbit plane between the line of nodes and the eccentricity vector and is given by

$$\omega = \arccos\left(\frac{\vec{n}\cdot\vec{e}}{\|\vec{n}\|\|\vec{e}\|}\right) \tag{A.16}$$

Finally, the true anomaly of the orbiting object specifies its angular location along the orbit with respect to periapsis. It is the angle between the position vector in the orbit plane of the object and the eccentricity vector, and is thus computed as follows

$$\nu = \arccos\left(\frac{\vec{e}\cdot\vec{r}}{\|\vec{e}\|\|\vec{r}\|}\right) \tag{A.17}$$

A.3 Radial-Transverse-Normal Reference Frame

The Radial-Transverse-Normal (RTN) frame is located at the center of mass of an orbiting object and is not fixed to the body of the object. Rather, this frame rotates according to the object's orbital motion. The radial axis, R, with unit vector $\hat{r}$, is always aligned with the position vector pointing from the center of mass of the central attractor to the center of mass of the object. The normal axis, N, with unit vector $\hat{n}$, is always normal to the object's orbit plane. The transverse axis, T, with unit vector $\hat{t}$, completes the right-handed basis vector set and is given by $\hat{t} = \hat{n} \times \hat{r}$. A diagram showing the RTN frame relative to the inertial frame for an orbiting object is shown in figure A.6 below.

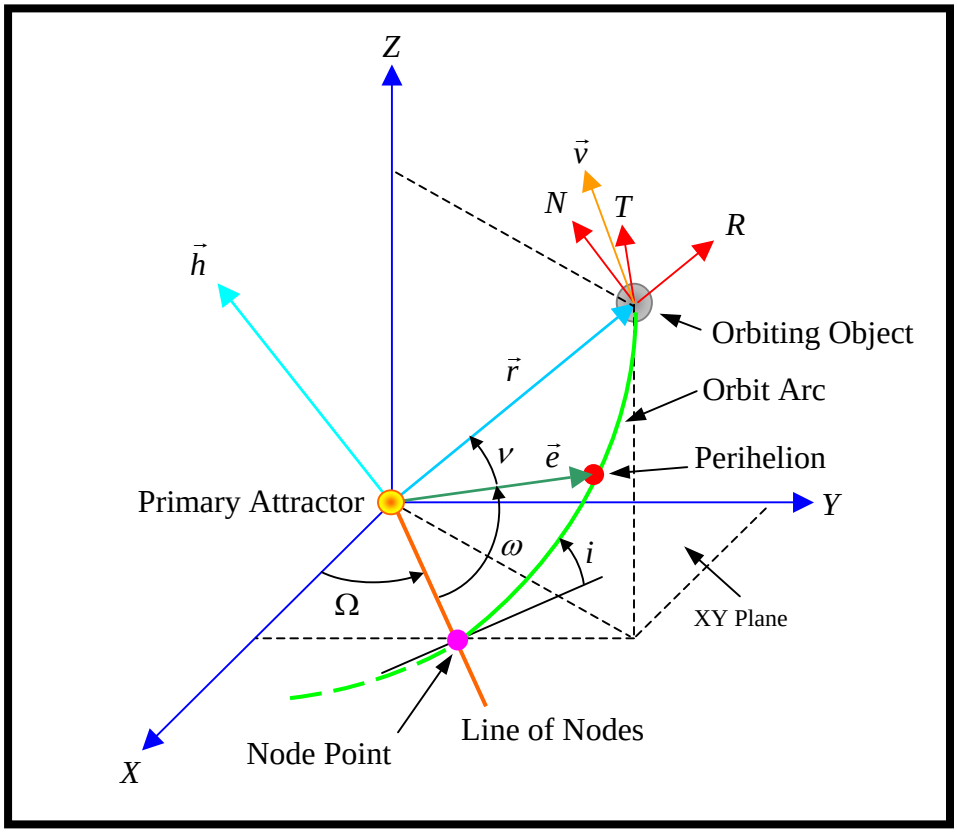

Figure A.6: RTN Reference Frame and Orbital Geometry

Vectors are easily converted from the RTN frame to the inertial frame and vice versa. This operation is crucial for the optimal deflection algorithms presented in this work. Construction of this linear transformation is accomplished by performing a sequence of rotations where the first rotation is a positive rotation about the Z axis through the angle Ω as shown in figure (A.7) below.

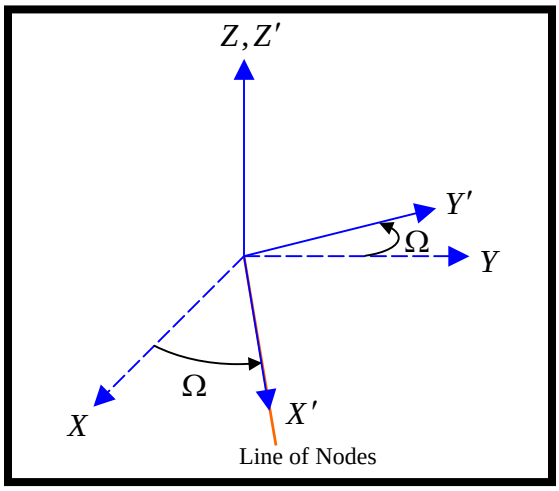

Figure A.7: First Rotation About The Z Axis

The following rotation matrix can be derived from analyzing the geometry in figure A.7

$$\underline{R}_{XYZ'}^{XYZ}(\Omega) = \begin{bmatrix} \cos(\Omega) & \sin(\Omega) & 0 \\ -\sin(\Omega) & \cos(\Omega) & 0 \\ 0 & 0 & 1 \end{bmatrix} \tag{A.18}$$

As seen in figure (A.7) above, this rotation brings the X axis into alignment with the line of nodes, at which point the X axis becomes the X' axis.

The next rotation in the sequence is a positive rotation about the X' axis through angle i as shown in figure (A.8) below.

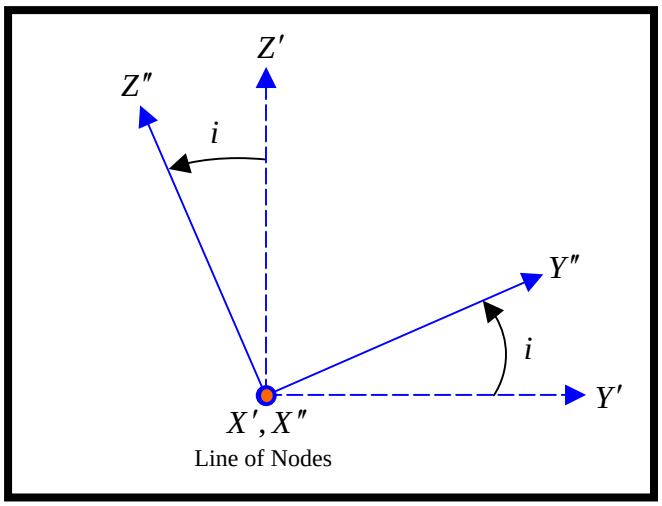

Figure A.8: Second Rotation About The X', X'' Axis

The transformation matrix corresponding to the rotation illustrated in figure A.8 is

$$\underline{R}_{X''Y''Z''}^{XYZ'}(i) = \begin{bmatrix} 1 & 0 & 0 \\ 0 & \cos(i) & \sin(i) \\ 0 & -\sin(i) & \cos(i) \end{bmatrix} \tag{A.19}$$

The third and final rotation in the sequence is a positive rotation about the $Z'', Z''', \hat{N}$ axis through the angle $\omega + \nu$ as shown in figure (A.9) below.

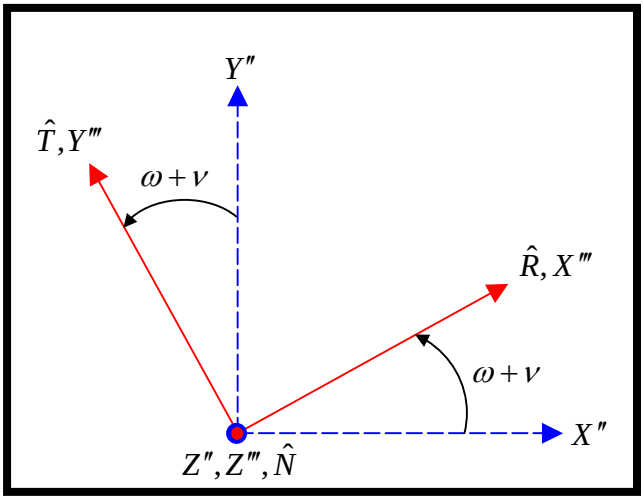

Figure A.9: Third and Final Rotation About The $Z'', Z''', \hat{N}$ Axis

The rotation matrix corresponding to the rotation illustrated in figure A.9 is

$$\underline{R}_{RTN}^{X''Y''Z''}(\omega+\nu) = \begin{bmatrix} \cos(\omega+\nu) & \sin(\omega+\nu) & 0 \\ -\sin(\omega+\nu) & \cos(\omega+\nu) & 0 \\ 0 & 0 & 1 \end{bmatrix} \tag{A.20}$$

The total transformation matrix that transforms vectors coordinated in the XYZ frame to vectors coordinated in the RTN frame is computed by multiplying the rotation matrices for each rotation in the sequence as shown in equations (A.21) below.

$$\begin{aligned} \vec{r}_{RTN} &= \underline{R}_{RTN}^{X''Y''Z''}(\omega+\nu)\underline{R}_{X''Y''Z''}^{X'Y'Z'}(i)\underline{R}_{X'Y'Z'}^{XYZ}(\Omega)\vec{r}_{XYZ} \\ \vec{r}_{RTN} &= \underline{R}_{RTN}^{XYZ}\vec{r}_{XYZ} \end{aligned} \tag{A.21}$$

Carrying out the matrix multiplications called for in equations (A.21) yields the product of equations (A.18), (A.19), and (A.20) as

$$\underline{R}_{RTN}^{XYZ} = \begin{bmatrix} \cos(\omega+\nu)\cos(\Omega) - \cos(i)\sin(\Omega)\sin(\omega+\nu) & \cos(\omega+\nu)\sin(\Omega) + \cos(i)\cos(\Omega)\sin(\omega+\nu) & \sin(i)\sin(\omega+\nu) \\ -\sin(\omega+\nu)\cos\Omega - \cos(i)\sin(\Omega)\cos(\omega+\nu) & -\sin(\omega+\nu)\sin\Omega + \cos(i)\cos(\Omega)\cos(\omega+\nu) & \sin(i)\cos(\omega+\nu) \\ \sin(i)\sin(\Omega) & -\sin(i)\cos(\Omega) & \cos(i) \end{bmatrix} \quad \text{(A.22)}$$

The matrix given in (A.22) is the desired transformation matrix that transforms vectors coordinated in the XYZ frame to vectors coordinated in the RTN frame. To transform vectors from the RTN frame to the XYZ frame, the transpose of equation (A.22) is used.

A.4 Earth-Centered Inertial Reference Frame

The Earth-Centered Inertial (ECI) frame is centered at the center of mass of the Earth and does not rotate with Earth. The Z axis is aligned with Earth's spin axis, which is tilted by approximately 23.5° from the Z axis of the HCI frame. The X axis of the ECI frame is aligned with the X of the HCI frame and hence also points to the first point in Aries. A diagram of the ECI frame is given in figure A.10 below.

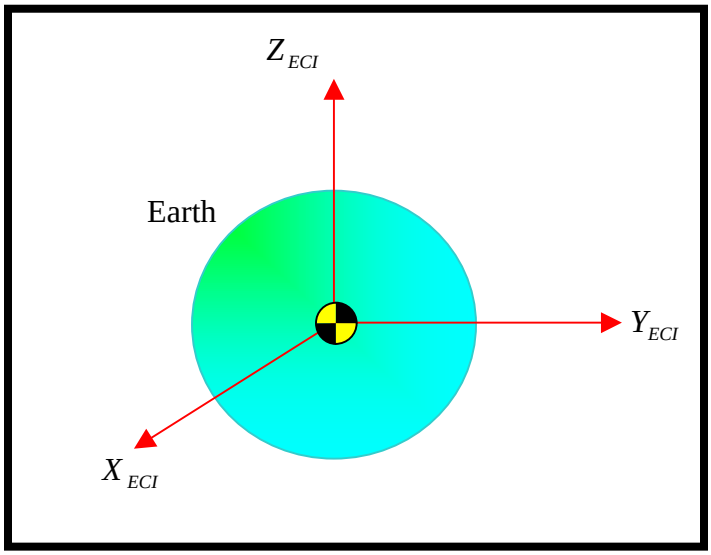

Figure A.10: The Earth-Centered Inertial (ECI) Reference Frame

A.4.1 Transformation to Heliocentric Inertial Reference Frame

Vectors in the ECI frame are readily transformed to vectors in the HCI frame by rotating about the X axis through the angle of the tilt of the Earth's rotation axis with respect to the plane of the ecliptic. This angle is typically referred to as the obliquity, ε, and is nominally equal to 23.5°. Slight periodic variations in the obliquity must be taken into account for extreme accuracy and are not detailed here. The Earth's spin axis also nutates and precesses very slightly, which must be accounted for in order to be absolutely precise. These considerations are also not

detailed here. Consult any astrodynamics text for a full treatment of these topics. Figure A.11 below illustrates the rotation of the ECI frame to the HCI frame.

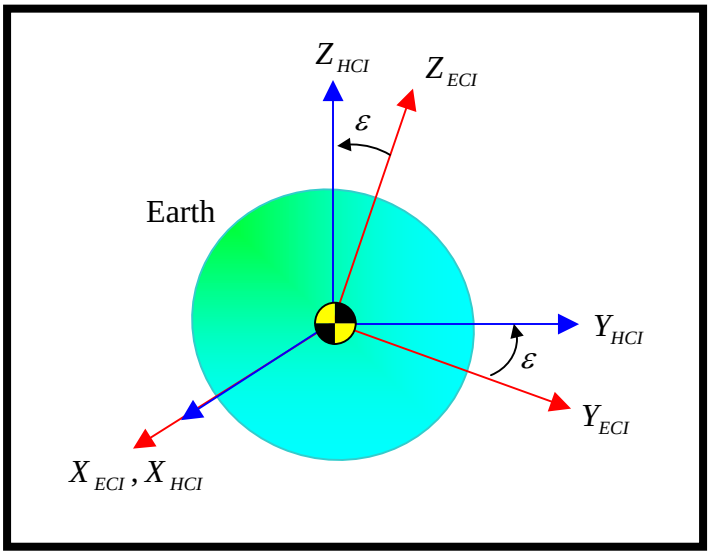

Figure A.11: Rotation of the ECI Frame to the HCI Frame

The rotation matrix that accomplishes this transformation is given by

$$\underline{R}_{HCI}^{ECI} = \begin{bmatrix} 1 & 0 & 0 \\ 0 & \cos(\varepsilon) & -\sin(\varepsilon) \\ 0 & \sin(\varepsilon) & \cos(\varepsilon) \end{bmatrix} \tag{A.23}$$

A.5 Earth-Centered, Earth-Fixed Reference Frame

The Earth-Centered, Earth-Fixed (ECEF) reference frame is centered at the center of mass of the Earth and the Z axis is aligned with the Earth's spin axis. The X axis of the ECEF frame always points directly through the 0° longitude line and hence this frame rotates with the Earth.

A.5.1 Transformation to Earth-Centered Inertial Reference Frame

Vectors in the ECEF frame are readily rotated to the ECI frame by a simple rotation about their common Z axis through an angle known as the Greenwich Hour Angle (GHA), represented by θ. A diagram showing the relationship between the ECEF and the ECI frame is given in figure A.12 below.

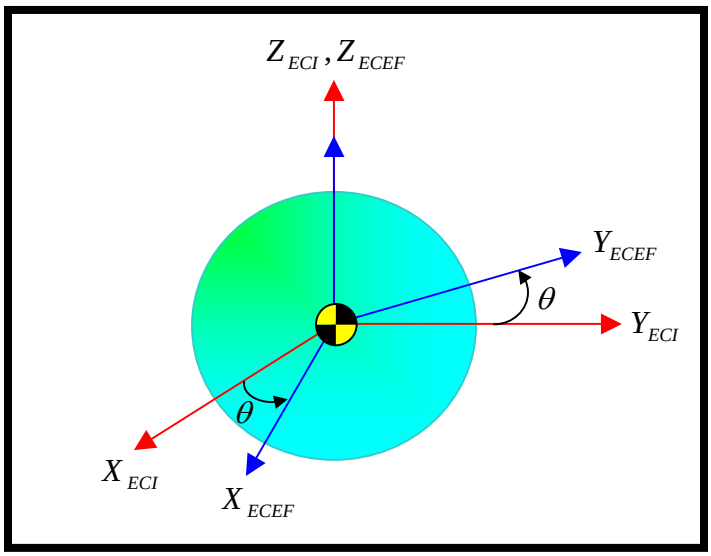

Figure A.12: ECEF and ECI Reference Frames

The rotation matrix that transforms vectors from the ECEF frame to the ECI frame is given by

$$\underline{R}_{ECI}^{ECEF} = \begin{bmatrix} \cos(\theta) & -\sin(\theta) & 0 \\ \sin(\theta) & \cos(\theta) & 0 \\ 0 & 0 & 1 \end{bmatrix} \tag{A.24}$$

The GHA can be readily computed for a given Julian Date (JD) according to the following formulations.

$$T_{UT1} = \frac{JD - 2451545.0}{36525} \tag{A.25}$$

$$GHA = 67310.5481 + \left((876600 \times 3600) + 8640184.812866\right)T_{UT1} + 0.093104T_{UT1}^2 - \left(6.2 \times 10^{-6}\right)T_{UT1}^3 \tag{A.26}$$

APENDIX B: ORBITAL MOTION SIMULATION

Numerical simulation of dynamic systems is an integral tool for engineering analysis in general and spacecraft mission design in specific. Therefore, a robust orbital dynamics simulation system was developed, using the Matlab® numerical computing environment and programming language to facilitate the analyses in this work. The mathematical and algorithmic aspects of this simulation architecture are developed below.

B.1 Gravitational Physics

The orbital simulations are accomplished using a generalized N-body simulator engine with a numerical integration routine at its core. The numerical integration routine used to integrate the ordinary differential equations (ODEs) of motion is `ode45`, a Matlab® function that provides robust integration of ODEs with 4^{th} order accuracy, 5^{th} order error control, and adaptive step-sizing. The core mathematics from which the differential equations for orbital motion are derived follows directly from Newton's law of gravitation, given by

$$\vec{F}_{ij} = -\frac{Gm_i m_j}{\left\|\vec{r}_{ij}\right\|^3}\hat{r}_{ij} \tag{B.1}$$

where

$\vec{F}_{ij}$ = the gravitational force vector of the *i*th body acting on the *j*th body

m_i = the mass of the *i*th body

m_j = the mass of the *j*th body

$\vec{r}_{ij}$ = the position vector of the *j*th body with respect to the *i*th body

A diagram illustrating the geometry associated with equation (B.1) is shown in figure B.1 below.

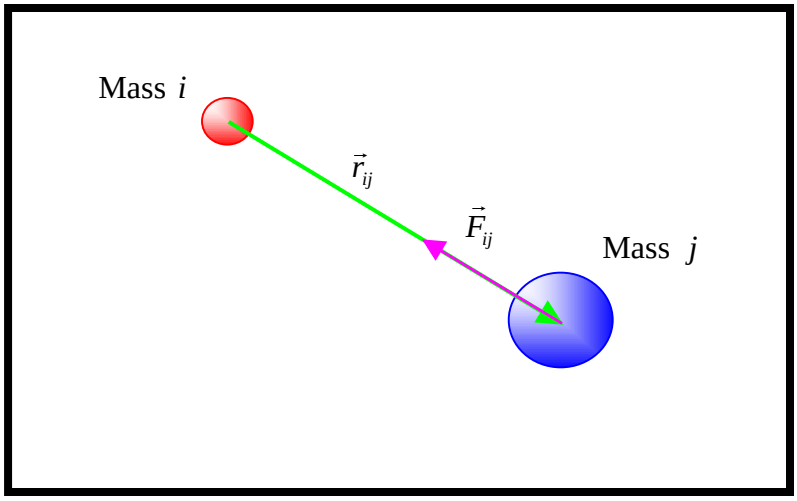

Figure B.1: Gravitation Between Two Point Masses

For an N-body system, each body in the system will experience a force due to every other body in the system, meaning that each body has N-1 gravitational forces acting upon it due to the remaining bodies. Thus, the total gravitational force acting on the i th body is obtained by summing the forces, yielding the following equation

$$\sum \vec{F}_i = -G \sum_{i=1}^{n} \sum_{\substack{j=1 \\ j \neq i}}^{n} \frac{m_i m_j}{\left\| \vec{r}_{ji} \right\|^3} \hat{r}_{ji} \qquad \text{(B.2)}$$

where

G = the universal gravitational constant

$\vec{r}_{ji}$ = the position of body i with respect to body j , $\left(\vec{r}_i - \vec{r}_j\right)$

The position of a given body as a function of time is obtained by numerically integrating the total acceleration of that body, which is obtained by dividing the total force acting on that body by the mass of that body, as shown in the following equation.

$$\ddot{\vec{r}}_i = \frac{\sum \vec{F}_i}{m_i} = -G\sum_{\substack{j=1 \\ j\neq i}}^{n} \frac{m_j}{\left\|\vec{r}_{ji}\right\|^3} \hat{r}_{ji} \tag{B.3}$$

where

$\ddot{\vec{r}}_i$ = the total acceleration of body i as a function of time

The ultimate objective is to obtain the position of each body as a function of time, written as $\vec{r}_i(t)$. The total acceleration on each body can be expressed in terms of this quantity as follows, producing a second order differential equation

$$\ddot{\vec{r}}_i(t) = \frac{d^2}{dt^2}\left(\vec{r}_i(t)\right) \tag{B.4}$$

This system must be reduced to first order so that numerical integration techniques may be applied, and this is achieved by taking advantage of the fact that the acceleration is the first time derivative of the velocity and the velocity is the first time derivative of the position, yield the following combined first order system:

$$\begin{aligned} \dot{\vec{r}}_i(t) &= \frac{d}{dt}\left(\vec{r}_i(t)\right) \\ \ddot{\vec{r}}_i(t) &= \frac{d}{dt}\left(\dot{\vec{r}}_i(t)\right) \end{aligned} \tag{B.5}$$

Simultaneous numerical integration of equations (B.5) produces a time history of the position, velocity, and acceleration of each body. Since the position and velocity of a body define its dynamic state at any time, it is convenient to represent this information compactly in a state vector and state vector derivative as follows.

$$\vec{R}(t) = \begin{bmatrix} \vec{r}(t) \\ \dot{\vec{r}}(t) \end{bmatrix}$$
$$\dot{\vec{R}}(t) = \begin{bmatrix} \dot{\vec{r}}(t) \\ \ddot{\vec{r}}(t) \end{bmatrix} \tag{B.6}$$

where

$\vec{R}(t)$ = the system state vector

$\dot{\vec{R}}(t)$ = time derivative of the system state vector

For the purposes of numerical integration, the ordering of elements in the state vector is arbitrary, with the restriction that the order of elements in the state vector corresponds directly to the order of elements in the state vector's derivative. The convention in this work is that position vector and velocity vector components are grouped according to coordinate axis in the state vector.

Since this work will be solely concerned with dynamic systems which reside in physical, i.e., three dimensional, space, the positions, velocities, and accelerations will always be of dimension three. The fourth dimension of time is always the independent variable. The designations for the three dimensional axes are x, y, and z with orthonormal basis vectors denoted by $\hat{i}$, $\hat{j}$, and $\hat{k}$, respectively. The resulting orthogonal coordinate system is depicted in figure B.2 below.

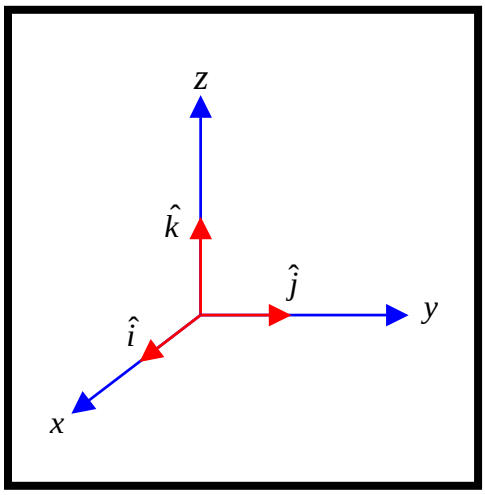

Figure B.2: Generalized Three Dimensional Reference Frame

Furthermore, all coordinate systems used in this work, unless specifically stated to be otherwise, are right-handed, meaning that the $\hat{i}$ and $\hat{j}$ basis vectors are co-planar and orthonormal and the $\hat{k}$ basis vector is constructed by the operation $\hat{i} \times \hat{j} = \hat{k}$.

The position, velocity, and acceleration vectors may thus be expressed as linear combinations of their components as follows.

$$\begin{aligned} \vec{r} &= r_x\hat{i} + r_y\hat{j} + r_z\hat{k} = \begin{bmatrix} r_x \\ r_y \\ r_z \end{bmatrix} \\ \dot{\vec{r}} &= \dot{r}_x\hat{i} + \dot{r}_y\hat{j} + \dot{r}_z\hat{k} = \begin{bmatrix} \dot{r}_x \\ \dot{r}_y \\ \dot{r}_z \end{bmatrix} \\ \ddot{\vec{r}} &= \ddot{r}_x\hat{i} + \ddot{r}_y\hat{j} + \ddot{r}_z\hat{k} = \begin{bmatrix} \ddot{r}_x \\ \ddot{r}_y \\ \ddot{r}_z \end{bmatrix} \end{aligned} \tag{B.7}$$

As mentioned previously, the convention in this work is that the position and velocity components are grouped together according to coordinate axis in the state vector and, consequently, in the state vector derivative as follows:

$$\vec{R} = \begin{bmatrix} r_{x_i} \\ \dot{r}_{x_i} \\ r_{y_i} \\ \dot{r}_{y_i} \\ r_{z_i} \\ \dot{r}_{z_i} \\ \cdot \\ \cdot \\ \cdot \end{bmatrix}, \dot{\vec{R}} = \begin{bmatrix} \dot{r}_{x_i} \\ \ddot{r}_{x_i} \\ \dot{r}_{y_i} \\ \ddot{r}_{y_i} \\ \dot{r}_{z_i} \\ \ddot{r}_{z_i} \\ \cdot \\ \cdot \\ \cdot \end{bmatrix} \tag{B.8}$$

where

$i = 1,2,...,n$

$n =$ the number of bodies in the system

Newton's second law, which states that the force is equal to the product of the mass and the acceleration, only holds true in an inertial, or non-accelerating (no linear acceleration, no rotational velocity or acceleration) reference frame. This fundamental law of motion is what allows equation (B.1) to be written. Hence, the positions, velocities, and accelerations of all bodies in the system will be referenced to a predefined inertial reference frame as shown in figure B.3 below.

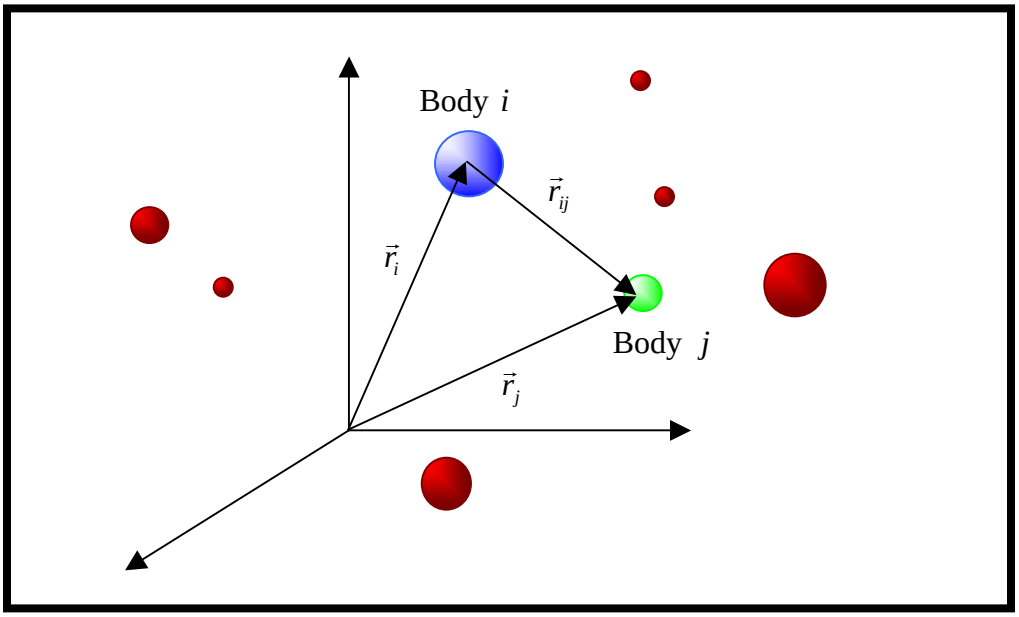

Figure B.3: System of N Bodies in an Inertial Reference Frame

The equations derived herein are implemented in a series of computer codes to allow for the propagation of an N-body system motivated solely by mutual gravitation with a given set of initial conditions. This simulation software is used to perform all the orbital analyses presented in this work.

B.2 Solar System Simulation

One final note regarding the simulation methods employed within is that for the purposes of simulating the motion of planets, NEOs, and spacecraft traveling in the solar system, the center of mass of the Sun is constrained to always be at the origin of the HCI frame. This is accomplished by not including the Sun in the system state vector and instead accounting for its gravitational influence by modifying equation (B.3) above as follows.

$$\ddot{\vec{r}}_i = -G\sum_{\substack{j=1 \\ j\neq i}}^{n} \frac{m_j}{\left\|\vec{r}_{ji}\right\|^3}\hat{r}_{ji} - \frac{Gm_{SUN}}{\left\|\vec{r}_i\right\|^3}\hat{r}_i \qquad \text{(B.9)}$$

APPENDIX C: NEO SCIENCE INSTRUMENTS

This appendix contains detailed information on selected scientific sensors that are useful characterizing NEO properties. The NEAR spacecraft successfully used these sensors in its study of the asteroid Eros and therefore they, and improved versions of them, are good choices for future NEO science missions. The information in this appendix was obtained from NEAR mission specifications.

C.1 Multi-Spectral Imager

In order to measure the rotation rates, size, and shape of the target NEO, a multi-spectral imager (MSI) can be used, shown in figure C.1. In addition to being able to map the surface of the NEO, the MSI is able to analyze surface composition of the NEO with its seven color filter capability. The seven color filters have a capability ranging from wavelengths of 450 nm to 1050 nm and were designed primarily for identifying iron-containing silicate minerals based on the surface reflection of sunlight, giving the unit a maximum surface resolution between 3 and 5 meters. This resolution is achieved at a range of 35 km based on preliminary research. If the orbit altitude is increased to 100 km, then the MSI is capable of a resolution of 9.6×16.2 m. Additionally, the MSI will contain one broadband filter to aid in low-light observations and navigation. The entire unit including support electronics has a mass of 7.7 kg and a power requirement of 6.92 Watts [34].

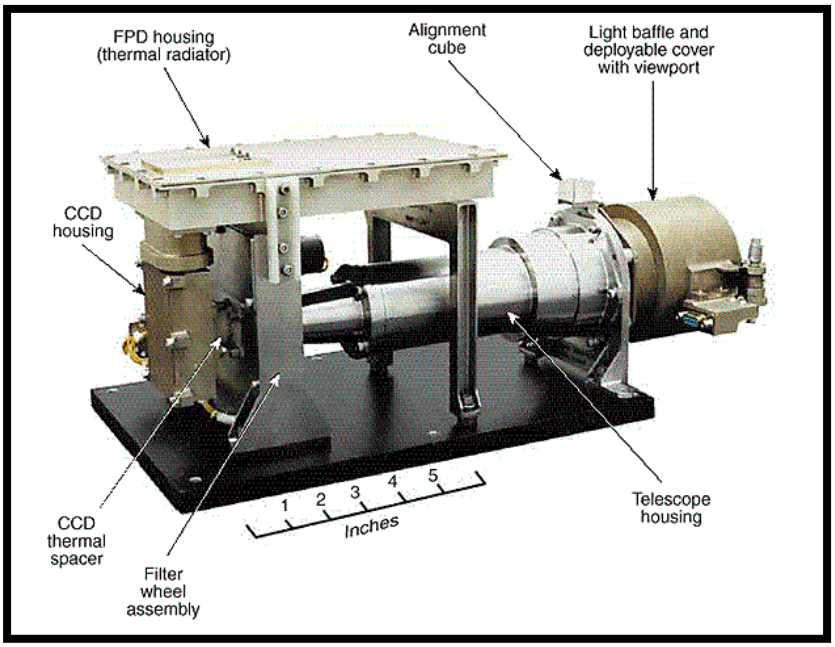

Figure C.1: Multi-Spectral Imager [34]

C.2 Near-Infrared Spectrograph

The Near-Infrared Spectrograph (NIS), shown in figure C.2 below, helps determine the mineral composition of the target NEO. When the sunlight reflects off the surface of the NEO different minerals produce different reflected spectra. The NIS is capable of viewing and analyzing these different spectra to determine what minerals are present. The NIS focuses on near-infrared wavelengths between 800-2700 nm. Light waves reflected between 800 nm and 1506 nm are directed into a 32-element germanium detector by a 1-D gold mirror, while wavelengths between 1348 nm and 2732 nm are directed into a 32-element indium-gallium arsenide detector with the same mirror. The unit is capable of a 140° field of view and resolution of 1.3×1.3 km from a 100 km altitude orbit. If the altitude above the NEO is reduced to 35 km, then the NIS is capable of imaging the surface at 300 m resolution. The NIS has a total mass of 15.15 kg and a power consumption of 15.1 Watts [35].

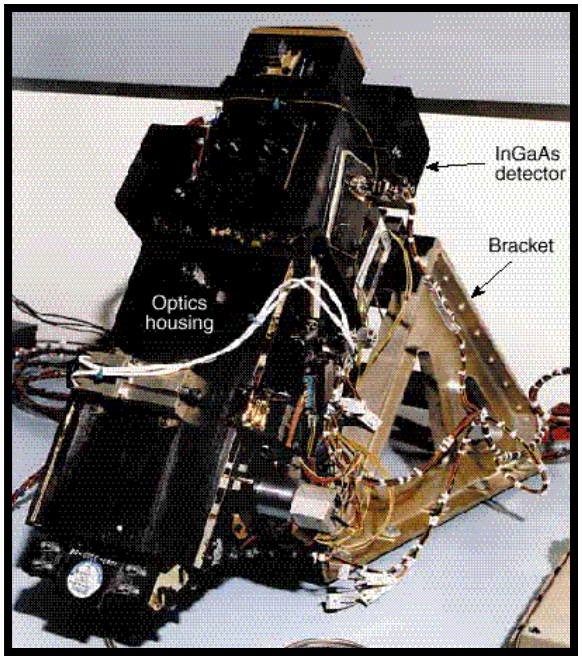

Figure C.2: Near-Infrared Spectrograph [35]

C.3 X-Ray/Gamma-Ray Spectrometer

The sensor that aids in elemental composition analysis of a NEO is the X-Ray/Gamma-Ray Spectrometer (XGRS), shown in figure C.3 below. The XGRS functions by collecting x-ray and gamma ray emissions from the NEO caused by x-ray fluorescence due to solar excitation and cosmic rays, respectively. The collected x-rays allow the measurement of the amounts of Mg, Al, Si, Ca, Ti, and Fe down to surface resolutions of 5 m at a range of 35 km. Conversely, the gamma rays will indicate the abundances of O, Si, Fe, H, and any radioactive elements. The XGRS has a power consumption of 24 W with a total mass of 26.9 kg [36].

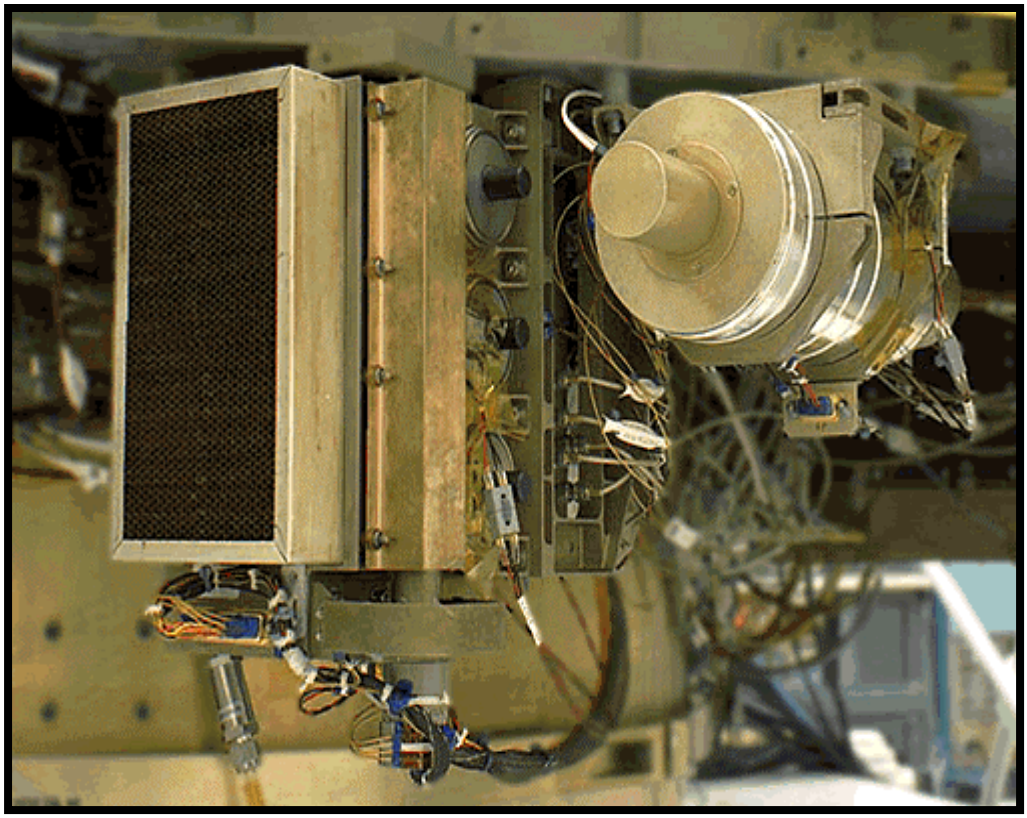

Figure C.3: X-Ray/Gamma-Ray Spectrometer [36]

C.4 Magnetometer

If nuclear devices are to be detonated near the NEO for the purposes of deflection, the magnetic field of the target NEO, if one is present, needs to be investigated to find its strength and geometry so that after the nuclear device has detonated any changes to the magnetic field can be recorded. In addition, any effects caused by solar wind can be measured. In order to measure the magnetic field, a three-axis fluxgate magnetometer capable of measuring magnetic fields from DC to 10 Hz will be used, shown in figure C.4 below. The magnetometer can measure magnetic field strengths from 4 nT to 65,536 nT with a minimum 10 nT field strength measurement at 35 km from the surface. The mass of the unit is 1.5 kg and it has a power requirement of 1.5 Watts [37].

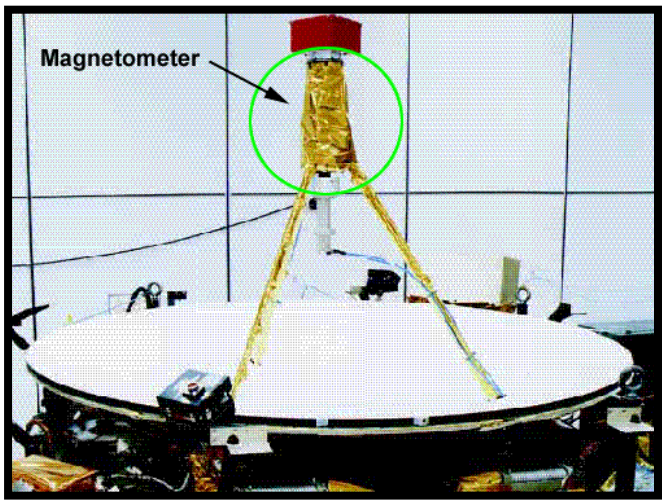

Figure C.4: Magnetometer [37]

C.5 Laser Rangefinder

Complete NEO characterization requires a detailed analysis of the shape of the NEO so that size, volume, and density can be estimated. In order to create detailed maps of the surface of the target NEO, a Laser Rangefinder (LR), shown in figure C.5 below, will be utilized to map the topography of the surface. The LR uses a 1.064 mm wavelength pulsed diode-pumped neodymium–yttrium–aluminum–garnet laser to determine the height of the spacecraft above the surface of the NEO. The LR measures the time that it takes the laser to reflect off the NEO and return to the spacecraft and, since the speed of light is constant, the distance can then be ascertained. The maximum altitude for accurate ranging is 50 km. The sensor has a mass of 5 kg, an average power consumption of 16.5 Watts, and a peak power usage of 20.7 Watts. The laser has an energy output of 15 mJ and a divergence of 235 μrad [38].

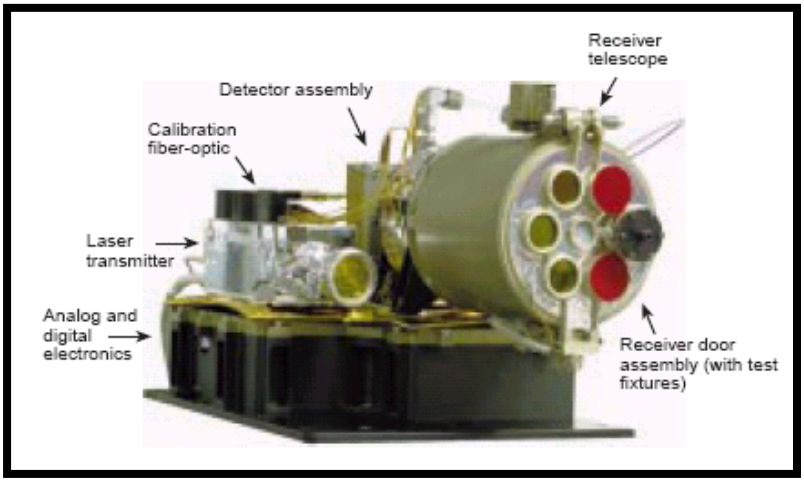

Figure C.5: Laser Rangefinder [38]

APPENDIX D: HISTORICAL NEO IMPACTS

This appendix presents a large table of some of the recorded NEO impacts during human history over the past several thousand years, beginning in 1420 BCE and extending up to near the present day (1998).

Table D.1: Listing of Historical NEO Impacts [1]

Damage, Injuries, Deaths, and Very Close Calls

Date	*Place*	*Source*	*Event*
c. 1420 B.C.	Israel	Joshua 10:11	Lethal meteorite fall
476	I-hsi and Chin-ling, China	Yau *et al.* (1994)	"Thundering chariots" "like granite" fell to ground; vegetation was scorched
580	France	*History of the Franks*	Great fireball and blast; Orleans and nearby towns burned
06/25/588	China	Yau *et al.* (1994)	"Red-colored object" fell with "noise like thunder" into furnace; exploded; burned several houses
01/14/616	China	Yau *et al.* (1994)	Ten deaths reported in China from meteorite shower; seige towers destroyed
679	Coldingham, England	Anglo-Saxon Chronicle	Monastery destroyed by "fire from heaven"
764	Nara, Japan	*Met.* 1, 300	Meteorite strikes house
810	Upper Saxony	Vita Caroli Magni	Charlemagne's horse startled by meteor; throws him to ground
1064	Chang-chou, China	Yau *et al.* (1994)	Daytime fireball, meteorite fall; fences burned
1321–1368	O-chia district, China	Yau *et al.* (1994)	Iron rain kills people, animals, damages houses
1369	Ho-t'ao, China	Yau *et al.* (1994)	"Large star" fell, starts fire, soldiers injured
2-3/1490	Ch'ing-yang, Shansi, China	Yau *et al.* (1994)	Stones fell like rain; more than 10,000 killed
10-11/1504	China	Yau *et al.* (1994)	"Large star" fell with "noise like thunder", garden burned
09/14/1511	Cremona, Lombardy, Italy		Monk killed with several birds, a sheep
1620	Punjab, India	*Philos. Mag.* [1] **16,** 294	Hot iron fell, burned grass; made into dagger, knife, two sabres
1639	China	Yau *et al.* (1994)	Large stone fell in market; tens killed; tens of houses destroyed
1648	Ship near Malacca		Two sailors reported killed on board ship en route from Japan to Sicily
1654	Milano, Italy		Monk reported killed by meteorite
8-9 1661	China	Yau *et al.* (1994)	Meteorite smashes through roof; no injuries
11/07/1670	China	Yau *et al.* (1994)	Meteorite fall, breaks roof beam of house
10/11/1761	Chamblan, France	*Mem. Acad. Dijon* 1 *C. R. Acad. Sci.* **7,** 76	House struck and burned by meteorite
07/24/1790	Barbotan and Agen, Gasc., France	*Philos. Mag.* [1] **16,** 293	Meteorite crushes cottage, kills farmer and some cattle
06/16/1794	Siena, Italy		Child's hat hit; child uninjured
12/19/1798	Benares, India		Building struck
10/30/1801	Suffolk, England	*Times* 11/3 3d	"Dwelling-houfe of Mr. Woodroffe, miller, near Horringer-mill, Suffolk, was set on fire by a meteor, and entirely confumed, together with a ftable adjoining."
07/04/1803	E. Norton, England		White Bull public house struck, chimney knocked down, grass burned; flight nearly horizontal
12/13/1803	Massing, Czech.		Building struck
07/1810	Shahabad, India	*Philos. Mag.* [1] **37,** 236	Great stone fell; five villages burned; several killed

Table D.1 (Continued)

11/10/1823	Waseda, Japan	*Met.* 1, 300	Meteorite strikes house
01/16/1825	Oriang (Malwate), India		Man reported killed, woman injured by meteorite fall
02/27/1827	Mhow, India	*Philos. Mag.* [4] **25,** 447	Man struck on arm, tree broken
11/13/1835	Belley, Dept de l'Ain, France	*Annuaire* (1836)	Fireball sets fire to barn
12/11/1836	Macao, Brazil		Several homes damaged, several oxen killed by meteorite
1841	Chiloe Archipel., Chile	*C. R. Acad. Sci.* **12,** 1196	Fire caused by meteorite fall
5-6 1845	Ch'ang-shou, Szechwan, China	Yau *et al.* (1994)	Stone meteorite damages more than 100 tombs
07/14/1847	Braunau, Bohemia		A 37-lb iron smashes through roof into room where three children are sleeping; no serious injuries
10/17/1850	Szu-mao, China	Yau *et al.* (1994)	Meteorite falls through roof of house
12/09/1858	Ausson, France		Building hit
05/01/1860	New Concord, Ohio		Colt struck and killed
08/08/1868	Pillistfer, Estonia		Building struck
01/01/1869	Hessle, Sweden		Man missed by few meters
01/23/1870	Nedagolla, India		Man stunned by meteorite
12/07/1872	Banbury, England	*Nature* **7,** 112	Fireball fells trees, wall
06/30/1874	Chin-kuei Shan, Ming-tung Li, China	Yau *et al.* (1994)	Thunderstorm; huge stone fell, crushed cottage, killed child
02/16/1876	Judesegeri, India		Water tank struck
01/03/1877	Warrenton, Missouri		Man missed by few meters
01/21/1877	De Cewsville, Ontario		Man missed by few meters
01/14/1879	Newtown, Indiana	*Paducah Daily News*	Leonidas Grover reported killed in bed (probable hoax)
01/31/1879	Dun-le-Poelier, France	C. Flammarion	Farmer reported killed by meteorite
11-12 1879	Huang-hsiang, China	Yau *et al.* (1994)	Rain of stones; many houses damaged; sulfur smell
11/19/1881	Großliebenthal, Russia		Man reported injured by meteorite
03/19/1887	Barque *J.P.A.*, N. Atlantic	*Am. J. Met.* 4 (1887)	Fireball "fell into the water very close alongside"
11/22/1893	Zabrodii, Russia		Building struck
02/10/1896	Madrid, Spain		Explosion; windows smashed, wall felled
03/11/1897	New Martinsville, W. Virginia	*NYT* 1:4	Man knocked out, horse killed; walls pierced
11/04/1906	Diep River, S. Africa		Building struck
09/05/1907	Hsin-p'ai Wei, Weng-li, China	Yau *et al.* (1994)	Stone fell; whole family crushed to death
12/07/1907	Bellefontaine, Ohio	*NYT* 1:4	Meteorite starts fire, destroys house
06/30/1908	Tunguska valley, Siberia		Two reportedly killed, many injured by Tunguska blast
05/29/1909	Shepard, Texas	*NYT* 1:6	Meteor drops through house
04/27/1910	Mexico	*NYT*	Giant meteor bursts, falls in mountains, starts forest fire

Table D.1 (Continued)

06/16/1911	Kilbourn, Wisconsin	*NYT* 8/8/32 17:6	Meteorite struck barn
06/28/1911	Nakhla, Egypt		Dog struck and killed by meteorite
07/19/1912	Holbrook, Arizona		Building struck; 14,000 stones fell; man missed by a few meters
01/09/1914	W. France	*NYT* 1:7	Meteor explosions break windows
11/22/1914	Batavia, New York	*NYT* 1:8	Meteorites damage farm
01/18/1916	Baxter, Missouri		Building struck
12/03/1917	Strathmore, Scotland		Building struck
06/30/1918	Richardton, N. Dakota		Building struck
07/15/1921	Berkshire Hills, Massachusetts	*NYT* 15:2	Meteor starts fire in Berkshires
12/21/1921	Beirut, Syria		Building hit
02/02/1922	Baldwyn, Mississippi		Man missed by 3 m
04/24/1922	Barnegat, New Jersey	*NYT* 1:2	Rocked buildings, shattered windows, clouds of noxious gas
05/30/1922	Nagai, Japan		Person missed by several meters
07/06/1924	Johnstown, Colorado		Man missed by 1 m
04/28/1927	Aba, Japan		Girl struck and injured by dubious meteorite
12/08/1929	Zvezvan, Yugoslavia	*NYT* III 1:2	Meteor hits bridal party, kills 1
08/13/1930	Brazil	*Obs.* 115, 250 (1995) *The Sciences* 36, 14	Brazilian "Tunguska event"; fire and "depopulation"
06/10/1931	Malinta, Ohio	*NYT* 6/11 3:4	Blast, crater, smell of sulfur, windows broken in farmhouse; four telephone poles snapped, wires down
09/08/1931	Hagerstown, Maryland	*NYT* 9/9 14:2	Meteor crashes through roof in Hagerstown
08/04/1932	Sao Christovao, Brazil	*NYT* 6:5	Fall unroofs warehouse
08/10/1932	Archie, Missouri	*NYT* 8/13 17:6	Homestead struck, person missed by <1 m
02/24/1933	Stratford, Texas	*NYT* 3/25 17:1	Bright fireball, 4-lb metallic mass; grass burned
08/08/1933	Sioux Co., Nebraska		Man missed by a few meters
02/16/1934	Texas	*NYT* 2/17 32:3	Pilot swerves to "avoid crash"
02/18/1934	Seville, Spain	*Seattle Times* 02/23/34	House struck, burned
09/28/1934	California	*NYT* 1:3	A pilot "escapes" shower
08/11/1935	Briggsdale, Colorado	*NYT* 21:2	Man narrowly missed by meteorite
03/14/1936	Red Bank, New Jersey	*NYT* 3/17 23:3	Meteorite through shed roof
04/02/1936	Yurtuk, USSR		Building struck
10/19/1936	Newfoundland	*NYT* 10/20 27:7	Fisherman's boat set on fire by meteorite
03/31/1938	Kasamatsu, Japan	*Met.* 1, 300	Meteorite pierces roof of ship
06/16/1938	Pantar, Phillipines		Several buildings struck
06/24/1938	Chicora, Pennsylvania		A cow struck and injured
09/29/1938	Benld, Illinois		Garage and car struck by 4-lb stone
07/10/1941	Black Moshannon Park, Pennsylvania		Person missed by 1 m
04/06/1942	Pollen, Norway		Person missed by 1 m
05/16/1946	Santa Ana, Nuevo Leon	*NYT* 9:4	Meteorite destroys many houses, injures 28
11/30/1946	Colford, Gloucestershire, UK	*NYT* 7:6	Telephones knocked out, boy knocked off bicycle

Table D.1 (Continued)

02/12/1947	Sikhote Alin, nr. Vladivostok	*NYT* 4/29 14:3	Iron meteorites fall; cratering
09/21/1949	Beddgelert, Wales		Building struck
11/20/1949	Kochi, Japan		Hot meteoritic stone enters house through window
05/23/1950	Madhipura, India		Building struck
09/20/1950	Murray, Kentucky	*NYT* 9/21 33:7	Several buildings struck
12/10/1950	St. Louis, Missouri		Car struck
03/03/1953	Pecklesheim, FRG		Person missed by several meters
01/07/1954	Dieppe, France	*NYT* 1/9 2:6	Meteorite—blinding explosion, smashed windows
11/28/1954	Sylacauga, Alabama	*NYT* 86:2 and *Met.* 1, 125	Mrs. Annie Hodges struck by 4-kg meteorite that crashed through roof, destroyed radio
01/17/1955	Kirkland, Washington	*Met.* 2, 56	Two irons break through amateur astronomer's observatory dome; one sets a fire
02/29/1956	Centerville, S. Dakota		Building hit
10/13/1959	Hamlet, Indiana		Building hit
02/23/1961	Ras Tanura, Saudi Arabia		Loading dock struck
09/06/1961	Bells, Texas	*Met.* 2, 67	Meteorite strikes roof of house
04/26/1962	Kiel, FRG		Building hit
12/24/1965	Barwell, England		Two buildings and a car struck
07/11/1967	Denver, Colorado		Building struck
04/12/1968	Schenectady, New York	*Met.* 4, 171	House hit
04/25/1969	Bovedy, N. Ireland		Building hit
08/07/1969	Andreevka, USSR		Building hit
09/16/1969	Suchy Dul, Czechoslovakia		Building hit
09/28/1969	Murchison, Australia		Building hit
04/08/1971	Wethersfield, Connecticut		House struck by meteorite
08/02/1971	Havero, Finland		Building hit
03/15/1973	San Juan Capistrano, California		Building hit
10/27/1973	Canon City, Colorado		Building hit
08/18/1974	Naragh, Iran		Building hit
01/31/1977	Louisville, Kentucky		Three buildings and a car struck
05/07/1979	Cilimus, Indonesia	Catalogue	Meteorite fell in garden
05/13/1981	Salem, Oregon		Building hit
11/08/1982	Wethersfield, Connecticut	*JRAS Canada* 85, 263 *NYT* 11/10 1:1 and 1/2/83 I 33:5	Pierced roof of house
06/15/1984	Nantong, PRC		Man missed by 7 m
06/30/1984	Aomori, Japan		Building struck
08/22/1984	Tomiya, Japan		Two buildings hit
09/30/1984	Binningup, Australia		Two sunbathers missed by 5 m
12/05/1984	Cuneo, Italy		Strong explosion, blinding flash; windows broken; daytime fireball "bright as Sun"

Table D.1 (Continued)

12/10/1984	Claxton, Georgia		Mailbox destroyed by meteorite
01/06/1985	La Criolla, Argentina		Farmhouse roof pierced, door smashed; 9.5-kg stone misses woman by 2 m
07/29/1986	Kokubunji, Japan		Several buildings hit
03/01/1988	Trebbin, GDR		Greenhouse struck by meteorite
05/18/1988	Torino, Italy		Building struck
06/12/1989	Opotiki, New Zealand		Building hit
08/15/1989	Sixiangkou, PRC		Building hit
04/07/1990	Enschede, Netherlands	*New Sci.*, 6/9/90, 37	House hit by believed fragment of Midas
07/02/1990	Masvingo, Zimbabwe		Person missed by 5 m
1991	Tahara, Japan		Meteorite struck deck of car-transport ship; made crater
08/31/1991	Noblesville, Indiana	*Sky & Telescope* 4/92	Meteorite fall missed two boys by 3.5 m
08/14/1992	Mbale, Uganda	*Met.* 29, 246	Forty-eight stones fall; roofs damaged, boy struck on head
10/09/1992	Peerskill, New York	*S.E.A.N.*	Car trunk, floor pierced by meteorite
10/20/1994	Coleman, Michigan	*Met. Pl. Sci.* 32, 781	Meteorite penetrated roof of house (1997)
1995	Neagari, Japan		Meteorite penetrated car trunk
04/11/1997	Chambrey, France	*Arizona Daily Star*, 4/12/97	Meteorite penetrated roof of car; set fire
06/13/1998	Portales, New Mexico	*Arizona Daily Star*	Meteorite penetrated barn roof
07/12/1998	Kitchener, Ontario	*Sky & Telescope* 2/99	Meteorite falls 1 m from golfer

Key: Catalogue, A. L. Graham, Catalogue of Meteorites (1985); *JRAS, Journal of the Royal Astronomical Society; Met., Meteoritics; Met. Pl. Sci, Meteoritics and Planetary Science; New Sci, New Scientist; NYT, The New York Times; Obs, The Observatory; S.E.A.N., Scientific Events Alert Network* (presently called *Bulletin of the Global Volcanism Network*).

APPENDIX E: SELECTED SOURCE CODE

This appendix presents selected source code used to perform the analyses within this work. Only the most pertinent codes have been included, omitting many of the smaller supporting functions in the software architecture.

```
% Begin function.
function opt_NEO_def_scan(scenario_file)

   % Record the start time of the optimal NEO deflection search so that the
   % total elapsed real-time may be computed for the user once the search
   % is complete.
   t0_total = clock;

   %=========================================================================%
   %= Load scenario file.                                                   =%
   %=========================================================================%
   eval(scenario_file);

   % Convert the simulation time step from days to seconds. This time step
   % is the interval at which the simulation stores values.
   dt_sim = dt_sim * 86400;

   %=========================================================================%
   %= Check that the specified output directory exists.                     =%
   %=========================================================================%
   if(~exist(output_dir,'dir'))
      error('Specified output directory does not exist.');
   else
      a = num2str(t0_total(1));
      b = num2str(t0_total(2));
      c = num2str(t0_total(3));
      d = num2str(t0_total(4));
      e = num2str(t0_total(5));
      f = num2str(floor(t0_total(6)));
      t_str = sprintf('%s_%s_%s_%s_%s_%s', a, b, c, d, e, f);
      save_file_name = sprintf('%s/%s_%s', output_dir, output_file_root,
t_str);
   end

   %=========================================================================%
   %= Run baseline simulation.                                              =%
   %=========================================================================%
   [base_sys_state, base_time] = baseline_simulation(scenario_file);

   % Loop over all the time indices in the system state matrix returned
   % from the baseline simulation.
   for(ind=1:length(base_time))

      % Extract the heliocentric inertial position vector at the current
      % time index for the NEO.
      r_i(1,1) = base_sys_state(ind, 1);
      r_i(2,1) = base_sys_state(ind, 3);
      r_i(3,1) = base_sys_state(ind, 5);

      % Extract the heliocentric inertial velocity vector at the current
      % time index for the NEO.
      v_i(1,1) = base_sys_state(ind, 2);
```

```
      v_i(2,1) = base_sys_state(ind, 4);
      v_i(3,1) = base_sys_state(ind, 6);

      % Compute the NEO's heliocentric keplerian orbital elements at the
      % current time index.
      [a, e, i, RAAN, arg_peri, true_anom] = r_v_to_kep_elem(r_i, v_i, ...
                                                             mu_sun);
      % Store the NEO's position and velocity.
      NEO_data.x_pos(ind) = r_i(1);
      NEO_data.x_vel(ind) = v_i(1);
      NEO_data.y_pos(ind) = r_i(2);
      NEO_data.y_vel(ind) = v_i(2);
      NEO_data.z_pos(ind) = r_i(3);
      NEO_data.z_vel(ind) = v_i(3);

      % Store the NEO's true anomaly.
      NEO_data.true_anom(ind) = true_anom;

      % Store the NEO's argument of perihelion.
      NEO_data.arg_peri(ind) = arg_peri;

      % Store the NEO's right ascension of the ascending node.
      NEO_data.RAAN(ind) = RAAN;

      % Store the NEO's orbital inclination.
      NEO_data.i(ind) = i;

      % Store the Earth's position and velocity.
      Earth_data.x_pos(ind) = base_sys_state(ind, 7);
      Earth_data.x_vel(ind) = base_sys_state(ind, 8);
      Earth_data.y_pos(ind) = base_sys_state(ind, 9);
      Earth_data.y_vel(ind) = base_sys_state(ind, 10);
      Earth_data.z_pos(ind) = base_sys_state(ind, 11);
      Earth_data.z_vel(ind) = base_sys_state(ind, 12);

      if(num_obj > 2)
         k = 13;
         for(ind2=1:num_obj-2)
            OTHER_data(ind2).x_pos(ind) = base_sys_state(ind, k);
            OTHER_data(ind2).x_vel(ind) = base_sys_state(ind, k+1);
            OTHER_data(ind2).y_pos(ind) = base_sys_state(ind, k+2);
            OTHER_data(ind2).y_vel(ind) = base_sys_state(ind, k+3);
            OTHER_data(ind2).z_pos(ind) = base_sys_state(ind, k+4);
            OTHER_data(ind2).z_vel(ind) = base_sys_state(ind, k+5);
            k = k + 6;
         end
      end

   end

   % Free the memory storing the entire baseline system state over time.
   clear base_sys_state;

   % Prepare the time scan vector.
   if(~isempty(time_scan_vec))
      time_scan_vec = time_scan_vec*86400.0;
      time_scan_TOL = time_scan_TOL*86400.0;
      for(ind=1:length(time_scan_vec))
         if(time_scan_vec(ind) >= 0)
            time_scan_vec(ind) = time_scan_vec(ind) + base_time(1);
         else
            time_scan_vec(ind) = time_scan_vec(ind) + base_time(end);
         end

         if((time_scan_vec(ind) > base_time(end)) | (time_scan_vec(ind) <
base_time(1)))
```

```
            error('One or more time scan values are out of range.');
         end
      end
   else
      % Convert the time scan parameters from units of [days] to units of
      % [sec].
      time_scan_res   = time_scan_res   * 86400.0;
      time_scan_TOL   = time_scan_TOL   * 86400.0;
      time_scan_init  = time_scan_init  * 86400.0;
      time_scan_final = time_scan_final * 86400.0;

      % Ensure that the time scan values are in the range of the baseline
      % data.
      if((time_scan_init < base_time(1)) | (time_scan_init >=
base_time(end)))
         time_scan_init = base_time(1);
      end
      if((time_scan_final >= base_time(end)) | (time_scan_final <
base_time(1)))
         time_scan_final = base_time(end);
      end

      time_scan_vec = (time_scan_init:time_scan_res:time_scan_final);
   end

   % Search through the vector of actual times for the baseline
   % simulation data points and store the indices for the actual times that
   % match the desired times to scan, within tolerance.
   for(ind1=1:length(time_scan_vec))
      for(ind2=1:length(base_time))
         if(abs(base_time(ind2) - time_scan_vec(ind1)) <= time_scan_TOL)
            time_scan_indices(ind1) = ind2;
            break;
         end
      end
   end

   % Validate the time scan indices.
   if(exist('time_scan_indices'))
      for(ind=1:length(time_scan_indices))
         if(time_scan_indices(ind) == 0)
            error('A time index has not been initialized.');
         end
      end
   else
       error('A time index has not been initialized.');
   end


   if(start_true_anom_scan_at_t_scan == 1)
       true_anoms_to_scan = NEO_data.true_anom(min(time_scan_indices):end);
   else
       true_anoms_to_scan = NEO_data.true_anom;
   end


   k = 1;
   if(~isempty(true_anom_vec))
       for(ind1=1:length(true_anom_vec))
           for(ind2=1:length(true_anoms_to_scan))
               if(abs(true_anoms_to_scan(ind2) - true_anom_vec(ind1)) <=
true_anom_TOL)
                   if(k == 1)
                       true_anom_indices(k) = ind2+(min(time_scan_indices));
                       k = k + 1;
                   else
```

```
                        if(abs(ind2 - true_anom_indices(k-1)) > 10) % 10 is
just something that works (a bit of an overkill even) when dt_sim = 0.1
days.
                            true_anom_indices(k) =
ind2+(min(time_scan_indices));
                            k = k + 1;
                        end
                    end
                end
            end

            % Validate the true anom scan indices.
            if(exist('true_anom_indices'))
                for(ind=1:length(true_anom_indices))
                    if(true_anom_indices(ind) == 0)
                        error('A true anomaly index has not been initialized.');
                    end
                end
            else
                error('A true anomaly index has not been initialized.');
            end
        end

        if(exist('true_anom_indices'))
            scan_indices_tot = sort([time_scan_indices true_anom_indices]);
        else
            scan_indices_tot = sort(time_scan_indices);
        end

        k = 1;
        for(ind=1:length(scan_indices_tot))
            if(ind == 1)
                scan_ind_vec(k) = scan_indices_tot(ind);
                k = k + 1;
            else
                dup_flag = 0;
                for(ind2=1:(k-1))
                    if(scan_ind_vec(ind2) == scan_indices_tot(ind))
                        dup_flag = 1;
                        break;
                    end
                end
                if(dup_flag == 0)
                    scan_ind_vec(k) = scan_indices_tot(ind);
                    k = k + 1;
                end
            end
        end

        clear time_scan_indices;

        time_scan_indices = scan_ind_vec;

        clear scan_ind_vec;

        % Prepare the azimuth scan vector.
        if(isempty(azimuth_scan))
           azimuth_scan = (azimuth_init:azimuth_res:azimuth_final);
        end
        azimuth_scan = azimuth_scan*(pi/180);

        % Prepare the elevation scan vector.
        if(isempty(elevation_scan))
           elevation_scan = (elevation_init:elevation_res:elevation_final);
        end
```

```
   elevation_scan = elevation_scan*(pi/180);

   % Convert the magnitude of the deflection delta-v from units of [cm/s]
   % to [km/s].
   dv_mag = dv_mag/100000;

   % Initialize the master index of the deflection data results.
   master_index = 1;

   % Compute the total number of search combinations based on user input
   % for the optimal deflection search parameters.
   num_searches = length(time_scan_indices)*length(azimuth_scan)* ...
                  length(elevation_scan);

   % Display a message informing the user of the number of searches that
   % will be performed.
   disp(sprintf('\nNumber of searches to perform -> %d\n', num_searches));

   % Generate unpopulated orbital element structures for each body to be
   % used for the iterated deflection simulations..
   for(loop_index=1:num_obj)
      [orb_data_curr(loop_index)] = generate_orb_data_struct;
   end

   % Initialize the masses of all bodies.
   orb_data_curr(1).mass = orb_data(NEO_orb_index).mass;
   orb_data_curr(2).mass = orb_data(EARTH_orb_index).mass;
   if(num_obj > 2)
      for(ind=3:num_obj)
         orb_data_curr(ind).mass = orb_data(ind).mass;
      end
   end

   clear orb_data;

   % Display a message informing the user that the optimal deflection
   % search is beginning.
   disp(sprintf('\nBeginning optimal deflection search iterations...\n'));


   % Begin optimal NEO deflection search iterations loops.
   for(loop_index_time=1:length(time_scan_indices))

      % Store the current time index.
      time_index = time_scan_indices(loop_index_time);

      for(loop_index_az=1:length(azimuth_scan))

         for(loop_index_el=1:length(elevation_scan))

            % Compute the deflection delta-v vector in the NEO-centered RTN
            % frame.
            dv_vec_RTN(1,1) =
dv_mag*cos(elevation_scan(loop_index_el))*sin(azimuth_scan(loop_index_az));
            dv_vec_RTN(2,1) =
dv_mag*cos(elevation_scan(loop_index_el))*cos(azimuth_scan(loop_index_az));
            dv_vec_RTN(3,1) = dv_mag*sin(elevation_scan(loop_index_el));

            % Retrieve the necessary orbital elements for the NEO at the
            % current time index to construct the transformation matrix
            % from the NEO's RTN frame to the heliocentric inertial frame.
            true_anom = NEO_data.true_anom(time_index);
            arg_peri  = NEO_data.arg_peri(time_index);
            RAAN      = NEO_data.RAAN(time_index);
            i         = NEO_data.i(time_index);
```

```
            % Rotate the deflection delta-v vector from the RTN frame to
            % the inertial frame.
            [dv_vec_INRTL] = rot_RTN2INERTIAL(true_anom, arg_peri, RAAN, i,
dv_vec_RTN);

            % Initialize the NEO's state at the time of deflection,
            % including the applied deflection delta-v vector.
            orb_data_curr(1).x_pos = NEO_data.x_pos(time_index);
            orb_data_curr(1).x_vel = NEO_data.x_vel(time_index) +
dv_vec_INRTL(1);
            orb_data_curr(1).y_pos = NEO_data.y_pos(time_index);
            orb_data_curr(1).y_vel = NEO_data.y_vel(time_index) +
dv_vec_INRTL(2);
            orb_data_curr(1).z_pos = NEO_data.z_pos(time_index);
            orb_data_curr(1).z_vel = NEO_data.z_vel(time_index) +
dv_vec_INRTL(3);

            % Initialize the Earth's state at the time of deflection.
            orb_data_curr(2).x_pos = Earth_data.x_pos(time_index);
            orb_data_curr(2).x_vel = Earth_data.x_vel(time_index);
            orb_data_curr(2).y_pos = Earth_data.y_pos(time_index);
            orb_data_curr(2).y_vel = Earth_data.y_vel(time_index);
            orb_data_curr(2).z_pos = Earth_data.z_pos(time_index);
            orb_data_curr(2).z_vel = Earth_data.z_vel(time_index);

            if(num_obj > 2)
               for(ind=3:num_obj)
                  orb_data_curr(ind).x_pos = OTHER_data(ind-
2).x_pos(time_index);
                  orb_data_curr(ind).x_vel = OTHER_data(ind-
2).x_vel(time_index);
                  orb_data_curr(ind).y_pos = OTHER_data(ind-
2).y_pos(time_index);
                  orb_data_curr(ind).y_vel = OTHER_data(ind-
2).y_vel(time_index);
                  orb_data_curr(ind).z_pos = OTHER_data(ind-
2).z_pos(time_index);
                  orb_data_curr(ind).z_vel = OTHER_data(ind-
2).z_vel(time_index);
               end
            end

            % Set the initial time for the deflection simulation.
            t0 = base_time(time_index);

            % Compute the final time for the deflection simulation.
            tf = base_time(end);

            % Run the Solar System N body simulator.
            [f, time_curr, t_elapsed_curr] =
Solar_System_N_body_sim(orb_data_curr, t0, dt_sim, tf, options);

            % Form a formatted time string for the current deflection
            % simulation's elapsed time.
            [cur_def_sim_t_str] = format_elapsed_time(t_elapsed_curr);

            % Display a message informing the user that the current
            % deflection simulation is complete and how long it took to
            % run.
            disp(sprintf('\nDeflection simulation [ %d ] complete in: [ %s
].\n', master_index, cur_def_sim_t_str));

            for(ind=1:length(time_curr))
               rel_NEO_wrt_earth(1) = f(ind,1) - f(ind,7);
               rel_NEO_wrt_earth(2) = f(ind,3) - f(ind,9);
               rel_NEO_wrt_earth(3) = f(ind,5) - f(ind,11);
```

```
                deflection_data(master_index).NEO_Earth_dist(ind) =
norm(rel_NEO_wrt_earth);

                rel_NEO_wrt_earth_orig(1) = NEO_data.x_pos(time_index-1+ind)
- Earth_data.x_pos(time_index-1+ind);
                rel_NEO_wrt_earth_orig(2) = NEO_data.y_pos(time_index-1+ind)
- Earth_data.y_pos(time_index-1+ind);
                rel_NEO_wrt_earth_orig(3) = NEO_data.z_pos(time_index-1+ind)
- Earth_data.z_pos(time_index-1+ind);
                deflection_data(master_index).NEO_Earth_dist_orig(ind) =
norm(rel_NEO_wrt_earth_orig);

                if(store_rel_pos_other == 1)

                    if(num_obj > 2)

                        ss = 13;

                        for(ww=1:length(OTHER_data))


                            rel_pos_other(1) = f(ind,1) - f(ind,ss);
                            rel_pos_other(2) = f(ind,3) - f(ind,ss+2);
                            rel_pos_other(3) = f(ind,5) - f(ind,ss+4);


deflection_data(master_index).OTHER_rel(ww).rel_pos(ind) =
norm(rel_pos_other);

                            ss = ss + 6;
                        end

                    end

                end

            end

            % CORRECT PERFORMANCE INDEX!
            deflection_data(master_index).def_NEO_mag =
min(deflection_data(master_index).NEO_Earth_dist) -
min(deflection_data(master_index).NEO_Earth_dist_orig);


            % CONWAY'S PERFORMANCE INDEX!
            % indd = length(time_curr);
            % aa = f(end,1) - NEO_data.x_pos(time_index-1+indd);
            % bb = f(end,3) - NEO_data.y_pos(time_index-1+indd);
            % cc = f(end,5) - NEO_data.z_pos(time_index-1+indd);
            % deflection_data(master_index).def_NEO_mag = norm([aa bb cc]);


            deflection_data(master_index).def_traj_times = time_curr;

            % Store the current deflection delta-v vector azimuth.
            deflection_data(master_index).azimuth =
azimuth_scan(loop_index_az);

            % Store the current deflection delta-v vector elevation.
            deflection_data(master_index).elevation =
elevation_scan(loop_index_el);

            % Store the time index at which the deflection was applied.
            deflection_data(master_index).time_index_of_deflection =
time_index;
```

```
            % Display a message informing the user that the current optimal
            % deflection search iteration is complete.
            disp(sprintf('\nOptimal search iteration [ %d ] of [ %d ]
complete (%f percent).\n', master_index, num_searches,
100*(master_index/num_searches)));

            % Increment the master deflection data index.
            master_index = master_index + 1;

         end

      end

   end

   % Decrement the master index since it was incremented after the final
   % iteration.
   master_index = master_index - 1;

   % Compute the elapsed real time for the optimal NEO deflection search.
   elapsed_search_time = etime(clock,t0_total);

   % Format the total elapsed time string.
   [total_time_str] = format_elapsed_time(elapsed_search_time);

   % Save all data for later post-processing.
   save(save_file_name);

   % Display a message informing the user that the optimal NEO deflection
   % search is complete and how long it took.
   disp(sprintf('\n>>>>> Optimal Deflection Scan Complete in [ %s ]
<<<<<\n', total_time_str));

% End function.
return
```

```
% Begin function.
function opt_NEO_def_scan_post_proc(load_file_name)

   % Load the optimal deflection results data from file.
   load(load_file_name);

   physical_constants;

   for(ind=1:master_index)

      deflection_data(ind).true_anom =
NEO_data.true_anom(deflection_data(ind).time_index_of_deflection);
      deflection_data(ind).arg_peri  =
NEO_data.arg_peri(deflection_data(ind).time_index_of_deflection);
      deflection_data(ind).RAAN      =
NEO_data.RAAN(deflection_data(ind).time_index_of_deflection);
      deflection_data(ind).i         =
NEO_data.i(deflection_data(ind).time_index_of_deflection);
      deflection_data(ind).time_of_deflection =
base_time(deflection_data(ind).time_index_of_deflection);

      el = deflection_data(ind).elevation;
      az = deflection_data(ind).azimuth;
      dv_vec_RTN(1,1) = dv_mag*cos(el)*sin(az);
      dv_vec_RTN(2,1) = dv_mag*cos(el)*cos(az);
      dv_vec_RTN(3,1) = dv_mag*sin(el);

      NEO_vel_vec_INRTL(1,1) =
NEO_data.x_vel(deflection_data(ind).time_index_of_deflection);
      NEO_vel_vec_INRTL(2,1) =
NEO_data.y_vel(deflection_data(ind).time_index_of_deflection);
      NEO_vel_vec_INRTL(3,1) =
NEO_data.z_vel(deflection_data(ind).time_index_of_deflection);

      true_anom =
NEO_data.true_anom(deflection_data(ind).time_index_of_deflection);
      arg_peri  =
NEO_data.arg_peri(deflection_data(ind).time_index_of_deflection);
      RAAN      =
NEO_data.RAAN(deflection_data(ind).time_index_of_deflection);
      i         = NEO_data.i(deflection_data(ind).time_index_of_deflection);

      [NEO_vel_vec_RTN] = rot_INERTIAL2RTN(true_anom, arg_peri, RAAN, i,
NEO_vel_vec_INRTL);

      theta =
acos(dot(NEO_vel_vec_RTN,dv_vec_RTN)/(norm(NEO_vel_vec_RTN)*norm(dv_vec_RTN)
));
      theta = theta*180/pi;
      if(theta < 0)
         theta = theta + 360.0;
      end
      deflection_data(ind).theta = theta;

   end

   max_def = 0;
   for(ind=1:master_index)
      if(deflection_data(ind).def_NEO_mag > max_def)
         max_def = deflection_data(ind).def_NEO_mag;
         max_def_index = ind;
      end
   end


%    % Code to pick out Conway's "near-optimal" solution.
```

```
%    max_def = 0;
%    max_def_index1 = max_def_index;
%    for(ind=1:master_index)
%       if(ind ~= max_def_index1)
%           if((deflection_data(ind).def_NEO_mag > max_def)) %%% &
((deflection_data(ind).azimuth*180/pi) < 100))
%               max_def = deflection_data(ind).def_NEO_mag;
%               max_def_index = ind;
%           end
%       end
%    end
%    disp('>>>>>>>>>>>> WARNING!!! CONWAY'S NEAR-OPTIMAL BEING USED!!!
<<<<<<<<<<<<<');



   t_ind_max_def = deflection_data(max_def_index).time_index_of_deflection;
   az_max_def = deflection_data(max_def_index).azimuth;
   el_max_def = deflection_data(max_def_index).elevation;

   NEO_vel_at_max_def_INRTL(1,1) = NEO_data.x_vel(t_ind_max_def);
   NEO_vel_at_max_def_INRTL(2,1) = NEO_data.y_vel(t_ind_max_def);
   NEO_vel_at_max_def_INRTL(3,1) = NEO_data.z_vel(t_ind_max_def);

   true_anom = NEO_data.true_anom(t_ind_max_def);
   arg_peri = NEO_data.arg_peri(t_ind_max_def);
   RAAN = NEO_data.RAAN(t_ind_max_def);
   i = NEO_data.i(t_ind_max_def);

   [NEO_vel_at_max_def_RTN] = rot_INERTIAL2RTN(true_anom, arg_peri, RAAN, i,
NEO_vel_at_max_def_INRTL);

   dv_vec_RTN(1,1) = dv_mag*cos(el_max_def)*sin(az_max_def);
   dv_vec_RTN(2,1) = dv_mag*cos(el_max_def)*cos(az_max_def);
   dv_vec_RTN(3,1) = dv_mag*sin(el_max_def);

   vecs(1,1,1) = dv_vec_RTN(1,1);
   vecs(1,2,1) = dv_vec_RTN(2,1);
   vecs(1,3,1) = dv_vec_RTN(3,1);

   vecs(2,1,1) = NEO_vel_at_max_def_RTN(1,1);
   vecs(2,2,1) = NEO_vel_at_max_def_RTN(2,1);
   vecs(2,3,1) = NEO_vel_at_max_def_RTN(3,1);

   vector_plot3d(vecs);

   % Print out the results of the optimal NEO deflection search in terms
   % of the overall maximum (optimal with respect to deflection magnitude)
   % NEO deflection..
   disp(sprintf('\n>>>>> OPTIMAL DEFLECTION SEARCH RESULTS <<<<<'));
   disp(sprintf('=========================================='));
   disp(sprintf('Maximum Deflected Distance from Earth ----------------------
-------> %f [km]', max_def));
   disp(sprintf('Time after Detection at which Deflection was Applied ------
-------> %f [years]',
deflection_data(max_def_index).time_of_deflection/86400.0/365.25));
   disp(sprintf('NEO True Anomaly at which Deflection was applied ----------
-------> %f [deg]', deflection_data(max_def_index).true_anom));
   disp(sprintf('Azimuth of Optimal Deflection Vector ----------------------
-------> %f [deg]', deflection_data(max_def_index).azimuth*180/pi));
   disp(sprintf('Elevation of Optimal Deflection Vector --------------------
-------> %f [deg]', deflection_data(max_def_index).elevation*180/pi));
   disp(sprintf('Angle between NEO velocity Vector and Optimal Deflection
Vector --> %f [deg]', deflection_data(max_def_index).theta));

   % Locate the maximum deflection for each deflection time.
```

```
   for(ind=1:length(time_scan_indices))
      max_def = 0;
      for(ind2=1:master_index)
         if(deflection_data(ind2).time_index_of_deflection ==
time_scan_indices(ind))
            if(deflection_data(ind2).def_NEO_mag > max_def)
               max_def_index = ind2;
               max_def = deflection_data(ind2).def_NEO_mag;
            end
         end
      end
      max_deflections(ind) = max_def;
      plot_times(ind) = base_time(time_scan_indices(ind));
      max_deflections_indices(ind) = max_def_index;
   end

   for(ind=1:length(max_deflections_indices))
      true_anom_max_defs(ind) =
deflection_data(max_deflections_indices(ind)).true_anom;
   end

   figure
   plot(plot_times/86400/365.25, true_anom_max_defs, 'go')
   grid on
   xlabel('Time After Detection [years]')
   ylabel('True Anomaly at Deflection [deg]')

   figure
   plot(plot_times/86400/365.25, max_deflections, 'bo')
   grid on
   xlabel('Time After Detection [years]')
   ylabel('Maximum Deflection [km]')

   figure
   for(i=1:master_index)
      if(i == 1)
         hold on
      end
      if(bw_flag == 1)

plot(deflection_data(i).azimuth*180/pi,deflection_data(i).def_NEO_mag,'r-o')
      else

plot(deflection_data(i).azimuth*180/pi,deflection_data(i).def_NEO_mag,'r-o')
      end

   end
   grid on
   xlabel('Azimuth [deg]')
   ylabel('Deflection [km]')

   figure
   for(i=1:master_index)
      if(i == 1)
         hold on
      end
      if(bw_flag == 1)

plot(deflection_data(i).elevation*180/pi,deflection_data(i).def_NEO_mag,'r-
o')
      else

plot(deflection_data(i).elevation*180/pi,deflection_data(i).def_NEO_mag,'r-
o')
      end
```

```
   end
   grid on
   xlabel('Elevation [deg]')
   ylabel('Deflection [km]')

   figure
   if(bw_flag == 1)
       plot(deflection_data(master_index).def_traj_times/86400/365.25,
deflection_data(max_def_index).NEO_Earth_dist,'g')
   else
       plot(deflection_data(master_index).def_traj_times/86400/365.25,
deflection_data(max_def_index).NEO_Earth_dist,'g')
   end
   grid on
   xlabel('Time From Sim Start [years]')
   ylabel('NEO-Earth Distance DEFLECTED [km]')

   figure
   if(bw_flag == 1)
       plot(deflection_data(master_index).def_traj_times/86400/365.25,
deflection_data(max_def_index).NEO_Earth_dist_orig,'b')
   else
       plot(deflection_data(master_index).def_traj_times/86400/365.25,
deflection_data(max_def_index).NEO_Earth_dist_orig,'g')
   end
   grid on
   xlabel('Time From Sim Start [years]')
   ylabel('NEO-Earth Distance ORIGINAL [km]')

   k = 1;
   for(ind=1:length(azimuth_scan))
      for(ind2=1:length(elevation_scan))
         def_mags(ind,ind2) = deflection_data(k).def_NEO_mag/max_def;
         k = k + 1;
      end
   end

   figure
   imagesc(def_mags);
   colorbar;

    figure
    ind = 1;
    for(loop_index_az=1:length(azimuth_scan))
         for(loop_index_el=1:length(elevation_scan))
             def_mat(loop_index_az, loop_index_el) =
deflection_data(ind).def_NEO_mag;
             ind = ind + 1;
         end
    end

    surf(elevation_scan*(180/pi), azimuth_scan*(180/pi), def_mat);

    xlabel('Elevation [deg]')
    ylabel('Azimuth [deg]')
    zlabel('Deflection [km]')


% End function.
Return
```

```
%==================%
%= Program Header =%
%==================%
%
% Purpose:    Simulate the motion of a N body system acting under the
%             effects of mutual gravitation.
%
% Inputs:     orb_data - a vector of orbital data structures, one
%                        for each body, containing dynamic information
%                        including the initial state (position and
%                        velocity) and mass.
%             t0       - initial time value for the simulation.
%             dt_sim   - time step at which to store state information.
%             tf       - final time value for the simulation.
%             options  - pre-defined numerical integration parameters for
%                        the built-in Matlab routine ode45(). this is an
%                        optional input argument. if not provided, this
%                        program will default to a set of strict numerical
%                        integration tolerances.
%
% Outputs:    f        - matrix containing the positions and velocities for
%                        each body over the time interval of the
%                        simulation, as generated by ode45().
%             t        - a vector of times that correspond to each position
%                        and velocity for each body over the time interval
%                        of the simulation.
%
% Usage:      [f, t, t_elapsed] = N_body_sim(orb_data, t0, dt_sim, tf,
options)
%

% Begin function.
function [f, t, t_elapsed] = Solar_System_N_body_sim(orb_data, t0, dt_sim,
tf, options)

   % Load physical constants.
   physical_constants;

   % If no options are provided for the ode45() routine by the user, set
   % the tolerances for the numerical integration to strict values to
   % ensure accuracy. Note that this may result in noticably increased
   % numerical integration time.
   if(nargin < 5)

      options = odeset('reltol', 1e-11, 'abstol', 1e-9);

   end

   % Determine the number of bodies to simulate from the number of orbital
   % data structures passed into this function.
   num_bodies = length(orb_data);

   % Initialize the total system state vector index.
   k = 1;

   % Populate the total system state vector index by extracting the state
   % vector components from each orbital data structure.
   for(i=1:num_bodies)

      % Extract the state vector components and assign them to the
      % appropriate place in the total system state vector.
      R(k)   = orb_data(i).x_pos;
      R(k+1) = orb_data(i).x_vel;
      R(k+2) = orb_data(i).y_pos;
      R(k+3) = orb_data(i).y_vel;
      R(k+4) = orb_data(i).z_pos;
```

```
      R(k+5) = orb_data(i).z_vel;

      % Increment the total system state vector index.
      k = k + 6;

      % Extract the mass for the current body and populate the vector which
      % contains the masses of all bodies.
      mass(i) = orb_data(i).mass;

   end

   % Set the placeholder flag required by ode45() to "empty." this flag is
   % required when passing additional arguments to the derivatives routine
   % supplied to ode45(). additional arguments are anything else in
   % addition to the system state vector and the time.
   FLAG = '';

   % Record the time immediately before the numerical integration of the
   % system state begins so that the elapsed real time required to simulate
   % the system can be computed.
   t_start = clock;

   % Numerically integrate the system state via the built-in Matlab routine
   % ode45().
   [t, f] = ode45('Solar_System_N_body_derivs', (t0:dt_sim:tf), R, ...
                  options, mass, G, m_sun, num_bodies);


   % Compute the real-time elapsed during the numerical integration.
   t_elapsed = etime(clock, t_start);

% End function.
Return
```

```
%==================%
%= Program Header =%
%==================%
%
% Purpose:    Compute the derivative of the state
%             vector for an N-body system of the Solar System.
%
% Inputs:     t     - the time index of the simulation.
%             R     - the system state vector.
%             FLAG  - variable required by this function.
%             m     - vector of masses for each body in the state vector.
%             G     - gravitational constant.
%             m_sun - mass of the sun.
%             n     - number of bodies in the state vector.
%
% Outputs:    R_dot - the time derivative of the system state vector. this
%                     vector must be shaped as a column vector.
%
% Usage:      [R_dot] = Solar_System_N_body_derivs(t, R, FLAG, m, G, n)
%
% Notes:      o This function is not intended to be called stand-alone,
%               although that is possible. It is intended to be called in
%               an automated fashion by the built-in Matlab routine
%               ode45().
%
% Date of last modification: 9/14/2005

%Begin function.
function [R_dot] = Solar_System_N_body_derivs(t, R, FLAG, m, G, m_sun, n)

   % Initialize state vector index.
   k = 1;

   % Loop over all masses.
   for(i=1:n)

      % Extract the position components from the state vector.
      r(1,i) = R(k);
      r(2,i) = R(k+2);
      r(3,i) = R(k+4);

      % Increment the state vector index.
      k = k + 6;

   end

   % Initialize state vector derivative index.
   k = 2;

   % Loop over all masses.
   for(i=1:n)

      % Initialize the acceleration components to zero.
      r2dot(1) = 0;
      r2dot(2) = 0;
      r2dot(3) = 0;

      % Compute the cube of the distance of the current mass from the Sun.
      r_mag = norm(r(:,i));
      r_mag_3 = r_mag^3;

      % Loop over all other masses.
      for(j=1:n)

         % Only compute if j is not equal to i.
         if(j ~= i)
```

```
            % Compute relative position vector.
            rij = r(:,j) - r(:,i);

            % Compute relative position vector magnitude.
            rij_mag = norm(rij);

            % Compute the cube of the relative position vector magnitude.
            rij_mag_3 = rij_mag^3;

            % Compute accelerations.
            r2dot(1) = r2dot(1) + ((G*m(j))/rij_mag_3)*rij(1);
            r2dot(2) = r2dot(2) + ((G*m(j))/rij_mag_3)*rij(2);
            r2dot(3) = r2dot(3) + ((G*m(j))/rij_mag_3)*rij(3);

         end

      end

      % Include the gravitational acceleration due to the Sun.
      r2dot(1) = r2dot(1) - ((G*m_sun)/r_mag_3)*r(1,i);
      r2dot(2) = r2dot(2) - ((G*m_sun)/r_mag_3)*r(2,i);
      r2dot(3) = r2dot(3) - ((G*m_sun)/r_mag_3)*r(3,i);

      % Load the state vector derivatives.
      R_dot(k)   = r2dot(1);
      R_dot(k+2) = r2dot(2);
      R_dot(k+4) = r2dot(3);

      % Increment the state vector derivative index.
      k = k + 6;

   end

   % Initialize the state vector derivative index.
   k = 1;

   % Loop over the velocity elements of the state vector derivative.
   while(k <= ((6*n)-1))

      % Set the derivatives of the positions equal to the velocities.
      R_dot(k) = R(k+1);

      % Increment the state vector derivative index.
      k = k + 2;
   end

   % Return a column vector for the ode45() function.
   R_dot = R_dot';

% End function.
Return
```

```
%%%%%%%%%%%%%%%%%%%%%%%%%%%%%%%%%%%%%%%%%%%%%%%%%%%%%%%%%%%%%%%%%%%%%%%%%%%%
%%%%%%%%%%%%%%%%%%%%%%%%%%%%%%%%%%%%%%%%%%%%%%%%%%%%%%%%%%%%%%%%%%%%%%%%%%%%
%%%%%%%%%%%%%%%%%%%%%%%%%%%%%%%%%%%%%%%%%%%%%%%%%%%%%%%%%%%%%%%%%%%%%%%%%%%%
%%%%%%%%%%%%%%%%%%%%%%%% ORBITAL SCENARIO INPUT FILE %%%%%%%%%%%%%%%%%%%%%%%%
%%%%%%%%%%%%%%%%%%%%%%%%%%%%%%%%%%%%%%%%%%%%%%%%%%%%%%%%%%%%%%%%%%%%%%%%%%%%
%%%%%%%%%%%%%%%%%%%%%%%%%%%%%%%%%%%%%%%%%%%%%%%%%%%%%%%%%%%%%%%%%%%%%%%%%%%%
%%%%%%%%%%%%%%%%%%%%%%%%%%%%%%%%%%%%%%%%%%%%%%%%%%%%%%%%%%%%%%%%%%%%%%%%%%%%
%=========================================================================%
%= Set output file directory.                                            =%
%=========================================================================%
output_dir = '';
%=========================================================================%
%= Set output filename root.                                             =%
%=========================================================================%
output_file_root = '';
%=========================================================================%
%=========================================================================%
%=============== SET OPTIMAL DEFLECTION SEARCH PARAMETERS ================%
%=========================================================================%
%=========================================================================%
% >>>>>>>>>>>>>> TIME <<<<<<<<<<<<<<<<<<<<<<<<<<<<<<<<<<<<<<<<<<<<<<<<<<< %
time_scan_init  = [];                                                % [days]
time_scan_res   = [];                                                % [days]
time_scan_final = [];                                                % [days]
time_scan_vec   = [];                                                % [days]
time_scan_TOL   = [];                                                % [days]
% >>>>>>>>>>>>>> TRUE ANOMALY <<<<<<<<<<<<<<<<<<<<<<<<<<<<<<<<<<<<<<<<<< %
true_anom_init  = [];                                                 % [deg]
true_anom_res   = [];                                                 % [deg]
true_anom_final = [];                                                 % [deg]
true_anom_vec   = [];                                                 % [deg]
true_anom_TOL   = [];                                                 % [deg]
% >>>>>>>>>>>>>> AZIMUTH <<<<<<<<<<<<<<<<<<<<<<<<<<<<<<<<<<<<<<<<<<<<<<<< %
azimuth_init    = [];                                                 % [deg]
azimuth_res     = [];                                                 % [deg]
azimuth_final   = [];                                                 % [deg]
azimuth_scan    = [];                                                 % [deg]
% >>>>>>>>>>>>>> ELEVATION <<<<<<<<<<<<<<<<<<<<<<<<<<<<<<<<<<<<<<<<<<<<< %
elevation_init  = [];                                                 % [deg]
elevation_res   = [];                                                 % [deg]
elevation_final = [];                                                 % [deg]
elevation_scan  = [];                                                 % [deg]
% >>>>>>>>>>>>>> DELTA-V <<<<<<<<<<<<<<<<<<<<<<<<<<<<<<<<<<<<<<<<<<<<<<<< %
dv_mag          = ;                                                  % [cm/s]
%=========================================================================%
%=========================================================================%
%=========================================================================%
%= Set meta simulation options.                                          =%
%=========================================================================%
store_rel_pos_other = 0;
start_true_anom_scan_at_t_scan = 1;
%=========================================================================%
%= Set simulation parameters.                                            =%
%=========================================================================%
%=========================================================================%
%= Error tolerance options for Matlab's ode45() numerical integrator.    =%
%=========================================================================%
options = odeset('reltol', , 'abstol', );
%=========================================================================%
%= Time step at which the numerical integrator should store results.     =%
%=========================================================================%
dt_sim = ;                                                           % [days]
%=========================================================================%
%= Load physical constants into the variable space.                      =%
%=========================================================================%
physical_constants;
```

```
%=========================================================================%
%= Set the desired number of total sim objects, NOT counting the sun.    =%
%=========================================================================%
num_obj = 2;
%=========================================================================%
%= Generate an unpopulated data structure for each object.               =%
%=========================================================================%
for(ind=1:num_obj)
    [orb_data(ind)] = generate_orb_data_struct;
end
%=========================================================================%
%= Generate unpopulated epoch data structures for NEO and all objects.   =%
%=========================================================================%
[epoch_data_NEO]      = generate_epoch_data_struct;
[epoch_data_INIT_ALL] = generate_epoch_data_struct;
%=========================================================================%
%= Generate unpopulated epoch data structure for event time.             =%
%=========================================================================%
[epoch_data_EVENT] = generate_epoch_data_struct;
%=========================================================================%
%= Set the event time.                                                   =%
%=========================================================================%
epoch_data_EVENT.year    = ;                                % [year]
epoch_data_EVENT.month   = ;                                % [month]
epoch_data_EVENT.day     = ;                                % [day]
epoch_data_EVENT.hours   = ;                                % [hour (UT)]
epoch_data_EVENT.minutes = ;                                % [minutes (UT)]
epoch_data_EVENT.seconds = ;                                % [seconds (UT)]
epoch_data_EVENT.JD      = ;                                % [JD]
epoch_data_EVENT.MJD     = ;                                % [MJD]
%=========================================================================%
% Set the orbital data structure indices.                                =%
%=========================================================================%
NEO_orb_index   = 1;
EARTH_orb_index = 2;
%=========================================================================%
%= Load orbital ephemeris data.                                          =%
%=-----------------------------------------------------------------------=%
%= Note: The NEO is always the first in the array of data structures.    =%
%=========================================================================%
%=========================================================================%
% >>>>>>>>>>>> NEO <<<<<<<<<<<<<<<<<<<<<<<<<<<<<<<<<<<<<<<<<<<<<<<<<<<< %
%=========================================================================%
orb_data(NEO_orb_index).a         = ;                           % [km]
orb_data(NEO_orb_index).e         = ;                           % [ - ]
orb_data(NEO_orb_index).i         = ;                           % [deg]
orb_data(NEO_orb_index).RAAN      = ;                           % [deg]
orb_data(NEO_orb_index).arg_peri  = ;                           % [deg]
orb_data(NEO_orb_index).mean_anom = ;                           % [deg]
orb_data(NEO_orb_index).mass      = ;                           % [kg]
%=========================================================================%
%= Set the epoch for the above NEO state information.                    =%
%=========================================================================%
epoch_data_NEO.year    = ;                                % [year]
epoch_data_NEO.month   = ;                                % [month]
epoch_data_NEO.day     = ;                                % [day]
epoch_data_NEO.hours   = ;                                % [hour (UT)]
epoch_data_NEO.minutes = ;                                % [minutes (UT)]
epoch_data_NEO.seconds = ;                                % [seconds (UT)]
epoch_data_NEO.JD      = ;                                % [JD]
epoch_data_NEO.MJD     = ;                                % [MJD]
%=========================================================================%
% >>>>>>>>>>>> EARTH <<<<<<<<<<<<<<<<<<<<<<<<<<<<<<<<<<<<<<<<<<<<<<<<<< %
%=========================================================================%
orb_data(EARTH_orb_index).a         = ;                         % [km]
orb_data(EARTH_orb_index).e         = ;                         % [ - ]
```

```
orb_data(EARTH_orb_index).i         = ;                                 % [deg]
orb_data(EARTH_orb_index).RAAN      = ;                                 % [deg]
orb_data(EARTH_orb_index).arg_peri  = ;                                 % [deg]
orb_data(EARTH_orb_index).mean_anom = ;                                 % [deg]
orb_data(EARTH_orb_index).mass      = ;                                 % [kg]
%=========================================================================%
% >>>>>>>>>>>> ALL OTHER SIMULATION OBJECTS <<<<<<<<<<<<<<<<<<<<<<<<<< %
%=========================================================================%
%
%=========================================================================%
%= Set the epoch for the initial state information for all objects other =%
%= than the NEO above.                                                   =%
%=-----------------------------------------------------------------------=%
%= Note: It is assumed that all objects other than the NEO, including    =%
%=       the Earth, have the same epoch for their initial conditions.    =%
%=========================================================================%
epoch_data_INIT_ALL.year    = ;                                 % [year]
epoch_data_INIT_ALL.month   = ;                                 % [month]
epoch_data_INIT_ALL.day     = ;                                 % [day]
epoch_data_INIT_ALL.hours   = ;                                 % [hour (UT)]
epoch_data_INIT_ALL.minutes = ;                                 % [minutes (UT)]
epoch_data_INIT_ALL.seconds = ;                                 % [seconds (UT)]
epoch_data_INIT_ALL.JD      = ;                                 % [JD]
epoch_data_INIT_ALL.MJD     = ;                                 % [MJD]
%=========================================================================%
%= Fully populate the orbital data structures.                           =%
%=========================================================================%
for(ind=1:num_obj)
   [orb_data(ind)] = populate_orb_data_struct(orb_data(ind), mu_sun);
end
%=========================================================================%
%= Fully populate the epoch data structures.                             =%
%=========================================================================%
[epoch_data_NEO]      = populate_epoch_data_struct(epoch_data_NEO);
[epoch_data_INIT_ALL] = populate_epoch_data_struct(epoch_data_INIT_ALL);
[epoch_data_EVENT]    = populate_epoch_data_struct(epoch_data_EVENT);
%%%%%%%%%%%%%%%%%%%%%%%%%%%%%%%%%%%%%%%%%%%%%%%%%%%%%%%%%%%%%%%%%%%%%%%%%%%
%%%%%%%%%%%%%%%%%%%%%%%%%%%%%%%%%%%%%%%%%%%%%%%%%%%%%%%%%%%%%%%%%%%%%%%%%%%
%%%%%%%%%%%%%%%%%%%%%%%%%%%%%%%%%%%%%%%%%%%%%%%%%%%%%%%%%%%%%%%%%%%%%%%%%%%
%%%%%%%%%%%%%%%%%%%% END ORBITAL SCENARIO INPUT FILE %%%%%%%%%%%%%%%%%%%%%%%
%%%%%%%%%%%%%%%%%%%%%%%%%%%%%%%%%%%%%%%%%%%%%%%%%%%%%%%%%%%%%%%%%%%%%%%%%%%
%%%%%%%%%%%%%%%%%%%%%%%%%%%%%%%%%%%%%%%%%%%%%%%%%%%%%%%%%%%%%%%%%%%%%%%%%%%
%%%%%%%%%%%%%%%%%%%%%%%%%%%%%%%%%%%%%%%%%%%%%%%%%%%%%%%%%%%%%%%%%%%%%%%%%%%
```

REFERENCES

1. Lewis, John S. *Comet and Asteroid Impact Hazards on a Populated Earth*, Academic Press, 2000, San Diego, CA

2. D. Morrison, *et al.* "Impacts and the public: communicating the nature of the impact hazard" *Mitigation of Hazardous Asteroids and Comets*, Cambridge University Press, 2004

3. B.A. Conway "Optimal interception and deflection of Earth-approaching asteroids using low-thrust electric propulsion" *Mitigation of Hazardous Asteroids and Comets*, Cambridge University Press, 2004

4. Update on the Spaceguard Survey and on Asteroid Apophis http://impact.arc.nasa.gov/news_detail.cfm?ID=162 (August 2005)

5. Bottke, *et al.* "Recent progress in interpreting the nature of the near-Earth object population" *Mitigation of Hazardous Asteroids and Comets*, Cambridge University Press, 2004

6. Near Earth Asteroid Rendezvous, *Asteroid Types.* http://near.jhuapl.edu/eros/astertypes.html (September 2003)

7. Chesley, *et al.* "Earth impactors: orbital characteristics and warning times" *Mitigation of Hazardous Asteroids and Comets*, Cambridge University Press, 2004

8. Deep Impact: Mission Results: Excavating Comet Tempel 1 http://deepimpact.jpl.nasa.gov/results/excavating.html (November 2005)

9. Asphaug, Erik "Interior structures for asteroids and cometary nuclei" *Mitigation of Hazardous Asteroids and Comets*, Cambridge University Press, 2004

10. D. Idle "TALON and CRADLE – Systems for the Rescue of Tumbling Spacecraft and Astronauts – A Preliminary Design", Ph.D. Dissertation, The University of Texas at Austin, 1989

11. Wiesel, William E. *Spaceflight Dynamics*, Irwin McGraw-Hill, Boston, Massachusetts, 1989

12. Holsapple, Keith A. “About deflecting asteroids and comets” *Mitigation of Hazardous Asteroids and Comets*, Cambridge University Press, 2004

13. Robert A. Rohde and Richard A. Muller (2005). “Cycles in fossil diversity.” *Letters to Nature*, Vol. 434, March 10, 2005, 208-210

14. NASA – Near Earth Object Program http://www.nasa.gov/audience/foreducators/postsecondary/features/F_Near_Earth_Program.html (November 2005)

15. A. J. Ball, *et al.* “Lander and penetrator science for near-Earth object mitigation studies” *Mitigation of Hazardous Asteroids and Comets*, Cambridge University Press, 2004

16. Asteroid Vaporization Energy Analysis http://www.stardestroyer.net/Empire/Tech/Beam/Asteroid.html (November 2005)

17. Gritzner, *et al.* “Mitigation technologies and their requirements” *Mitigation of Hazardous Asteroids and Comets*, Cambridge University Press, 2004

18. Wilkins, Peter A. Computer rendering of asteroid model using Lightwave software (November 2005)

19. Spotlight on “Angels and Demons” http://public.web.cern.ch/Public/Content/Chapters/Spotlight/SpotlightAandD-en.html (November 2005)

20. Thorton, Stephen T. and Rex, Andrew *Modern Physics for Scientists and Engineers*, Thomson Learning, Inc., 2002

21. Sang-Young Park and I. Michael Ross (1999). “Two-Body Optimization for Deflecting Earth-Crossing Asteroids” *Journal of Guidance, Control, and Dynamics* Vol. 22, No.3, May-June 1999, 415-420

22. Database of Near-Earth Asteroids, *1991 RB* http://earn.dlr.de/nea/J91R00B.htm (November 2005)

23. Siding Spring Exploratory http://www.sidingspringexploratory.com.au (November 2005)

24. Orbit Simulation, *Asteroid (1991 RB)* http://neo.jpl.nasa.gov/cgi-bin/db?name=1991+RB (November 2005)

25. NEODys: quick search (search string = “1991RB”) http://newton.dm.unipi.it/cgi-bin/neodys/neoibo?quicksearch:0;main (November 2005)

26. *The Astronomical Almanac For The Year 2005*, Washington: U.S. Government Printing Office, London: The Stationary Office, 2005

27. Lynch, David K. and Peterson, Glenn E. “Athos, Porthos, Aramis & D’Artagnan: Four Planning Scenarios for Planetary Protection”, The Aerospace Corporation, 2004

28. Lyon (France) – World Sites Atlas http://www.sitesatlas.com/Europe/France/Lyon.htm (November 2005)

29. List of All U.S. Nuclear Weapons http://nuclearweaponarchive.org/Usa/Weapons/Allbombs.html (November 2005)

30. Pratt & Whitney – Products – Space – RL 10 http://www.pratt-whitney.com/prod_space_rl10.asp (April 2004)

31. ELV Mission Analysis Launch Vehicle Information http://elvperf.ksc.nasa.gov/elvMap/staticPages/perf_query1.html (April 2004)

32. NSSDC Master Catalog Display *NEAR Shoemaker* http://nssdc.gsfc.nasa.gov/database/MasterCatalog?sc=1996-008A (November 2005)

33. Schweickart, R. “A Call to (Considered) Action” Presented at the National Space Society International Space Development Conference, Washington, DC May, 2005

34. John Hopkins University/Applied Physis Laboratory, (1998). *NEAR Multispectral Imager*. Near Earth Asteroid Rendezvous. http://near.jhuapl.edu/fact_sheets/MSI.pdf (September 2003)

35. John Hopkins University/Applied Physis Laboratory, (1998). *NEAR Near-Infrared Spectrometer*. Near Earth Asteroid Rendezvous. http://near.jhuapl.edu/fact_sheets/NIS.pdf (September 2003)

36. John Hopkins University/Applied Physis Laboratory, (1998). *NEAR X-Ray/Gamma-Ray Spectrometer*. Near Earth Asteroid Rendezvous. http://near.jhuapl.edu/fact_sheets/XGRS.pdf (September 2003)

37. John Hopkins University/Applied Physis Laboratory, (1998). *NEAR Magnetometer*. Near Earth Asteroid Rendezvous. http://near.jhuapl.edu/fact_sheets/MAG.pdf (September 2003)

38. John Hopkins University/Applied Physis Laboratory, (1998). *NEAR Laser Rangefinder*. Near Earth Asteroid Rendezvous. http://near.jhuapl.edu/fact_sheets/NLR.pdf (September 2003)